

https://dspace.org/

Electric return current distribution through train wagons in AC railway systems

Clay, James

2016-09-16
http://hdl.handle.net/10539/21045

Downloaded from a DSpace repository. https://dspace.org/



ELECTRIC RETURN CURRENT DISTRIBUTION THROUGH TRAIN WAGONS IN AC RAILWAY SYSTEMS

RESEARCH DISSERTATION

School of Electrical and Information Engineering
University of the Witwatersrand, Johannesburg

Author:	James Clay
Student Number:	325609
Due Date:	May 2016
Research Title:	Electric Return Current Distribution through Train Wagons in AC Railway Systems
Supervisor:	Prof Ivan Hofsajer

DECLARATION

I, James William Clay, Student Number 325609, hereby declare that this dissertation is my own unaided work, except where explicitly indicated otherwise. It is being submitted to the Faculty of Engineering and the Built Environment at the University of the Witwatersrand, Johannesburg as part of a Degree of Master of Science in Engineering. This dissertation has not been submitted before for any degree or examination to any other University.

Signed: 

Date: 30th May 2016

ABSTRACT

The electric railway environment has long been considered electromagnetically unfriendly and has been plagued by electromagnetic interference. Recently, it has been found that a substantial percentage of return current flows through the couplers of moving trains. This current has been the cause of electromagnetic interference in neighbouring systems and the electrical erosion of wagon bearings.

This document provides a brief background around the observed current in the wagon couplers of electric trains as well as the effects thereof. Information from railway experts is presented in the form of a literature survey in order to establish a high level understanding of electric railway configurations and the challenges that have been experienced with the various configurations.

The document goes on to establish a theoretical background of the concepts expanded upon in the development of a system model. Some theoretical discussion included is the concept of power factors, basic magnetic circuits, internal inductance, the proximity effect, mutual-inductance, the dot convention and multi-conductor transmission lines.

Once the theoretical background is established, the development of a system model is proposed and presented. The model that is proposed considers the supply infrastructure configuration, locomotive or locomotive consist and a single wagon which is cascaded to form a train. This model is the culmination of the research.

Following the system model development, the model was tested against measured data both from Sweden (external) and South Africa (internal) to give confidence in the model.

The model was used to perform investigations of various conditions on the current distribution in a train. Some interesting observations that were made include the uneven distribution of current exiting the axles of a wagon, as well as the idea that higher frequency components of the return current will tend to travel in the couplers of the train, whilst lower frequency components will tend to travel through the electrical supply infrastructure such as the rails.

TABLE OF CONTENTS

Declaration i

Abstract ii

List of Figures vii

List of Tables xiv

List of Symbols xvi

List of Abbreviations xviii

CHAPTER 1 Introduction 1

1.1 Overview of Transnet Freight Rail and their Observations 3

1.2 Problem Statement 3

1.3 Initial Investigation Findings 4

CHAPTER 2 Background & Literature Survey 5

2.1 Traction Supply Infrastructure 5

2.2 Electromagnetic Interference (EMI) in Traction Systems 6

2.3 Supply System Configuration 9

2.4 Stray Return Currents 11

2.4.1 Stray Currents in DC Infrastructure 12

2.4.2 Stray Currents in AC Infrastructure 16

2.5 Electrical Continuity of Conductors 17

2.6 Return Current Distribution 18

CHAPTER 3 Theoretical Discussion 20

3.1 The Magnetic Circuit 20

3.2 Internal Inductance 22

3.3 Proximity Effect 23

3.4 Mutual Inductance between Magnetic Circuits 23

3.5 The Dot Convention 23

3.6 Multi-conductor Transmission Lines 25

CHAPTER 4 Model Development 27

4.1 The Locomotive Model 27

4.1.1 Energy Flow through a Locomotive 27

4.1.2 Power Electronics in Modern Locomotives 28

4.1.3 The Single Source Locomotive Model 28

4.1.4 The Multiple Source Locomotive Model 30
4.1.5 The Multiple Source Locomotive Model Parameters 31
4.2 The Supply Infrastructure 32
4.2.1 The Ideal Supply Model 32
4.2.2 The Lumped Impedance Supply Model 33
4.2.3 The Multiple Transmission Line Supply Model 34
4.2.4 The Inclusion of Rail-to-Mast Bonds in Supply Model 40
4.2.5 The Parallel Supply Model 42
4.3 The Wagon Model 43
4.3.1 The Ideal Wagon Model 43
4.4 Wagon Model Verification 47
CHAPTER 5 Measured Data 48
5.1 Ekman et al. Measurements 48
5.1.1 Train and Infrastructure configuration 48
5.1.2 Transducer locations 49
5.1.3 Measurement results 49
5.2 Transnet Freight Rail Measurements 50
5.2.1 Train and Infrastructure configuration 50
5.2.2 Transducer locations 51
5.2.3 Measurement results 51
CHAPTER 6 Simulation Model 54
6.1 Main Simulation Circuit 54
6.1.1 Simulation Settings and Configuration 56
6.1.2 Infrastructure and Sub-Station Feeds 57
6.1.3 Locomotive Consist 58
6.1.4 Wagons 58
6.2 Simulation Sub-Circuits 59
6.2.1 Wagon Set Sub-Circuits 59
6.2.2 Individual Wagon Sub-Sub-Circuit 60
CHAPTER 7 Simulation Model Data 62
7.1 Simulated Model Verification 62
7.1.1 Ekman et al. Measurements 62
7.1.2 Transnet Freight Rail Measurements 67

7.2 Discrepancies between Ekman et al. and Transnet Freight Rail Wagon Model Parameters 73
7.3 Summary of Results and Observations 74
CHAPTER 8 Investigation & Discussion 75
8.1 Return Current distribution in Wagon Wheels 75
8.1.1 Current distribution in the Axles of a Single Wagon 75
8.2 Return Current distribution in Wagon Couplers 78
8.3 Effect of Wagon Model 78
8.3.1 Wagon Coupler to Coupler Resistance 79
8.3.2 Wagon Coupler to Wheel Resistance 80
8.3.3 Wagon Coupler to Coupler Inductance 82
8.4 Discussion Summary 84
CHAPTER 9 Conclusion 85
References 87
APPENDIX A Activity Diagram of Research 90
APPENDIX B Argument Structure of Research 91
APPENDIX C Wagon Model Verification: Experimental Methodology 92
C.1 Experiment Location 92
C.2 Experiment Apparatus 93
C.3 Transnet Freight Rail Safety Requirements 97
C.4 Experimental Method 98
C.4.1 Measurements on Wheel D1 98
C.4.2 Measurements on Wheel C1 100
C.4.3 Measurements on Wheel B1 101
C.4.4 Measurements on Wheel A1 103
C.5 Isolation of the Wagon 104
C.6 Electrical Connections to the Wagon 105
C.7 Self-Inductance Introduced by Test Apparatus 109
APPENDIX D Wagon Model Verification: Experimental Results Analysis 111
D.1 Setup of Simultaneous Equations from Wagon Measurements 111
D.1.1 Measurements on Axle D1 112
D.1.2 Measurements on Axle C1 115
D.1.3 Measurements on Axle B1 119
D.1.4 Measurements on Axle A1 123

D.2 Solving Simultaneous equations 127

APPENDIX E Transnet Freight Rail Coal Line Measurements: Experimental Methodology 131

E.1 Experiment Location 131

E.2 Experiment Apparatus 131

E.3 Experimental Method 145

APPENDIX F LTSpice NetLists 146

F.1 Main Simulation Circuit Netlist (LTSpice Generated) 146

F.2 Wagon Set Sub-Circuit Netlist (LTSpice Generated) 149

F.3 Individual Wagon Sub-Sub-Circuit Netlist (LTSpice Generated) 149

APPENDIX G Octave Simulation Source Code 154

G.1 Wagon Parameter Iterative Determination Simulation Code 154

G.2 Wagon Parameter Matrix Calculation Verification Simulation Code 157

LIST OF FIGURES

Figure 1: Diagram illustrating a simplified equivalent model of the AC traction system. 10

Figure 2: Diagram illustrating a simplified equivalent model of the dual feed AC traction system. 10

Figure 3: Diagram illustrating a simplified equivalent model of the DC traction system. 10

Figure 4: Diagram illustrating a simplified equivalent model of the one way DC traction supply system. 11

Figure 5: Diagram illustrating the equivalent circuit model of the typical harmonic filter at DC sub-stations in South Africa adapted from [2]. 11

Figure 6: Diagram illustrating a simple equivalent model of the DC traction system 13

Figure 7: Diagram illustrating a simple equivalent model of a 25 kV AC traction system utilizing the booster transformer scheme. 17

Figure 8: Diagram illustrating a simple equivalent model of a 2 x 25 kV AC traction system utilizing the auto transformer scheme. 17

Figure 9: Diagram illustrating the possible return current paths immediately subsequent to the locomotive. 18

Figure 10: Diagram to show magnetic field created around a conductor carrying current, adapted from [21]. 20

Figure 11: Diagram to show multiple conductors around a point $\boldsymbol{p}$. 21

Figure 12: Diagram to 2 current carrying loops with dot convention. 24

Figure 13: Diagram illustrating a 3 conductor MTL. 26

Figure 14: Diagram to show the simplified flow of power in a modern locomotive feeding from an AC supply. 27

Figure 15: Diagram to show the simplified flow of power in a modern dual voltage locomotive feeding from a DC supply. 28

Figure 16: Diagram to show the ideal current source model of a modern locomotive utilising on-board power electronics. 29

Figure 17: Diagram to show the harmonic content found in a typical modern locomotive utilising power electronics, extracted from [25]. 30

Figure 18: Diagram to show the multiple current source model of a modern locomotive utilising on-board power electronics. 31

Figure 19: Diagram to show the multiple current source model of a modern locomotive utilising on-board power electronics. 32

Figure 20: Diagram to show the ideal AC sub-station supply model. 33

Figure 21: Diagram to show the lumped impedance supply model. 33

Figure 22: Diagram to show the typical supply infrastructure layout on the Transnet Coal Line. 34

Figure 23: Diagram to show the typical supply infrastructure geometrical dimensions on the Transnet Coal Line. 36

Figure 24: Diagram to show the typical supply infrastructure geometrical dimensions on the Transnet Coal Line inclusive of wagons modelled as a continuous drawbar. 37

Figure 25: Diagram illustrating the typical Coal Line supply configuration with a train as a MTL. 39

Figure 26: Diagram to show the extended lumped impedance supply model per meter inclusive of oscillating rail-to-mast bond. 42

Figure 27: Diagram to show the Lumped Impedance, Parallel Supply Model. 43

Figure 28: Diagram to show the Ideal Wagon Model. 44

Figure 29: Diagram to show the reduced ideal wagon model from axle symmetries. 45

Figure 30: Diagram to show the reduced ideal wagon model from physical wagon symmetries. 46

Figure 31: Diagram to show the reduced complex wagon model. 47

Figure 32: Graph showing the measurement results for line and coupler currents obtained by Ekman et al. during measurements in Sweden, extracted from [19]. 49

Figure 33: Graph showing the measurement results for line and coupler currents obtained during measurements on the South African Coal Line. 51

Figure 34: Graph showing the measurement results for the 1st coupler currents against distance, obtained during measurements on the South African Coal Line. 53

Figure 35: Simulation circuit diagram showing the main simulation circuit model in LTSpice. 55

Figure 36: Figure showing the simulation settings and configuration for the main simulation circuit, extracted from Figure 35. 56

Figure 37: Figure showing the simulation settings and configuration for the main simulation circuit, extracted from Figure 35. 56

Figure 38: Figure showing the supply feed subsequent to the train for the main simulation circuit, extracted from Figure 35. 57

Figure 39: Figure showing the supply feed preceding the train as well as the locomotive consist for the main simulation circuit, extracted from Figure 35. 58

Figure 40: Figure showing the wagon sub-circuits for the main simulation circuit, extracted from Figure 35. 59

Figure 41: Figure showing the wagon set sub-circuits to be included in the main simulation circuit. 60

Figure 42: Figure showing the individual wagon sub-sub-circuits to be included in the wagon set sub-circuit. 61

Figure 43: Graph showing the Ekman et al. measured primary current and the simulated primary current. 63

Figure 44: Graph showing the Ekman et al. measured 1st coupler current and the simulated 1st coupler current. 64

Figure 45: Graph showing the Ekman et al. measured 20th coupler current and the simulated 20th coupler current. 65

Figure 46: Graph showing the Ekman et al. measured 51st coupler current and the simulated 51st coupler current. 66

Figure 47: Graph showing the Transnet measured primary current and the simulated primary current. 68

Figure 48: Graph showing the Transnet measured 1st coupler current and the simulated 1st coupler current. 69

Figure 49: Graph showing the Transnet measured 100th coupler current and the simulated 100th coupler current. 70

Figure 50: Graph showing the Transnet measured 150th coupler current and the simulated 150th coupler current. 71

Figure 51: Graph showing the waveforms of the current through the nodes of the 1st wagon of the Coal Line train. 76

Figure 52: Graph showing the harmonic content of the current through the nodes of the 1st wagon of the Coal Line train. 77

Figure 53: Graph showing the harmonic content of the current through the nodes of the 1st wagon of the Coal Line train as a percentage of their respective total current. 77

Figure 54: Graph showing current distribution in the couplers of the wagons of a Coal Line train. 78

Figure 55: Graph showing current distribution in the couplers of the wagons of a Coal Line train under varying coupler to coupler resistance. 79

Figure 56: Graph showing current distribution in the couplers of the wagons of a Coal Line train under varying coupler to coupler resistance, as a percentage of the 1st coupler current. 80

Figure 57: Graph showing current distribution in the couplers of the wagons of a Coal Line train under varying coupler to wheel resistance. 81

Figure 58: Graph showing current distribution in the couplers of the wagons of a Coal Line train under varying coupler to wheel resistance, as a percentage of the 1st coupler current. 82

Figure 59: Graph showing current distribution in the couplers of the wagons of a Coal Line train under varying wagon heights. 83

Figure 60: Graph showing current distribution in the couplers of the wagons of a Coal Line train, as a percentage of the 1st coupler current, under varying wagon heights 83

Figure 61: Photograph showing the yard section used to conduct wagon measurements. 92

Figure 62: Photograph showing the experiment apparatus in the storage crate during the wagon measurements 94

Figure 63: Photograph showing the experiment apparatus for the wagon measurements. 95

Figure 64: Photograph showing the experiment setup at the experiment location during the wagon measurements 95

Figure 65: Photograph showing the experiment setup for DC measurements at the experiment location during the wagon measurements..... 96

Figure 66: Photograph showing the experiment setup for AC measurements at the experiment location during the wagon measurements..... 96

Figure 67: Photograph showing the warning notice not to couple to or move the wagon set which was under testing during the wagon measurements. 98

Figure 68: Diagram showing electrical connections to the wagon nodes to take measurements on the wheel $\boldsymbol{D1}$ during wagon measurements..... 99

Figure 69: Diagram showing electrical connections to the wagon nodes to take measurements on the wheel $\boldsymbol{C1}$ during wagon measurements. 100

Figure 70: Diagram showing electrical connections to the wagon nodes to take measurements on the wheel $\boldsymbol{B1}$ during wagon measurements..... 102

Figure 71: Diagram showing electrical connections to the wagon nodes to take measurements on the wheel $\boldsymbol{A1}$ during wagon measurements. 103

Figure 72: Photograph showing the paper isolation between the wagon wheels and rail during the wagon measurements. 105

Figure 73: Photograph showing the filing of surfaces to which electrical contacts were made during the wagon measurements..... 106

Figure 74: Photograph showing the solder connections between conductors and the nodes of the wagon during the wagon measurements..... 108

Figure 75: Photograph showing the return conductive wire in close proximity to the wagon body to avoid creating loop areas and inductances during the wagon measurements. 110

Figure 76: Diagram to show the reduced complex wagon model..... 111

Figure 77: Diagram showing electrical connections to the wagon nodes to take measurements on the wheel $\boldsymbol{D1}$ during wagon measurements..... 112

Figure 78: Circuit diagram of wagon model whilst under measurements on the wheel $\boldsymbol{D1}$. 113

Figure 79: Graph showing wagon node voltages and supply current during measurements on the wheel $\boldsymbol{D1}$. 114

Figure 80: Diagram showing electrical connections to the wagon nodes to take measurements on the wheel $\boldsymbol{C1}$ during wagon measurements. 116

Figure 81: Circuit diagram of wagon model whilst under measurements on the wheel $\boldsymbol{C1}$. 117

Figure 82: Graph showing wagon node voltages and supply current during measurements on the wheel $\boldsymbol{C1}$. 118

Figure 83: Diagram showing electrical connections to the wagon nodes to take measurements on the wheel $\boldsymbol{B1}$ during wagon measurements. 120

Figure 84: Circuit diagram of wagon model whilst under measurements on the wheel $\boldsymbol{B1}$. 121

Figure 85: Graph showing wagon node voltages and supply current during measurements on the wheel $\boldsymbol{B1}$. 122

Figure 86: Diagram showing electrical connections to the wagon nodes to take measurements on the wheel $\boldsymbol{A1}$ during wagon measurements. 124

Figure 87: Circuit diagram of wagon model whilst under measurements on the wheel $\boldsymbol{A1}$. 125

Figure 88: Graph showing wagon node voltages and supply current during measurements on the wheel $\boldsymbol{A1}$. 126

Figure 89: Photograph showing the Transnet Freight Rail data acquisition system on one of their test coaches. 132

Figure 90: Photograph showing the front of the Transnet Freight Rail patch panel on one of their test coaches. 133

Figure 91: Photograph showing the back of the Transnet Freight Rail patch panel on one of their test coaches. 134

Figure 92: Photograph showing the front of the Transnet Freight Rail fiber optic receivers on one of their test coaches. 136

Figure 93: Photograph showing the connection from the optic receivers to the patch panel on one of Transnet Freight Rail's test coaches. 137

Figure 94: Photograph showing the fiber optic cables entering one of the Transnet Freight Rail test coaches. 138

Figure 95: Photograph showing the connection of the optic cables to the receivers on one of Transnet Freight Rail's test coaches. 139

Figure 96: Photograph showing the front of the fibre optic transmitter on one of Transnet Freight Rail's test coaches. 140

Figure 97: Photograph showing an overview of equipment found on one of Transnet Freight Rail's test coaches. 141

Figure 98: Photograph showing placement of the current clamp around the draw bar of one Transnet Freight Rail's coal wagon sets. 142

Figure 99: Photograph showing placement of the connection from the current clamp to the optic transmitter on one Transnet Freight Rail's coal wagon sets. 143

Figure 100: Photograph showing the remote logger used to measure wagon currents at significant distance from the Transnet Freight Rail test coach..... 144

Figure 101: Photograph showing the remote logger and current clamp used to measure wagon currents at significant distance from the Transnet Freight Rail test coach..... 145

LIST OF TABLES

Table 1: Table showing the approximated harmonic content of a class 19E locomotive. 32

Table 2: Table showing the electrical and physical parameters of the conductors typically found on the Coal Line, [26]–[28]. 34

Table 3: Table showing the distance between conductors typically found on the Coal Line, extended from Table 2. 38

Table 4: Table showing the cross-sectional area and radius of conductors typically found on the Coal Line, extended from Table 2 and [28]. 39

Table 5: Table showing the self-inductance and mutual-inductance of conductors typically found on the Coal Line as lumped parameters per meter. 40

Table 6: Table showing ratio of 1st coupler current in the 20th and 51st couplers during measurements performed by Ekman et al., extracted from [19]. 50

Table 7: Table showing ratio of 1st coupler current in the 100th and 150th couplers during measurements performed on the South African Coal Line 52

Table 8: Table showing ratio of 1st coupler current in the 20th and 51st couplers during measurements performed by Ekman et al. in comparison to simulated data, extracted from [19]. 66

Table 9: Table showing ratio of primary current in the 1st, 20th and 51st couplers during measurements performed by Ekman et al. in comparison to simulated data, extracted from [19]. 66

Table 10: Table showing ratio of 1st coupler current in the 100th and 150th couplers during measurements performed by Transnet Freight Rail in comparison to simulated data. 71

Table 11: Table showing ratio of primary current in the 1st, 100th and 150th couplers during measurements performed by Transnet Freight Rail in comparison to simulated data. 71

Table 12: Table showing wagon parameters obtained through wagon measurements against those used in the simulation. 73

Table 13: Table showing the experiment apparatus list and quantity requirements for the wagon measurements 93

Table 14: Table showing the supply voltages tested and measurements taken during wagon measurements on wheel $\boldsymbol{D1}$. 99

Table 15: Table showing the supply voltages tested and measurements taken during wagon measurements on wheel $\boldsymbol{C1}$. 101

Table 16: Table showing the supply voltages tested and measurements taken during wagon measurements on wheel $\boldsymbol{B1}$. 102

Table 17: Table showing the supply voltages tested and measurements taken during wagon measurements on wheel $\boldsymbol{A1}$. 104

Table 18: Table showing signals recorded whilst performing in-service wagon coupler current measurements. 145

LIST OF SYMBOLS

%	=	Percentage
Fe	=	Iron
Fe^{2+}	=	Ferrous
e^-	=	Electron
O_2	=	Oxygen
H_2O	=	Water
OH^-	=	Hydroxide
Ω	=	Ohms
φ	=	Phase angle between voltage and current °
H	=	Magnetic field intensity
r	=	Radius of a circle m
π	=	Pi
i	=	Current A
B	=	Magnetic flux density T
μ	=	Permeability
μ_0	=	Permeability of free space ($4\pi 10^{-7}\ henry/meter$)
μ_r	=	Relative permeability
Φ	=	Magnetic flux
A	=	Cross-sectional area m^2
λ	=	Flux linkage
N	=	Number of turns of a coil
l_{ii}	=	Self-inductance of the i^{th} loop H
d_{i0}	=	Distance between the i^{th} conductor and the 0^{th} conductor m
r_{w0}	=	Radius of the 0^{th} conductor m
r_{wi}	=	Radius of the i^{th} conductor m
l_{ij}	=	Mutual-inductance between the i^{th} and j^{th} loop H
d_{j0}	=	Distance between the j^{th} conductor and the 0^{th} conductor m
M_{ij}	=	Mutual-inductance between the i^{th} and j^{th} loop H
M	=	Induction Motor
P_{Loco}	=	Power drawn in a locomotive W
V_{Loco}	=	Voltage supplied to a locomotive V

I_{Loco}	=	Current drawn by a locomotive A
d	=	Distance m
i_{Feeder}	=	Current through the feeder conductor A
$i_{Catenary}$	=	Current through the catenary conductor A
$i_{Contact}$	=	Current through the contact conductor A
i_{Wagon}	=	Current through the wagon coupler A
$i_{Left\ rail}$	=	Current through the left rail conductor A
$i_{Right\ rail}$	=	Current through the right rail conductor A
i_{Return}	=	Current through the return conductor A
i_0	=	Current through the reference conductor A
$span$	=	Distance between mast poles m
$Z_{conductor}$	=	Lumped impedance of the bond Ω/m
Z_{bond}	=	Impedance of the rail-to-mast bond between the rail and the return conductor Ω/m
R	=	Resistance Ω
°	=	Degrees
pf	=	Power Factor

LIST OF ABBREVIATIONS

19E	Class 19 Electric Locomotive
AC	Alternating Current
Auto	Automatic
BE	Braking Effort
Bo-Bo	Four wheels on two axles
BPP	Brake Pipe Pressure
C	Capacitance
CCD	Car Control Device
Co-Co	Six wheels on two axles
Conv.	Converter
DC	Direct Current
DPF	Displacement Power Factor
ECP	Electronically Controlled Pneumatic
EMI	Electromagnetic Interference
et al.	et alia: and others
FFT	Fast Fourier Transform
GNU	GNU's Not Unix!
GPS	Global Positioning System
IGBT	Insulated Gate Bipolar Transistors
Inv.	Inverter
L	Inductance
LTSpice	Linear Technology Simulation Program with Integrated Circuit Emphasis
MatLab	MATrix LABoratory
MTL	Multiple Transmission Line
Netlist	Textual description of a circuit
OHTE	Over Head Track Equipment
PCC1	Power Conversion Cubicle 1
PCC2	Power Conversion Cubicle 2
PWM	Pulse Width Modulation
RBCT	Richards Bay Coal Terminal
RC	Resistive, Capacitive

RLC	Resistive, Inductive, Capacitive
RMS	Root Mean Square
SPICE	Simulation Program with Integrated Circuit Emphasis
TE	Tractive Effort
TFR	Transnet Freight Rail
THD	Total Harmonic Distortion
TPF	Total Power Factor

CHAPTER 1
INTRODUCTION

The railway industry has developed from the primitive beginnings of steam powered engines to the advanced electronically controlled induction traction motors found in today's modern locomotives. However, these great strides in technology have not come without cost.

Electromagnetic Interference (EMI) in railway infrastructure has been one of the hurdles which we have faced due to our advances and one which we still face today. This interference particularly plagues the railway signaling system and various methods to reduce electromagnetic interference have been employed to minimize the effects.

This being said, Electromagnetic Interference is also present in other railways systems which have not been granted the same attention in reducing the effects. This is due to the level of reliance on different systems. Sub-systems related to operational safety are of more concern and are justly addressed as a priority.

As new and advanced technologies are introduced into the railway environment, more Electromagnetic Interferences in sub-systems are identified. One such effect of Electromagnetic Interference was the failure of on-board computers on Transnet Freight Rail's Coal wagons.

Transnet Freight Rail is the largest freight logistics company in South Africa, and moves their client's commodities by rail. Transnet Freight Rail is no exception to the difficulties experienced with the introduction of advancing technologies.

In fact, Transnet Freight Rail Engineers observed numerous failures in some sub-systems on-board their trains with the introduction of Electronically Controlled Pneumatic Brakes on their Coal Corridor. This led to an investigation into the causes of the device failures and the discovery of unanticipated high return current levels found in the couplers of their Coal train wagons. The current originates from the sub-stations feeding the railway, travelling along the railway supply infrastructure to the electric locomotives and is intended to return to the sub-station through return conductors and the rails.

Although these wagon currents were observed by Transnet Freight Rail Engineers as well as technical staff from another railway company in Sweden, the understanding of the mechanisms affecting the levels of the current were not understood. Both countries identified that there is return current running through the couplers of the train wagons under Alternating Current infrastructure. This prompted further research into the mechanisms affecting the current level in the couplers of a train.

The research presented in this dissertation is focused on the development of an applicable circuit simulation model to represent the return current levels observed in the couplers of trains which operate in AC territory.

The research was focused on the current levels found in Alternating Current infrastructure, as this was the infrastructure under which both railway companies witnessed their findings. This is not to say that there are low levels of current in the couplers of a train under Direct Current infrastructure. Electrical return current levels in the couplers of a train under Direct Current infrastructure could be investigated as an extension to the research presented herein.

The outcome of the research is an electrical circuit simulation model that can be used to predict the return current levels in the couplers of a train by adjusting various parameters to the conditions of the train. Some of these parameters include the infrastructure geometrical configuration and the sizes of conductors which affects the resistivity of the conductor as well as the self-inductance and mutual-inductance of and between conductors.

Additionally, the sub-station feeding arrangement is also taken into consideration. Whether the feeding arrangement is a single feed, or dual feeding sub-stations, and the sub-station voltages and frequencies will have effect on the expected current levels found in the couplers of a train.

Further, one of the dominant configurable set of parameters is that of the wagon model. Different railway operators will use different wagon designs and suppliers which will affect the wagon model parameters.

Before utilizing the system simulation model, all these configurable parameters must be determined experimentally or theoretically. Thereafter, tuning of the model to match measured coupler currents must occur.

Once the model is correctly representing measured results, the model can be used to predict the current levels in the couplers of the train. Various abnormal conditions can also be investigated by adjusting the system model parameters accordingly.

As an extension of this concept, an investigation and discussion chapter is included in this dissertation which investigates the effects of such conditions at a high level.

The conclusion of the research is the system model to predict the return current levels through the couplers of a train under Alternating Current infrastructure.

1.1 Overview of Transnet Freight Rail and their Observations

Transnet Freight Rail (TFR) is a large freight logistics company in South Africa. The company operates a heavy haul coal corridor between the coal mines north of Ermelo and the Richards Bay Coal Terminal (RBCT).

The operator runs coal trains between Ermelo and Richards Bay typically using a six locomotive lead consist[1] and two hundred trailing wagons. The corridor spans a distance of approximately 500 km.

In order to increase capacity, operational efficiency and safety as well as keeping up-to-date with technological advancements, Transnet Freight Rail began implementing a new electronically controlled braking system on their Coal Line wagons. This new braking system is called Electronically Controlled Pneumatic (ECP) brakes.

Conventionally, wagon brakes are controlled by regulating the Brake Pipe Pressure (BPP). This brake pipe runs the length of the train. Each pneumatic brake cylinder on each wagon is coupled to this pneumatic pipe and responds to the Brake Pipe Pressure by applying and releasing wagon brakes. The Brake Pipe Pressure is controlled by the locomotive consist[1], where the driver can apply and release brakes using a handle.

The implementation of ECP brakes means that the Brake Pipe Pressure is maintained at a high pressure and acts as an air supply rather than a control mechanism. Each wagon is equipped with a reservoir, and an on-board computer named the Car Control Device (CCD). Additionally, electrical conductors run the length of the train to supply power and control instructions to each on-board computer.

1.2 Problem Statement

Transnet Freight Rail has, during and subsequent to the roll out of the new ECP technology, experienced failures of onboard equipment such as Car Control Devices found on train wagons. These CCDs control the wagon brakes subsequent to receiving commands from the lead locomotive of the train. Because these failures are associated with the train braking system, reliability of this train sub-system is of utmost importance.

These failures led Transnet to conduct testing in order to identify the root cause of the failures [1].

[1] **Consist** – A locomotive consist refers to a group of locomotives coupled together to provide higher tractive and braking effort than a single locomotive.

1.3 Initial Investigation Findings

Through the preliminary investigation carried out by Transnet staff, it was established that a significant amount of return current is travelling through the couplers of the train wagons.

The return path of the current to the sub-station has always been thought to be the rails and the overhead return conductor, which is true for the majority of return current found between the train and the sub-station. However the current distribution through the train, the rail and the return conductor for the length of the train has not been of great concern in the past. This was because the current distribution seemed to have little to no effect on the operations of the train. With the use of a current transducer, high current levels were found to be present in the couplings of the train.

It was found that the CCD failures typically occurred at moments when the current through the coupler of the train were high. This was as a result of the high coupler currents causing Electromagnetic Interference on the ECP power and control conductors, and hence CCD failures [1].

During the investigation, it was also observed that the magnitude of the current, measured with respect to the distance travelled along the railway formed a fairly consistent pattern.

Deviations in the patterns were investigated and it was found that the change in pattern was caused by a change in the surrounding infrastructure. Specifically, missing and defective rail-to-mast bonds were accurately identified by monitoring the coupler current patterns. Further, when a rail-to-mast bond was missing or defective, the coupler current magnitude would be higher than the average magnitude compared to when rail-to-mast bonds were present and operational.

One immediately implementable solution to the failures of the CCDs, was the investigation and correction of any missing or defective rail-to-mast bonds on the coal corridor.

Although the problem of failing CCDs on the coal corridor could be solved, the mechanisms affecting the coupler current were not fully understood. In order to better understand the mechanisms affecting the coupler current, the research presented in this dissertation was initiated. The outcome of the research is to better understand the mechanisms affecting the coupler current and investigate the possibility of future development of an in-service monitoring system to identify where rail-to-mast bonds are missing or defective.

CHAPTER 2
BACKGROUND & LITERATURE SURVEY

Electromagnetic interference (EMI) in railway infrastructure has been one of the challenges which we have experienced due to our technological advances and one which we still face today. Various methods to reduce electromagnetic interference have been employed to minimize EMI effects.

The question of alternative means of traction is raised given the difficulties introduced by the use of the electric locomotive. The use of diesel locomotives would alleviate these EMI issues that electric locomotives introduce. Not only would the problem of EMI be solved, but the phenomena of corrosion in metallic and reinforced concrete structures in proximity to the railway would no longer be of concern. Further, the capital outlay would be considerably lower for diesel tractive effort as the catenary infrastructure would no longer be required.

However, the efficiency of electric locomotives cannot be ignored [2]. Heavy haul railways which are consuming large amounts of power often prefer electric traction due to the substantially lower running costs.

With the use of electric locomotives, supporting catenary supply infrastructure is required. This infrastructure is inclusive of current conductors to the electric locomotives and utilizes the rails and a return conductor as a return current path back to the sub-station.

It has recently been found that the current distribution, in the immediate vicinity of the train, across the return paths to the sub-station is not as previously predicted or assumed. Substantial current has been found to flow through wagons of the train. The discussion of these current paths will be presented section 2.6.

In the past, this has not been a topic of concern as there have only been a few negative results noticed. However, the value of the information that could potentially be extracted from monitoring these current distributions has also not been explored. Thus developing a model to describe the current distributions and the influences thereof can prove beneficial, and is the reasoning behind this research.

2.1 Traction Supply Infrastructure

Apart from a minority of exceptions such as three-phase electrification, two types of supply infrastructure are used in electric railway systems. These are single phase Alternating Current (AC) supply and Direct Current (DC) supply [3], [4].

The original advantage of DC infrastructure was that the vehicle mounted equipment was minimal. DC traction motors could be powered directly from the supply voltage in series for slow speeds and parallel for high speeds [4].

The voltage levels for the AC infrastructure are typically 25 kV or 15 kV with the less common 50 kV also being used in some areas. The operating frequency is mainly 50 Hz or 60 Hz, which is dependent on the national grid supply frequency [3], [4]. Some of the older infrastructure operates on 16⅔ Hz and 25 Hz in order to enable the operation of older locomotives which use DC traction motors and older on-board converter technologies [3], [4].

Higher voltage infrastructure proves more economic for heavy-haul railways as a lower current is drawn for the same amount of power consumed. This lower current results in lower i^2R losses in the supply system.

DC voltage levels range from 500 V mostly found on tramway systems to the most common 3 kV [3].

The South African freight rail network consists mainly of 3 kV DC infrastructure, constituting to more than 13 000 km of track. The DC sub-stations can be found at an approximate spacing of 10 km as well as single-phase 25 kV AC at 50 Hz. Less common is the single-phase 50 kV AC at 50 Hz supply infrastructure which services the rail line between Sishen and Saldanha [2].

2.2 Electromagnetic Interference (EMI) in Traction Systems

Neglecting electromagnetic interference in railways systems would prove to be dire to the point of halting operations due to the importance of the signaling systems and on-board electronics. Although the research presented in this dissertation does not include the EMI manifestations that have been observed as a result of wagon currents, it is important to identify and understand the sources which can introduce a EMI in neighboring systems as this highlights the need to understand and be able to minimize the causes of EMI such as high wagon currents.

Electromagnetic interference can be defined as the appearance of any unwanted voltage or current or electromagnetic field which is generated by one system in another. The system generating the disturbance is referred to as the source, and the system affected, the receiver [5].

The railway environment is generally classified as electromagnetic interference unfriendly due to its amalgamation of power, information and communications [5]–[7].

R. Hill (1997), in his paper *Electromagnetic Compatibility – Disturbance Sources and Equipment Susceptibility* [5] presents the idea that EMI in railway traction systems can be categorized into three specific groups, these being:

(i) Internal Interference:
- This is interference in railway systems caused by railway systems. An example of such would include interference in the safety signaling system caused by the traction power supply system.

(ii) Outgoing Interference:
- This is interference in an external system which is caused by railway systems. Stray or leakage currents (discussed further in section 2.4) causing corrosion or interference in electrical equipment is a prime example of outgoing interference.

(iii) Incoming Interference:
- This is interference received by railway systems caused by external systems. The transmission of utility power in proximity to the railway can cause interference in the railway signaling systems.

In addition to the malfunctioning of railway systems, EMI can also pose a risk to personnel safety. High step and touch potentials as a result of EMI are a risk to personnel [5].

Modern locomotives which make use of switching electronics can cause over-voltages and power quality degradation [5], [8]–[10]. These can affect electrical equipment and cause premature failure due to insulation breakdown [8].

Electromagnetic Interference is a result of the coupling between the EMI source and the receiver. The principle coupling mechanisms are [7]:

(i) Conductive (galvanic) Coupling:
- Galvanic coupling is found when the source and receiver share a conductor. Signaling circuits are often plagued with EMI as they generally share the running rails as a conductor with the traction supply system.

(ii) Inductive Coupling:
- Changes in the magnetic flux caused by the source can induce $L.di/dt$ voltages in the circuitry of the EMI receiver. Two parallel conductors are a prime example of equipment susceptible to inductive coupling.

(iii) Capacitive Coupling:
- Capacitive coupling can either be static where a high voltage conductor and a nearby metallic object form a capacitive potential divider, or dynamic where the changes in the electric field result in $C.dV/dt$ currents in the circuitry of the EMI receiver.

(iv) Radiative Coupling:
- EMI can result from high frequency effects such as arcing and/or fast current of voltage switching.

In order to address and minimize electromagnetic interference in the railway environment, the possible sources of internal and outgoing EMI should be identified. Such sources could include, however are not limited to [5]:

(i) Rectifier Sub-stations (discussed further in section 2.3):
- Switching transients originating in the pulse rectifiers in DC traction sub-stations introduce EMI into the traction supply. Further, an unbalance in the rectifier circuit, different magnitude in the incoming power supply phases or abnormal operating conditions can also lead to EMI being introduced into the system.

(ii) Transformer Sub-stations:
- The three-phase transmission lines feeding the AC traction sub-stations could be carriers or EMI which will introduced into the traction supply system through the AC transformers. This EMI found on the three-phase transmission line can be a result of corona discharge or nearby conductors, or partial discharge or micro-arcs at metallic contacts or across insulator surfaces.

(iii) Transmission of Traction Power:
- Earth leakage or stray currents can be considered receivers of EMI, but their existence can also be the source or EMI. The insulators found in the traction supply infrastructure are also susceptible to partial discharges across their surfaces which could result in EMI in neighboring systems.

(iv) Locomotives:
- Power electronic devices utilizing switching or high currents to convert power to traction motors can be the source of EMI. Further, EMI from arcing caused by pantograph jump, main circuit breaker operations, or the commutators of DC traction motors is also possible.

(v) Signaling or Track Side Equipment:
- Stereotypically, signaling and track side equipment are EMI receivers, however in some situations they can act as the source of EMI.

Zhezhelenko, et al. (2009) [8] wrote a paper which focused on the possible solutions of resonant modes found in single phase AC railways. The need to dampen these resonant modes arose from the risk of electrical equipment failure due to high levels of harmonic distortion and voltage imbalance [8].

Three solutions to dampen resonant modes are brought forward by Zhezhelenko, et al. [8]. The first solution is the installation of a first-order RC filter on either the locomotive or the sub-station. The surge impedance termination of a second-order RLC filter is provided as a second solution. Zhezhelenko, et al. proposed that this filter be installed at the open end of the traction section. The second-order filter has a lower filter resistor current and hence the electrical rating of filter components is reduced as well as the losses. The third solution suggested by Zhezhelenko, et al. is the combination of an active power filter and a passive RLC filter installed at the end of the traction feeder.

The resonant modes occur at frequencies defined by the length of the traction network, regardless of the locomotive position in this network. Zhezhelenko, et al. suggest that these frequencies decrease with increasing feeder lengths but lie typically in the range of 2 – 30 kHz [8].

S. Baranowski, et al. (2012) [6] provided a model and simulation of the transient noise created by a sub-station. Their measurements were performed with varying currents and the measurements were analyzed in the time and frequency domains [6]. One of their findings was that the nominal current directly affects the transient voltage levels at frequencies below 40 kHz but seemed to have no direct relationship at frequencies above 40 kHz [6].

In the paper by K. Yuuki, et al. (2010) [11] EMI is classified into two groups or frequencies as follows:

(i) Frequencies less than 10 kHz:
- These harmonics on the catenary line are usually caused by the high frequency switching of the power conversion units (inverters and converters) on-board the locomotives.

(ii) Frequencies less than a few MHz:
- These frequencies are typically a result of common mode current. These currents are enabled by stray capacitances.

Yuuki, et al. suggest that for EMI with frequencies around 100 kHz, common mode current is usually the dominant cause [11].

Although Electromagnetic Interference causes and mechanisms have been discussed, it is important to remember that EMI in railway systems is not the focus of this research but rather a result of the coupler current which is present.

2.3 Supply System Configuration

The typical railway supply infrastructure consists of sub-stations, connected to the national grid, which supply power to an overhead line or catenary system. The running rails and return conductor act as the return path to the sub-station [3], [4], [7].

AC sections are separated by “neutral sections” or “dead sections” to avoid circulating AC currents, whilst DC sections are continuous with sub-stations feeding the catenary in parallel [3]. This means that should a sub-station in a DC section fail, it can be isolated from the catenary, and the next sub-station will supply power to the section. However, if an AC sub-station fails, the section which that particular sub-station was supplying power to will remain unpowered until the problem is rectified. Figure 1 and Figure 3 describe the simplified equivalent models for the AC and DC traction supply systems respectively. In order to address this reliability concern in AC systems, dual feeding arrangements also

exist. A simplified representation of the dual feed AC traction system is provided in Figure 2.

Alternative supply and return conductors such as a third rail supply are used; however these are not as common as the above mentioned configuration. This being said, it is common for a return conductor which is connected to the return rails to be connected at regular intervals [3], [4], [12].

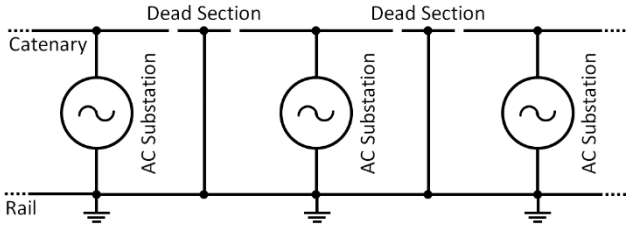


Figure 1: Diagram illustrating a simplified equivalent model of the AC traction system.

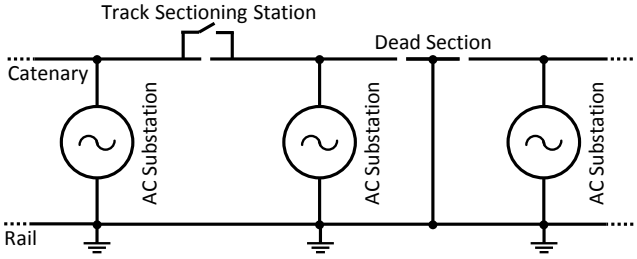


Figure 2: Diagram illustrating a simplified equivalent model of the dual feed AC traction system.

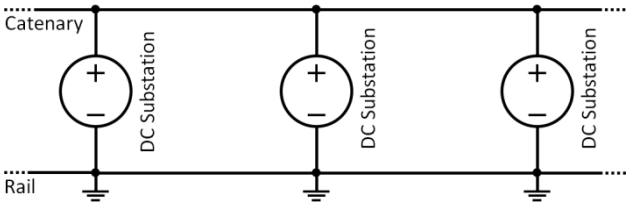


Figure 3: Diagram illustrating a simplified equivalent model of the DC traction system.

Expanding the model for the DC traction supply system, it must be noted that the DC traction power is rectified from the three-phase AC utility supply. This rectification is often performed through the use of six, twelve or twenty four pulse circuits [4]. As a result of this means of rectification, regenerated power from the locomotives in braking cannot be transferred back onto the national grid or utility supply [4]. This can be seen graphically in Figure 4.

During rectification of the AC power to DC power, harmonics are introduced on the catenary supply due to these pulse circuits. In an effort to reduce these harmonics, series resonant filters are installed at the output of the rectifiers in the South African railways. The resonant frequencies of these filters is typically 600 Hz, 1200 Hz and in some cases 2400 Hz [2]. Figure 5 show the equivalent circuit model of the typical harmonic filters installed at the outputs of the DC sub-stations in South Africa.

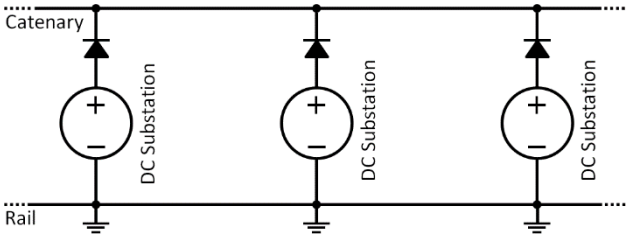


Figure 4: Diagram illustrating a simplified equivalent model of the one way DC traction supply system.

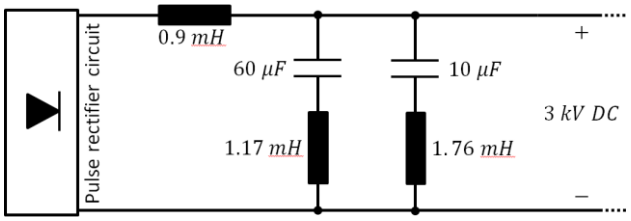


Figure 5: Diagram illustrating the equivalent circuit model of the typical harmonic filter at DC sub-stations in South Africa adapted from [2]**.**

The discussions in this section have provided a background overview of typical supply configuration. The configuration utilized by Transnet Freight Rail and in this research is discussed further in section 4.2.

2.4 Stray Return Currents

Stray return currents can cause damage to metallic objects in proximity to the railway as well as being environmentally undesirable. Stray currents can cause erosion of metallic objects such as water pipes through the mechanism of electrolysis [3], [4], [7], [9], [12]–[17]. Current will flow through the path of least impedance, whether it be the intended path or otherwise [14]. It is for this reason that stray currents must be mitigated as far as possible.

Stray return currents resulting from electric railway installations have been widely documented [3], [4], [7], [9], [12]–[17]. Despite this, it proves difficult to accurately model stray return currents as an equivalent electrical circuit due to the complexity of the phenomena, and that the model would be restricted to only very simple geometry [14], [17].

2.4.1 Stray Currents in DC Infrastructure

Before absorbing the theory of stray DC currents it should be noted that stray DC currents are discussed in this dissertation as a background and reference. The research presented herein focusses on AC infrastructure and hence a thorough understanding of stray DC currents is not of crucial importance. This by no means indicates that coupler current in DC territory is not of concern, but rather that it falls outside the scope of research of this dissertation. The high likelihood of stray DC currents in railway infrastructure, as discussed below, encourages further in-depth research into return current paths in DC territory.

This being said, stray current is closely related to the DC railway infrastructure. The DC railway typically uses the running rails as a return path for the current due to economic reasons. Because of this there is a resultant voltage drop on the running rails which alludes to stray current leaking into the earth and imbedded structures in the earth [13]–[15]. These stray currents play a major role in the corrosion of rails and buried metallic structures in proximity to the railway. Additional to causing undesirable corrosion of metallic objects through the mechanism of electrolysis, these stray currents can also result in interference with signaling systems [13].

In order to form a brief understanding of the mechanism of corrosion, one must momentarily delve into the field of chemistry and the methods of conduction for different materials.

In metallic conductors, the current flow is electronic, meaning that charge is transferred through the flow of electrons. However, current flow in electrolytes, such as earth and concrete, is ionic. This means that for leakage current in DC systems to occur, an electron to ion transfer must occur as the current leaves the rails and enters the earth [15].

It must be stated that this electron to ion transfer occurs during direct current leakage such as that typically found in DC traction supply systems, and not during the induced effects found in AC traction supply systems.

When current leaves the rail to the earth, oxidation or an electron producing reaction occurs [15] and can be seen in equation (1) below. Should this reaction be frequent, it will become visible as corrosion.

$$Fe \rightarrow Fe^{2+} + 2e^{-} \tag{1}$$

In contrast, when the leakage current returns to the rail, an electron-consuming reaction occurs. Should this reaction take place in an oxygenated environment [15], which is typically the case, it can be described by equation (2).

$$O_2 + 2H_2O + 4e^- \rightarrow 4OH^- \quad (2)$$

An iron-reduction reaction is not thermodynamically preferred and so iron does not generally plate onto the rails when current returns to the rails.

From these chemical equations it is clear that corrosion will occur at instances where current leaves a metallic object to an electrolyte, however not when current enters a metallic object from an electrolyte.

In the paper compiled by M. Alamuti, et al. (2011) [13] four methods of decreasing the leakage or stray current to the earth is suggested. The first is to decrease the rail resistance and hence the voltage drop across the running rails. The second is by increasing the rail-to-earth resistance and minimizing the opportunity for current to leak onto the earth. Thirdly, Alamuti, et al. suggest designing systems with a higher operating DC voltage and thus a lower return current for the same amount of power. Lastly, it is suggested that the traction sub-stations be located closer to one another, however this greatly increases the construction costs of the railway [13]. These four methods or reducing leakage current in DC traction supply systems is echoed and supported by I. Cotton, et al. (2005) [15].

Closely related to the rail-to-earth resistivity, various earthing schemes of the traction supply system exist. These include solid earthed, diode earthed, floating and thyristor earthed schemes [13], [15]. The various earthing schemes are graphically described in Figure 6.

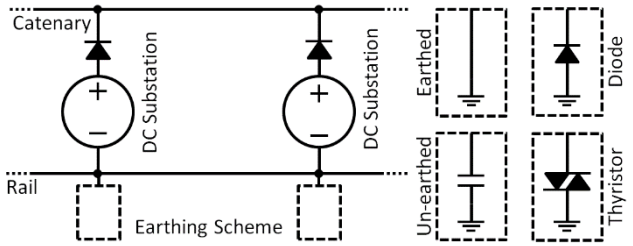


Figure 6: Diagram illustrating a simple equivalent model of the DC traction system

The first earthing scheme detailed is the unearthed scheme. In this scheme, the rails have no intentional connection to the earth thus creating a floating rail. This means that a high rail-to-earth impedance exists which limits stray current [13], [15].

An opposite of the unearthed scheme, is the directly earthed scheme which reduces the rail voltage, thus assisting in meeting safety requirements. Its main objective is to guarantee circuit continuity and also to ensure that personnel in the vicinity of the railway cannot be exposed to dangerously high voltages [13]. It is found that this scheme has many stray current problems [13].

Alamuti, et al. performed simulations which indicated that there is a strong correlation between the stray currents and the rail potentials in both earthed and unearthed schemes.

This relationship was found to be linear [13]. This notion is also detailed by I. Cotton, et al. (2005) [15] in their paper *Stray Current Control in DC Mass Transit Systems* and R. Hill (1997) [7] in his paper *Electric Railway Traction – Electromagnetic Interference in Traction Systems*.

Consider an example of a locomotive drawing $1000\ A$, located $1000\ m$ from the DC sub-station and the rails having a resistance of $20\ m\Omega/\text{km}$. Through the use of Ohm's law it can be deduced that there will be a voltage drop of $20\ V/\text{km}$ of track. Depending on whether the earthed or unearthed scheme is employed, this voltage can appear in one of two ways.

In the unearthed scheme, where the rails and the negative DC bus are "floating", this voltage drop of $20\ V/\text{km}$ will be seen as a rail voltage of $10\ V$ to remote earth at the locomotive and $-10\ V$ to remote earth at the DC sub-station.

However, in the earthed scheme, where the rails and the negative DC bus are connected to ground, this voltage drop of $20\ V/\text{km}$ will be seen as a rail voltage of $20\ V$ to remote earth at the locomotive and $0\ V$ to remote earth at the DC sub-station.

The polarity of the potential between the rail and remote earth will determine direction in which the leakage current will flow.

If it is assumed that the voltage drop per meter is linear as per the papers of M. Alamuti, et al. (2011) and I. Cotton, et al. (2005), it will be noticed that voltage to remote earth midway between the sub-station and the locomotive will be $0\ V$ for the unearthed scheme. This means that from the locomotive to midway, there will be a positive potential between rail and remote earth resulting in leakage current flowing from the rails and causing corrosion. From the midway to the sub-station, the a negative rail to remote earth potential will exist causing leakage current to flow back from earth into the rails. It should be noted that based on the chemical reactions detailed by equations (1) and (2), no corrosion of the rails will occur from midway to the sub-station.

However, in the earthed scheme, the rail remote earth potential is positive for the length of the track. This results in leakage current from the rails to the earth for the entire length between the locomotive and the sub-station, causing corrosion of the rails over the entire distance [15].

The third earthing scheme identified by Alamuti, et al. and Cotton, et al. is the diode-earthed scheme. Alamuti, et al. state that recent practical and theoretical studies have shown that in this scheme, high touch potentials as well as stray currents may exist simultaneously [13]. The negative busbar at the traction sub-station is connected to the earth through diodes in this scheme. The diodes act to limit rail voltage by providing a short circuit path to earth whenever the rail voltage exceeds the diodes threshold [13].

The use of stray current collection mats located beneath the track at regular intervals as well as beneath the sub-station is employed [13]. The diode-earthed scheme allows for current to flow back from the earth or current collector mats and prevents traction current flowing into the earth of current collection mats [13].

Finally, the thyristor-earthed scheme is highlighted by Alamuti, et al. In this fourth scheme a floating negative automatic earthing switch is created. This earthing switch consists of DC voltage and current monitoring circuits as well as two thyristors which provide bidirectional controlled current flow [13]. These are all located at the traction sub-station. The scheme acts to limit the rail voltage by activating the corresponding thyristor. The activation of the thyristors is dependent on the polarity of the rail potential. The activated thyristor continues to allow current flow until the current reduces to zero or the polarity reverses across the thyristor [13].

The results of the simulations performed by Alamuti, et al. indicate that the corrosion hazard in unearthed schemes are approximately eight times that of solidly earthed schemes [13].

After comparing the results of their simulations, Alamuti, et al. conclude that the diode-earthed scheme results in the highest level of rail-to-earth voltage followed by the unearthed scheme and thyristor-earthed scheme. Unsurprisingly, this leaves the earthed scheme with the lowest rail-to-earth voltage [13].

Alamuti, et al. state that the most hazardous stray current resulting in corrosion of metallic objects initiates from a negative rail voltage [13] which is supported by equations (1) and (2). From their simulations, the unearthed scheme provides the best protection against stray currents and the associated effects. This is followed by thyristor-earthed, diode-earthed and solidly-earthed schemes respectively [13].

From their paper, it can be seen that a trade-off exists between the stray current levels causing corrosion and the rail voltage levels required to meet safety regulations [13]. This is verified by Hill in his paper detailing traction power supplies [4] and L. Ardizzon, et al. (2003) in their paper about electric traction and electrolytic corrosion [14].

Apart from the various earthing schemes to balance the trade-off between rail voltage and leakage currents, the solution of stray or leakage current collection systems is brought forward by I. Cotton, et al. (2005) [15], F. Fichera, et al. (2013) [16] and N. Dekker (1999) [17]. The concept behind the stray current collection systems is to “catch” any leakage current prior to causing corrosive damage to nearby metallic objects. This current catching infrastructure often comprises of the reinforcements in the concrete track bed. The reinforcement is bonded along its length to provide a continuous path for current to the sub-station. In order to avoid corrosion of the reinforcement, the reinforcement is deliberately bonded to the DC negative bus at the sub-station.

2.4.2 Stray Currents in AC Infrastructure

Although more prevalent in DC infrastructure, stray currents also occur in AC infrastructure. A. Mariscotti, et al. (2005) as well as L. Ardizzon, et al. (2003) suggest that the important parameters which influence the amount of stray current are rail-to-earth conductance, earthed return conductors-to-earth conductance and earth resistivity [9], [14].

In their paper, Mariscotti, et al. suggest that the return current of traction systems can be characterized by a set of transfer functions which depend on frequency, geometrical arrangement of conductors, the earthing arrangement, distance between the locomotive and the measuring point, feeding arrangement, leakage to earth of the rails and earth conductivity [9], [10]. Further, in their analysis, the traction line is modelled as a Multiple Transmission Line (MTL) which achieves an accuracy level of within 20% in the frequency range of 50 Hz - 50 kHz [10].

Preliminary investigations by Mariscotti, et al. indicate that the dielectric constant of soil can vary in capacitance terms, between overhead conductors and rails, by less than 10%. Larger variations are expected to be seen in rail-to-earth and rail-to-rail capacitance terms [9].

Conclusions made by Mariscotti, et al. suggest that the amount of stray current for the low frequency range is proportional to the conductance-to-earth of the return conductor [9].

In AC infrastructure, two alternative configurations to the simple configuration are employed to mitigate stray return currents. These are the use of Booster Transformers and Auto Transformers. The notion behind both these setups is that the transformer is rated at full traction current and acts as a 1:1 current transformer thus forcing the same magnitude of current in the return conductor as is flowing in the supply conductor [3], [4], [7], [12], [18]. This means that stray currents are "forced" to approximately zero. Grounding of the return conductor to the rails at regular intervals is often utilized in the booster transformer scheme. Figure 7 and Figure 8 show the equivalent circuit diagrams and current flow of the booster transformer and auto transformer respectively.

The principle of operation between the booster and auto transformer schemes are contrasting. The booster transformer scheme acts to balance currents whilst the auto transformer scheme acts to balance voltages [4].

The booster and auto transformers are installed along the rail line. Booster Transformers are installed typically every 3 km and Auto Transformers every 8 to 10 km. Transnet Freight Rail installed Booster transformers on their coal corridor.

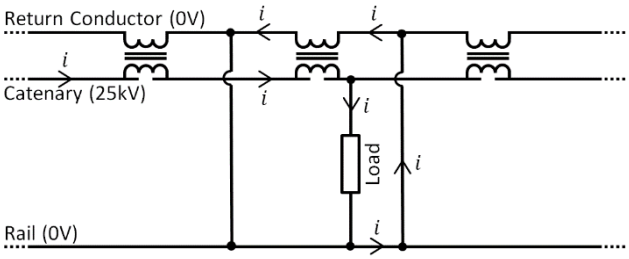


Figure 7: Diagram illustrating a simple equivalent model of a 25 kV AC traction system utilizing the booster transformer scheme.

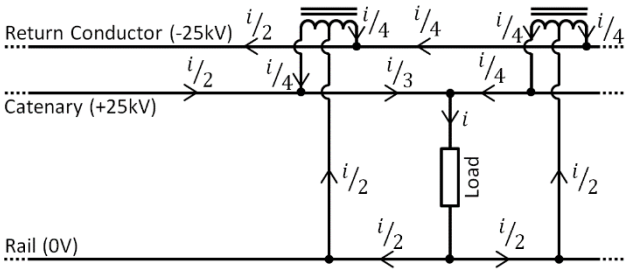


Figure 8: Diagram illustrating a simple equivalent model of a 2 x 25 kV AC traction system utilizing the auto transformer scheme.

2.5 Electrical Continuity of Conductors

The papers by P. Szacsvay (2011) [3], suggest that the most vulnerable part of the traction return circuit is not the rails but in fact the the bonding cables and connections [3]. These bonds are seen in Figure 7 and Figure 8 as the connection between the rail and the return conductor.

The rails are robust and sturdy when compared to the electrical bonds connecting sections of rails or connecting the rail to the return conductor. Not only are these cables more likely to become damaged, their connections to the rail can also become loose or may not be installed correctly.

Should one of these bonds be missing or faulty, the return current flows the path of least impedance to the sub-station, which could consist of the closest bond or in the form of stray currents.

Szacsvay also recommends that in DC traction systems with the rail as a return conductor, that both rails be used as the return path [3]. This will reduce the impedance of the return conductor and so minimize the voltage drop across the return conductor. Additionally, the second rail acts as a redundant return conductor in the event that the electrical connection in the first rail is broken.

2.6 Return Current Distribution

Little research into the path of the return current through the train has been conducted, as it has mostly been considered as negligible or having little effect. However, the paper by J. Ekman, et al. (2009) [19] suggests that there is a significant percentage of current in the couplings of the train. The conductive characteristics of wagons and couplings allow for the train to act as an alternative path for return current. This is due to the fact that the current will divide among the available paths based on their impedance. This is illustrated in Figure 9.

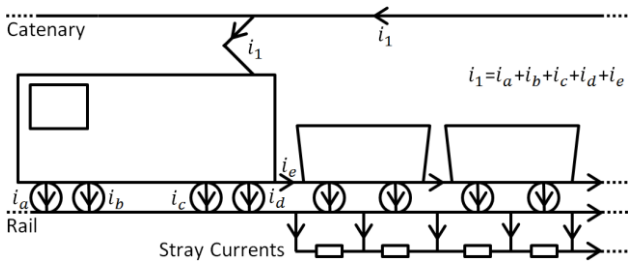


Figure 9: Diagram illustrating the possible return current paths immediately subsequent to the locomotive.

Ekman et al. indicate that the current corrosion noticed in the bearings of wagons was as a direct result of this current found in the couplings [19].

Ekman et al. put forward the premise that, at locations where these current appear to be particularly high in the couplings, it could indicate failing or defective electrical equipment due to an observed difference in current magnitude resulting from the change in impedance of the return path such as a broken or missing bond. The missing or broken bond would mean that there is no electrical connection from the rail to the mast, thus increasing the impedance to the return conductor. The current will thus not travel through a defective bond, but remain in the rails and couplers.

Another notion that Ekman et al. conveys is that environmental variances could also affect the percentage of return current seen through the couplings of a train. Ekman et al. makes particular reference to changes in the water table [19].

Modern railway rolling stock, particularly some found in the South African environment have electronic systems on-board. For example, some wagons have Electronically Controlled Pneumatic braking systems. To achieve this, a signal cable must run the length of the train which provides both power to the electronics as well as transmits braking commands. Because this cable runs in close proximity to the couplers, current flowing through the couplers can have, and have had, a noticeable effect on the correct operation of these devices as a result of interference caused by this coupler current [1].

Ekman et al. proposes a solution to minimize the coupling currents by making the couplings of the electric locomotive electrically isolated from the locomotive itself [19].

This idea removes the conductive path through the coupling and forces return current directly into the rail. One must question whether this is a desirable situation as this offers as quick fix to the damages caused by the current through the couplings but does not address the root cause of the coupling currents.

Interestingly, through Ekman et al.'s experimental research, it was found that a high amount of current returns to the rails through the bearings and wheels of wagons towards end of the train as compared to the wagons closer to the locomotives [19]. This suggests that mutual inductance between the catenary line and the train as well as electrical impedances account for the current distribution through the train [19].

This notion that Ekman et al. has brought forward is discussed further in CHAPTER 8. CHAPTER 8 follows the system model development discussed in CHAPTER 4 and the system model verification discussed in CHAPTER 7. CHAPTER 8 investigates various conditions which could affect the coupler current found in a train such as the increase or decrease of coupling and impedance paths.

CHAPTER 3
THEORETICAL DISCUSSION

In order to analyze the mechanism of electromagnetic coupling suspected to effect the current distribution along a train, an approximate circuit model of the system must be developed. This model will aid in theorizing the causes of the electromagnetic incompatibility, predict the effects of the presence of this coupling, and also analyze the possible benefits of the presence of this coupling. Thus a model of the system is developed. However, before a circuit model is developed, the theory relating to the mechanisms contributing to the model is investigated in this chapter.

3.1 The Magnetic Circuit

The supply infrastructure is, practically speaking, a collection of conductors carrying current. Thus, it is useful to investigate the magnetic field around a single conductor and then extend this to multiple conductors.

Figure 10 shows the magnetic field (H) that is produced when a conductor carries a current (i) [21]–[23].

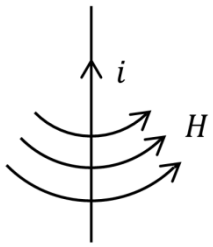


Figure 10: Diagram to show magnetic field created around a conductor carrying current, adapted from [21].

From Ampere's circuit law [21]–[23], the line integral of the magnetic field intensity around a closed path containing a single current carrying conductor is equal to the current in the conductor as seen in equation (3).

$$\oint \boldsymbol{H} \cdot \boldsymbol{dl} = i \tag{3}$$

If the closed path is considered to be a circular contour, equation (3) can be simplified to equation (4), with r being the radius of the circle, as shown below. This is equivalent to the Biot-Savart law [23].

$$\oint \boldsymbol{H} \cdot \boldsymbol{dl} = i$$
$$H2\pi r = i$$
$$H = \frac{i}{2\pi r} \tag{4}$$

This means that the magnetic field intensity created by a current carrying conductor at a distance r from the centre of the conductor can be calculated using equation (4).

This can be extended to multiple conductors, each of which is carrying a current. Using the theory of super position, each current carrying conductor will cause magnetic field intensity on a point in space, and the resultant magnetic field intensity, at this point in space, is equal to the sum of the individual effects from each of the conductors. Multiple conductors are depicted in Figure 11 and the resulting equation (5) is derived based on super position.

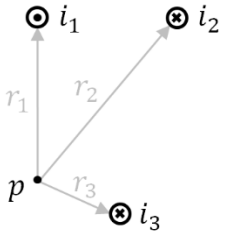


Figure 11: Diagram to show multiple conductors around a point p.

Thus:
$$H_p = H_1 + H_2 + H_3$$
$$= \frac{i_1}{2\pi r_1} + \frac{-i_2}{2\pi r_2} + \frac{-i_3}{2\pi r_3} \tag{5}$$

This can be extended to any amount of conductors through simple manipulation of equation (5).

Further, the magnetic flux density, B, exists wherever there is a magnetic field intensity, H. These two quantities form the fundamental magnetic field vectors. The two quantities are mathematically related as shown in equations (6) and (7) if found in a linear, homogeneous and isotropic medium [21]–[23].

$$B = \mu H \qquad Wb/m^2 \text{ or } T \tag{6}$$
$$= \mu_0 \mu_r H \qquad Wb/m^2 \text{ or } T \tag{7}$$

where:
- μ is the permeability of the medium.
- μ_0 is the permeability of free space ($4\pi 10^{-7}\ henry/meter$).
- μ_r is the relative permeability of the medium.

This means that the magnetic flux density is directly dependent on the magnetic material or medium and its associated magnetic properties.

Materials which are magnetisable are generally non-linear with respect to magnetic fields. In these materials, B and H are related through a hysteresis curve [22].

Further, the magnetic flux, Φ, through a cross sectional area, A, with magnetic flux density, B, is calculated as per equation (8) [21]–[23].

$$\Phi = BA \tag{8}$$

The inductance of a coil, L, is defined as the flux linkage, λ, of the coil per ampere of the current, i, which it carries. The flux linkage can be calculated using the by the number of turns of the coil, N, as well as the magnetic flux through the core of the coil [21], [22]. The flux linkage formula is shown by equation (9) and the inductance of a coil is shown by equation (10).

$$\lambda = N\Phi \tag{9}$$

$$L = \frac{\lambda}{i} \tag{10}$$

This shows that any circuit element with an inductive element will experience a current through the inductive component based on the magnetic flux to which the inductor or exposed. Or alternatively, any circuit element with an inductive component will create a magnetic flux as a result of the current flowing through the inductive component. This theory applies to both the catenary model, which would be the source of the magnetic field, as well as the wagon model in which currents are induced.

If the surrounding medium of the inductive component is linear, homogeneous and isotropic, such as air, then the current in the loop is directly proportional to the magnetic flux through the loop, as per (10). From Faraday's Law of induction, the voltage applied to the loop, or induced in the loop is:

$$V = \frac{d\lambda}{dt} = L\frac{dI}{dt} \tag{11}$$

This is known as the self-inductance of the circuit.

3.2 Internal Inductance

The discussion to this point has considered the magnetic flux external to a wire or cable. Internal inductance of cables, although present, is generally assumed negligible in comparison to external inductance [22]. For the purposes of this research, this is assumed to be true.

3.3 Proximity Effect

In the event that two current carrying conductors are relatively close to one another, within the range of a few radii, the current distribution through the cross-section of conductors will be effected. The current will be concentrated on the side towards the other conductor. This is known as the proximity effect [22]. Due to the conductors being spaced far from one another compared to their radii in this research, the proximity effect is deemed to be negligible.

3.4 Mutual Inductance between Magnetic Circuits

When more than one magnetic circuit are in proximity of one another, each circuit will have a flux which penetrates the other circuit/s. This will result in inductive coupling between the circuits. This is generally referred to as the mutual inductance between the circuits or loops. If one of the loops carries a current, I_1, which causes a flux, λ_2, through the surface of a second loop, a mutual inductance exists:

$$M_{12} = \frac{\lambda_2}{I_1} \tag{12}$$

Further, the flux in each loop is a super position of the loop's self-inductance and the mutual-inductances from the other loops.

$$\begin{aligned} \lambda_1 &= L_{11}I_1 + \cdots + M_{1i}I_i + \cdots + M_{1n}I_n \\ &\vdots \\ \lambda_n &= M_{n1}I_1 + \cdots + M_{ni}I_i + \cdots + L_{nn}I_n \end{aligned}$$

Similarly, this can be represented as a matrix:

$$\boldsymbol{\lambda} = \boldsymbol{LI}$$

where: $\boldsymbol{\lambda} = \begin{bmatrix} \lambda_1 \\ \vdots \\ \lambda_i \\ \vdots \\ \lambda_n \end{bmatrix}$ and $\boldsymbol{L} = \begin{bmatrix} L_{11} & \cdots & M_{1i} & \cdots & M_{1n} \\ \vdots & \ddots & \vdots & \ddots & \vdots \\ M_{i1} & \vdots & L_{ii} & \vdots & M_{in} \\ \vdots & \ddots & \vdots & \ddots & \vdots \\ M_{n1} & \cdots & M_{ni} & \cdots & L_{nn} \end{bmatrix}$ and $\boldsymbol{I} = \begin{bmatrix} I_1 \\ \vdots \\ I_i \\ \vdots \\ I_n \end{bmatrix}$

3.5 The Dot Convention

Loops carrying current influence one another, as described in section 3.4. There exists a self-inductance of the loop and mutual inductances from neighbouring loops. The dot convention is the resolution to place a dot on the individual inductors in order to identify the loop orientations with respect to one another, and hence the effect each loop has on every other loop. The inductor describing the loop is marked with a positive terminal and negative terminal as well as placing a dot defining its orientation. Subsequent to this, the equations describing the voltage across each inductor can be established.

Figure 12 shows 2 current carrying loops in proximity to one another. The current direction for each loop is defined. The inductive elements representing the induction of each loop are then assigned voltage polarity and dot convention.

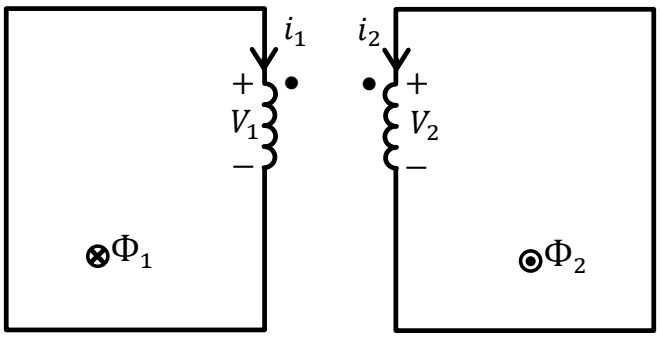


Figure 12: Diagram to 2 current carrying loops with dot convention.

The Faraday Law voltages induced in each loop is represented as V_1 and V_2. The voltage equations can are then formulated with the signs of the terms omitted.

$$V_1 = (*)L_{11}\frac{dI_1}{dt} + (*)M_{12}\frac{dI_2}{dt}$$

$$V_2 = (*)L_{22}\frac{dI_2}{dt} + (*)M_{12}\frac{dI_1}{dt}$$

The signs for the self and each mutual inductance is then determined using the following rules [22]:

Self-Inductance:	(+) if	Current enters + voltage terminal
	(-) if	Current enters - voltage terminal
Mutual-Inductance:	(+) at the dotted end if	Current in the other loops enters • of its inductance
	(-) at the dotted end if	Current in the other loops does not enter • of its inductance

Using these rules, the voltage equations can be finalized:

$$V_1 = L_{11}\frac{dI_1}{dt} + M_{12}\frac{dI_2}{dt}$$

$$V_2 = L_{22}\frac{dI_2}{dt} + M_{12}\frac{dI_1}{dt}$$

3.6 Multi-conductor Transmission Lines

The self-inductance and mutual-inductance discussed above are useful in formulating equations which describe the coupling between Multi-conductor Transmission Lines (MTL). These inductance equations as well as the self and mutual capacitances describe the MTL equations. This being said, the self and mutual capacitances are ignored and considered negligible. This is justified during the verification of the system model in CHAPTER 7. The MTL equations can be used to determine the interference in each loop caused by neighbouring loops [22].

Following derivations, formulas for MTL conductor's self-inductance and mutual-inductance are obtained. The derivation of the formulae is not detailed in this document, however the interested reader may review the derivations in [22], [24]. The resulting per-unit-length formulae for MTL conductors which are not above an infinite ground plane are shown in equations (13) and (14). These equations are in reference to a "zeroth", 0^{th} conductor. The 0^{th} conductor acts as the return path for all the other conductors of the multi-conductor transmission line. This is illustrated in Figure 13.

Self-inductance:

$$l_{ii} = \frac{\mu_0}{2\pi} ln \frac{d_{i0}^2}{r_{w0} r_{wi}} \tag{13}$$

where:
- l_{ii} is the self –inductance of the i^{th} loop.
- μ_0 is the permeability of free space ($4\pi 10^{-7}\ henry/meter$).
- d_{i0} is the distance between the i^{th} conductor and the 0^{th} conductor.
- r_{w0} is the radius of the 0^{th} conductor.
- r_{wi} is the radius of the i^{th} conductor.

$$l_{ij} = l_{ji} = \frac{\mu_0}{2\pi} ln \frac{d_{i0} d_{j0}}{d_{ij} r_{w0}} \tag{14}$$

where:
- l_{ij} is the mutual –inductance between the i^{th} and j^{th} loop.
- μ_0 is the permeability of free space ($4\pi 10^{-7}\ henry/meter$).
- d_{i0} is the distance between the i^{th} conductor and the 0^{th} conductor.
- d_{j0} is the distance between the j^{th} conductor and the 0^{th} conductor.
- r_{w0} is the radius of the 0^{th} conductor.

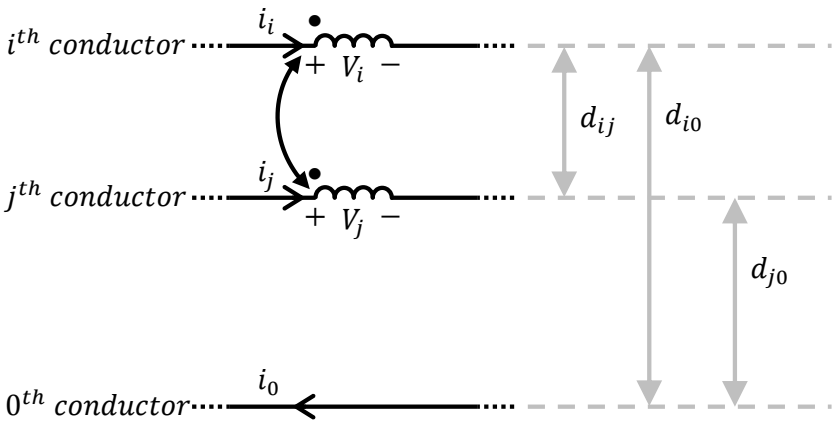


Figure 13: Diagram illustrating a 3 conductor MTL.

The theoretical basis established in this chapter is used to develop the system model which is the amalgamation of three sub-models being the locomotive or locomotive consist model, the supply model and the wagon model. The development of these models is described in CHAPTER 4.

CHAPTER 4
MODEL DEVELOPMENT

From the previous sections of this document, a basis of theoretical understanding has been established. This chapter discusses the environment in which the systems and sub-systems exist as well as a development of a circuit models which describe the sub-systems based on their surrounding environment and the theoretical background already established.

4.1 The Locomotive Model

4.1.1 Energy Flow through a Locomotive

The energy flow through today's modern locomotives follows a typical topology. In the case of AC voltage locomotives, the voltage from the catenary supply is applied to a large transformer, often referred to as the main transformer. This is described in the simplified model in Figure 14.

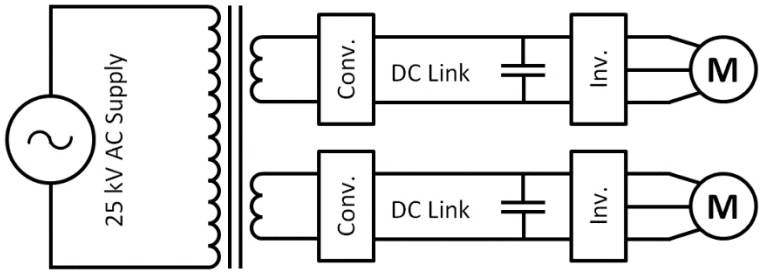


Figure 14: Diagram to show the simplified flow of power in a modern locomotive feeding from an AC supply.

The main transformer steps the large single phase voltage down to a more practical voltage for manipulation. The transformer's secondary windings (typically more than one) are connected to a converter which rectifies the voltage and outputs the power onto the DC link as depicted in Figure 14.

When discussing the flow of power from DC catenary infrastructure, the DC link becomes the entry point to the locomotive power system. Because DC catenary voltage is already rectified and the voltage magnitude is a convenient value, the supply from the catenary is connected to the DC link and bypasses the main transformer and the converter. This can be seen in Figure 15.

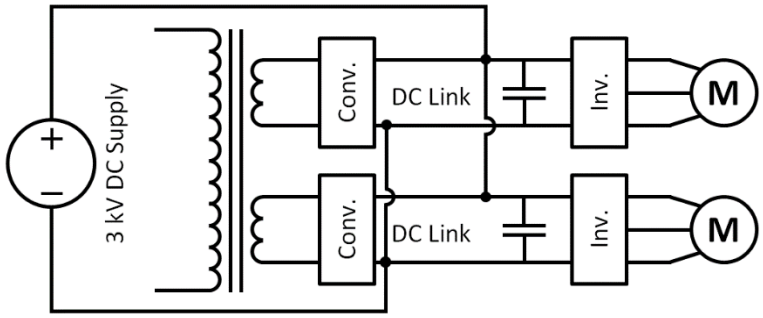


Figure 15: Diagram to show the simplified flow of power in a modern dual voltage locomotive feeding from a DC supply.

The inverter then feeds from the DC link, regardless of AC or DC supply, and outputs the required voltage and frequency in three phases to the traction motor/s. The voltage and frequency is variable and the control system will determine the required parameters based on various algorithms which consider notch commanded by the driver, wheel slip, rotor speed and others.

It should be noted that the converter and inverter roles are switched during regenerative braking. Locomotives with this feature act as generators which convert kinetic energy to electrical energy and use this conversion as a means of braking the train.

4.1.2 Power Electronics in Modern Locomotives

The operation of modern locomotives is through the use of Pulse Width Modulation (PWM) which drives the switching of Insulated Gate Bipolar Transistors (IGBTs) located in the locomotive's power conversion cubicles. Because of these advanced techniques of power conversion, the power factor of modern locomotives can be approximated to one.

This use of power electronics to switch high currents at high speeds introduces switching transients into the system. It proves particularly difficult to predict the magnitude and frequency of these harmonics due to the fact that the locomotive control system is constantly changing switching parameters based on the notch commanded by the driver, the speed of the locomotive, jerk control (method of minimizing the in train forces experienced by the couplers), DC link voltage, catenary voltage and various other parameters.

4.1.3 The Single Source Locomotive Model

Due to the fact that modern locomotives have an approximated power factor of unity due to the addition of advanced on-board power electronics to the locomotive, the locomotive can be primarily modeled as a controlled current source as shown in Figure 16 below.

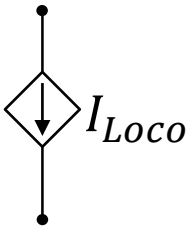


Figure 16: Diagram to show the ideal current source model of a modern locomotive utilising on-board power electronics.

The instantaneous value of I_{Loco}, as depicted in Figure 16, can be determined by the rating of the locomotive, and the line voltage. This is assuming that the locomotive is operating continuously at full rating. This is assumed for the sake of simplicity, but is extended further during the course of research to include operations at reduced power (lower traction command or coasting).

As an example, if a locomotive is rated at 3 MW (P_{Loco}) and the line voltage supplied to the locomotive is 25 kV_{rms} (V_{Loco}), the current flowing through the locomotive (I_{Loco}) can simply be equated using the power formula as seen in (15).

$$Power = Voltage \times Current \tag{15}$$

Thus, as a continuation of the example, the locomotive parameters can be calculated:

$$\begin{aligned} P_{Loco} &= V_{Loco} \times I_{Loco} \\ \therefore I_{Loco} &= \frac{P_{Loco}}{V_{Loco}} \\ &= \frac{3\ 000\ 000}{25\ 000} \\ &= 120\ A \end{aligned}$$

As an extension of this ideal model, the regenerative braking function of the locomotive can be included. When a locomotive enters regenerative braking mode, the locomotive will act as a power source instead of a power sink or load. By simply inverting the current value of the locomotive model, I_{Loco}, to reflect $-I_{Loco}$, the locomotive itself becomes a power source.

Although this locomotive model is simple to use and understand, the effects of harmonics due to the use of the power electronics cannot be ignored and must be included in the locomotive model. Thus the multiple source locomotive model is proposed in section 4.1.4.

4.1.4 The Multiple Source Locomotive Model

The on-board power electronics found in modern locomotives adds the benefit of simplifying the model of the locomotive as a power sink with unity power factor. However, this being said, the on-board power electronics also adds complexity due to the harmonic content that is introduced into the system. This can be seen by the current vs frequency plot in Figure 17.

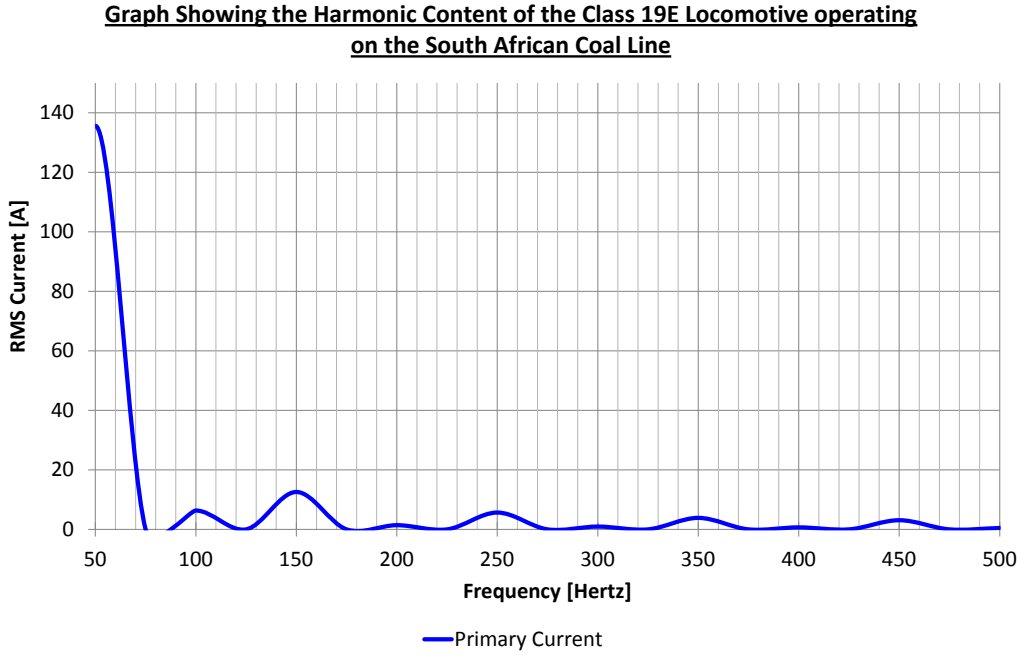


Figure 17: Diagram to show the harmonic content found in a typical modern locomotive utilising power electronics, extracted from [25]**.**

From Figure 17, it is clear that although the fundamental frequency, being $50\ Hz$, has the largest magnitude, substantial current magnitudes at higher frequencies also exist. Thus, the single current source model will prove inadequate in modeling the higher frequency components found in the supply line. It is for this reason that the single current source model is extended to the multiple source current model. Each current source will be at the frequency and magnitude of a harmonic which is found through measured data such as that shown in Figure 17. The multiple current source model can be seen in Figure 18. The number of sources can be varied depending on the level of accuracy required.

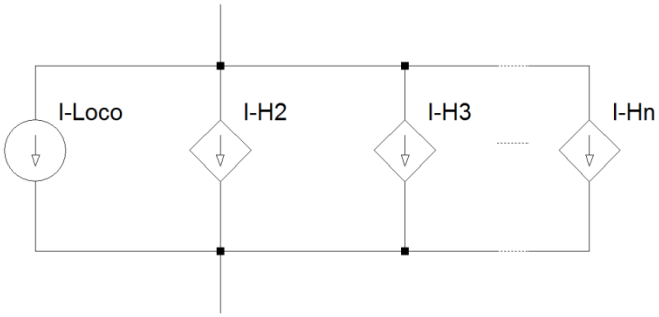


Figure 18: Diagram to show the multiple current source model of a modern locomotive utilising on-board power electronics.

It is at this point that the idea of the "unity" power factor of the locomotive should be questioned.

The return current leaves the locomotive through brushes on the axles of the wheels and into the rail which acts as the conductive path returning to the sub-station. This being said, the couplers on the locomotive can also act as a conductive path should another locomotive or wagon be coupled to the locomotive. This means that in a bo-bo configured locomotive (locomotive with four axles), the return current has the choice of six return paths, two couplers and four wheels. In the case of a co-co configured locomotive (locomotive with six axles), there will be eight return paths for current.

This being said, there will exist differing impedance paths through the nodes. This will directly affect the current magnitude division between the nodes. For the purposes of the research, the axles of the locomotive consist are considered as a single node with a resistive path. The coupler of the locomotive consist connecting to the first wagon of the train is also considered as a second node with its own resistive path. This is depicted in Figure 19. The resistive values are to be determined or tuned during simulations.

4.1.5 The Multiple Source Locomotive Model Parameters

In order to estimate the parameters of the components or elements of the locomotive model, the harmonic content of the locomotive must be observed. Based on the harmonic testing performed during the commissioning of the class 19E locomotive, the amplitude of the harmonics can be estimated. Extracted from Figure 17 are results in Table 1 which gives the expected amplitude of the harmonics of the locomotive.

Table 1: Table showing the approximated harmonic content of a class 19E locomotive.

Harmonic order	Frequency [Hz]	Observed Current [A]	Percentage of Fundamental
Fundamental	50	136.6	100%
2	100	1.3	4.7%
3	150	12.6	9.3%
4	200	1.4	1%
5	250	5.7	4.2%
6	300	0.9	0.7%
7	350	3.9	2.9%
8	400	0.7	0.5%
9	450	3.1	2.3%
10	500	0.5	0.3%

The result of this extrapolation and the assumptions made is a locomotive model with parameters which can be used for simulations. Figure 19 below, shows the preliminary multiple current source locomotive model for simulation purposes. The model parameters are configured for the applicable simulation conditions.

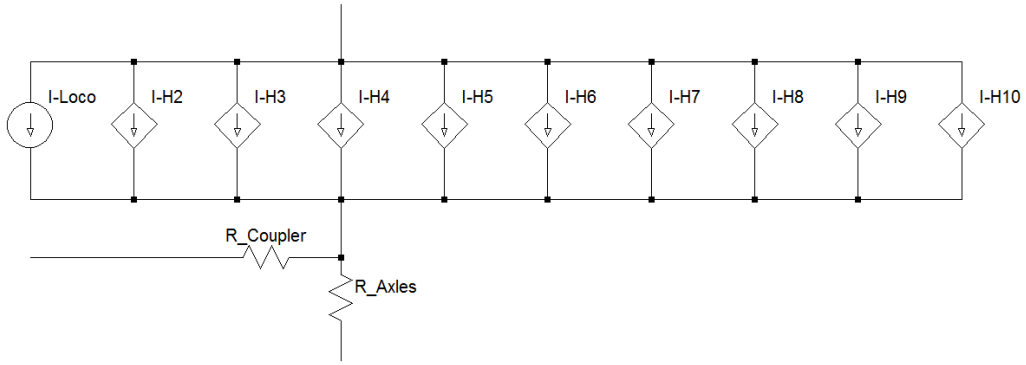


Figure 19: Diagram to show the multiple current source model of a modern locomotive utilising on-board power electronics.

4.2 The Supply Infrastructure

4.2.1 The Ideal Supply Model

The power supply infrastructure to the locomotive can be modelled very simply, with only an ideal source, or with added levels of complexity. Each level of complexity that is added will result in a more accurate model. Initially, the simple ideal source model feeding power to the locomotive is proposed, as can be seen in Figure 20.

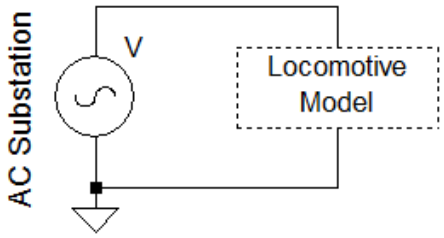


Figure 20: Diagram to show the ideal AC sub-station supply model.

This model means that the voltage supplied by the sub-station will be equal in magnitude and phase as the voltage at the locomotive. This is clearly not the case, as the transmission line will cause a voltage drop as it is non-ideal and has impedance due to its physical attributes and/or makeup. It is for this reason that the lumped impedance supply model is proposed in section 4.2.2.

4.2.2 The Lumped Impedance Supply Model

The transmission line of any power transmission system will have resistive, inductive and capacitive elements to it. These attributes will result in the voltage magnitude and phase being altered. The impedance of the line will usually be specified per kilometer, thus a lumped model can be used such that the impedance is a function of the distance (d) of the locomotive from the sub-station. This model is shown in Figure 21.

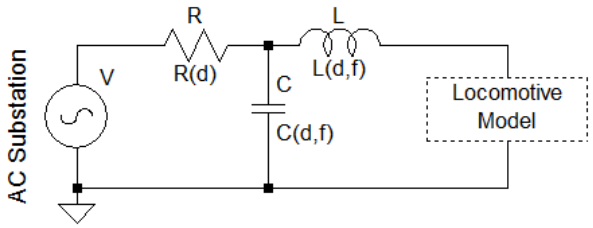


Figure 21: Diagram to show the lumped impedance supply model.

From Figure 21, it is clear that, depending on the transmission line parameters; there will be a voltage drop and phase shift along the transmission line. This means that the voltage at the output of the AC sub-station and the voltage at the input of the locomotive will be different in magnitude and phase; however they will be related through the parameters of the transmission line.

This model is a simple description of the power feeding circuit; however, there are multiple conductors as opposed to a single conductor carrying current to and from the locomotive. Thus the model must be extended in order to achieve an acceptable level of accuracy. The Multiple Transmission Line model is proposed in section 4.2.3.

4.2.3 The Multiple Transmission Line Supply Model

The Over Head Track Equipment (OHTE) refers to the transmission lines from the sub-station to the locomotives. This comprises of a number of current carrying conductors. The typical conductors and their geometrical layout are illustrated in Figure 22.

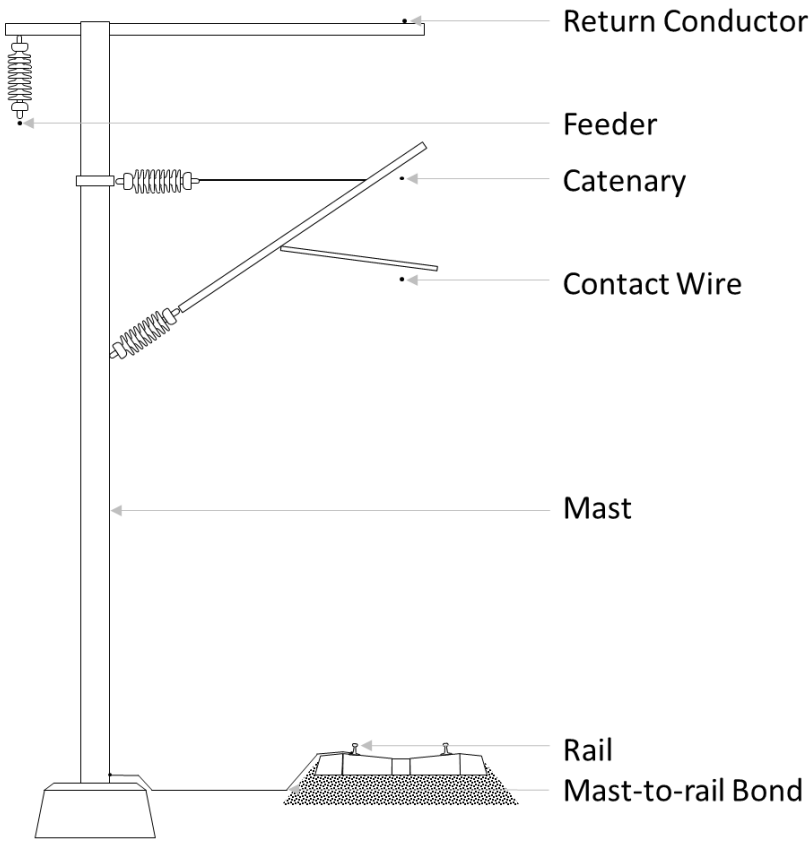


Figure 22: Diagram to show the typical supply infrastructure layout on the Transnet Coal Line.

Recognizing that the multiple conductors will have an effect on the supply model, they must be taken into account. In order to do this, the typical infrastructure layout must be considered as well as the electrical parameters of each conductor.

The relevant electrical and physical parameters of each conductor described in Figure 22 can be found in Table 2 based on the fundamental frequency of $50\ Hz$.

Table 2: Table showing the electrical and physical parameters of the conductors typically found on the Coal Line, [26]–[28]**.**

	Units	Material	Ermelo - Vryheid	Vryheid - Richards Bay
Contact Wire	mm^2	HD Cu	107	161
Self-Impedance	Ω/km		0.2186+j0.8006	0.1616+j0.7881

	Units	Material	Ermelo - Vryheid	Vryheid - Richards Bay
Catenary Wire	mm^2	HD Cu	65	80
Self-Impedance	Ω/km		0.3230+j0.8106	0.2851+j0.8043
Return Conductor	mm^2	AAC	150	250
Self-Impedance	Ω/km		0.2316+j0.7831	0.1574+j0.7666
Additional Return Conductor	mm^2	AAC	150	None
Self-Impedance	Ω/km		0.2316+j0.7831	
Feeder Wire	mm^2	AAC	150	150
Self-Impedance	Ω/km		0.2316+j0.7831	0.2316+j0.7831
Rail	mm^2	Steel	7686	7686
Self-Impedance	Ω/km		0.04+j0.95	0.04+j0.95
Span Length	m		71	67
Contact Wire Height (Normal)	m		5.15	5.2
Overall Impedance	Ω/km		0.169+j0.369	0.135+j0.321
Drawbar	mm^2	Steel	12933	12933

The geometrical configuration and dimensions of the conductors are described in Figure 23.

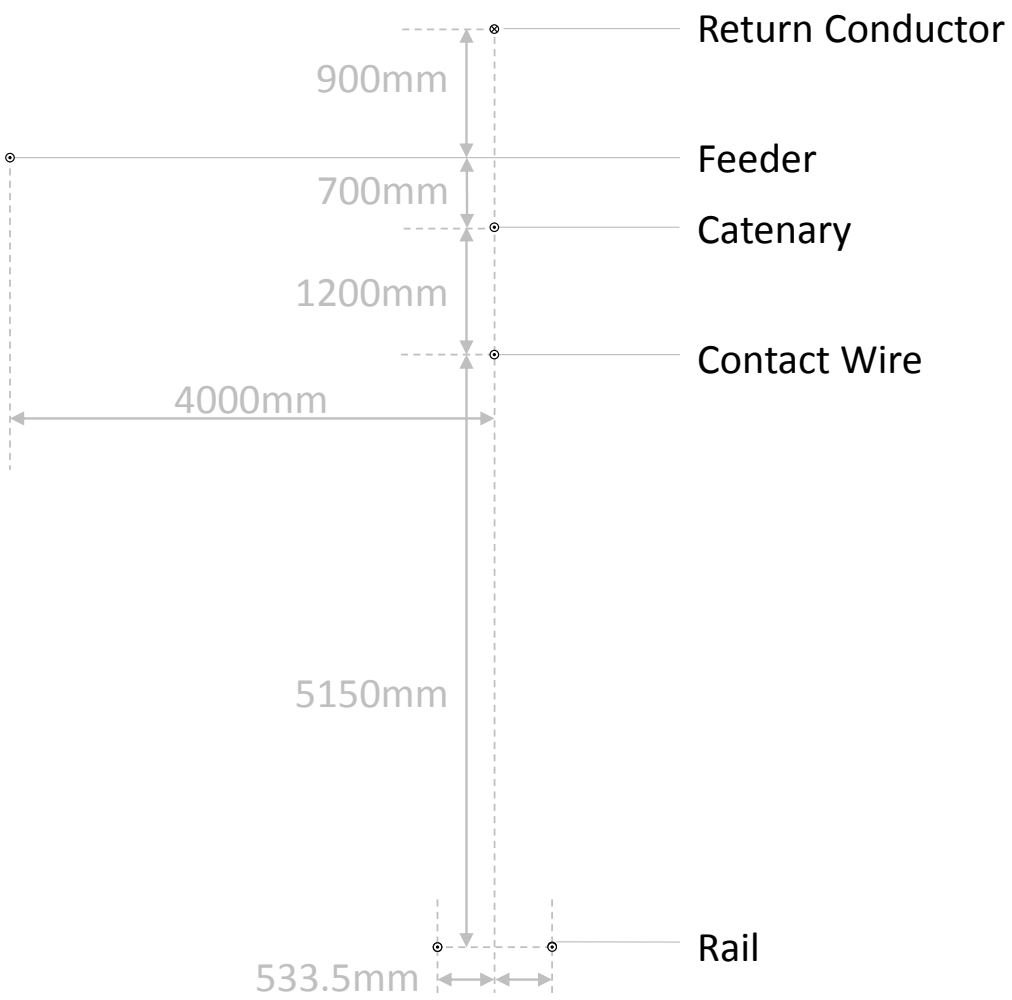


Figure 23: Diagram to show the typical supply infrastructure geometrical dimensions on the Transnet Coal Line.

Using the theoretical background provided in CHAPTER 3, the line parameters in Table 2 and the geometrical configuration of the current carrying conductors, a Multiple Transmission Line (MTL) model is derived for the supply system.

In order to simplify the model, and avoid unnecessary complexity, the current carrying conductors, inclusive of the rails, are estimated to be circular conductors with equivalent cross-sectional area. Similarly, the wagons are of an extremely complex physical shape, thus they are estimated to be a continuous drawbar at a height of approximately 3 meters from the rails. These values were obtained during the simulations of CHAPTER 7 as they resulted in acceptable simulation results when compared to measurement results.

Drawbars are permanent connections between wagons, similar to the coupler; however a drawbar cannot be disconnected, thus creating sets of wagons. Typically, on the Coal Line these wagon sets consist of four single wagons.

The size and height from the rails of this wagon approximation as a drawbar will affect the self-impedance of the coupler conductors and mutual-inductance with other conductors. This change in impedances is investigated further in CHAPTER 8. The approximation of the wagon radii and height must be tuned to the appropriate simulation conditions such that the system model reflects measure results.

Thus, Figure 23 can be revised to include the current path through the wagons of the train modelled as a continuous drawbar. This revised diagram can be seen in Figure 24.

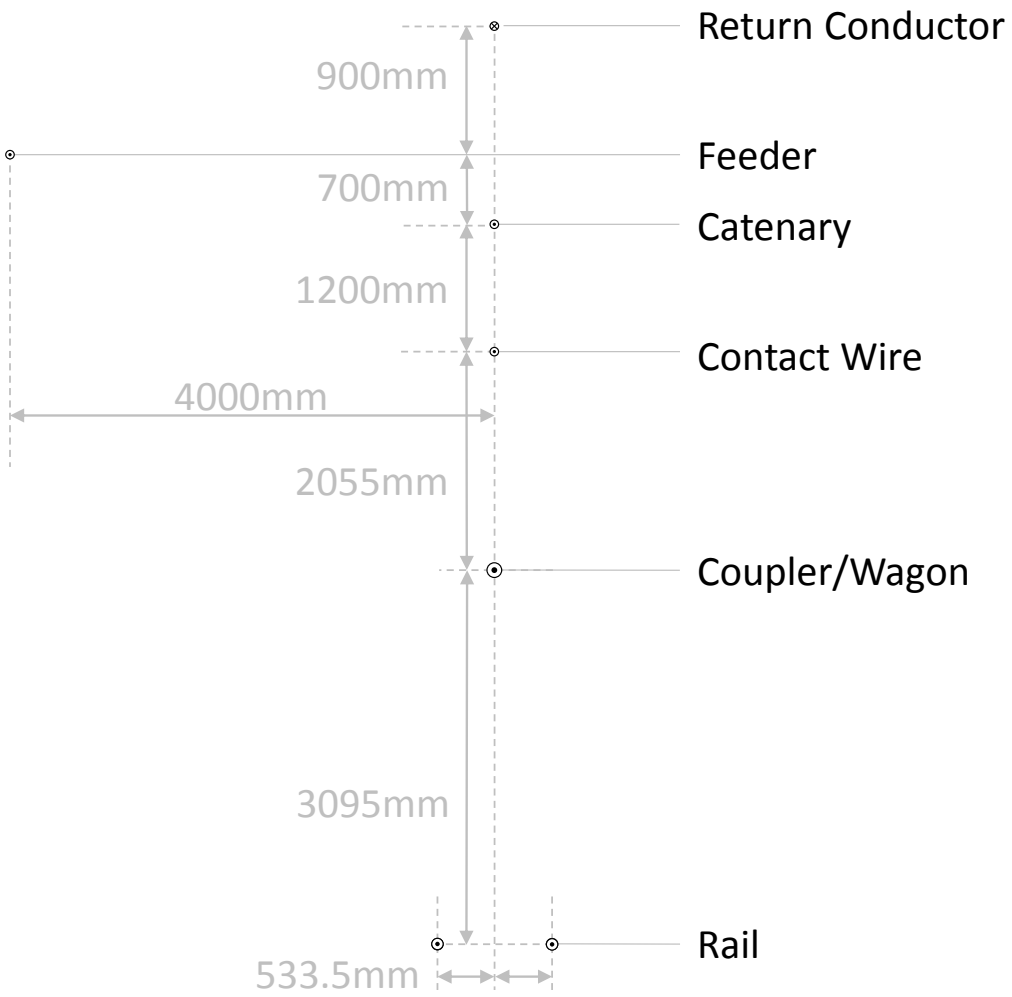


Figure 24: Diagram to show the typical supply infrastructure geometrical dimensions on the Transnet Coal Line inclusive of wagons modelled as a continuous drawbar.

For ease of reference, the distance between individual current carrying conductors is extracted from Figure 24 and presented in Table 3.

Table 3: Table showing the distance between conductors typically found on the Coal Line, extended from Table 2.

Distances (m)	Reference	Return Conductor	Feeder	Catenary	Contact Wire	Wagon	Left Rail	Right Rail
Reference	0.000	7.950	8.100	6.350	5.150	3.095	0.533	0.533
Return Conductor	7.950	0.000	4.100	1.600	2.800	4.855	7.968	7.968
Feeder	8.100	4.100	0.000	4.061	4.428	5.625	7.856	8.382
Catenary	6.350	1.600	4.061	0.000	1.200	3.255	6.372	6.372
Contact Wire	5.150	2.800	4.428	1.200	0.000	2.055	5.178	5.178
Wagon	3.095	4.855	5.625	3.255	2.055	0.000	3.140	3.140
Left Rail	0.533	7.968	7.856	6.372	5.178	3.140	0.000	1.067
Right Rail	0.533	7.968	8.382	6.372	5.178	3.140	1.067	0.000

In essence, the supply infrastructure and couplers/wagons are modelled as per the theoretical approach of Figure 13. This is illustrated in Figure 25. It should be noted that the reference or 0^{th} conductor is placed level to and between the rails. The reference conductor is used for calculation purposes. In theory the current which the reference conductor will carry is the sum of the other conductors, being zero. In practicality, the reference conductor does not exist.

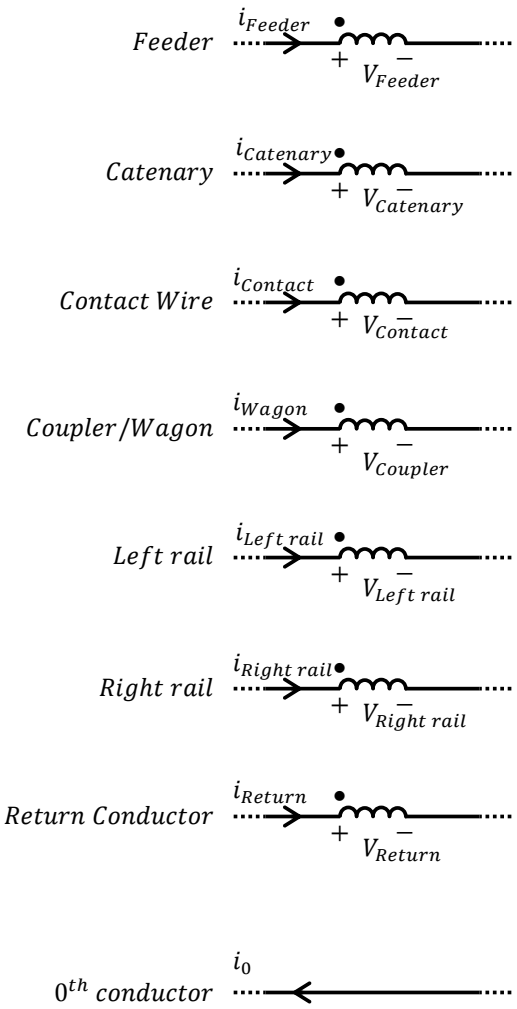


Figure 25: Diagram illustrating the typical Coal Line supply configuration with a train as a MTL.

Using the respective average cross-sectional areas, each current carrying conductor can be estimated to solid cylindrical conductor with radius calculated using the conductor's cross-sectional area and the formula for the area of a circle. This estimation is performed for all current carrying conductors. These radii are shown for individual conductors in Table 4

Table 4: Table showing the cross-sectional area and radius of conductors typically found on the Coal Line, extended from Table 2 and [28]**.**

	Ermelo – Vryheid Cross Sectional Area (mm^2)	Ermelo – Vryheid Radius (m)
Contact Wire	107	0.005836022
Catenary Wire	65	0.004548642
Return Conductor	150	0.006909883
Additional Return Conductor	150	0.006909883
Feeder Wire	150	0.006909883
Rail	7686	0.049462408

	Ermelo – Vryheid Cross Sectional Area (mm^2)	Ermelo – Vryheid Radius (m)
Drawbar	12933	0.102840480

Again, referring to the theoretical background provided in CHAPTER 3, equations (13) and (14) allow for the calculation of self-inductance and mutual-inductance of the supply model conductors inclusive of the couplers/wagons. This is possible using the values found in Table 3 and Table 4. This results in the self-inductances and mutual-inductances per meter shown in Table 5.

Table 5: Table showing the self-inductance and mutual-inductance of conductors typically found on the Coal Line as lumped parameters per meter.

Inductances (H/m)	Return	Feeder	Catenary	Contact Wire	Wagon	Left Rail	Right Rail
Return	2.82E-06	1.55E-06	1.69E-06	1.53E-06	1.32E-06	8.69E-07	8.69E-07
Feeder	1.55E-06	2.83E-06	1.50E-06	1.44E-06	1.29E-06	8.75E-07	8.62E-07
Catenary	1.69E-06	1.50E-06	2.81E-06	1.66E-06	1.35E-06	8.68E-07	8.68E-07
Contact Wire	1.53E-06	1.44E-06	1.66E-06	2.68E-06	1.40E-06	8.68E-07	8.68E-07
Wagon	1.32E-06	1.29E-06	1.35E-06	1.40E-06	1.42E-06	8.66E-07	8.66E-07
Left Rail	8.69E-07	8.75E-07	8.68E-07	8.68E-07	8.66E-07	1.34E-06	7.30E-07
Right Rail	8.69E-07	8.62E-07	8.68E-07	8.68E-07	8.66E-07	7.30E-07	1.34E-06

4.2.4 The Inclusion of Rail-to-Mast Bonds in Supply Model

The supply model developed thus far has considered the 2-dimensional or cross sectional view of the infrastructure. This has allowed the model format to be lumped parameters as a function of their length or the distance from the supply.

In order for the development of a more robust model, the effects along the length of the track must also be considered. Transnet Freight Rail's Coal line infrastructure has such components in the form of rail-to-mast bonds at intervals on the track.

In order to physically earth the mast poles, return conductors and rails together, bonding straps known as rail-to-mast bonds are installed at intervals along the transmission line. These bonds create an electrical short between the rail, the mast pole and the return conductor which ensure safe touch potentials for maintenance or other personnel working in the vicinity of the railway. These mast-to-rail bonding straps are typically installed on every fifth mast pole.

The major parameter affecting the impedance between the rail and the return conductor is the impedance of the rail over the distance. The lumped impedance model of these bonds must be an oscillating function as these bonds will repeat every fifth mast pole. This oscillation is necessary as the impedance will increase as it passes a bond, and decrease as it approaches the next bond.

For the sake of mathematical simplicity, this oscillating function will be described using a sine function, however can be extended to a triangular function, or other, should the application so require. Also, it should be noted that the inductive element of the rail-to-mast bonds are considered negligible in comparison to the perpendicular transmission line conductors. Thus the rail-to-mast bond is considered purely resistive. The oscillating function is derived as follows:

$$Z_{bond} = Z_{conductor}\left(\frac{span}{2} \times \left(\sin\left(\frac{d}{5 \times span}\right) + 1\right) + 15.42\right)$$

where:

d	is the distance of from the sub-station.
$span$	is the distance between mast poles (either $71m$ or $65m$).
$Z_{conductor}$	is the impedance of the bond in Ω/m.
Z_{bond}	is the impedance of the bonding between the rail and the return conductor at distance d.

These parameters lead to an extended lumped impedance model which describes the parameters of each conductor as well as the bonding between the rail and the return conductor as can be seen in Figure 26.

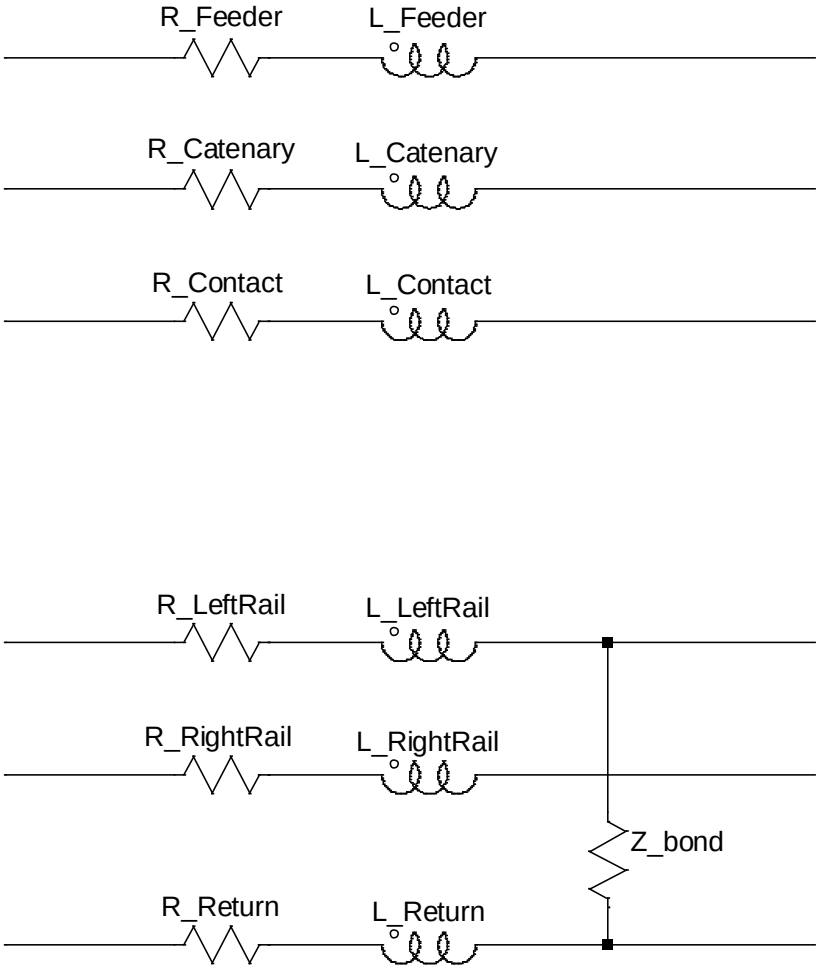


Figure 26: Diagram to show the extended lumped impedance supply model per meter inclusive of oscillating rail-to-mast bond.

4.2.5 The Parallel Supply Model

As described in the literature survey in CHAPTER 2, the AC supply network is broken into sections, each in phase with one phase of the three phase supply from the national grid. As an extension of this idea of AC sections, the idea of parallel sub-station feeding is introduced to the model [26].

Along the coal line, the sections are fed from either end of the section, and in some sections a triple feed exists [26]. The benefits of this parallel feeding system is that the current supply is shared between the transformers in the sub-stations and the voltage drop seen at the locomotive input is reduced [26]. The equivalent circuit model of the parallel feeding arrangement can be seen in Figure 27.

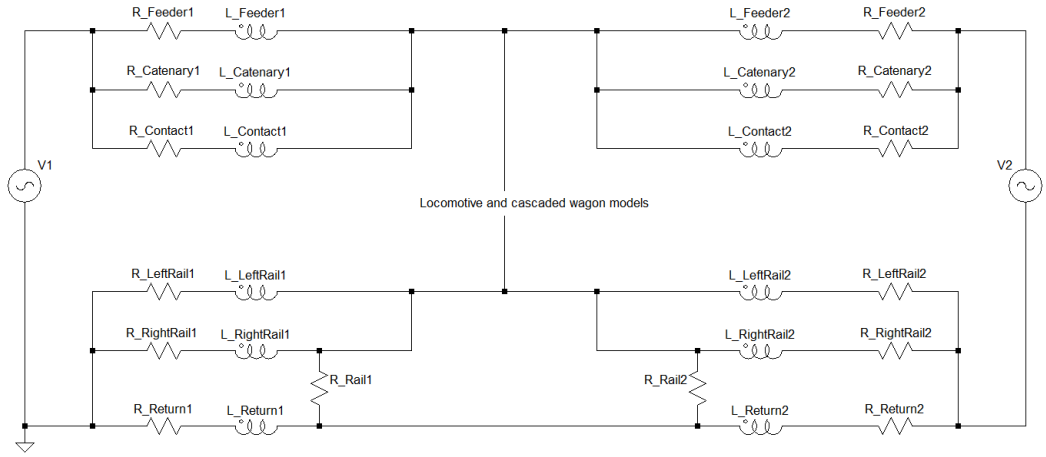


Figure 27: Diagram to show the Lumped Impedance, Parallel Supply Model.

4.3 The Wagon Model

4.3.1 The Ideal Wagon Model

Although not historically included in locomotive and supply system modelling, the wagon model must be included in this research as it is the crux of the return current distribution through a train.

Firstly, we consider that the wagon generally has 10 points at which current can enter and/or exit the wagon. These paths are the eight wheels (four axels) and the two couplers. Similar to the various return paths seen in the locomotive model in section 4.1.4, the various paths are initially modelled as an arrangement of resistors. Each node is connected to each other node through resistive impedance. This model can be seen below in Figure 28.

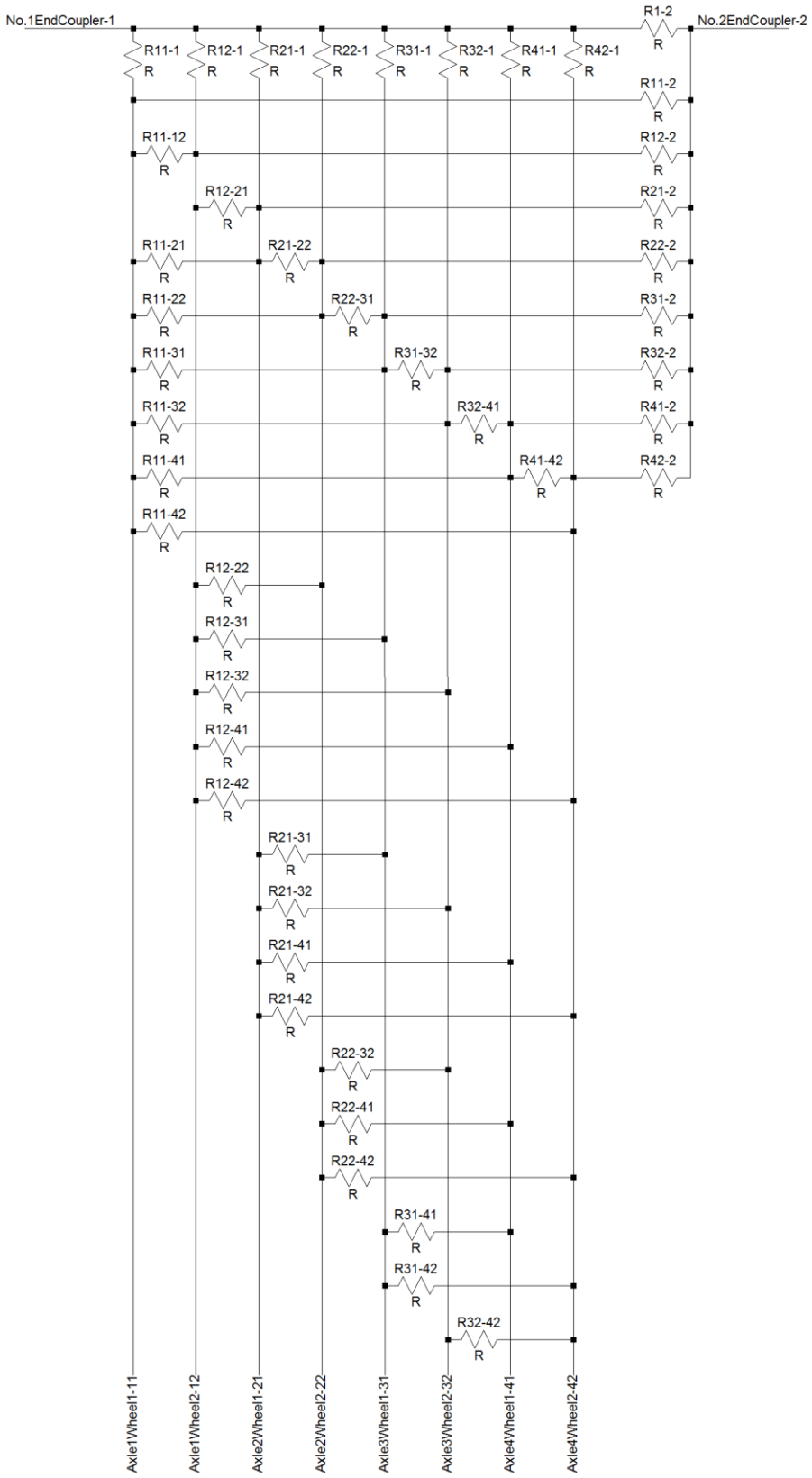


Figure 28: Diagram to show the Ideal Wagon Model.

It is expected that the values of the all resistors will not be equal, although symmetries will exist. In order to simplify the wagon model from the complex grid of resistors, some assumptions regarding the symmetry of the wagons is made.

It is assumed that the wheels and axle sets are symmetrical about the centre of the wagon. This means that each axel with two wheels is considered a node. The resistor network is thus simplified to the circuit diagram shown in Figure 29.

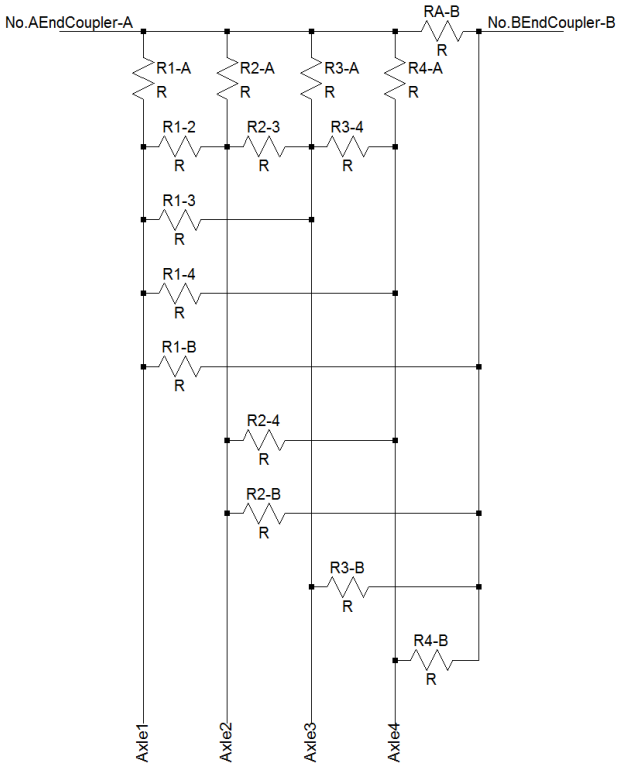


Figure 29: Diagram to show the reduced ideal wagon model from axle symmetries.

Further symmetries of the wagon are considered. The electrical path from coupler A to axle 1 is assumed to be identical to axle 2. Thus element $R_{1-A} = R_{2-A}$. The same assumption is made from coupler A to axle 3 and axle 4, so $R_{3-A} = R_{4-A}$.

Similarly, the same train of thought is applied to the axles from the opposite coupler. This results in the equivalents of $R_{1-B} = R_{2-B}$ and $R_{3-B} = R_{4-B}$. Further, whether observing from coupler A or coupler B, symmetries will be observed such as $R_{1-A} = R_{4-B}$ and $R_{2-A} = R_{3-B}$.

The impedance between axle 1 and axle 3 is assumed to be identical to that between axle 1 and axle 4. This means that $R_{1-3} = R_{1-4}$. Further, the impedance between axle 2 and

axle 3 is assumed to be identical to that between axle 2 and axle 4, so that $R_{2-3} = R_{2-4}$. These are also physically symmetrical so $R_{1-3} = R_{1-4} = R_{2-3} = R_{2-4}$.

Taking all the physical symmetries into consideration the wagon model is revised. Figure 30 is the graphical representation of the reduced wagon model based on the physical symmetries discussed.

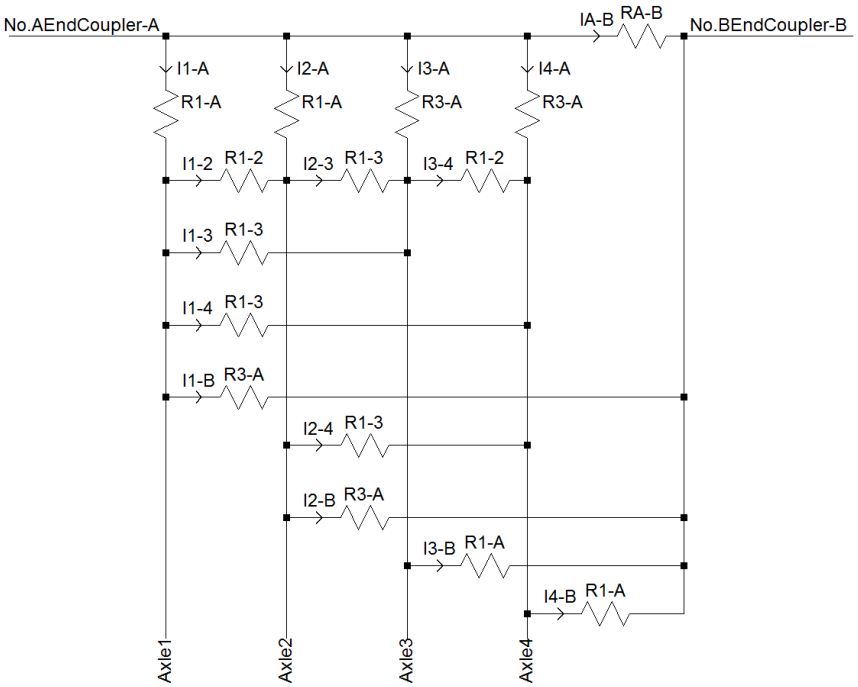


Figure 30: Diagram to show the reduced ideal wagon model from physical wagon symmetries.

Now that the reduced ideal model has been established, the inductive and capacitive elements can also be included in the model. For the purposes of this research, it is assumed, that the capacitive elements are negligible as the voltage that is expected between the nodes of the wagon should be very low. This is proven during the investigation and measurements of the wagon presented in APPENDIX C and APPENDIX D. Thus the capacitive elements between the nodes of the wagon model are not included. The inductive elements are included in the model; however the investigation and measurements of the wagon presented in APPENDIX C and APPENDIX D concludes that most of these inductive elements are negligible.

Each resistor in the reduced ideal wagon model proposed in Figure 30 is extended to have an inductive element, such that the resistor and inductor are in series. The complex wagon model will now include these inductive elements and can be seen in Figure 31.

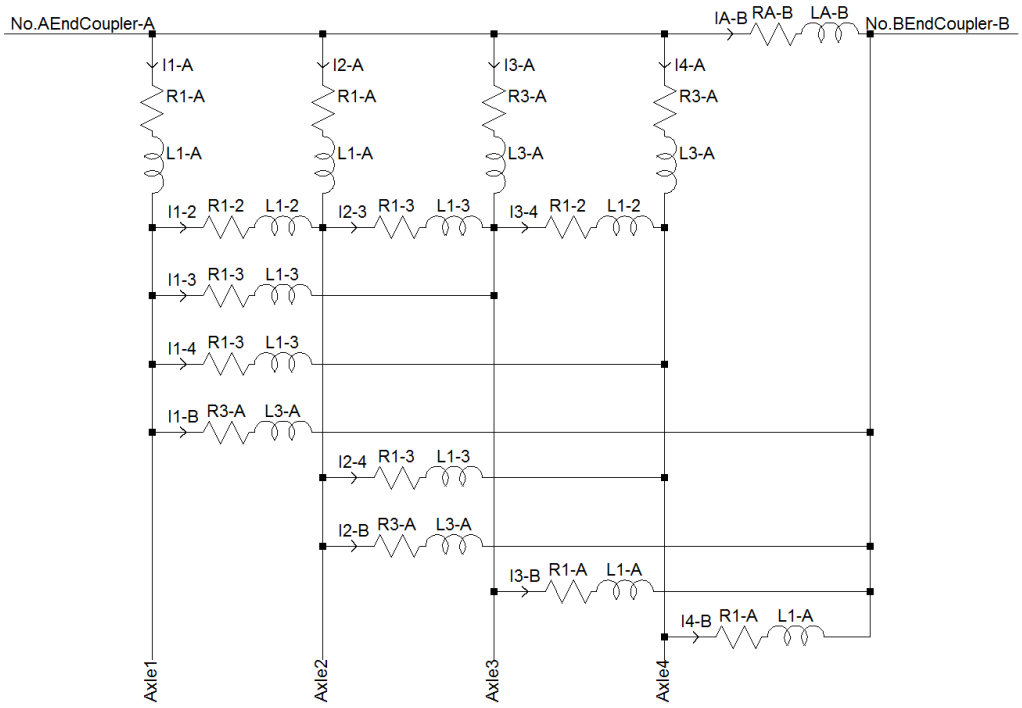


Figure 31: Diagram to show the reduced complex wagon model.

4.4 Wagon Model Verification

In order to use the wagon model in simulations and further in the research, verification of the model needed to occur. The method of wagon model verification was through static measurements on a wagon. The verification procedure and resulting calculations are found in APPENDIX C and APPENDIX D respectively.

For ease for reference, the resulting model parameters are determined to be:

- $R_{A-B} = 0.72\ \Omega$
- $R_{1-A} = 200\ \Omega$
- $R_{1-2} = 1500\ \Omega$
- $R_{1-3} = 1500\ \Omega$
- $R_{3-A} = 120\ \Omega$

The wagon model, excluding coupler to coupler inductance, is the same as that of Figure 30 with the above mentioned parameters. This is due to the determination that the inductive components to the wheels are negligible.

CHAPTER 5
MEASURED DATA

Once the model of the system is established, verification of the model must occur. The model is verified using two sources of measured data. The measured data is described in this chapter, with simulated data is presented in CHAPTER 7 and then the comparison between measured and simulated data is discussed in CHAPTER 8.

The sources of measured data, for the purposes of this research, are the data measured and presented by Ekman et al. in their paper [19] as well as measurements performed by Transnet Freight Rail on a revenue earning, in-service coal train.

This chapter will discuss the measurements obtained from both sources as well as their surrounding conditions as far as the information is available.

5.1 Ekman et al. Measurements

Ekman et al. published a paper documenting their observations of return current flowing through the couplers of wagons in Sweden. The investigation was initiated by a higher than anticipated replacement of wagon bearings which was the result of electrical erosion. This led to research into the cause of the electrical erosion [19].

The measurements performed by Ekman et al. that are to be used in the verification of the system model developed through this research can be found in [19]. The measurements were conducted on the 5th of April 2006 between 10:00 and 13:00.

5.1.1 Train and Infrastructure configuration

Iron ore from the Swedish mines to the harbors is transported though the utilization of 52 to 66 wagon trains. Typically, as described by Ekman et al., these trains are powered by one of three locomotive configurations; however the configuration used when performing the measurements used in this research, were 10.8 MW Bombardier locomotives. These exist in a consist of synchronized doubles with combined maximum power consumption is 10.8 MW.

The measurements were taken with a 52 wagon train, each with a capacity of 25 tons/axle. The length of the train totaled to 481.8 m.

The Swedish railway infrastructure differs from the South African environment in that Sweden makes use of 16 kV at 16.7 Hz as compared to the South African 25 kV at 50 Hz. Further, the electrical sub-stations are positioned approximately 100 km apart in comparison to the South African spacing of track sectioning stations being approximately

15 km, and sub-stations being approximately 30 km apart. The Swedish infrastructure also makes use of Auto Transformers, discussed in section 2.4.2, in some railway sections. These Auto Transformers are spaced at 10 km intervals. Other upgraded sections make use Booster Transformers as discussed in section 2.4.2. The South African Coal line does not make use of Auto Transformers.

5.1.2 Transducer locations

The coupler currents measured by Ekman et al. were the 1st wagon coupler, 20th wagon coupler and 51st wagon coupler. The primary line current drawn by the locomotive consist was also measured. These measurements were taken with respect to time.

5.1.3 Measurement results

The results obtained from the measurements conducted by Ekman et al. can be seen in Figure 32.

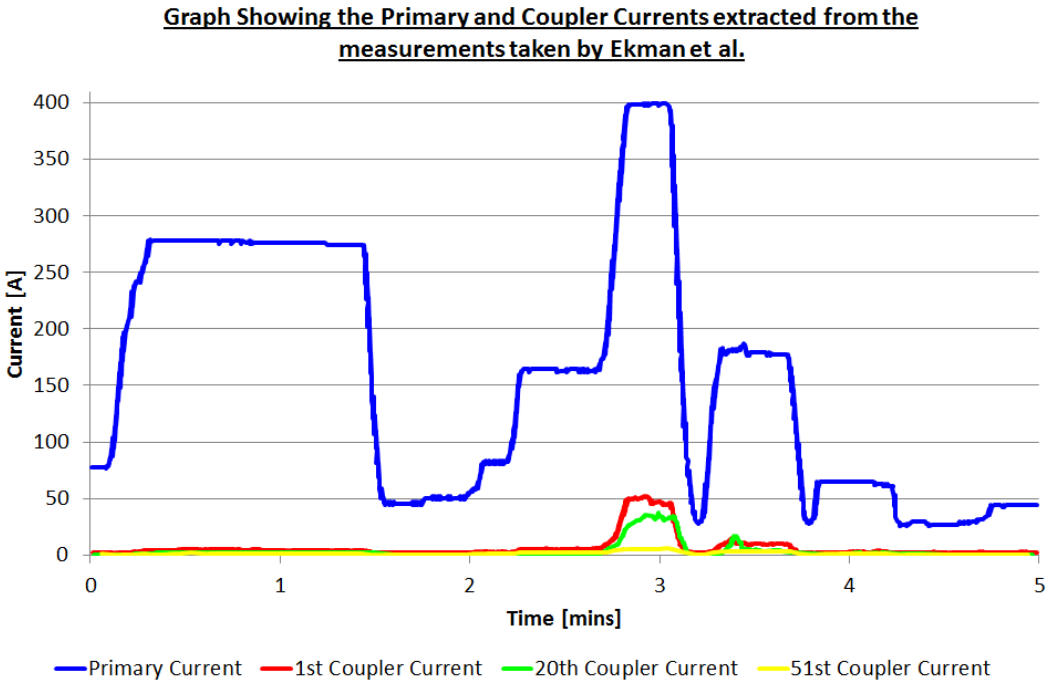


Figure 32: Graph showing the measurement results for line and coupler currents obtained by Ekman et al. during measurements in Sweden, extracted from [19].

The measurements were taken over a period of 5 minutes. During this time, two Auto Transformers were passed [19]. It is assumed, from the graphical data that these Auto Transformers were located at approximately 2 and 4 minutes respectively. Ekman et al. do not state where these Auto Transformers are located, however based on the coupler currents, these assumptions are made.

Ekman et al. also present a summary of the ratio of the 1st coupler current found in the measured trailing couplers.

Table 6: Table showing ratio of 1st coupler current in the 20th and 51st couplers during measurements performed by Ekman et al., extracted from [19]**.**

Coupler Number	Remaining Wagons	Percentage of 1st Coupler Current Expected	Percentage of 1st Coupler Current Experienced
1	52	100 %	100 %
20	33	63 %	74 %
51	2	3.85 %	10 %

These measurements presented by Ekman et al. will be used to verify the system model proposed in CHAPTER 4. The data comparison and model verification is presented in CHAPTER 8.

5.2 Transnet Freight Rail Measurements

As part of this research, wagon current measurements were performed using a revenue earning, in-service, coal train. The experimental method as well as explanations of the methods and equipment used to obtain these Transnet Freight Rail measurements can be found in APPENDIX E. The measurements were performed by the student as part of this research with the assistance of Transnet Freight Rail. For ease of reference, these measurements will be referred to as Transnet Freight Rail measurements.

The measurements were performed on the 5th of May 2015. The train departed from Ermelo depot at 10:45 and arrived at Richards Bay Coal Terminal at 22:40 [29].

The train number assigned for the trip was 4821 and the total load was 20 882 tons.

5.2.1 Train and Infrastructure configuration

The South African coal line operates from the coal mines north of Ermelo to Richards Bay Coal Terminal. The measurements taken were performed between Ermelo and Richards Bay Coal Terminal. This being said, only sections of data that are of interest are presented in this research.

The coal line operates significantly long trains consisting of 6 locomotives leading the train; with 200 wagons trailing the locomotive consist. The locomotives are each rated for a maximum power consumption of 3 MW. The wagons are rated at 21 tons/axle. The total length of the train is approximately 2.5 km.

The electrical supply to the locomotives is from electrical sub-stations spaced approximately 30 km apart [26]. The voltage at the sub-stations is 25 kV at 50 Hz. The use of Booster Transformers was employed on the Coal line.

5.2.2 Transducer locations

The test coach utilized during the measurements measured various signals from the locomotives, on-board systems and 1st wagon coupler current. Remote loggers were deployed to the 100th and 150th couplers. The measurement methodology is explained in more detail in APPENDIX E.

5.2.3 Measurement results

Once the measurements had been completed, the data was reviewed and a section of data was selected and extracted. The results of which can be seen in Figure 33.

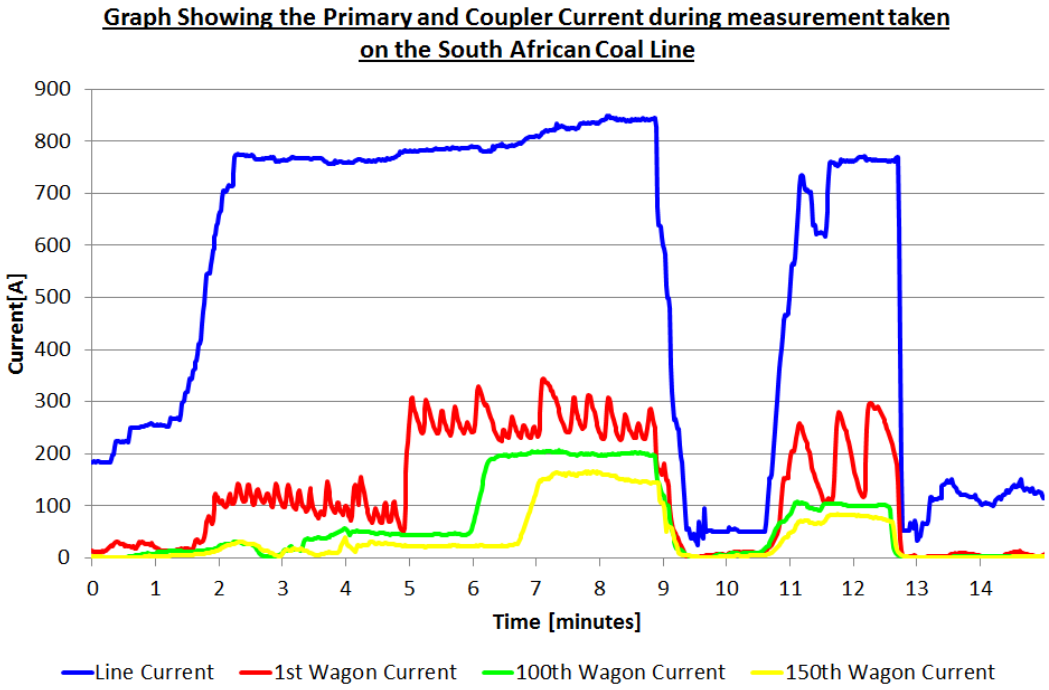


Figure 33: Graph showing the measurement results for line and coupler currents obtained during measurements on the South African Coal Line.

During the measurement period shown in Figure 33 the infrastructure affecting the current through the wagons was passed. The Coal line makes use of Booster Transformers which force the return current into the overhead return conductor [26], [30], [31].

The locomotive consist and leading wagon passed the Booster Transformer at approximately 5 minutes and thereafter the trailing wagons with the 100th wagon passing

at 6 minutes and the 150th wagon passing the Booster Transformer at approximately 6minutes and 45 seconds. This is seen in Figure 33 as each respective wagon coupler current increases directly after passing the Booster Transformer. This is a result of the direction of return current and whether the majority of current returns to the sub-station is in front of, or behind the train.

In comparison to Ekman et al., a summary of the ratio of the 1st coupler current found in the measured trailing couplers, as well as the percentage of total return current in presented in Table 7.

Table 7: Table showing ratio of 1st coupler current in the 100th and 150th couplers during measurements performed on the South African Coal Line.

Current	Remaining Wagons	Percentage of 1st Coupler Current Experienced	Percentage of Primary Current Experienced
Primary Current	200	318 %	100 %
1st Coupler	199	100 %	31 %
100th Coupler	100	75 %	24 %
150th Coupler	50	60 %	19 %

An additional observation that has been made from the measurements is that rail-to-mast bonds can be identified from the 1st coupler current. A pattern emerges such that the rail-to-mast bonds are located at each trough. This is where the return current has a low impedance connection to the overhead return conductor and hence the wagon current is small in comparison to when the rail-to-mast bond being some distance away.

Another observation that must be noted is the pattern seen on the 1st coupler current. Interestingly, the pattern is only found on the 1st coupler current. The pattern is missing from the primary current as well as the other coupler currents measured.

Before this research commenced, Transnet Freight Rail made observation of this pattern, and through investigations identified that the pattern was directly linked to the locations of the rail-to-mast bonds. In fact, defective bonds and their locations were identified to infrastructure maintenance personnel who performed independent investigations and repairs and confirmed that the identified bonds were defective.

Defective rail-to-mast bonds are identified by the typical periodicity of the pattern doubling. This means that if a rail-to-mast bond is defective or missing at a certain location, the current peak is normally higher than surrounding peaks and the troughs on either side of the high peak are approximately double the distance apart in comparison to

the other troughs. This can easily be seen if the 1st coupler current, as a percentage of the primary current, is plotted against distance. The reason for this is that any fluctuations in the primary current as a result of the driver handling of the train are reduced and that the rail-to-mast bonds are typically periodic. Plotting the data in this way allows for simpler interpretation. Taking an extract from the same data presented in Figure 63, the 1st coupler current as a percentage of the primary current of plotted against distance in Figure 34.

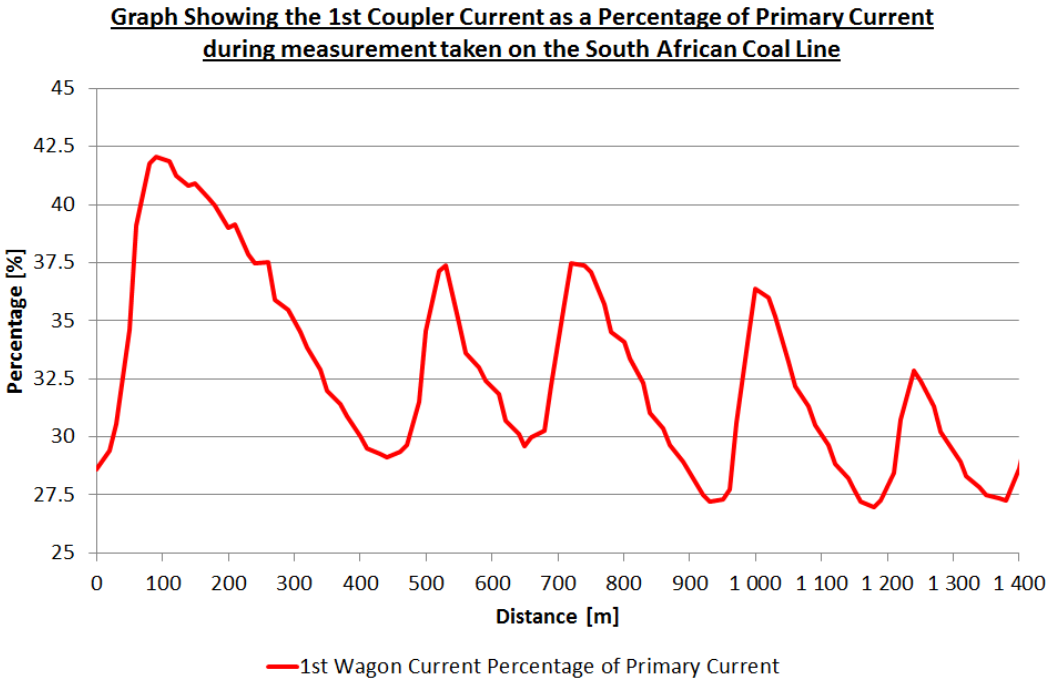


Figure 34: Graph showing the measurement results for the 1st coupler currents against distance, obtained during measurements on the South African Coal Line.

The first peak and its associated troughs can be seen to be higher than the proceeding peaks, and its troughs are spaced at a greater distance than the proceeding troughs in Figure 34. This is an indication that the rail-to-mast bond at this point is defective or missing.

These measurements taken on the South African Coal Line are used to test the system model proposed in CHAPTER 4. The data comparison and model verification is presented in CHAPTER 8.

CHAPTER 6
SIMULATION MODEL

The system model presented in CHAPTER 4 is imported into an electrical circuit simulation package for analysis, behavioral prediction and model verification.

The simulation package used in this research is LTSpice. LTSpice is freeware circuit simulation software which implements SPICE. LTSpice is developed and maintained by Linear Technology, a semi-conductor manufacturer.

It must be noted that although the LTSpice simulation package was utilized in this research, the system model developed in CHAPTER 4 can be imported to one of the many circuit simulation alternative software packages as so desired.

The system model is imported into LTSpice in two categories, namely the main circuit and sub circuits. This is done for modularity of the system model so that it may more easily be configured to different operating environments. These circuit categories will be elaborated in the sections that follow.

6.1 Main Simulation Circuit

The main circuit model is the starting point of the simulation. It contains all the simulation configurations and settings as well at the circuit which can easily be configured based on distance. Included in the main simulation circuit is the sub-station feeds subsequent to, and preceding the train as well as the locomotive consist. The individual wagons of the train, and the infrastructure in their vicinity, are included as sub-sub-circuits and are discussed in section 6.2.2.

The entire main simulation circuit model is illustrated in Figure 35 to give an overview of the circuit.

The sections contained in the main simulation circuit are the sub-station feeds, the modular wagons and the locomotive consist.

All of these sections are included in Figure 35 and can be identified, however in order to provide more details on each section, the sections will be individually discussed.

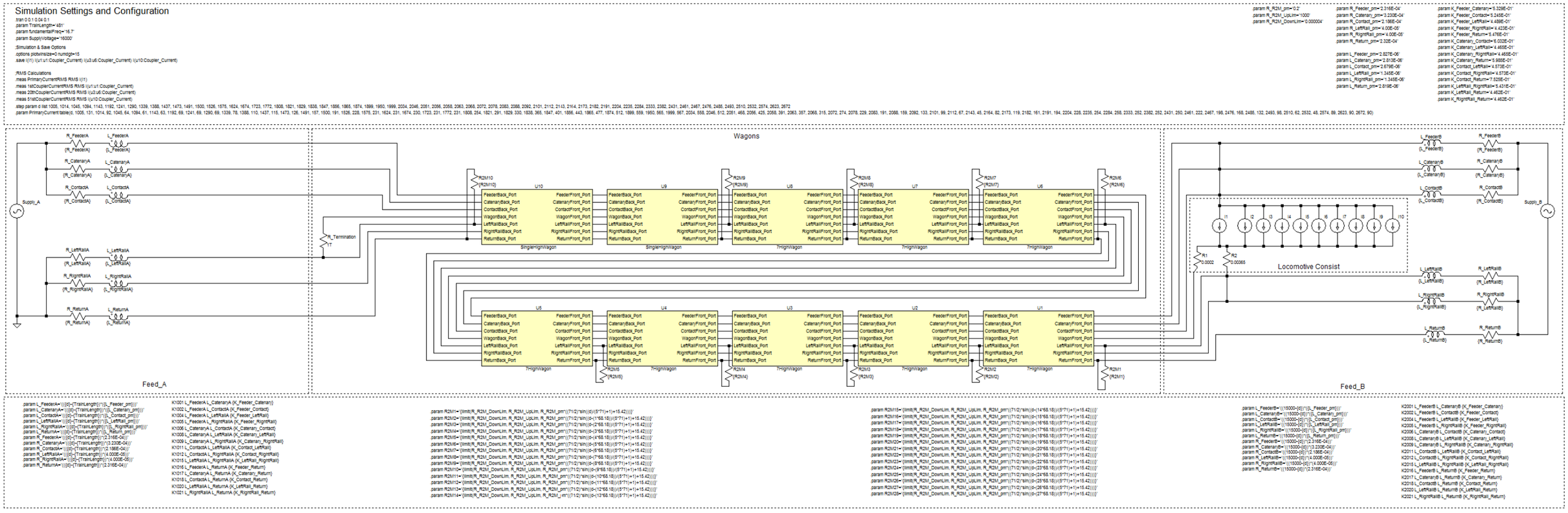


Figure 35: Simulation circuit diagram showing the main simulation circuit model in LTSpice.

6.1.1 Simulation Settings and Configuration

In order for the simulation package to perform the circuit simulation, the type of analysis, plotting options, saving options, measurement variables, stepping parameters and look up tables must be defined.

The stepping parameter is the distance which the train has travelled. This allows the simulation to be performed in distance intervals, whether periodic or not. Other parameters such as primary line current can then be defined at each distance in the form of a look up table.

Further, parameters common to components of the simulation are also initialized such as resistances per meter, inductances per meter and mutual conductance co-efficients. Figure 36 and Figure 37 illustrate the settings, configurations and initialization of parameters for the main simulation circuit.

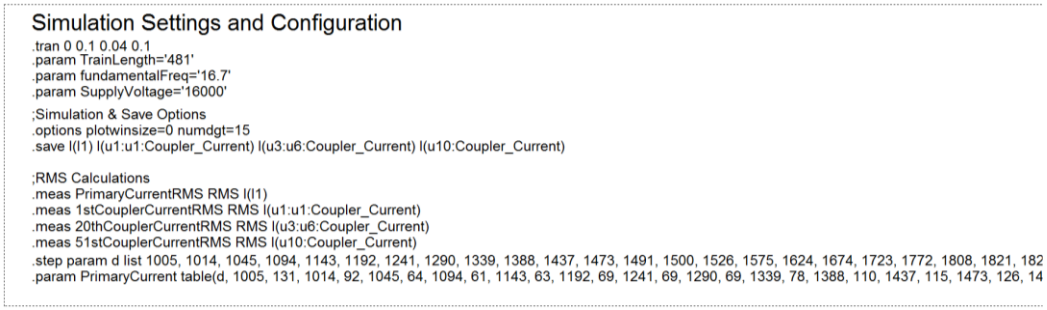


Figure 36: Figure showing the simulation settings and configuration for the main simulation circuit, extracted from Figure 35.

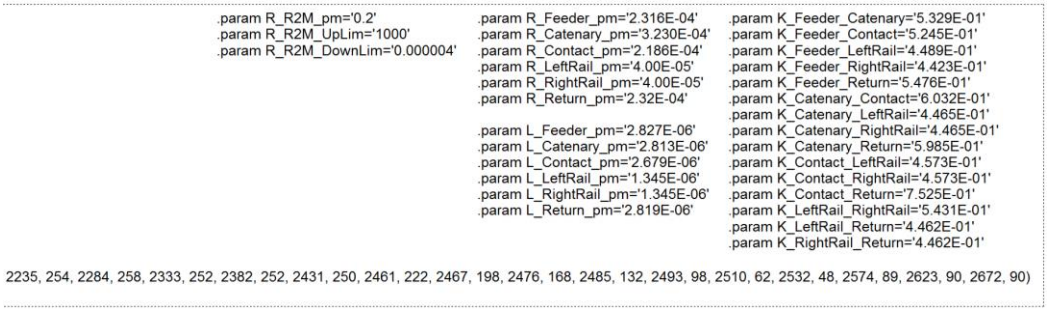


Figure 37: Figure showing the simulation settings and configuration for the main simulation circuit, extracted from Figure 35.

6.1.2 Infrastructure and Sub-Station Feeds

The supply feed from the sub-stations both subsequent to, and preceding the train, is included in the main simulation model. Due to their characteristics being defined by distance, they are modelled as lumped parameters. Figure 38 illustrates the circuit describing the power supply subsequent to the train while Figure 39 illustrates the power supply feed preceding the train. It should be noted that the characteristics of the models are determined by the stepped distance parameter "d".

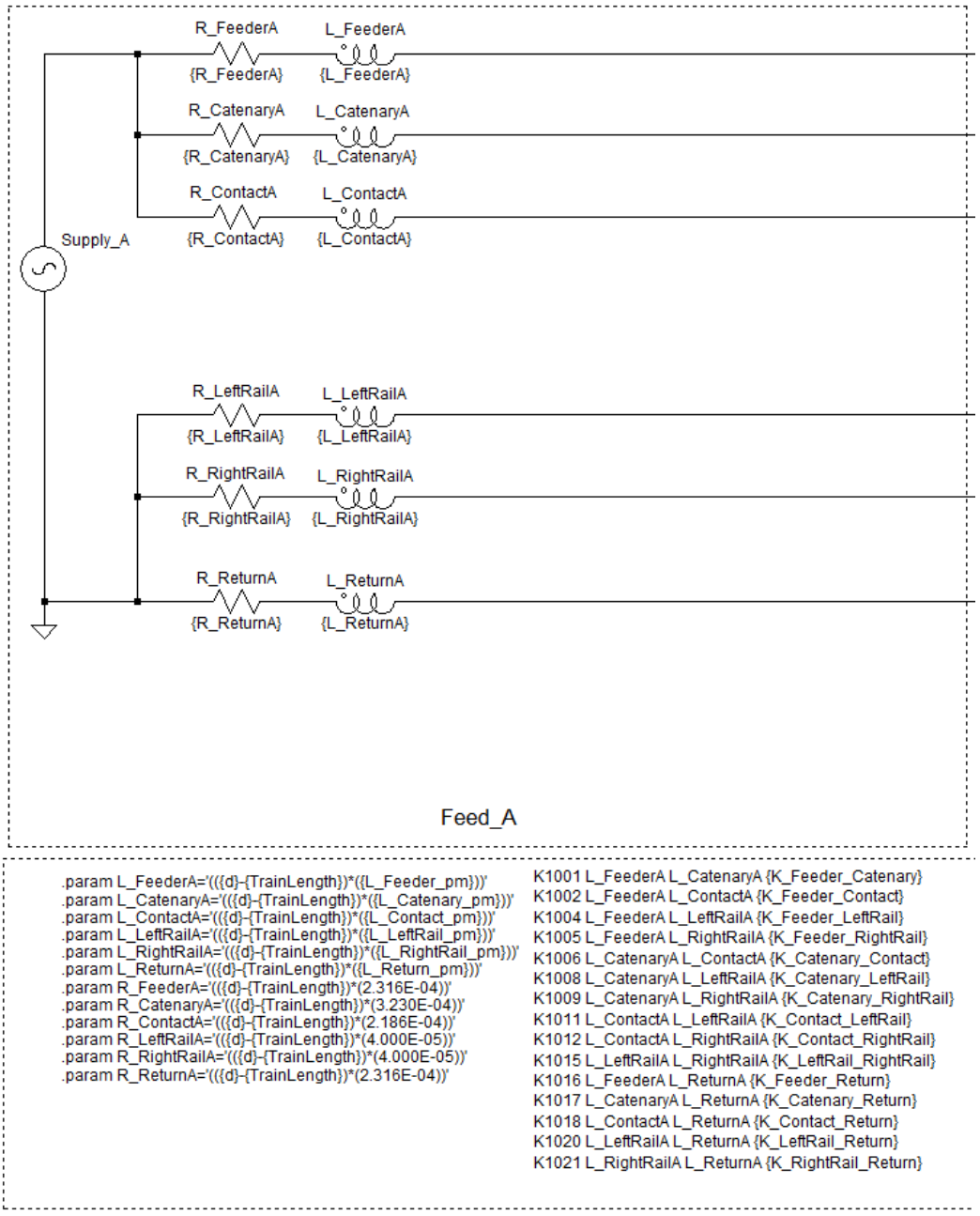


Figure 38: Figure showing the supply feed subsequent to the train for the main simulation circuit, extracted from Figure 35.

6.1.3 Locomotive Consist

The multiple source locomotive consist model which was developed in CHAPTER 4 is also illustrated in Figure 39. The model makes use of the defined fundamental frequency current source, with all harmonic sources as a proportional function of the fundamental.

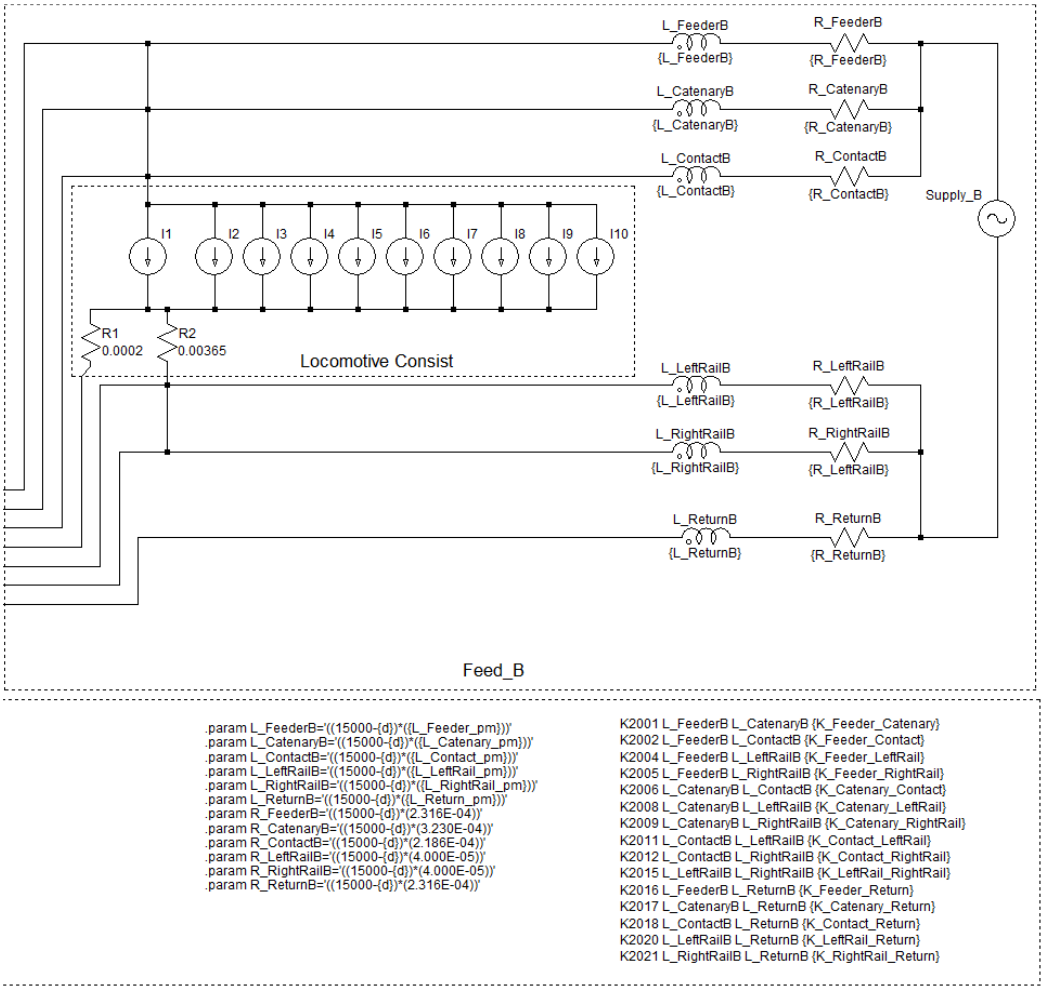


Figure 39: Figure showing the supply feed preceding the train as well as the locomotive consist for the main simulation circuit, extracted from Figure 35.

6.1.4 Wagons

Trains are configured based on operational requirements, thus differing trains will consist of different numbers of wagons. Thus the wagons are imported into the simulation package as sub-circuits.

For further simplification, individual wagons are grouped into sets equivalent to the distance between rail-to-mast bonds. Thus, each individual wagon is modelled as a sub-

sub-circuit, and each set of wagons between rail-to-mast bonds are modelled as sub-circuits. The set of sub-circuits that are included in the main simulation model are these wagon sets, illustrated in Figure 40.

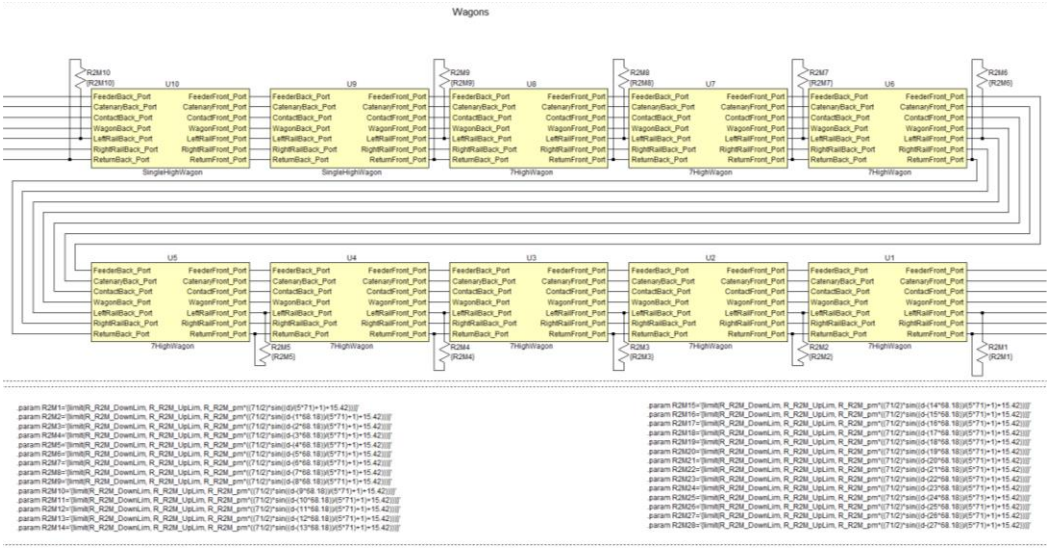


Figure 40: Figure showing the wagon sub-circuits for the main simulation circuit, extracted from Figure 35.

For reference purposes, the Spice Netlist for the Main Simulation Circuit can be found in APPENDIX F. This allows for simpler importation into other Spice based simulation packages as well as the ability to modify parameters and configurations, should the reader so wish.

6.2 Simulation Sub-Circuits

The simulation model presented in this chapter makes use of sub-circuits. Two sub-circuits are used extensively. The first is the wagon set sub-circuits which is in essence groups of the individual wagon sub-sub-circuits.

6.2.1 Wagon Set Sub-Circuits

The wagon simulation sets are defined by the distance between rail-to-mast bonds. In the case of this research this equates to approximately 7 wagons. Thus 7 individual wagon sub-sub-circuits are included in the wagon simulation set sub-circuit. Figure 41 illustrates the 7 individual wagons creating the wagon set sub-circuit.

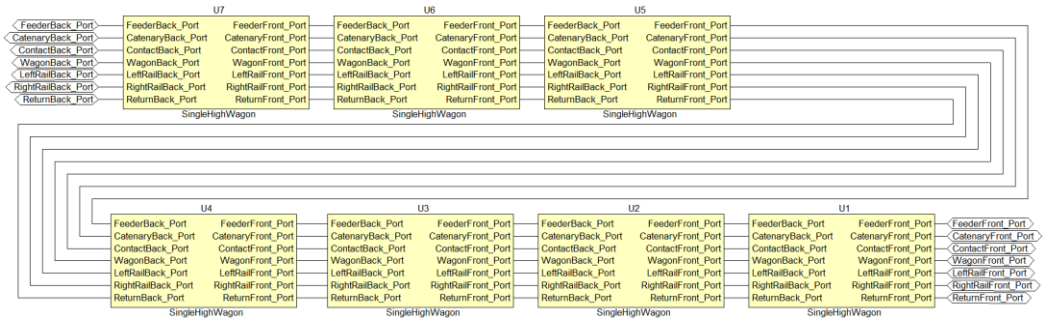


Figure 41: Figure showing the wagon set sub-circuits to be included in the main simulation circuit.

For reference purposes, the Spice Netlist for the wagon simulation set sub-circuit can be found in APPENDIX F. This allows for simpler importation into other Spice based simulation packages as well as the ability to modify parameters and configurations should the reader so wish.

6.2.2 Individual Wagon Sub-Sub-Circuit

Each individual wagon model, as developed in CHAPTER 4, is imported into the circuit simulation package as a sub-sub-circuit. The simulation model includes the infrastructure in the vicinity of the wagon so as to include mutual couplings with infrastructure. This can be seen in Figure 42.

The individual wagon model is sectioned between the nodes of the couplers and the axles. The resistance and inductance parameters are then defined as parameters as a function of the physical distances between the nodes [28], [32], [33].

Initially, per meter quantities are configured, thereafter each element is defined as a function of the distance between nodes and their relevant per meter quantities.

The sub-sub-circuit interfaces with the parent circuit though the use of ports. The front ports on the individual wagon sub-sub-circuit are the front feeder, front catenary, front contact, front coupler, front left rail, front right rail and front return. The back ports on the individual wagon sub-sub-circuit are the back feeder, back catenary, back contact, back coupler, back left rail, back right rail and back return.

For reference purposes, the Spice Netlist for the individual wagon sub-sub-circuit can be found in APPENDIX F. This allows for simpler importation into other Spice based simulation packages as well as the ability to modify parameters and configurations should the reader so wish.

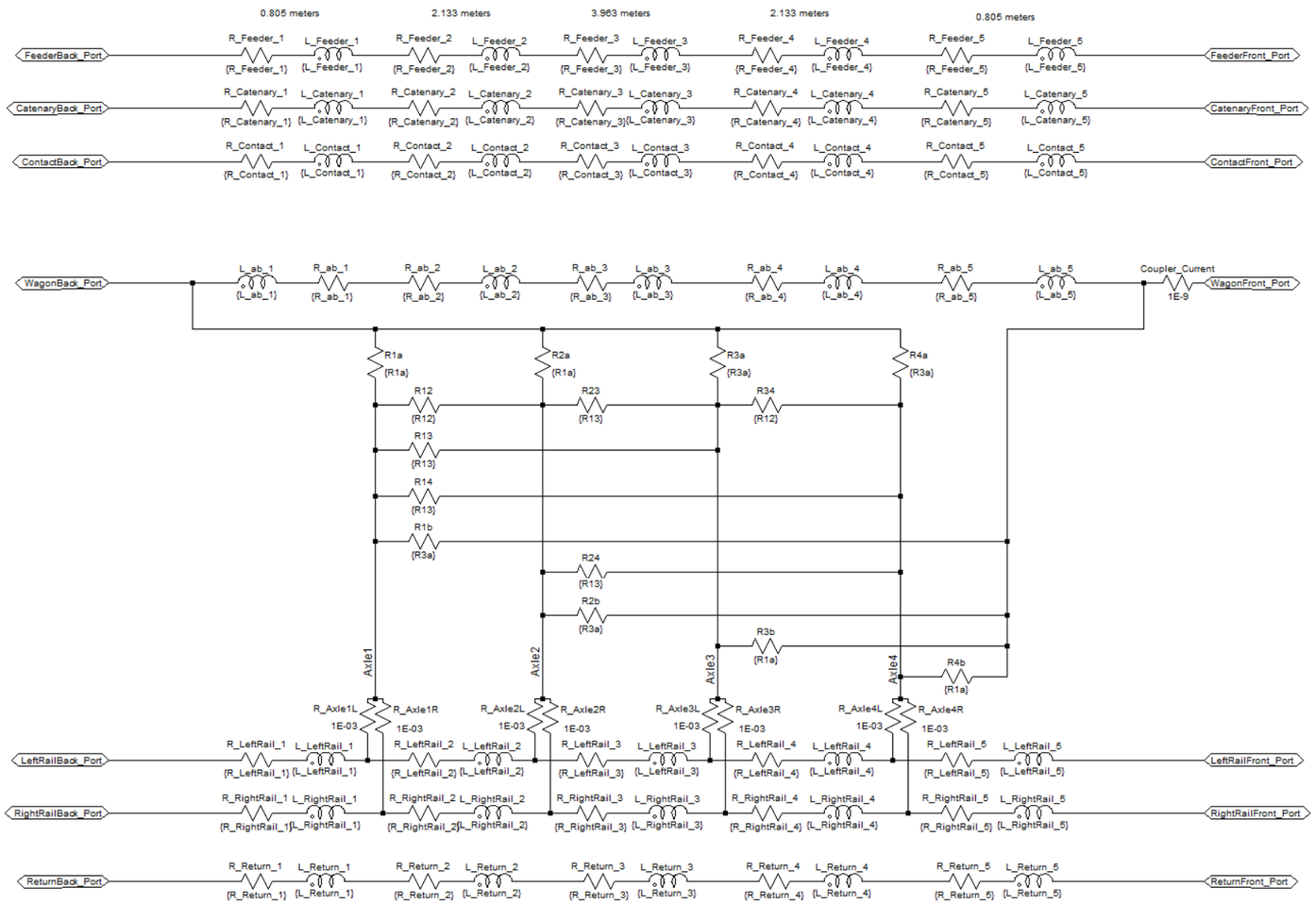
Parameter Configuration

```
.param Rab='0.003'
.param R1a='125'
.param R12='1200'
.param R13='1200'
.param R3a='125'


.param R_Feeder_pm='2.316E-04'
.param R_Catenary_pm='3.230E-04'
.param R_Contact_pm='2.186E-04'
.param R_ab_pm='{Rab}/9.034'
.param R_LeftRail_pm='4.00E-05'
.param R_RightRail_pm='4.00E-05'
.param R_Return_pm='2.32E-04'

.param L_Feeder_pm='2.827E-06'
.param L_Catenary_pm='2.813E-06'
.param L_Contact_pm='2.679E-06'
.param L_ab_pm='1.996E-06'
.param L_LeftRail_pm='1.345E-06'
.param L_RightRail_pm='1.345E-06'
.param L_Return_pm='2.819E-06'

.param K_Feeder_Catenary='5.329E-01'
.param K_Feeder_Contact='5.245E-01'
.param K_Feeder_ab='5.447E-01'
.param K_Feeder_LeftRail='4.489E-01'
.param K_Feeder_RightRail='4.423E-01'
.param K_Feeder_Return='5.476E-01'
.param K_Catenary_Contact='6.032E-01'
.param K_Catenary_ab='5.716E-01'
.param K_Catenary_LeftRail='4.465E-01'
.param K_Catenary_RightRail='4.465E-01'
.param K_Catenary_Return='5.985E-01'
.param K_Contact_ab='6.074E-01'
.param K_Contact_LeftRail='4.573E-01'
.param K_Contact_RightRail='4.573E-01'
.param K_Contact_Return='7.525E-01'
.param K_ab_LeftRail='5.287E-01'
.param K_ab_RightRail='5.287E-01'
.param K_ab_Return='3.621E-01'
.param K_LeftRail_RightRail='5.431E-01'
.param K_LeftRail_Return='4.462E-01'
.param K_RightRail_Return='4.462E-01'
```




```
.param Dist_1='0.805'

.param L_Feeder_1='({Dist_1}*{L_Feeder_pm})'
.param L_Catenary_1='({Dist_1}*{L_Catenary_pm})'
.param L_Contact_1='({Dist_1}*{L_Contact_pm})'
.param L_ab_1='({Dist_1}*{L_ab_pm})'
.param L_LeftRail_1='({Dist_1}*{L_LeftRail_pm})'
.param L_RightRail_1='({Dist_1}*{L_RightRail_pm})'
.param L_Return_1='({Dist_1}*{L_Return_pm})'

.param R_Feeder_1='{Dist_1}*{R_Feeder_pm}'
.param R_Catenary_1='{Dist_1}*{R_Catenary_pm}'
.param R_Contact_1='{Dist_1}*{R_Contact_pm}'
.param R_ab_1='{Dist_1}*{R_ab_pm}'
.param R_LeftRail_1='{Dist_1}*{R_LeftRail_pm}'
.param R_RightRail_1='{Dist_1}*{R_RightRail_pm}'
.param R_Return_1='{Dist_1}*{R_Return_pm}'

K1001 L_Feeder_1 L_Catenary_1 {K_Feeder_Catenary}
K1002 L_Feeder_1 L_Contact_1 {K_Feeder_Contact}
K1003 L_Feeder_1 L_ab_1 {K_Feeder_ab}
K1004 L_Feeder_1 L_LeftRail_1 {K_Feeder_LeftRail}
K1005 L_Feeder_1 L_RightRail_1 {K_Feeder_RightRail}
K1006 L_Feeder_1 L_Return_1 {K_Feeder_Return}
K1007 L_Catenary_1 L_Contact_1 {K_Catenary_Contact}
K1008 L_Catenary_1 L_ab_1 {K_Catenary_ab}
K1009 L_Catenary_1 L_LeftRail_1 {K_Catenary_LeftRail}
K1010 L_Catenary_1 L_RightRail_1 {K_Catenary_RightRail}
K1011 L_Catenary_1 L_Return_1 {K_Catenary_Return}
K1012 L_Contact_1 L_ab_1 {K_Contact_ab}
K1013 L_Contact_1 L_LeftRail_1 {K_Contact_LeftRail}
K1014 L_Contact_1 L_RightRail_1 {K_Contact_RightRail}
K1015 L_Contact_1 L_Return_1 {K_Contact_Return}
K1016 L_ab_1 L_LeftRail_1 {K_ab_LeftRail}
K1017 L_ab_1 L_RightRail_1 {K_ab_RightRail}
K1018 L_ab_1 L_Return_1 {K_ab_Return}
K1019 L_LeftRail_1 L_RightRail_1 {K_LeftRail_RightRail}
K1020 L_LeftRail_1 L_Return_1 {K_LeftRail_Return}
K1021 L_RightRail_1 L_Return_1 {K_RightRail_Return}
```

```
.param Dist_2='2.133'

.param L_Feeder_2='({Dist_2}*{L_Feeder_pm})'
.param L_Catenary_2='({Dist_2}*{L_Catenary_pm})'
.param L_Contact_2='({Dist_2}*{L_Contact_pm})'
.param L_ab_2='({Dist_2}*{L_ab_pm})'
.param L_LeftRail_2='({Dist_2}*{L_LeftRail_pm})'
.param L_RightRail_2='({Dist_2}*{L_RightRail_pm})'
.param L_Return_2='({Dist_2}*{L_Return_pm})'

.param R_Feeder_2='{Dist_2}*{R_Feeder_pm}'
.param R_Catenary_2='{Dist_2}*{R_Catenary_pm}'
.param R_Contact_2='{Dist_2}*{R_Contact_pm}'
.param R_ab_2='{Dist_2}*{R_ab_pm}'
.param R_LeftRail_2='{Dist_2}*{R_LeftRail_pm}'
.param R_RightRail_2='{Dist_2}*{R_RightRail_pm}'
.param R_Return_2='{Dist_2}*{R_Return_pm}'

K2001 L_Feeder_2 L_Catenary_2 {K_Feeder_Catenary}
K2002 L_Feeder_2 L_Contact_2 {K_Feeder_Contact}
K2003 L_Feeder_2 L_ab_2 {K_Feeder_ab}
K2004 L_Feeder_2 L_LeftRail_2 {K_Feeder_LeftRail}
K2005 L_Feeder_2 L_RightRail_2 {K_Feeder_RightRail}
K2006 L_Feeder_2 L_Return_2 {K_Feeder_Return}
K2007 L_Catenary_2 L_Contact_2 {K_Catenary_Contact}
K2008 L_Catenary_2 L_ab_2 {K_Catenary_ab}
K2009 L_Catenary_2 L_LeftRail_2 {K_Catenary_LeftRail}
K2010 L_Catenary_2 L_RightRail_2 {K_Catenary_RightRail}
K2011 L_Catenary_2 L_Return_2 {K_Catenary_Return}
K2012 L_Contact_2 L_ab_2 {K_Contact_ab}
K2013 L_Contact_2 L_LeftRail_2 {K_Contact_LeftRail}
K2014 L_Contact_2 L_RightRail_2 {K_Contact_RightRail}
K2015 L_Contact_2 L_Return_2 {K_Contact_Return}
K2016 L_ab_2 L_LeftRail_2 {K_ab_LeftRail}
K2017 L_ab_2 L_RightRail_2 {K_ab_RightRail}
K2018 L_ab_2 L_Return_2 {K_ab_Return}
K2019 L_LeftRail_2 L_RightRail_2 {K_LeftRail_RightRail}
K2020 L_LeftRail_2 L_Return_2 {K_LeftRail_Return}
K2021 L_RightRail_2 L_Return_2 {K_RightRail_Return}
```

```
.param Dist_3='3.963'

.param L_Feeder_3='({Dist_3}*{L_Feeder_pm})'
.param L_Catenary_3='({Dist_3}*{L_Catenary_pm})'
.param L_Contact_3='({Dist_3}*{L_Contact_pm})'
.param L_ab_3='({Dist_3}*{L_ab_pm})'
.param L_LeftRail_3='({Dist_3}*{L_LeftRail_pm})'
.param L_RightRail_3='({Dist_3}*{L_RightRail_pm})'
.param L_Return_3='({Dist_3}*{L_Return_pm})'

.param R_Feeder_3='{Dist_3}*{R_Feeder_pm}'
.param R_Catenary_3='{Dist_3}*{R_Catenary_pm}'
.param R_Contact_3='{Dist_3}*{R_Contact_pm}'
.param R_ab_3='{Dist_3}*{R_ab_pm}'
.param R_LeftRail_3='{Dist_3}*{R_LeftRail_pm}'
.param R_RightRail_3='{Dist_3}*{R_RightRail_pm}'
.param R_Return_3='{Dist_3}*{R_Return_pm}'

K3001 L_Feeder_3 L_Catenary_3 {K_Feeder_Catenary}
K3002 L_Feeder_3 L_Contact_3 {K_Feeder_Contact}
K3003 L_Feeder_3 L_ab_3 {K_Feeder_ab}
K3004 L_Feeder_3 L_LeftRail_3 {K_Feeder_LeftRail}
K3005 L_Feeder_3 L_RightRail_3 {K_Feeder_RightRail}
K3006 L_Feeder_3 L_Return_3 {K_Feeder_Return}
K3007 L_Catenary_3 L_Contact_3 {K_Catenary_Contact}
K3008 L_Catenary_3 L_ab_3 {K_Catenary_ab}
K3009 L_Catenary_3 L_LeftRail_3 {K_Catenary_LeftRail}
K3010 L_Catenary_3 L_RightRail_3 {K_Catenary_RightRail}
K3011 L_Catenary_3 L_Return_3 {K_Catenary_Return}
K3012 L_Contact_3 L_ab_3 {K_Contact_ab}
K3013 L_Contact_3 L_LeftRail_3 {K_Contact_LeftRail}
K3014 L_Contact_3 L_RightRail_3 {K_Contact_RightRail}
K3015 L_Contact_3 L_Return_3 {K_Contact_Return}
K3016 L_ab_3 L_LeftRail_3 {K_ab_LeftRail}
K3017 L_ab_3 L_RightRail_3 {K_ab_RightRail}
K3018 L_ab_3 L_Return_3 {K_ab_Return}
K3019 L_LeftRail_3 L_RightRail_3 {K_LeftRail_RightRail}
K3020 L_LeftRail_3 L_Return_3 {K_LeftRail_Return}
K3021 L_RightRail_3 L_Return_3 {K_RightRail_Return}
```

```
.param Dist_4='2.133'

.param L_Feeder_4='({Dist_4}*{L_Feeder_pm})'
.param L_Catenary_4='({Dist_4}*{L_Catenary_pm})'
.param L_Contact_4='({Dist_4}*{L_Contact_pm})'
.param L_ab_4='({Dist_4}*{L_ab_pm})'
.param L_LeftRail_4='({Dist_4}*{L_LeftRail_pm})'
.param L_RightRail_4='({Dist_4}*{L_RightRail_pm})'
.param L_Return_4='({Dist_4}*{L_Return_pm})'

.param R_Feeder_4='{Dist_4}*{R_Feeder_pm}'
.param R_Catenary_4='{Dist_4}*{R_Catenary_pm}'
.param R_Contact_4='{Dist_4}*{R_Contact_pm}'
.param R_ab_4='{Dist_4}*{R_ab_pm}'
.param R_LeftRail_4='{Dist_4}*{R_LeftRail_pm}'
.param R_RightRail_4='{Dist_4}*{R_RightRail_pm}'
.param R_Return_4='{Dist_4}*{R_Return_pm}'

K4001 L_Feeder_4 L_Catenary_4 {K_Feeder_Catenary}
K4002 L_Feeder_4 L_Contact_4 {K_Feeder_Contact}
K4003 L_Feeder_4 L_ab_4 {K_Feeder_ab}
K4004 L_Feeder_4 L_LeftRail_4 {K_Feeder_LeftRail}
K4005 L_Feeder_4 L_RightRail_4 {K_Feeder_RightRail}
K4006 L_Feeder_4 L_Return_4 {K_Feeder_Return}
K4007 L_Catenary_4 L_Contact_4 {K_Catenary_Contact}
K4008 L_Catenary_4 L_ab_4 {K_Catenary_ab}
K4009 L_Catenary_4 L_LeftRail_4 {K_Catenary_LeftRail}
K4010 L_Catenary_4 L_RightRail_4 {K_Catenary_RightRail}
K4011 L_Catenary_4 L_Return_4 {K_Catenary_Return}
K4012 L_Contact_4 L_ab_4 {K_Contact_ab}
K4013 L_Contact_4 L_LeftRail_4 {K_Contact_LeftRail}
K4014 L_Contact_4 L_RightRail_4 {K_Contact_RightRail}
K4015 L_Contact_4 L_Return_4 {K_Contact_Return}
K4016 L_ab_4 L_LeftRail_4 {K_ab_LeftRail}
K4017 L_ab_4 L_RightRail_4 {K_ab_RightRail}
K4018 L_ab_4 L_Return_4 {K_ab_Return}
K4019 L_LeftRail_4 L_RightRail_4 {K_LeftRail_RightRail}
K4020 L_LeftRail_4 L_Return_4 {K_LeftRail_Return}
K4021 L_RightRail_4 L_Return_4 {K_RightRail_Return}
```

```
.param Dist_5='2.133'

.param L_Feeder_5='({Dist_5}*{L_Feeder_pm})'
.param L_Catenary_5='({Dist_5}*{L_Catenary_pm})'
.param L_Contact_5='({Dist_5}*{L_Contact_pm})'
.param L_ab_5='({Dist_5}*{L_ab_pm})'
.param L_LeftRail_5='({Dist_5}*{L_LeftRail_pm})'
.param L_RightRail_5='({Dist_5}*{L_RightRail_pm})'
.param L_Return_5='({Dist_5}*{L_Return_pm})'

.param R_Feeder_5='{Dist_5}*{R_Feeder_pm}'
.param R_Catenary_5='{Dist_5}*{R_Catenary_pm}'
.param R_Contact_5='{Dist_5}*{R_Contact_pm}'
.param R_ab_5='{Dist_5}*{R_ab_pm}'
.param R_LeftRail_5='{Dist_5}*{R_LeftRail_pm}'
.param R_RightRail_5='{Dist_5}*{R_RightRail_pm}'
.param R_Return_5='{Dist_5}*{R_Return_pm}'

K5001 L_Feeder_5 L_Catenary_5 {K_Feeder_Catenary}
K5002 L_Feeder_5 L_Contact_5 {K_Feeder_Contact}
K5003 L_Feeder_5 L_ab_5 {K_Feeder_ab}
K5004 L_Feeder_5 L_LeftRail_5 {K_Feeder_LeftRail}
K5005 L_Feeder_5 L_RightRail_5 {K_Feeder_RightRail}
K5006 L_Feeder_5 L_Return_5 {K_Feeder_Return}
K5007 L_Catenary_5 L_Contact_5 {K_Catenary_Contact}
K5008 L_Catenary_5 L_ab_5 {K_Catenary_ab}
K5009 L_Catenary_5 L_LeftRail_5 {K_Catenary_LeftRail}
K5010 L_Catenary_5 L_RightRail_5 {K_Catenary_RightRail}
K5011 L_Catenary_5 L_Return_5 {K_Catenary_Return}
K5012 L_Contact_5 L_ab_5 {K_Contact_ab}
K5013 L_Contact_5 L_LeftRail_5 {K_Contact_LeftRail}
K5014 L_Contact_5 L_RightRail_5 {K_Contact_RightRail}
K5015 L_Contact_5 L_Return_5 {K_Contact_Return}
K5016 L_ab_5 L_LeftRail_5 {K_ab_LeftRail}
K5017 L_ab_5 L_RightRail_5 {K_ab_RightRail}
K5018 L_ab_5 L_Return_5 {K_ab_Return}
K5019 L_LeftRail_5 L_RightRail_5 {K_LeftRail_RightRail}
K5020 L_LeftRail_5 L_Return_5 {K_LeftRail_Return}
K5021 L_RightRail_5 L_Return_5 {K_RightRail_Return}
```

Figure 42: Figure showing the individual wagon sub-sub-circuits to be included in the wagon set sub-circuit.

CHAPTER 7
SIMULATION MODEL DATA

The simulation model is described in CHAPTER 6. In order to make use of this model for any purposes, it needs to be verified against the measured results as presented in CHAPTER 5.

Following the verification of the simulated model, the model can be used to predict current levels in couplers based on differing conditions.

7.1 Simulated Model Verification

7.1.1 Ekman et al. Measurements

Swedish railway operators have conducted a high level study into the current through the couplers of their iron ore trains [19]. The measurements which Ekman et al. presented, as well as the train configuration are described in CHAPTER 5.

The simulation model was configured to match the description of the measurement conditions provided by Ekman et al. [19]. Once the simulation model configuration was completed as far as possible, the simulation was allowed to run in order to predict the coupler currents through the train.

Following the completion of the simulation, the simulated data and the measured data could be compared to act as confirmation that the simulation model indeed predicts the coupler currents within explainable reason to the measured data.

The measured primary current from Ekman et al.'s data was first programmed into the simulation parameters. Figure 43 shows the comparison between the Ekman et al. measured primary current and the simulated primary current. These values are plotted as root-mean-square Amperes.

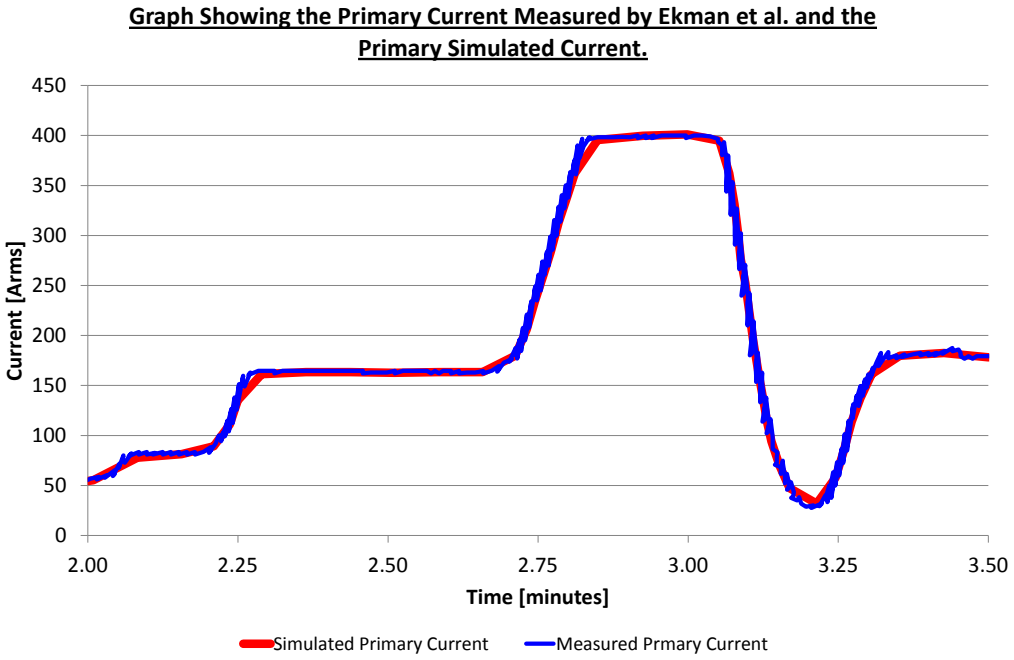


Figure 43: Graph showing the Ekman et al. measured primary current and the simulated primary current.

Figure 43 shows that the simulated primary current closely replicates the measured values.

The 1st coupler current which was measured by Ekman et al. is plotted against the simulated 1st coupler current in Figure 44. It can be seen that the measured current is somewhat erratic however it holds an average value proportional to the simulated primary current.

Various other factors which could affect the measured 1st coupler current such as in-train dynamic forces, irregular track conditions as well, as others cannot be considered due to the limited information provided by Ekman et al. [19].

The limited configuration information from Ekman et al. is an important point to recognize, as the simulation model cannot be verified with absolute certainty, however a degree of confidence in the model behavior can be achieved.

Taking this into consideration, it can be seen that the simulated data for the 1st coupler current follows the general trend and peak magnitude of the measured 1st coupler current.

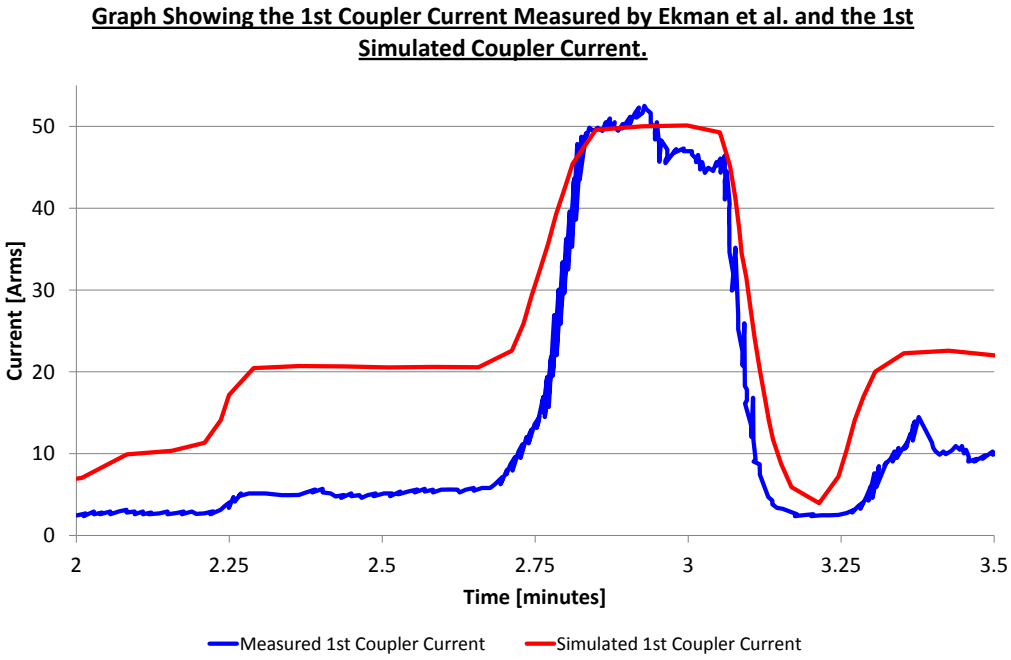


Figure 44: Graph showing the Ekman et al. measured 1st coupler current and the simulated 1st coupler current.

It should also be noted that the simulated 1st coupler current at 2.5 minutes is approximately 43% of the peak current value at 3 minutes. This correlates to the change in primary current in Figure 43. The simulation model is linear and this result proves this, however the discrepancy between simulated and measured 1st coupler current indicates that there was some non-linear effect on the measured current. Unfortunately due to the limited information regarding the measurements, this cannot be further investigated.

Similarly, the 20th coupler current which was measured by Ekman et al. is plotted against the simulated 20th coupler current in Figure 45. As with the 1st coupler current, it can be seen that the measured 20th coupler current is somewhat erratic however it holds an average value proportional to the measured primary current. Again, Ekman et al. [19] provide very little infrastructure configuration information and so the observations made in the simulation could very well be affected by unknown parameters.

The general trend and peak magnitude of the measured 20th coupler current is matched by the simulated 20th coupler current in Figure 45.

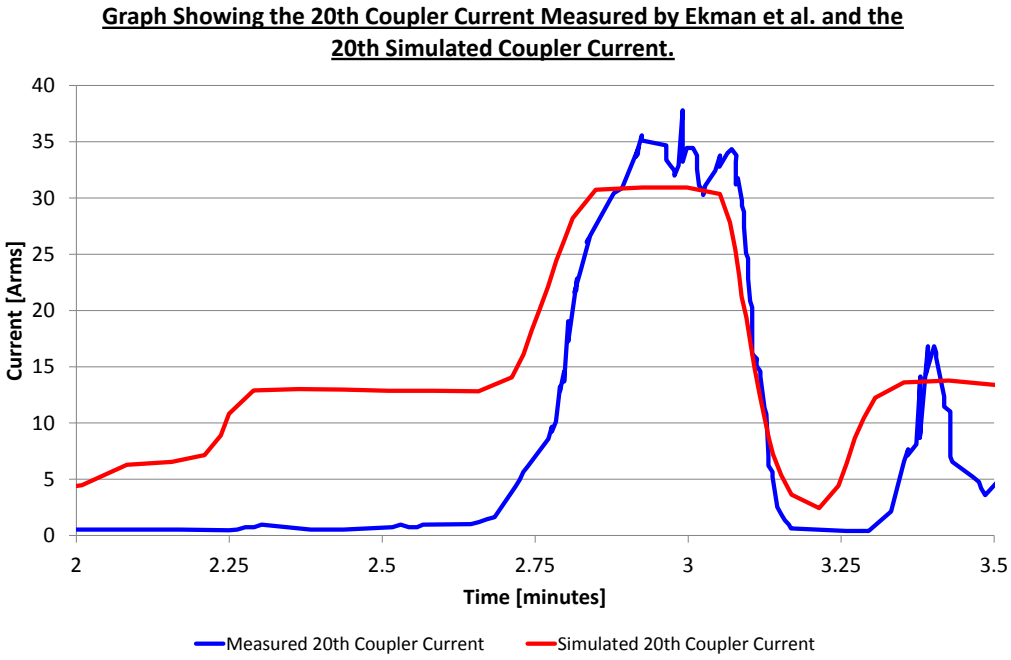


Figure 45: Graph showing the Ekman et al. measured 20th coupler current and the simulated 20th coupler current.

Again, the simulated 20th coupler current at 2.5 minutes is approximately 43% of the peak current value at 3 minutes. This correlates to the change in primary current in Figure 43. This is due to the linearity of the simulation model; however the discrepancy between simulated and measured 20th coupler current indicates was a non-linear effect on the measured current. This cannot be further investigated due to the limited information regarding the measurements provided by Ekman et al.

Finally, the comparison of the 51st coupler current measured by Ekman et al. to the simulated 51st coupler current is provided in Figure 46. The simulated 51st coupler current is seen to closely mimic the measured 51st coupler current with exception of small deviations.

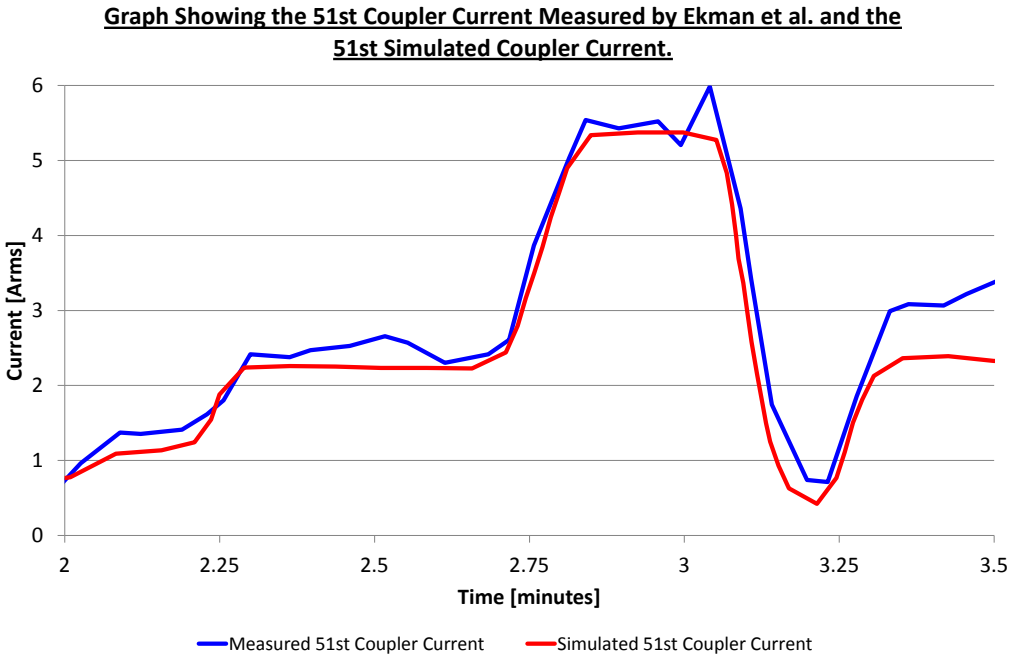


Figure 46: Graph showing the Ekman et al. measured 51st coupler current and the simulated 51st coupler current.

Table 8 and Table 9 make comparison of the coupler currents as a percentage of the 1st coupler current and the primary current respectively. This compares the coupler currents obtained from the Ekman et al. measurements to the simulated coupler currents.

Table 8: Table showing ratio of 1st coupler current in the 20th and 51st couplers during measurements performed by Ekman et al. in comparison to simulated data, extracted from [19].

Coupler Number	Remaining Wagons	Percentage of 1st Coupler Current Measured	Percentage of 1st Coupler Current Simulated
1	52	100 %	100 %
20	33	74 %	64.27 %
51	2	10 %	11.16 %

Table 9: Table showing ratio of primary current in the 1st, 20th and 51st couplers during measurements performed by Ekman et al. in comparison to simulated data, extracted from [19].

Coupler Number	Remaining Wagons	Percentage of Primary Current Measured	Percentage of Primary Current Simulated
1	52	12.71%	12.91 %
20	33	9.29 %	8.30 %
51	2	1.38 %	1.44 %

As can be seen from the simulation results presented in section 7.1.1, the simulation model data reflects similar results to those measured by Ekman et al. With more details surrounding the Ekman et al. measurements the simulation could be refined to produce more accurate results. This being said the simulation results demonstrate that the simulation model sufficiently represents the Ekman coupler current measurements and thus gives confidence in the model.

For reference, the wagon parameters that were used in the simulation to obtain the simulated data are presented below:

- $R_{ab} = 0.006\Omega$
- $R_{1a} = 1.7\Omega$
- $R_{12} = 10\Omega$
- $R_{13} = 10\Omega$
- $R_{3a} = 1.7\Omega$

These values were obtained through iterating the simulation with various parameter values until the configuration resulted in the Ekman et al. measured results. This method of parameter determination was necessary as the paper by Ekman et al. [19] does not provide actual wagon details.

7.1.2 Transnet Freight Rail Measurements

The measurements results obtained by Transnet Freight Rail are described in CHAPTER 5 of this research document.

The simulation model was configured to match the description of the measurement conditions that were experienced during the Transnet Freight Rail measurements. Once the simulation model configuration was completed, the simulation was allowed to run in order to predict the coupler currents through the train.

Following the completion of the simulation, the simulated data and the measured data was compared to act as verification that the simulation model indeed predicts the coupler currents within explainable reason to the measured data.

The measured primary current from the Transnet Freight Rail measurements was programmed into the simulation parameters. Figure 47 shows the comparison between the Transnet Freight Rail measured primary current and the simulated primary current. These values are plotted as root-mean-square Amperes.

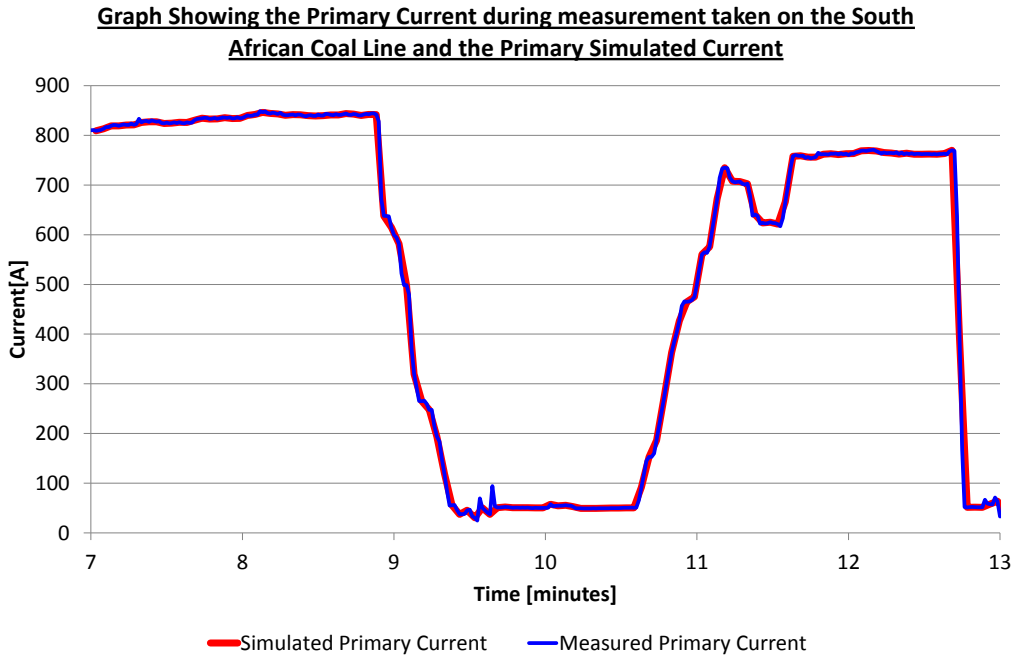


Figure 47: Graph showing the Transnet measured primary current and the simulated primary current.

Figure 47 shows that the simulated primary current closely replicates the measured values.

The 1st coupler current which was measured by Transnet Freight Rail is plotted against the simulated 1st coupler current in Figure 48.

It can be seen that the simulated current has an average value close to that of the measured primary current. Various other factors which could affect the measured 1st coupler current such as in-train dynamic forces and irregular track conditions as well as others were not considered when the measurements took place as the measurements were performed on an in-service train. This means that the train could not be stopped in a remote area to investigate the track and other conditions as this would cause a delay in train operations and loss in revenue.

Taking this into consideration, it can be seen that the simulated data for the 1st coupler current follows the general trend of the measured 1st coupler current.

It must also be noted that the simulated rail-to-mast bonds do not have the anticipated effect on the simulated data. This is a possible indication that the modelling of the rail-to-mast bonds is not simply a resistive effect, but also entails more complex and possibly non-linear characteristics. Further in-depth research into the rail-to-mast bonds and their interaction with the surrounding electrical infrastructure would be required to provide a more accurate rail-to-mast bond model. This further investigation does not fall within the scope of this research.

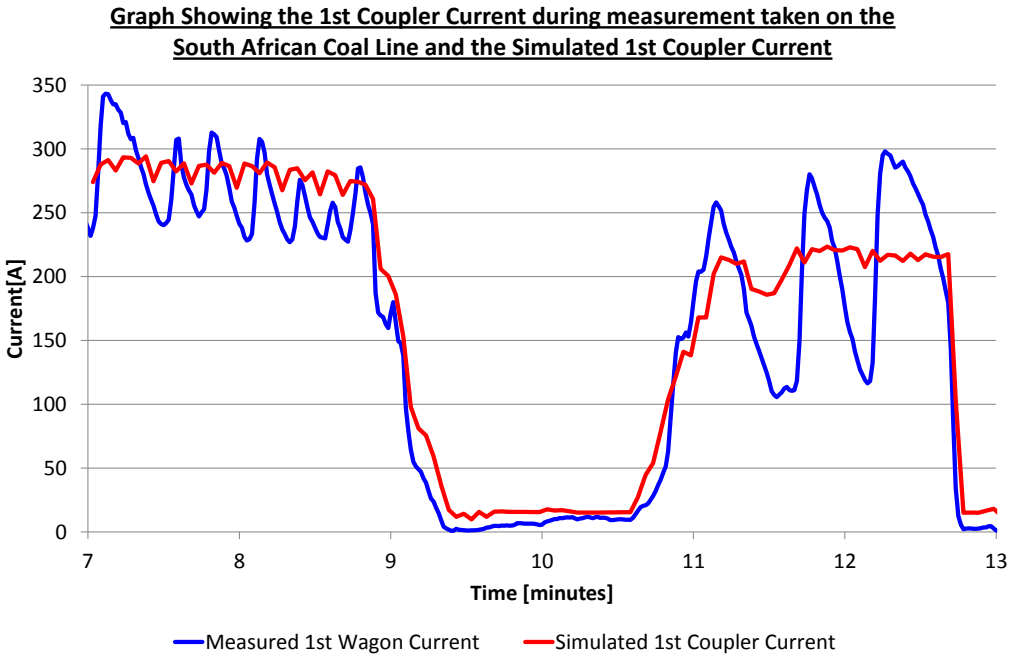


Figure 48: Graph showing the Transnet measured 1st coupler current and the simulated 1st coupler current.

Similarly, the 100th coupler current which was measured by Transnet Freight Rail is plotted against the simulated 100th coupler current in Figure 49. As with the 1st coupler current, it can be seen that the measured 100th coupler current holds an average value similar to the measured primary current. Also, the simulated current follows the rises and falls of the measured data.

The general trend and peak magnitude of the measured 100th coupler current is matched by the simulated 100th coupler current in Figure 49.

It should also be noted that between minutes 7 and 9, the simulated current is approximately the same as the measured current, in comparison to the visible difference in magnitude between the simulated 100th coupler current and the 100th measured coupler current between minutes 11 and 12.5. This indicates that the position of the train relative to feeding sub-stations may have a greater impact on the magnitude of coupler current than anticipated. Again, this would require further in-depth research to determine if this statement has any credibility.

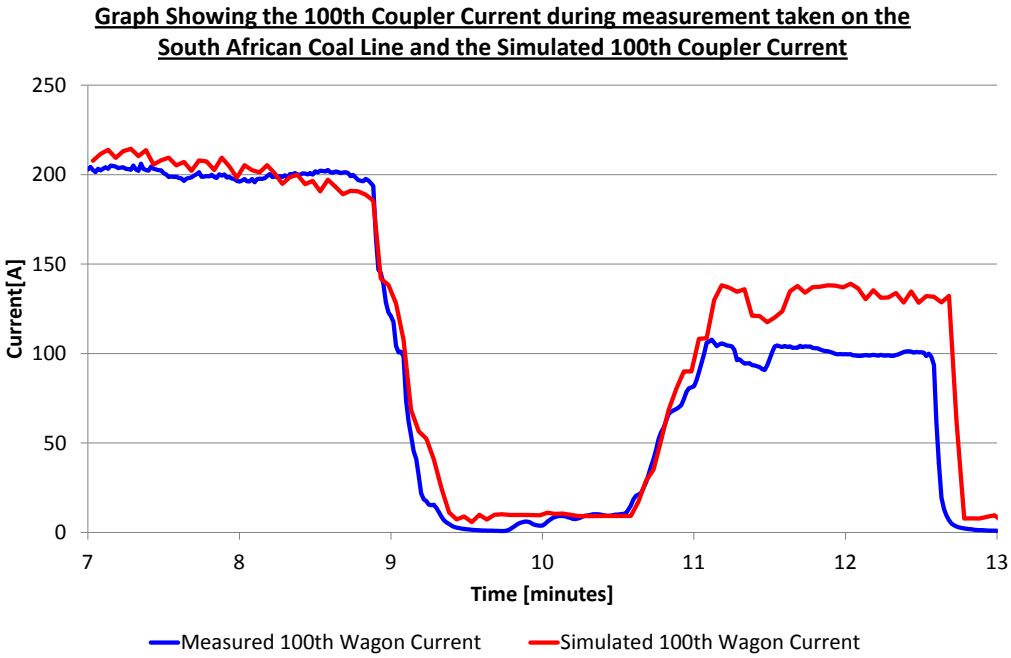


Figure 49: Graph showing the Transnet measured 100th coupler current and the simulated 100th coupler current.

Finally, the comparison of the 150th coupler current measured by Transnet Freight Rail to the simulated 150th coupler current is provided in Figure 50. The simulated 150th coupler current is seen to closely mimic the measured 150th coupler current with the exception of small deviations.

Again, similar to the 100th coupler current, it is observed that between minutes 7 and 9, the simulated current is approximately the same as the measured current, in comparison to the visible difference in magnitude between the simulated 150th coupler current and the 150th measured coupler current between minutes 11 and 12.5.

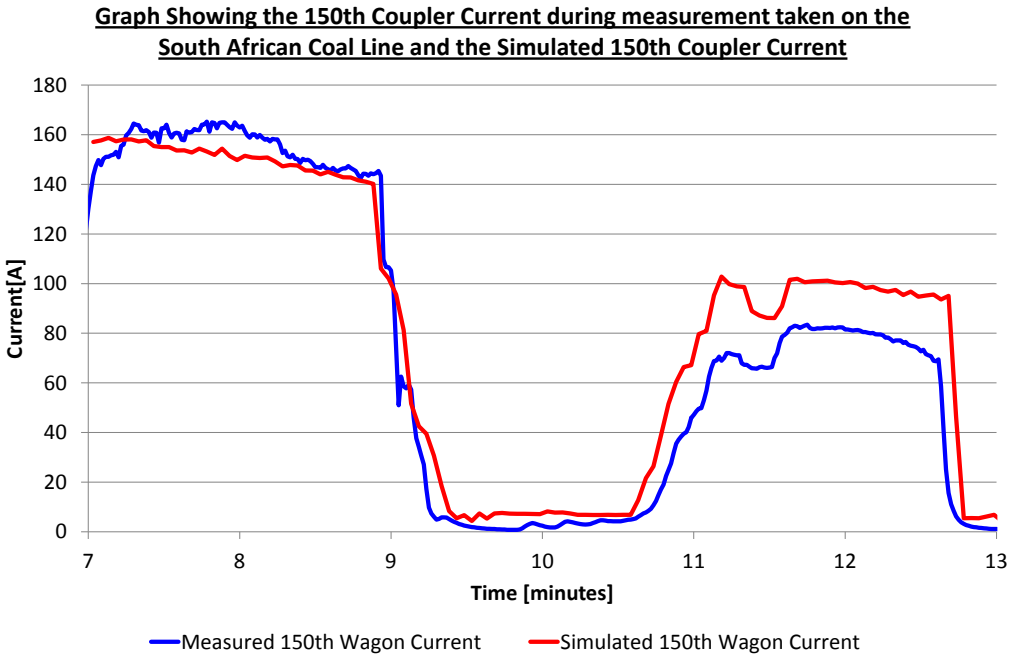


Figure 50: Graph showing the Transnet measured 150th coupler current and the simulated 150th coupler current.

Table 10 and Table 11 make comparison of the coupler currents as a percentage of the 1st coupler current and the primary current respectively. This compares the coupler currents obtained from the Transnet measurements to the simulated coupler currents.

Table 10: Table showing ratio of 1st coupler current in the 100th and 150th couplers during measurements performed by Transnet Freight Rail in comparison to simulated data.

Coupler Number	Remaining Wagons	Percentage of 1st Coupler Current Measured	Percentage of 1st Coupler Current Simulated
1	200	100 %	100 %
100	100	75 %	65.3 %
150	50	60 %	48.4 %

Table 11: Table showing ratio of primary current in the 1st, 100th and 150th couplers during measurements performed by Transnet Freight Rail in comparison to simulated data.

Coupler Number	Remaining Wagons	Percentage of Primary Current Measured	Percentage of Primary Current Simulated
1	200	31 %	31 %
100	100	24 %	20.3 %
150	50	19 %	15.1 %

As can be seen from the simulation results presented in section 7.1.2, the simulation model data reflects similar results to those obtained by Transnet Freight Rail. The simulation results demonstrate that the simulation model sufficiently represents the Transnet Freight Rail coupler current measurements and thus gives further confidence in the model.

For reference, the wagon parameters that were used in the simulation to obtain the simulated data are presented below:

- $R_{ab} = 0.0035\Omega$
- $R_{1a} = 100\Omega$
- $R_{12} = 1500\Omega$
- $R_{13} = 1500\Omega$
- $R_{3a} = 100\Omega$

These values were obtained through iterating the simulation with various parameter values until the configuration resulted in the Transnet measured results.

If these wagon parameters are compared to those obtained through the static wagon measurements that are presented in detail in APPENDIX D, it can be seen that with the exception of R_{ab}, the wagon parameters are within range of one another.

The discrepancy between the R_{ab} parameter is justified as the wagon on which static measurements were conducted had been standing for some time which could have allowed the development of rust or other contaminants affecting the electrical continuity from the coupler to the wagon body. These containments may not have significantly affected the other wagon parameters as they are considerably higher in magnitude compared to the small R_{ab} parameter. Further, when the train is under traction, the in-train forces will force the couplers against their pinions, forcing a good electrical connection.

Further, it can be seen from Table 12 that the measured parameter R_{1a} is differs from the value used in the simulations. Transnet Freight Rail makes use of earthling straps, made from copper to physically short the wagon body to the bogies and wheels. It has been noticed that occasionally, on the Coal line these straps are missing as a result of theft. The removal of this strap will have a direct result on the parameter R_{1a} and could be reason that the simulated and measured values differ.

For ease of reference the wagon parameters obtained during static wagon measurements and those used in the simulation are seen side by side in Table 12.

Table 12: Table showing wagon parameters obtained through wagon measurements against those used in the simulation.

Wagon Parameter Reference	Parameter Value Measured (Ω)	Parameter Value used in Simulation (Ω)
R_{ab}	0.72	0.0035
R_{1a}	200	100
R_{12}	1500	1500
R_{13}	1500	1500
R_{3a}	120	120

Further, the sensitivity of these wagon parameters as well as the self-inductance of the wagon and mutual-inductance with other conductors is investigated and presented in CHAPTER 8.

7.2 Discrepancies between Ekman et al. and Transnet Freight Rail Wagon Model Parameters

It must be noted that the wagon parameters obtained through iterative process for the Ekman model and Transnet Freight Rail model differ considerably. The question must be asked as to why these wagon models differ by such a degree.

The first response to this question would be the differences in physical wagon design. For example, Ekman et al. [19] do not provide sufficient information on the physical characteristics of their wagons, whilst Transnet Freight Rail wagon physical wagon characteristics are known. This means that the Ekman et al. wagons are an approximation based on limited information and would need further investigation and information to configure parameters which best reflect the wagon physical parameters.

Secondly, the wagon parameters are based on the wagons electrical response and not the wagon design. The actual response of the wagon to electrical stimulation and hence its parameters will be different if the wagon is not maintained to its designed specifications. For example, Transnet Freight Rail wagons are designed to include a wagon body to bogie earthing strap. This provides a good electrical connection between the wagon wheels and the wagon body. The reason that these straps form part of the wagon design is to force the wagon bodies to the same potential as their wheels. This ensures that a potential difference between the wagon bodies and their wheels or ground does not exist such that the touch potential is within Transnet safety regulations avoiding electrical shock to personnel.

This being said, during the course of the research it was found that many of these straps are missing and hence the resistivity between the wagon bodies (and couplers), to the wheels significantly increases. This is a result of neglected maintenance in the South African environment. The level of maintenance could be significantly different between South African Railways and Swedish railways.

7.3 Summary of Results and Observations

The simulation model was configured to represent both the Ekman et al. and Transnet Freight Rail infrastructure configurations as far as possible. The simulation results have yielded a confidence in the accuracy of the system model, however some observations were made.

The Ekman et al. measurements gave indication that there may possibly be further non-linear influences on the RMS wagon coupler current observed, when compared to the linear simulation model.

The characteristics of the coupler current were found to be in agreement between the measured data and simulation data for both Ekman et al. and Transnet Freight Rail.

The wagon parameters for both the Ekman et al. and Transnet Freight Rail simulations were obtained through iterative process. With exception of the coupler to coupler resistance, the Transnet Freight Rail wagon parameters are in agreement with those obtained through static measurements on a wagon. These measurements and their results are presented in APPENDIX C and APPENDIX D. The difference of the coupler to coupler resistance between the measured values in the values obtained through iteration is justified by the condition of the wagon under static measurement as compared to the average response of the wagons during dynamic measurements.

Similarly the discrepancies between the wagon parameters obtained for the Ekman et al. simulations and the Transnet Freight Rail wagon parameters is justified due to the lack of information regarding the Ekman et al. wagons [19] as well as the lack of suitable wagon maintenance in Transnet Freight Rail.

CHAPTER 8
INVESTIGATION & DISCUSSION

Following from the wagon model verification presented in CHAPTER 7, the system model can be used to investigate various different conditions and how the train may react to such conditions. Although this further investigation does not form an integral part of the research dissertation, it is included for interest and to show the benefits of the model.

The investigations presented in this chapter are by no means exhaustive. Many other conditions can be investigated as further research. The investigations presented in this chapter include the current distribution through the wagon wheels of a train, the current distribution in the wagon couplers and the effects of various wagon parameters on the behavior of the system model and results.

8.1 Return Current distribution in Wagon Wheels

As an extension of the investigation performed by Ekman et al., the return current distribution through the wagon wheels can be investigated. This investigation provides further information as to the current distribution between the nodes of a single wagon.

In order to perform this investigation, the Transnet Freight Rail system model was used, and the current through each wheel of the 1st wagon was observed.

8.1.1 Current distribution in the Axles of a Single Wagon

As an initial investigation, the current distribution in the wheels of the 1st wagon behind the locomotive consist is performed.

Figure 51 shows the waveforms of the currents through the front coupler, axle1 which is located behind the front coupler, axle2 which is located behind axle1, axle3 which is located behind axle2 and axle4 which is located behind axle3.

The magnitudes of the waveforms in the Figure 51 give an indication of the current distribution between the axles of the wagons. As can be seen, the axle closest to the entry point of the incoming current, axle1, has the highest current magnitude of all the axles, and this decreases which each axle moving away from the front coupler.

This means that the current is not distributed evenly in the axles of the wagon. If the wagon continuously faces the same direction, over time, any electrical erosion of the wheel bearings as proposed by Ekman et al. [19] will be more prevalent on axle1 than the other axles.

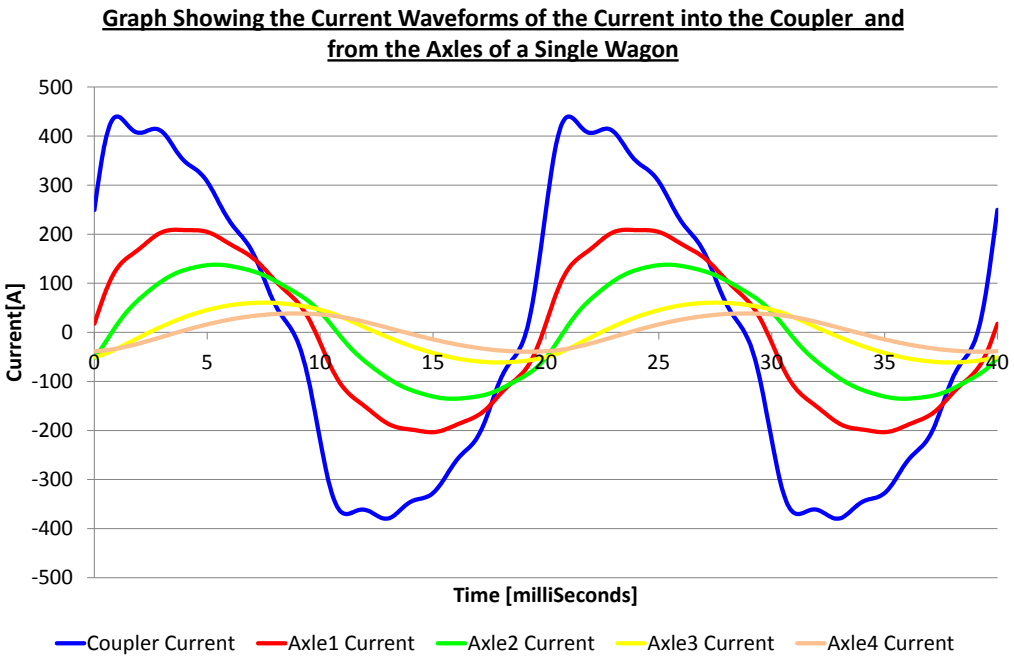


Figure 51: Graph showing the waveforms of the current through the nodes of the 1st wagon of the Coal Line train.

Figure 51 also gives an indication that the harmonic content of the current through the nodes differ. The coupler current looks to have the highest harmonic content and thereafter, in decreasing order, axle1, axle2, axle3 and axle4. This alludes to the hypothesis that the higher harmonics travel through the wagon couplers while the fundamental component and low harmonic components exit through the axles into the rails.

This being said, this investigation was performed with high rail-to-mast bond resistance. The distribution of the harmonic content may very well change when there is a lower impedance path to the return conductor. The observations could possibly reverse having the higher frequency components rather exiting through the axles to enter the return conductor. This hypothesis would need further investigation and verification.

To better understand the harmonic content distribution of the current through the nodes, a Fast Fourier Transform (FFT) is performed using LTSpice. The resulting plot is given in Figure 52.

The information provided in Figure 52 can be extended to represent the harmonic distribution in each node as a percentage of the nodes total current. This is presented in Figure 53. This verifies that the fundamental component indeed has a high percentage the axles than the coupler confirming that the higher frequency components will tend to travel through the couplers of the wagon rather than the rail.

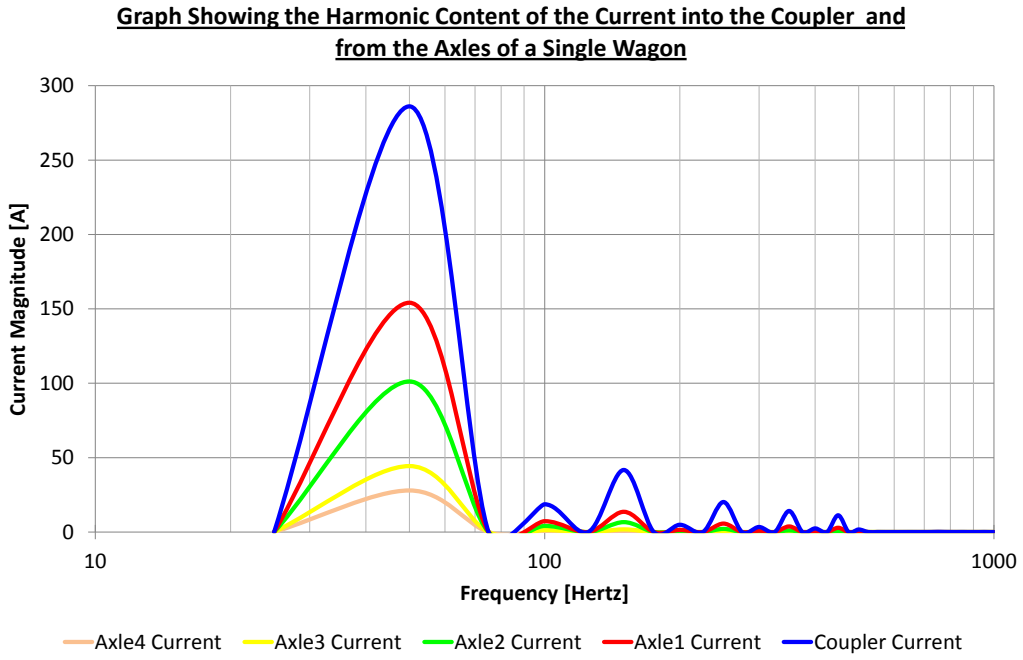


Figure 52: Graph showing the harmonic content of the current through the nodes of the 1st wagon of the Coal Line train.

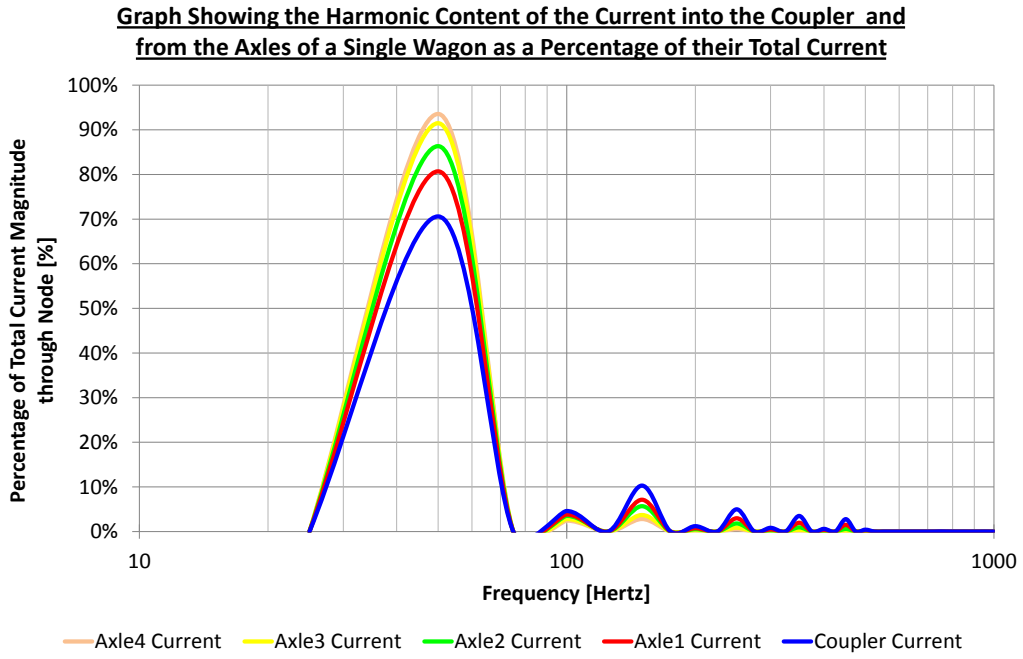


Figure 53: Graph showing the harmonic content of the current through the nodes of the 1st wagon of the Coal Line train as a percentage of their respective total current.

8.2 Return Current distribution in Wagon Couplers

In order understand the coupler current levels that are to be expected at various points along the train; the simulation model can be used to perform investigation into the RMS current levels through each coupler.

Using the simulation parameter configuration utilized to match the simulation data to the Transnet Freight Rail measured data; the coupler current levels in the train can be simulated. The results of the simulation are illustrated in Figure 54.

Figure 54 gives indication that the coupler current distribution through the train is non-linear. This shows that the current found in the coupler is affected by inductive components and not only resistive components. The concept is further investigated in sections 8.3.1 and 8.3.2.

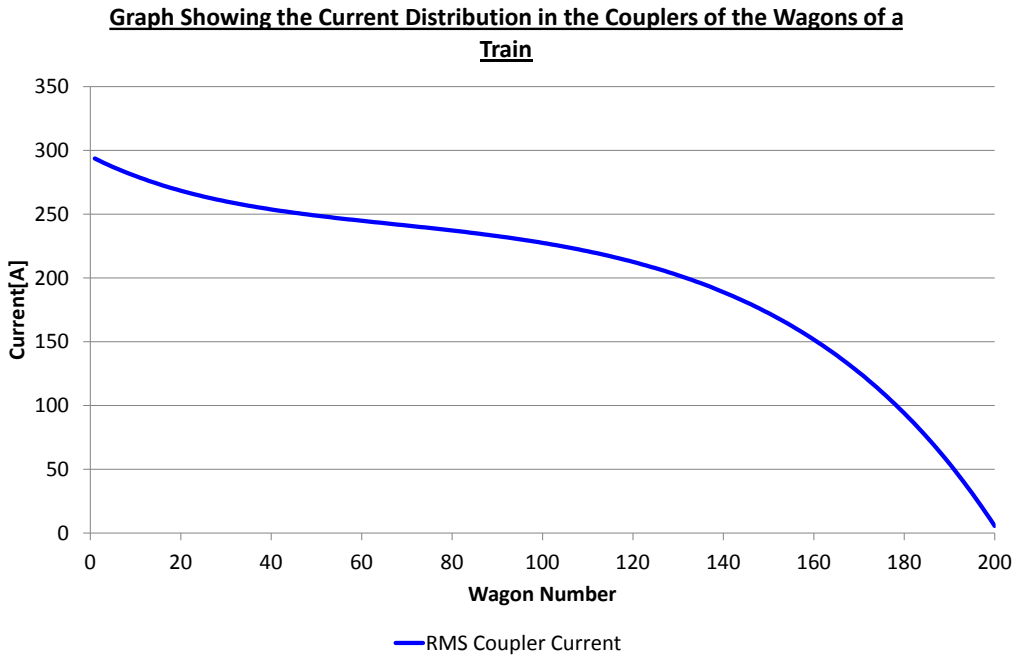


Figure 54: Graph showing current distribution in the couplers of the wagons of a Coal Line train.

8.3 Effect of Wagon Model

The effect of the wagon model parameters on the coupler current through the train, and the sensitivity thereof is investigated to give the research more meaning.

The wagon model is discussed in detail in CHAPTER 4, section 4.3 of this document. The wagon model contains both resistive and inductive elements. Varying these elements and observing the resulting coupler current distribution in the train will provide further insight into the mechanisms affecting the coupler currents. This investigation also gives direction as to the characteristics of the wagon that must be redesigned, should the coupler currents be causing undesired effects.

8.3.1 Wagon Coupler to Coupler Resistance

The coupler to coupler resistance, R_{ab}, was found to have significant influence on the coupler current levels during the simulations presented in section 7.1.2. The sensitivity of this parameter is investigated by varying the magnitude of R_{ab} and observing the effects on the coupler current distribution in the train.

Simulations were performed such that the coupler to coupler resistance, R_{ab}, was varied both above and below the R_{ab} value used in the Transnet Freight Rail model discussed in CHAPTER 7, section 7.1.2. The value of $R_{ab} = 0.0035\Omega$ is represented as 100 %. Figure 55 illustrates the results obtained from the simulations which vary R_{ab}. The figure shows the RMS current through the couplers of the train.

The foremost observation that is made from Figure 55 is that the coupler current RMS magnitudes are significantly affected by the coupler to coupler resistance of the wagons.

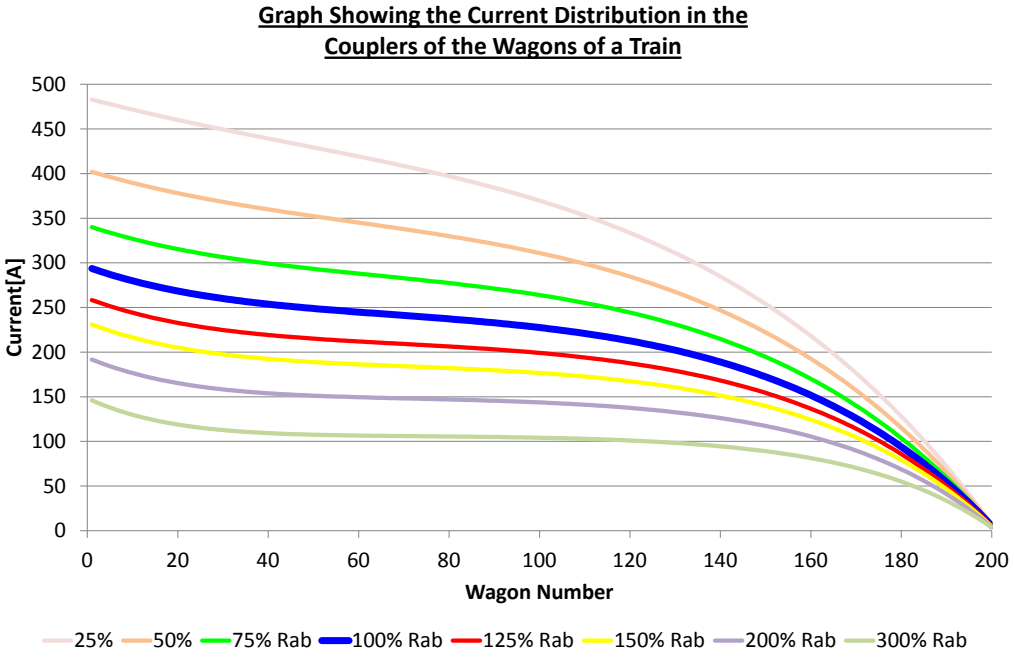


Figure 55: Graph showing current distribution in the couplers of the wagons of a Coal Line train under varying coupler to coupler resistance.

As an extension of the effects of the coupler to coupler resistance on the wagon currents, these currents can be plotted as a percentage of the 1st coupler current. This can be found in Figure 56. By representing the coupler current as a percentage of the 1st coupler current, we can establish if the return current carries further in the train at lower or higher coupler to coupler resistances whilst removing the effect that the coupler to coupler resistance has on the average current magnitude.

As can be seen in Figure 56, although there is some effect of the coupler to coupler resistance on the distribution of coupler current along the train, the effect is not significant.

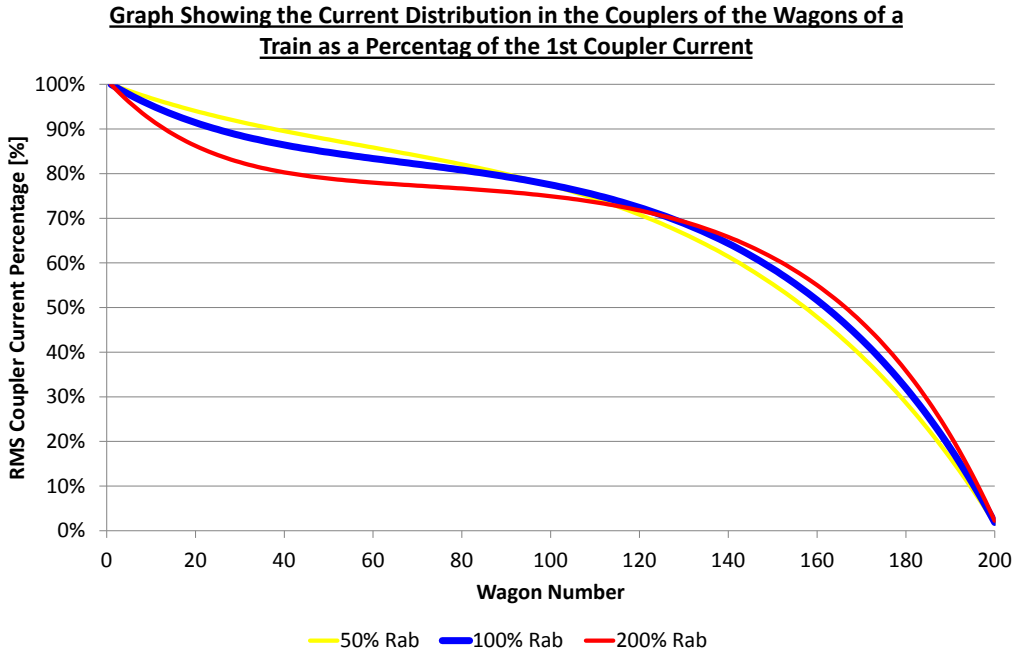


Figure 56: Graph showing current distribution in the couplers of the wagons of a Coal Line train under varying coupler to coupler resistance, as a percentage of the 1st coupler current.

8.3.2 Wagon Coupler to Wheel Resistance

Another wagon resistive parameter which will affect the coupler currents is the resistances between the couplers and the wagon wheels, namely R_{1a}, R_{12}, R_{13} and R_{3a}.

Representing the coupler to wheel resistive parameters used in the Transnet Freight Rail simulation of CHAPTER 7, section 7.1.2, being $R_{1a} = 100$, $R_{12} = 1500$, $R_{13} = 1500$ and $R_{3a} = 100$, as 100%, these parameter magnitudes were increased and decreased and their effect observed.

The results of the coupler current magnitudes along the length of the train are presented in Figure 57. It can be observed from this figure, that the average current magnitude is not

as greatly affected by the coupler to wheel resistances as by the coupler to coupler resistance as discussed in section 8.3.1.

A further observation is that the current distribution is affected by coupler to wheel resistances. The figure shows that with lower coupler to wheel resistances, the coupler current finds equilibrium based on the inductive components earlier on in the train, and is permitted to remain in this equilibrium for further in the train.

This is confirmed by plotting the coupler currents as a percentage of the 1st coupler current, which is provided in Figure 58.

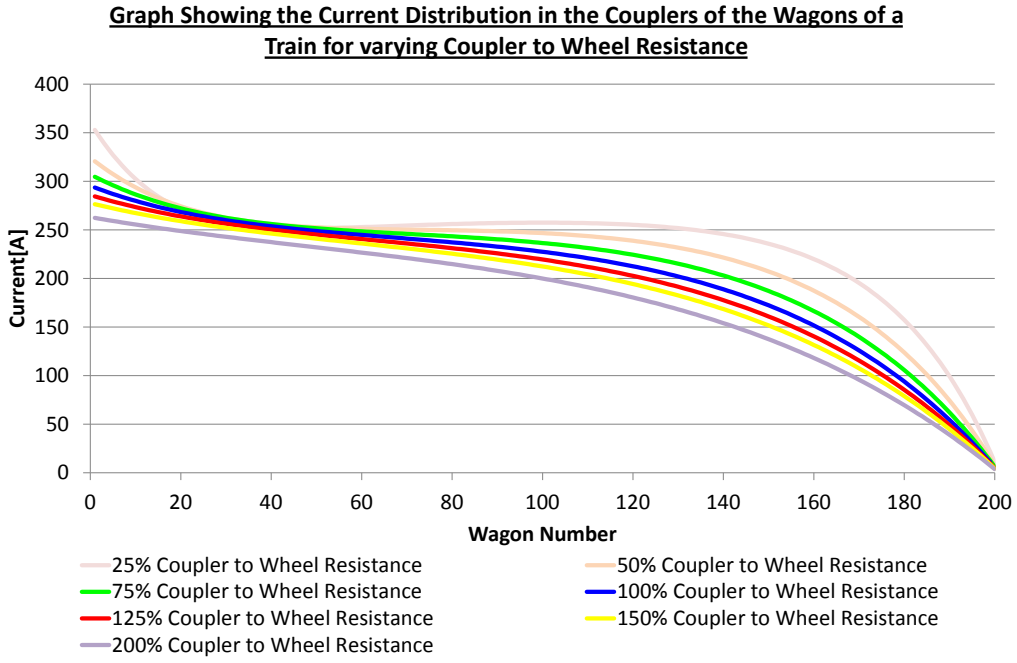


Figure 57: Graph showing current distribution in the couplers of the wagons of a Coal Line train under varying coupler to wheel resistance.

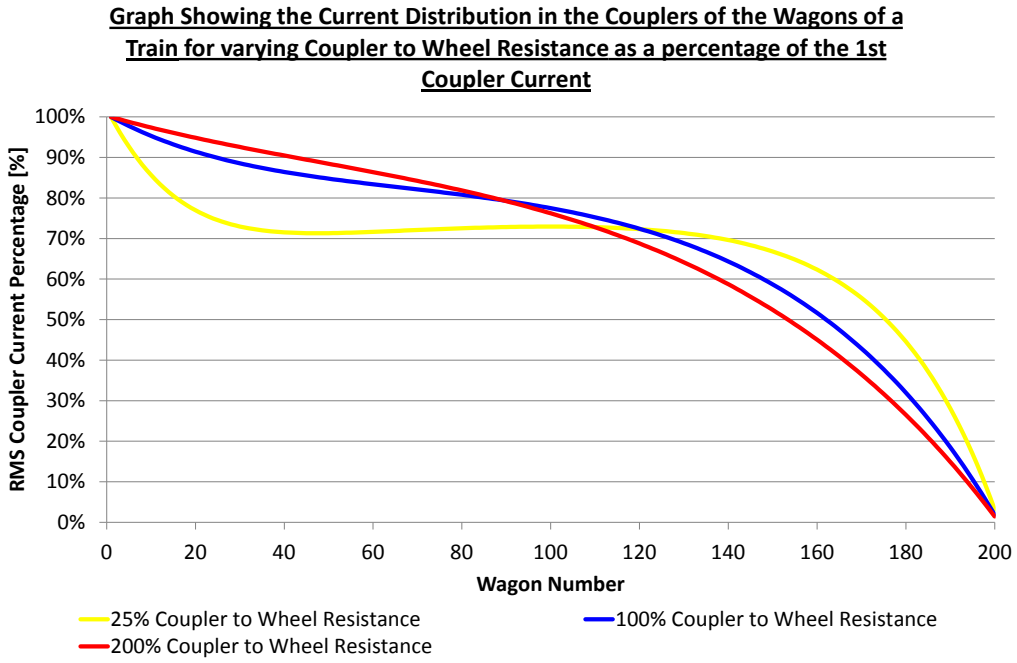


Figure 58: Graph showing current distribution in the couplers of the wagons of a Coal Line train under varying coupler to wheel resistance, as a percentage of the 1st coupler current.

8.3.3 Wagon Coupler to Coupler Inductance

CHAPTER 3 discusses the theoretical basis around which the system sub-models are derived or developed. One of the concepts discussed in CHAPTER 3 was the calculation of the self-inductance and mutual-inductances of an electrical conductor. The affecting characteristics of these inductances are the conductor's radius and its geometrical position to other conductors. Thus the effect of the wagon's height, and hence its self-inductance and mutual-inductance, is investigated to determine the effect of the coupler current distribution in the train.

8.3.3.1 Wagon Height Approximation

Using the wagon height approximation in the simulations of $3.095\ m$ to represent 100%, the wagon height is varied to establish its effects.

The coupler current distribution along the train is presented for varying wagon heights in Figure 59. This shows that the wagon height, and hence the mutual-inductance of the wagons with the surrounding electrical infrastructure conductors has effect on the average current magnitude in the couplers of the train.

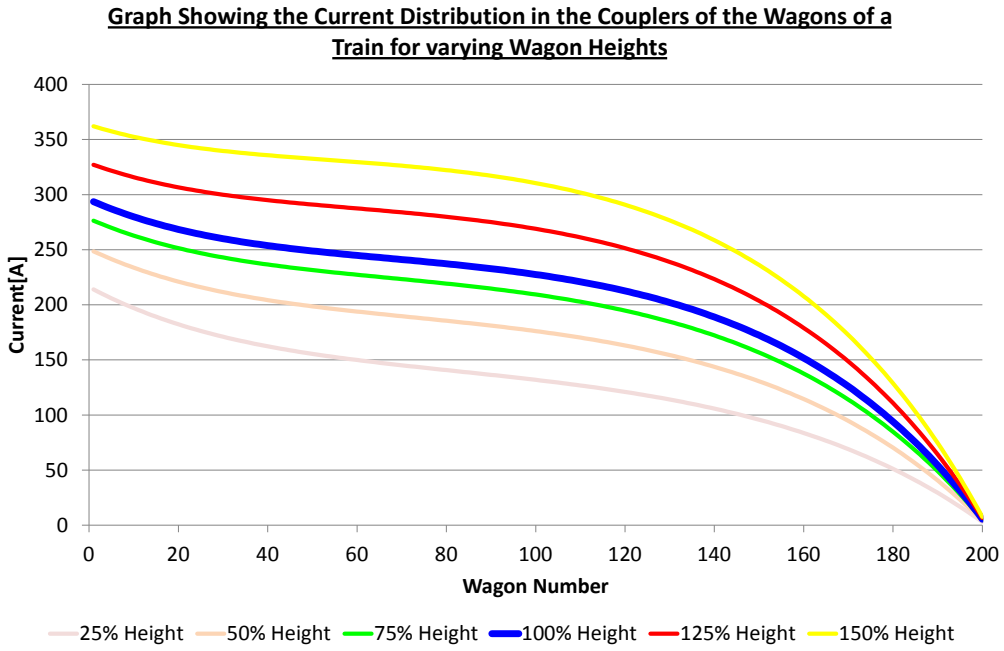


Figure 59: Graph showing current distribution in the couplers of the wagons of a Coal Line train under varying wagon heights.

Again, by plotting the coupler currents as a percentage of the 1st coupler current, a better understanding of the distribution of these current magnitudes is obtained. This is presented in Figure 60.

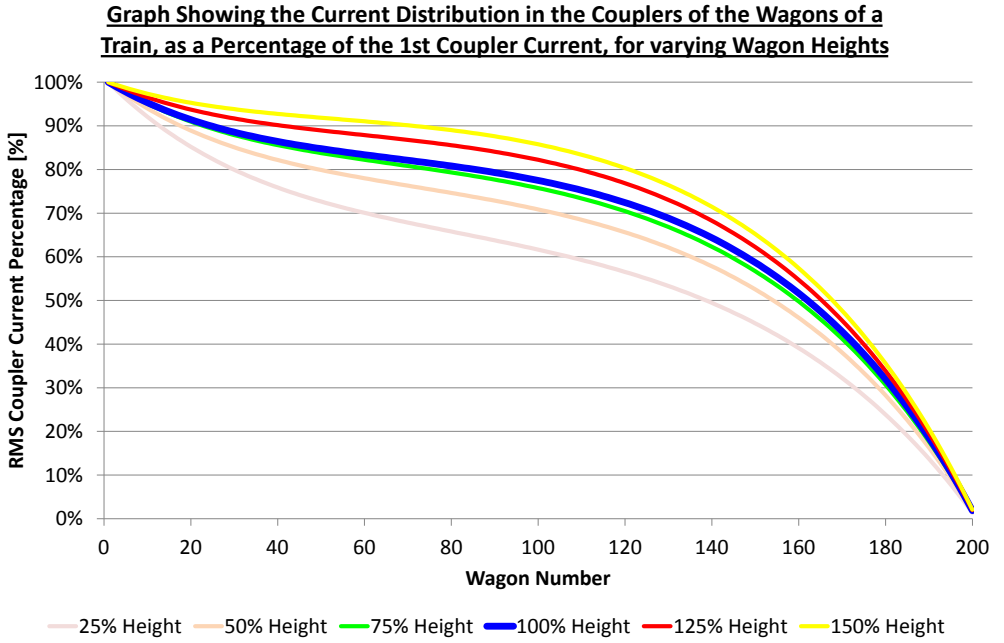


Figure 60: Graph showing current distribution in the couplers of the wagons of a Coal Line train, as a percentage of the 1st coupler current, under varying wagon heights.

It is also noted that the mutual-inductance between the wagons and the surrounding electrical conductor effects the coupler current distribution in a train.

8.4 Discussion Summary

From the investigations performed and the observations presented above, it is clear that there are many benefits to utilizing the system model to predict the behavior of the system under various conditions.

It has been found that the RMS current flowing through the wheels of a wagon into the rails is not evenly distributed. This could indicate that the wagon direction should periodically be rotated to avoid uneven electrical erosion of wagon bearings.

Further, during a railway operator's acquisition of new wagons, it may be beneficial to take into account that there is current present in the wheels. This consideration could include redesign of the electrical connection between the wagon body and wheels, such as carbon brushes. This being said, the results from section 8.3.2 indicate that a lower coupler to wheel resistances allow for the inductive coupling of the system to become dominant and thus allow for higher currents to travel further along the train. Detailed investigations, which fall outside the scope of this research, would be required to establish optimum design.

Under AC infrastructure, higher harmonics will tend to travel through the couplers of the train, whilst the lower frequency components will tend to exit to rails.

The coupler to coupler resistance of a wagon plays a significant role in the average coupler current magnitude. Should a railway be experiencing ill effects of coupler currents such as EMI or electrical erosion, they may wish to investigate means of increasing this parameter and thus reduce coupler current levels in the train.

Similar to the coupler to coupler resistance, the inductive coupling effects present in the system also pay a significant role in the average coupler current magnitude in the train. The contribution of both of these variables to the coupler current in the train shows that the coupler current is primarily a result of the inductive coupling of the wagons with the surrounding infrastructure as well as the distribution of current according to impedance paths.

The statement that the coupler current is affected by the impedance paths of the return encourages further study into the coupler currents which are expected in DC infrastructure. This was not included in the scope of this research but further investigations may indicate high coupler current levels in DC infrastructure.

CHAPTER 9
CONCLUSION

Transnet Freight Rail has observed unexpected distribution of return current, to the sub-station, through their coal trains which resulted in component failures due to Electromagnetic Interference. The existence of the current in the train couplers in AC territory prompted the research presented in this dissertation.

The research was approached by initially conducting a literature survey to provide some insights to the typical railway environment as well as the investigation of any other railway operators who have observed return current in the couplers of their trains. This identified a Swedish railway company as having observed coupler currents as a result of an investigation following premature wagon bearing failure due to electrical erosion.

Theoretical background has been discussed to provide an overview of the theoretical concepts used in the development of a system model.

The culmination of the research is the electrical system model that has been presented. The system model is an amalgamation of various sub-models. These sub-models being the infrastructure under which the train operates, the locomotive or locomotive consist model as well as the individual wagon model which is cascaded to form a train.

Each sub-model includes configurable parameters such that the system model can be adjusted to other operating corridors or railway operators.

Measurement data from the Swedish railway operator as well as Transnet Freight Rail was presented and subsequently used to test the model and the results endorsed confidence in the system model which has been developed and presented.

It was found that the system model simulation results represented the same characteristics as that of the measured data. However, the system model developed is linear, and the comparison against measured data from Sweden indicates that there could be complex non-linear effects influencing the coupler current which requires further investigation.

Further, the rail-to-mast bonds were represented as dynamic resistive components as a function of the train's displacement, however the results alluded that these bonds could be more complex than anticipated and require further investigation.

Following the comparison between the measured data and simulated data, further investigations using the system model were performed and presented. Through these

investigations, it was observed that the coupler to coupler resistance as well as the self-inductance and mutual-inductances in the system affect the magnitude of current found in the couplers of the train.

Further, the investigations show that with lower coupler to wheel resistances, the coupler current finds equilibrium based on the inductive components earlier on in the train, and is permitted to remain in this equilibrium for further in the train.

It was also noted that the distribution of current exiting the wagons of the train is not evenly distributed and the wheels closer to the front coupler carry more current than those behind them.

Through this research and the investigations, some recommendations are made for further research, investigations and system development.

Based on the distribution of current in the wheels or axles of the wagon, it is recommended that these be periodically rotated such that the electrical erosion will occur at approximately the same rate on all axles. This will mean that when wagon wheel bearings must be replaced, the entire set is replaced avoiding the need to pull the wagon set from service more frequently. It is also recommended that one set of wagons is not rotated and monitored to determine the magnitude of the effect of not rotating the wagons has against rotating the wagons.

If the operator desires to reduce the wagon coupler current magnitude to avoid electrical erosion of bearings and EMI in wagon electrical sub-systems, the coupler to coupler electrical resistivity can be increased to reduce coupler currents. This would be applicable to new wagon designs and must consider the mechanical and other implications that this may have.

The research and measurements have indicated that rail-to-mast pole bond defects can be identified by monitoring the coupler currents. It is recommended that further investigations into other defect identifications be performed, and a system developed to monitor the coupler currents on in-service trains and automatically identify defects and their locations to maintenance personnel prior to complete failure.

In conclusion, a simulation system model has been developed and simulation results have provided confidence in the model. The model presented as the contribution of the research and can be used in further research and/or investigations.

REFERENCES

[1] E. Tshivhilinge, P. du Plessis, and W. Mörs, “ECP Technology: CCD and TPS Failures - Supporting Investigation to Wagons Positioned right behind the Locomotives,” Johannesburg, 2012.

[2] B. Steyn, “Electromagnetic Compatibility of Power Electronic Locomotives and Railway Signalling Systems.pdf.” Rand Afrikaans University, Johannesburg, pp. 1–262, 1995.

[3] P. Szacsvay, “THE ELEPHANT and the FLEA LIVING with TRACTION RETURN,” no. July, 2011.

[4] R. J. Hill, “Electric railway traction, Part 3 Traction power supplies,” *POWER Eng. J.*, no. December, pp. 275–286, 1994.

[5] R. J. Hill, “Electric railway traction Part 6 Electromagnetic compatibility disturbance sources and equipment susceptibility,” no. February, pp. 31–39, 1997.

[6] S. (University of L. Baranowski, H. (University of L. Ouaddi, V. (IFSTTAR/LEOST) Deniau, J. (IFSTTAR/LEOST) Rioult, and G. (Alstom T. Nottet, “Modelisation of EM field radiated by catenaries and due to the railway power system,” 2012.

[7] R. J. Hill, “Electric railway traction Part 7 Electromagnetic interference in traction systems,” no. December, 1997.

[8] I. V Zhezhelenko, Y. L. Sayenko, A. V Gorpinich, V. V Nesterovych, and T. K. Baranenko, “Analysis of Resonant Modes in the Single-Phase Industrial AC Electrified Railway Systems,” in *Electrical Power Quality and Utilization*, 2009, pp. 9–12.

[9] A. Mariscotti, P. Pozzobon, and M. Vanti, “Distribution of the Traction Return Current in AT Electric Railway Systems,” *IEEE Trans. Power Deliv.*, vol. 20, no. 3, pp. 2119–2128, 2005.

[10] A. Mariscotti, “Distribution of the Traction Return Current in AC and DC Electric Railway Systems,” *IEEE Trans. Power Deliv.*, vol. 18, no. 4, pp. 1422–1432, Oct. 2003.

[11] K. Yuuki, H. Ueda, S. Shiraishi, S. Koizumi, and I. Yasuoka, “Study of EMI for Direct Drive Motor System in Railway Traction,” in *The 2010 International Power Electronics Conference*, 2010, pp. 1609–1613.

[12] C. Chou, Y. Hsiao, J. Wang, and Y. Hwang, “Distribution of earth leakage currents in railway systems with drain auto-transformers,” *IEEE Trans. Power Deliv.*, vol. 16, no. 2, pp. 271–275, Apr. 2001.

[13] H. Nouri, S. Jamali, and M. M. Alamuti, “Effects of earthing systems on stray current for corrosion and safety behaviour in practical metro systems,” *IET Electr. Syst. Transp.*, vol. 1, no. 2, pp. 69–79, Jun. 2011.

[14] L. Ardizzon, P. Pinato, and D. Zaninelli, “Electric traction and electrolytic corrosion : a software tool for stray currents calculation,” pp. 550–555.

[15] I. Cotton, C. Charalambous, P. Aylott, and P. Ernst, “Stray Current Control in DC Mass Transit Systems,” vol. 54, no. 2, pp. 722–730, 2005.

[16] F. Fichera, A. Mariscotti, I. S. Member, and A. Ogunsola, “Evaluating Stray Current from DC Electrified Transit Systems with Lumped Parameter and Multi-Layer Soil Models,” no. July, pp. 1187–1192, 2013.

[17] N. M. J. Dekker, “Stray Current Control - An Overview of Options,” 1999.

[18] H. Zhengqing, Z. Yuge, L. Shuping, and G. Shibin, “Modeling and Simulation for Traction Power Supply System of High-Speed Railway,” Chengdu, 2011.

[19] J. Ekman and A. Wisten, “Experimental Investigation of the Current Distribution in the Couplings of Moving Trains,” *IEEE Trans. Power Deliv.*, vol. 24, no. 1, pp. 311–318, Jan. 2009.

[20] G. Sandoval, “Power Factor in Electrical Power Systems with Non-Linear Loads,” no. 2.

[21] P. Sen, *Principles of Electric Machines and Power Electronics*. United States of America: John Wiley & Sons, Inc., 1997.

[22] C. R. Paul, *Inductance - Loop and Partial*. Hoboken, New Jersey: John Wiley & Sons, Inc., 2010.

[23] D. Jiles, *Introduction to Magnetism and Magnetic Materials*, Second Edi. Northwest: Chapman & Hall/CRC, Taylor & Francis Group, 1998.

[24] R. Perez, Ed., *Handbook of Electromagnetic Materials-CRC-Press (1995).pdf*. California: Academic Press, 1995.

[25] H. Takahashi, M. Matsuoka, and F. Harano, “EMC Retests results: AC territory with locomotives coupled condition (2,3,6 July, 2009),” Ventersdorp, 2009.

[26] R. S. Mann, “REPORT ON THE 25 kV AC TRACTION POWER SUPPLY REQUIREMENTS FOR THE TRANSPORT OF 30MTpa AND 40MTpa OF COAL BETWEEN ERMELO AND RICHARDS BAY.,” p. 40, 1979.

[27] S. De Waal and K. Steyn, “Railway Standards Platelaying UIC 60 Rail Profile Details (SKR-198-E1-E300).” Johannesburg, 1977.

[28] “Connecting Drawbar, H. E. Rotary & Non-rotary F Shank, 52152-1.” National Castings Inc., 1993.

[29] M. Modise, “Class 21E Fault Free Line Test from Ermelo to Richards Bay, Event List.” Transnet Freight Rail, Johannesburg, 2015.

[30] “Rail Network Infrastructure Diagram, BBB4827 ver 4.” Transnet Freight Rail, Johannesburg, 2006.

[31] “Small Scale - Ermelo to Richards Bay.” Transnet Freight Rail, Johannesburg.

[32] “Main Assembly CR-17 Wagon, PEW821B0000_D.” Transnet Rail Engineering, Kilner Park, 2012.

[33] Transnet, “S.A.R. Wheels and Axle, Two Wear - Wheels and Axles for Package Bearing Type D, CME152_12_A36.pdf.” Transnet Freight Rail, 1981.

APPENDIX A

ACTIVITY DIAGRAM OF RESEARCH

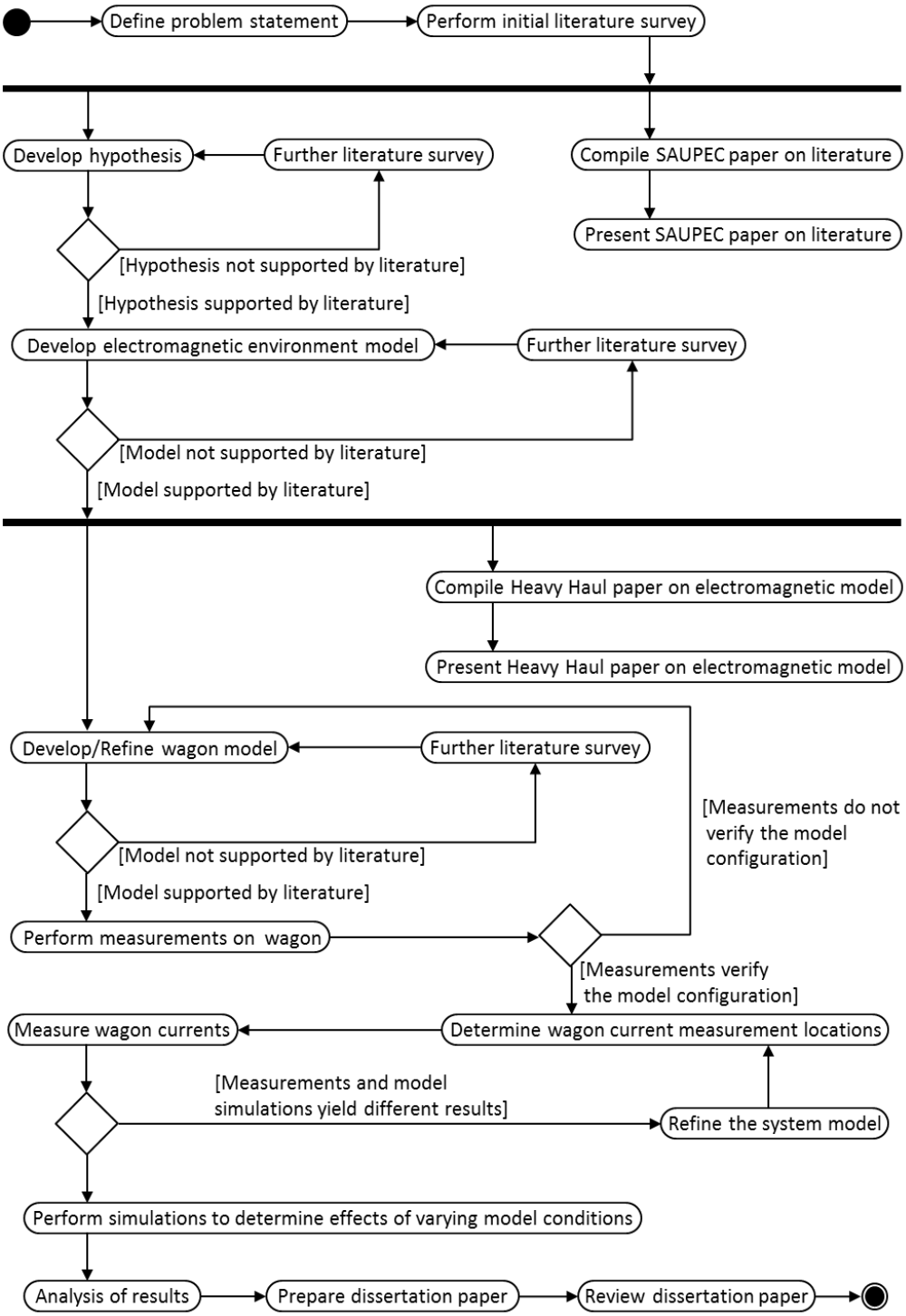


Figure A.1: Activity diagram depicting the process and flow of milestones and requirements for Masters Dissertation by research.

APPENDIX B

ARGUMENT STRUCTURE OF RESEARCH

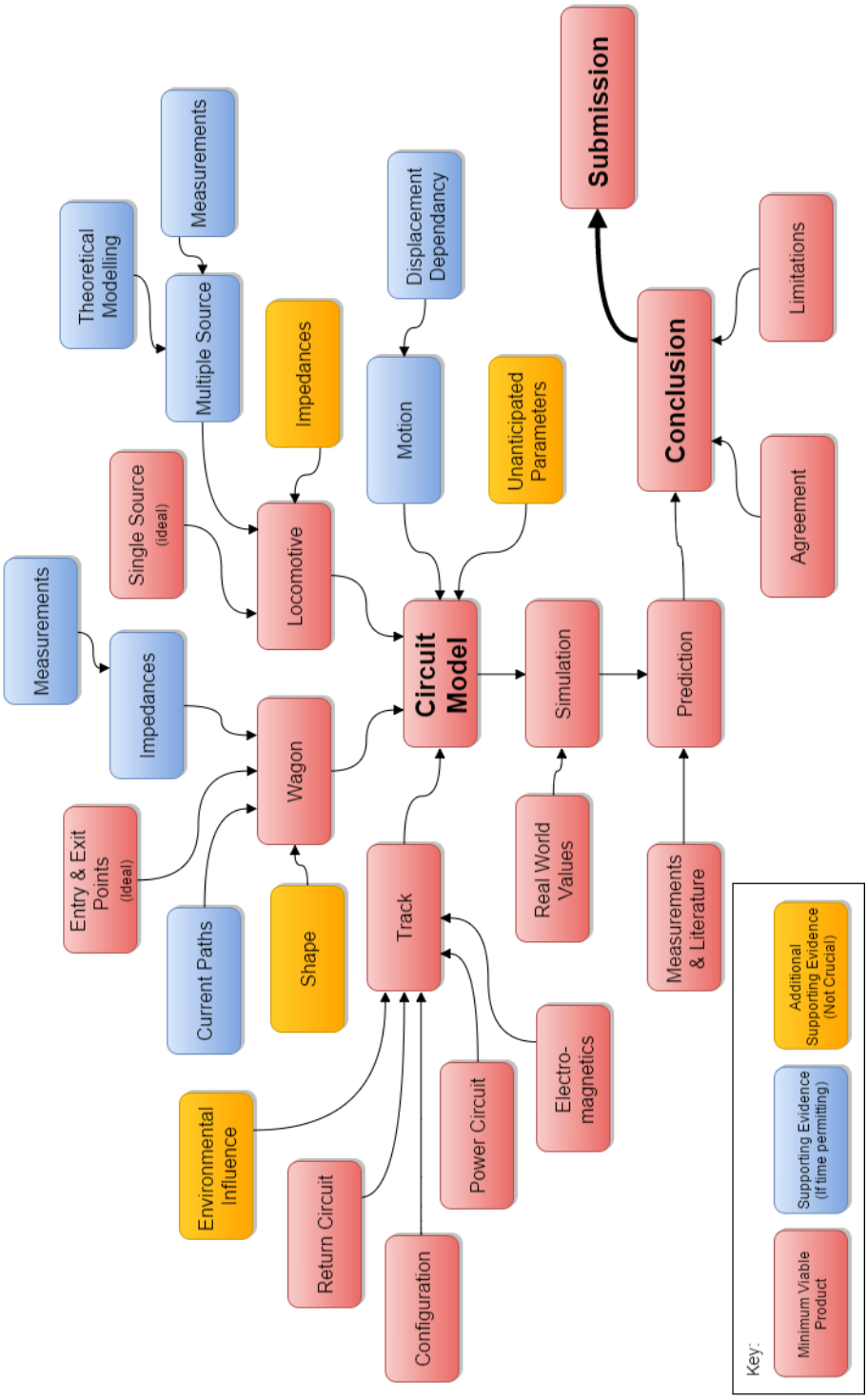


Figure B.1: Diagram illustrating the argument structure for Masters Dissertation by research.

APPENDIX C
WAGON MODEL VERIFICATION: EXPERIMENTAL METHODOLOGY

Once the theoretical wagon model is derived, which can be seen in CHAPTER 4, section 4.3 of the dissertation, verification and parameter determination of the wagon model was performed experimentally. The following section of the Appendices describes the experimental setup and methodology in verifying and determining parameter magnitudes of the wagon model.

C.1 Experiment Location

To ensure that there was no interference from surrounding railway infrastructure, an un-electrified yard location was selected to perform the wagon measurements. This can be seen in Figure 61 which depicts the wagon set on an un-electrified line section.



Figure 61: Photograph showing the yard section used to conduct wagon measurements.

It can be noticed that on the far left of the photograph in Figure 61, electrified sections can be seen. These were assumed to be a sufficient distance away to not cause interference with the measurements.

Further, measurements were performed at various AC and DC supply conditions to as further precautions of 50 Hz interference. Higher frequency measurements could be filtered if necessary to remove any 50 Hz interference observed in the measurements. This being said, filtering was not necessary and can be seen in the analysis on the experimental results in APPENDIX D.

The experiment location was considerably remote in the sense that motor vehicle transportation was required to access the site. No other resources were available at the location and so apparatus needed to be portable. The apparatus requirements are discussed in section C.2.

C.2 Experiment Apparatus

As the location of the wagon measurements was not located considerably close to any resources, all apparatus needed to be portable. Further, apparatus requiring 220 V AC 50 Hz power supply would need to be catered for through the use of battery packs and an inverter.

Considering the experiment location, the apparatus list was compiled and can be seen in Table 13, inclusive of approximate quantities.

Table 13: Table showing the experiment apparatus list and quantity requirements for the wagon measurements.

Description	Quantity
Wire	±50 meters
Electric Paint	1 tube
Gas soldering iron	1
Gas for soldering iron	1 tin
Matches/lighter	1
Solder	1 roll
Flux	1 tub
Duct Tape	1 roll
Cable Ties	1 pack
Marker	1
DC Power Supply	1
Function Generator	1
Leads	4 BNC to Banana 4 Banana to Banana sets
Inverter	1 (300 W)
12V DC battery (±7Ah)	4 per day
Multi-plug from Inverter	1
Multi-meter	1
Small AC Current Clamp	1
Scope-meter	1
Scope-meter Download Cable (Serial)	1
Serial Interface	1

Description	Quantity
Super Glue	1 tube
Chocolate Block (4)	1
Small Flat Screw Driver	1
Small Side Cutter	1
Small Metal File	1
Crate for storage	1

The apparatus was gathered and stored in a crate for easy transport to the experiment location. This can be seen in Figure 62.



Figure 62: Photograph showing the experiment apparatus in the storage crate during the wagon measurements.

The testing apparatus is owned by the Transnet Freight Rail, Technology Management, Traction Technology, Electrical Laboratory department. The apparatus was kindly made available to the responsible testing person (the student) for the duration of the wagon measurements.

The Electrical Laboratory department consists mainly of mobile testing resources and testing staff. These are in the form of "test coaches" which are specially designed coaches which can form part of a train and offer an expansive list of testing equipment. Due to the nature of work of the department, all their test equipment is calibrated on a yearly basis.

For reference, Figure 63, Figure 64, Figure 65 and Figure 66 illustrate the experimental apparatus at the testing location.



Figure 63: Photograph showing the experiment apparatus for the wagon measurements.



Figure 64: Photograph showing the experiment setup at the experiment location during the wagon measurements.



Figure 65: Photograph showing the experiment setup for DC measurements at the experiment location during the wagon measurements.



Figure 66: Photograph showing the experiment setup for AC measurements at the experiment location during the wagon measurements.

C.3 Transnet Freight Rail Safety Requirements

The experimental wagon measurements were conducted on Transnet Freight Rail premises. The Transnet Freight Rail Safety instructions were thus followed.

For the duration of the experiment, the responsible testing person (the student) gave notice to the control rooms on either end of the section. This is to inform the control rooms that there are personnel in the section so that the necessary precautions can be taken and warning given to drivers who will pass on adjacent lines.

The wagon measurements were conducted on a line adjacent to operational lines, thus diesel locomotives and/or trains would pass on the adjacent lines as per normal Transnet Freight Rail operations. During the passing of trains and/or locomotives, the testing would be paused, and the section cleared to make way for the passing train and/or locomotives. During the passing of the train and/or locomotives, the responsible testing person was required to make visual acknowledgement to the driver of the train and/or locomotives that he is aware that the train and/or locomotives will be passing before the driver proceeds to pass.

Further, for the duration of the tests, the control tower and train planner were notified that testing would be performed on the selected line. This was for safety as well as ensuring that the wagons under test are not allocated to a train for operation and hence moved.

In addition to notification to the train planner, notices were placed on the outer couplers of the wagon set. The notice was for the purpose of shunting cars such that, should the train planner arrange for the wagons to be shunted for service or other erroneously, the shunting driver will be made aware that the wagon set is under test and may not be moved. This notification can be seen in Figure 67.



Figure 67: Photograph showing the warning notice not to couple to or move the wagon set which was under testing during the wagon measurements.

C.4 Experimental Method

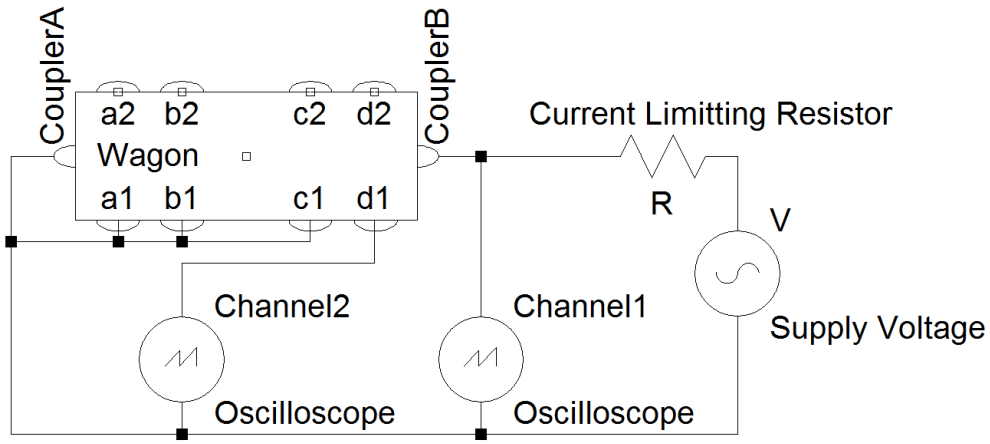
The determination of the model parameter magnitudes is performed by, isolating a single wagon from the rails, applying a voltage source across its couplers, and measuring the voltages at each node as well as the supply current.

The circuit was modified by creating a short circuit connection between all nodes not measured to the reference, or reference coupler. The supply voltage was then applied to the opposite coupler, without short circuit to the reference coupler. As an example, Figure 68 depicts the connections made to the nodes of the wagon during the measurements on the wheel closest to the voltage supply. An oscilloscope, or in the case of these measurements, a portable scope-meter was used to obtain the waveforms of the voltages and current, using an AC current clamp for AC measurements and a built-in ammeter of the multi-meter for DC measurements.

C.4.1 Measurements on Wheel D1

To perform measurements on wheel $D1$ of the wagon, wheels $A1$, $B1$ and $C1$ are connected to the reference, being $CouplerA$. This was achieved through the use of

conductive wire from each node to the reference. The supply voltage, both DC and AC at various frequencies, was then applied to $CouplerB$ in reference to $CouplerA$. Voltage measurements in reference to $CouplerA$ at wheel $D1$ were then taken. Figure 68 shows the electrical circuit diagram of the experimental setup for the measurements on wheel $D1$.



where: V is a frequency generator (variable frequency) or DC supply.

R is a current limiting resistor.

$CouplerA$ is the No.1 end coupler.

$a1, a2, b1, b2, c1, c2, d1, d2$ are wheel terminals.

$CouplerB$ is the No.2 end coupler.

Figure 68: Diagram showing electrical connections to the wagon nodes to take measurements on the wheel $D1$ during wagon measurements.

Once the circuit was configured, DC and AC supply voltages were applied to $CouplerB$. The voltages at $CouplerB$, wheel $D1$ and $CouplerA$ as well as the supply current were recorded. Table 14 shows the supply voltages and frequencies tested and the measurements recorded.

Table 14: Table showing the supply voltages tested and measurements taken during wagon measurements on wheel $D1$.

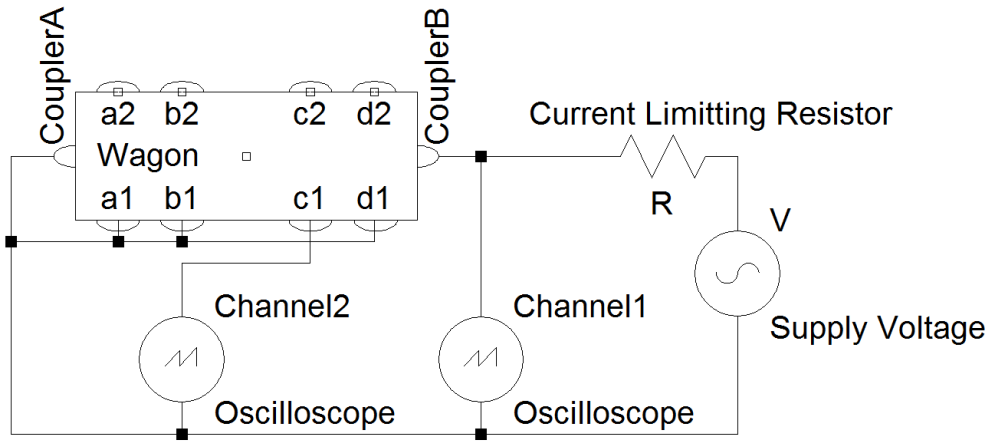
Supply Voltage Type	Supply Voltage Magnitude	Supply Voltage Frequency	Oscilloscope Channel 1 Measurement	Oscilloscope Channel 2 Measurement	Multi-Meter Measurement
DC	± 12 V	N/A	$CouplerB$	$CouplerA$	Supply Current
DC	± 12 V	N/A	$CouplerB$	$D1$	Supply Current
DC	± 24 V	N/A	$CouplerB$	$CouplerA$	Supply Current
DC	± 24 V	N/A	$CouplerB$	$D1$	Supply Current
AC	± 0.8 V	50 Hz	$CouplerB$	$CouplerA$	Supply Current
AC	± 0.8 V	50 Hz	$CouplerB$	$D1$	Supply Current
AC	± 0.8 V	50 Hz	$CouplerB$	$Supply\ Current$	Supply Current
AC	± 0.8 V	500 Hz	$CouplerB$	$CouplerA$	Supply Current
AC	± 0.8 V	500 Hz	$CouplerB$	$D1$	Supply Current
AC	± 0.8 V	500 Hz	$CouplerB$	$Supply\ Current$	Supply Current

Supply Voltage Type	Supply Voltage Magnitude	Supply Voltage Frequency	Oscilloscope Channel 1 Measurement	Oscilloscope Channel 2 Measurement	Multi-Meter Measurement
AC	± 0.8 V	5 kHz	$CouplerB$	$CouplerA$	Supply Current
AC	± 0.8 V	5 kHz	$CouplerB$	$D1$	Supply Current
AC	± 0.8 V	5 kHz	$CouplerB$	$Supply\ Current$	Supply Current

Once the measurements were recorded, circuit analysis was performed in order to determine the element magnitudes of the wagon model. This analysis is detailed in APPENDIX D.

C.4.2 Measurements on Wheel C1

To perform measurements on wheel $C1$ of the wagon, wheels $A1$, $B1$ and $D1$ are connected to the reference, being $CouplerA$. This was achieved through the use of conductive wire from each node to the reference. The supply voltage, both DC and AC at various frequencies, was then applied to $CouplerB$ in reference to $CouplerA$. Voltage measurements in reference to $CouplerA$ at wheel $C1$ were then taken. Figure 69 shows the electrical circuit diagram of the experimental setup for the measurements on wheel $C1$.



where: V is a frequency generator (variable frequency) or DC supply.
R is a current limiting resistor.
$CouplerA$ is the No.1 end coupler.
$a1, a2, b1, b2, c1, c2, d1, d2$ are wheel terminals.
$CouplerB$ is the No.2 end coupler.

Figure 69: Diagram showing electrical connections to the wagon nodes to take measurements on the wheel $C1$ during wagon measurements.

Once the circuit was configured, DC and AC supply voltages were applied to $CouplerB$. The voltages at $CouplerB$, wheel $C1$ and $CouplerA$ as well as the supply current were

recorded. Table 15 shows the supply voltages and frequencies tested and the measurements recorded.

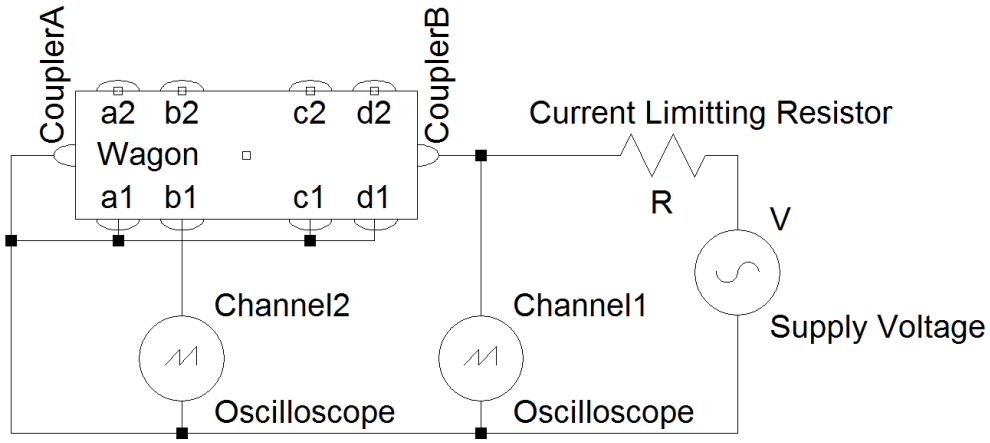
Table 15: Table showing the supply voltages tested and measurements taken during wagon measurements on wheel $C1$.

Supply Voltage Type	Supply Voltage Magnitude	Supply Voltage Frequency	Oscilloscope Channel 1 Measurement	Oscilloscope Channel 2 Measurement	Multi-Meter Measurement
DC	± 12 V	N/A	$CouplerB$	$CouplerA$	Supply Current
DC	± 12 V	N/A	$CouplerB$	$C1$	Supply Current
DC	± 24 V	N/A	$CouplerB$	$CouplerA$	Supply Current
DC	± 24 V	N/A	$CouplerB$	$C1$	Supply Current
AC	± 0.8 V	50 Hz	$CouplerB$	$CouplerA$	Supply Current
AC	± 0.8 V	50 Hz	$CouplerB$	$C1$	Supply Current
AC	± 0.8 V	50 Hz	$CouplerB$	$Supply\ Current$	Supply Current
AC	± 0.8 V	500 Hz	$CouplerB$	$CouplerA$	Supply Current
AC	± 0.8 V	500 Hz	$CouplerB$	$C1$	Supply Current
AC	± 0.8 V	500 Hz	$CouplerB$	$Supply\ Current$	Supply Current
AC	± 0.8 V	5 kHz	$CouplerB$	$CouplerA$	Supply Current
AC	± 0.8 V	5 kHz	$CouplerB$	$C1$	Supply Current
AC	± 0.8 V	5 kHz	$CouplerB$	$Supply\ Current$	Supply Current

Once the measurements were recorded, circuit analysis was performed in order to determine the element magnitudes of the wagon model. This analysis is detailed in APPENDIX D.

C.4.3 Measurements on Wheel B1

To perform measurements on wheel $B1$ of the wagon, wheels $A1$, $C1$ and $D1$ are connected to the reference, being $CouplerA$. This was achieved through the use of conductive wire from each node to the reference. The supply voltage, both DC and AC at various frequencies, was then applied to $CouplerB$ in reference to $CouplerA$. Voltage measurements in reference to $CouplerA$ at wheel $B1$ were then taken. Figure 70 shows the electrical circuit diagram of the experimental setup for the measurements on wheel $B1$.



where: V is a frequency generator (variable frequency) or DC supply.

R is a current limiting resistor.

$CouplerA$ is the No.1 end coupler.

$a1, a2, b1, b2, c1, c2, d1, d2$ are wheel terminals.

$CouplerB$ is the No.2 end coupler.

Figure 70: Diagram showing electrical connections to the wagon nodes to take measurements on the wheel $B1$ during wagon measurements.

Once the circuit was configured, DC and AC supply voltages were applied to $CouplerB$. The voltages at $CouplerB$, wheel $B1$ and $CouplerA$ as well as the supply current were recorded. Table 16 shows the supply voltages and frequencies tested and the measurements recorded.

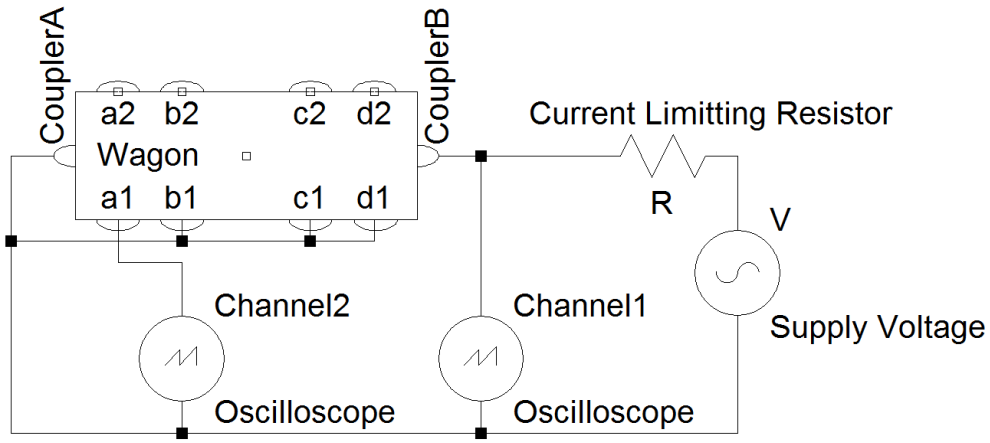
Table 16: Table showing the supply voltages tested and measurements taken during wagon measurements on wheel $B1$.

Supply Voltage Type	Supply Voltage Magnitude	Supply Voltage Frequency	Oscilloscope Channel 1 Measurement	Oscilloscope Channel 2 Measurement	Multi-Meter Measurement
DC	± 12 V	N/A	$CouplerB$	$CouplerA$	Supply Current
DC	± 12 V	N/A	$CouplerB$	$B1$	Supply Current
DC	± 24 V	N/A	$CouplerB$	$CouplerA$	Supply Current
DC	± 24 V	N/A	$CouplerB$	$B1$	Supply Current
AC	± 0.8 V	50 Hz	$CouplerB$	$CouplerA$	Supply Current
AC	± 0.8 V	50 Hz	$CouplerB$	$B1$	Supply Current
AC	± 0.8 V	50 Hz	$CouplerB$	$Supply\ Current$	Supply Current
AC	± 0.8 V	500 Hz	$CouplerB$	$CouplerA$	Supply Current
AC	± 0.8 V	500 Hz	$CouplerB$	$B1$	Supply Current
AC	± 0.8 V	500 Hz	$CouplerB$	$Supply\ Current$	Supply Current
AC	± 0.8 V	5 kHz	$CouplerB$	$CouplerA$	Supply Current
AC	± 0.8 V	5 kHz	$CouplerB$	$B1$	Supply Current
AC	± 0.8 V	5 kHz	$CouplerB$	$Supply\ Current$	Supply Current

Once the measurements were recorded, circuit analysis was performed in order to determine the element magnitudes of the wagon model. This analysis is detailed in APPENDIX D.

C.4.4 Measurements on Wheel A1

To perform measurements on wheel $A1$ of the wagon, wheels $B1$, $C1$ and $D1$ are connected to the reference, being $CouplerA$. This was achieved through the use of conductive wire from each node to the reference. The supply voltage, both DC and AC at various frequencies, was then applied to $CouplerB$ in reference to $CouplerA$. Voltage measurements in reference to $CouplerA$ at wheel $A1$ were then taken. Figure 71 shows the electrical circuit diagram of the experimental setup for the measurements on wheel $A1$.



where: V is a frequency generator (variable frequency) or DC supply.
R is a current limiting resistor.
$CouplerA$ is the No.1 end coupler.
$a1, a2, b1, b2, c1, c2, d1, d2$ are wheel terminals.
$CouplerB$ is the No.2 end coupler.

Figure 71: Diagram showing electrical connections to the wagon nodes to take measurements on the wheel $A1$ during wagon measurements.

Once the circuit was configured, DC and AC supply voltages were applied to $CouplerB$. The voltages at $CouplerB$, wheel $A1$ and $CouplerA$ as well as the supply current were recorded. Table 17 shows the supply voltages and frequencies tested the and measurements recorded.

Table 17: Table showing the supply voltages tested and measurements taken during wagon measurements on wheel $A1$.

Supply Voltage Type	Supply Voltage Magnitude	Supply Voltage Frequency	Oscilloscope Channel 1 Measurement	Oscilloscope Channel 2 Measurement	Multi-Meter Measurement
DC	± 12 V	N/A	$CouplerB$	$CouplerA$	Supply Current
DC	± 12 V	N/A	$CouplerB$	$A1$	Supply Current
DC	± 24 V	N/A	$CouplerB$	$CouplerA$	Supply Current
DC	± 24 V	N/A	$CouplerB$	$A1$	Supply Current
AC	± 0.8 V	50 Hz	$CouplerB$	$CouplerA$	Supply Current
AC	± 0.8 V	50 Hz	$CouplerB$	$A1$	Supply Current
AC	± 0.8 V	50 Hz	$CouplerB$	$Supply\ Current$	Supply Current
AC	± 0.8 V	500 Hz	$CouplerB$	$CouplerA$	Supply Current
AC	± 0.8 V	500 Hz	$CouplerB$	$A1$	Supply Current
AC	± 0.8 V	500 Hz	$CouplerB$	$Supply\ Current$	Supply Current
AC	± 0.8 V	5 kHz	$CouplerB$	$CouplerA$	Supply Current
AC	± 0.8 V	5 kHz	$CouplerB$	$A1$	Supply Current
AC	± 0.8 V	5 kHz	$CouplerB$	$Supply\ Current$	Supply Current

Once the measurements were recorded, circuit analysis was performed in order to determine the element magnitudes of the wagon model. This analysis is detailed in APPENDIX D.

C.5 Isolation of the Wagon

To allow for the wagon measurements, the wagon under test was required to be isolated from the rails. Should the wagon not be isolated from the rails, the rails would act as a conductive electrical connection between the wheels, thus modifying the circuit undesirably.

Various isolation methods were considered, however the most practical given the location was to place an insulating material between each wagon wheel and the rail. The material was not required to withstand high voltages as the test was performed in the low voltage range (less than 30V) however, the material needed to withstand the high force exerted by the wagon wheels on the rail. These wagons are specified to be 21 tons per axle. Assuming a gravitational acceleration contestant of approximately $9.81\ m/s^2$, this roughly calculates to a wheel to rail force of $103\ kN$.

Although a rather simple solution, the insulating material selected was newspaper with sufficient layers to withstand the wheel to rail force whilst still providing low voltage insulation as well as being flexible to avoid wagon derailment. Should the layering of the newspaper be in sufficient, the wheel to rail force would destroy the newspaper and create and electrical wheel to rail connection. In contrast, should the layering be excessive, this poses a risk to wagon derailment.

The newspaper isolation was placed in front of each wheel of the wagon. Special care was taken to ensure that the newspaper isolation covered the wheel flange in addition to the wheel surface. Thereafter, a diesel locomotive was used to shunt the wagon on top of the isolation. The result was that the each wheel had electrical isolation from the rail. Figure 72 provides visual illustration of the insulation between the wagon wheels and rail.

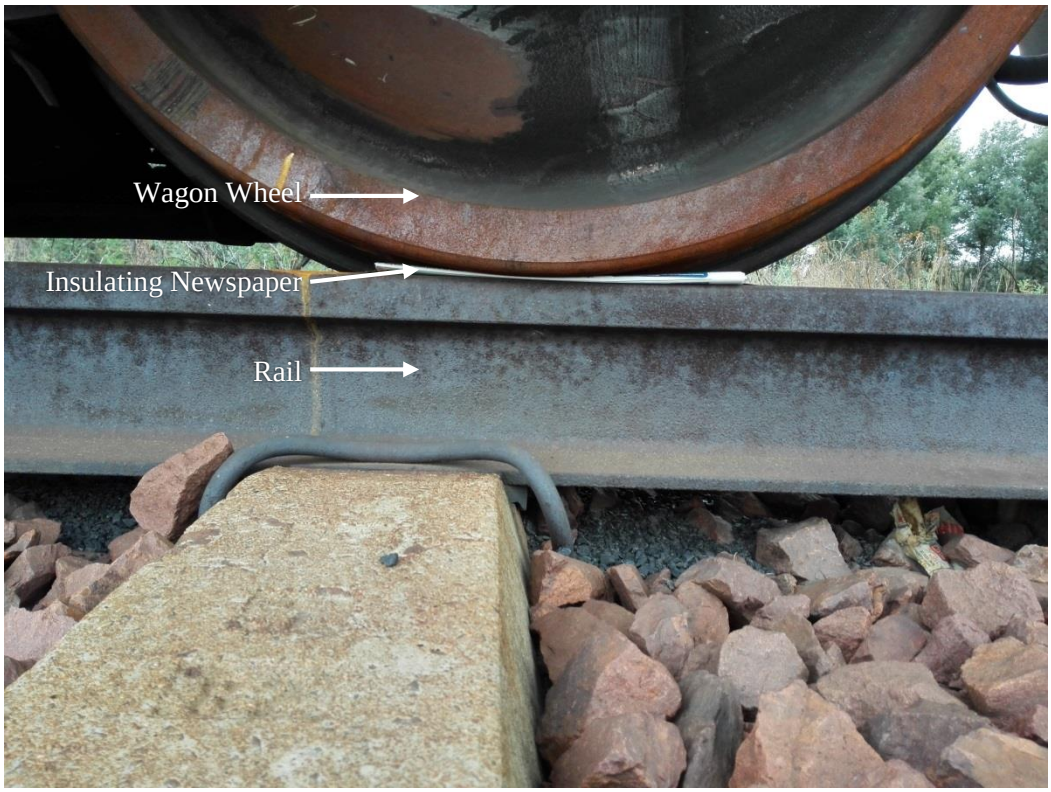


Figure 72: Photograph showing the paper isolation between the wagon wheels and rail during the wagon measurements.

C.6 Electrical Connections to the Wagon

The nodes of the wagon needed to be electrically connected to test apparatus in order to perform measurements. Electrical conductive wire was thus connected to each node. These wires could then be connected to test apparatus.

The wagon and wheels are manufactured from steel. Generally, the wagons and wheels experience rusting as well as being exposed to various contaminants. As a result, a direct electrical connection to the wheels and couplers is not possible. In order to allow for electrical connection, each node was filed using a small metal file. This allowed for a small section of steel to be exposed. This is illustrated in Figure 73 where a small section of the wagon wheel is filed to expose the underlying steel. An electrical conductive wire

to be connected to the node and thus used in the measurements can also be seen in the photograph.

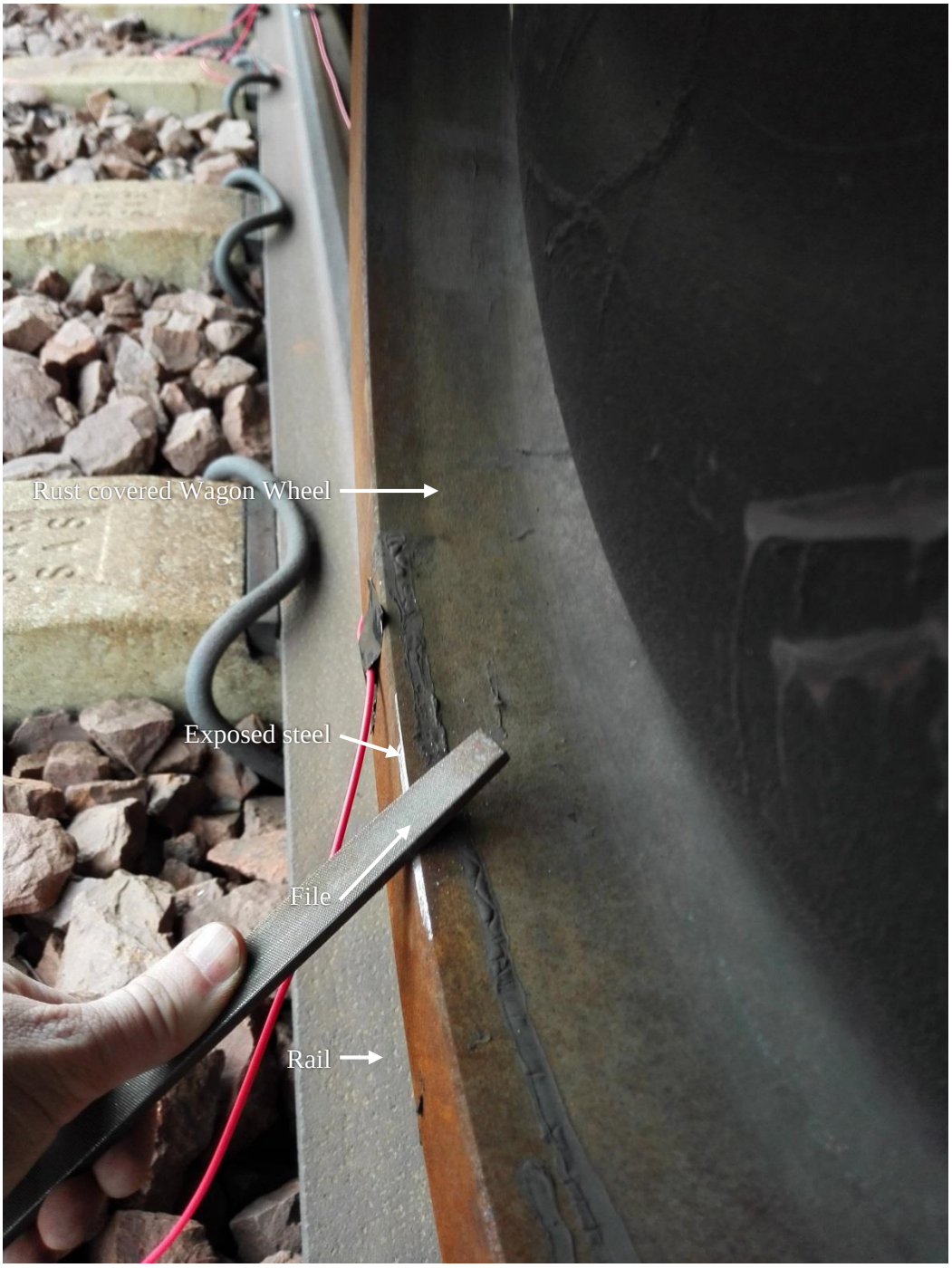


Figure 73: Photograph showing the filing of surfaces to which electrical contacts were made during the wagon measurements.

Once steel at each node was exposed, electrical conductive wire was secured to the wagon using duct tape. This secured the conductor to the wagon such that there would not be stresses on the area where the wire would make electrical connection to the node.

Subsequent to the securing to the conductive wires, the ends of the wires were soldered to the exposed steel of the nodes using a gas powered soldering iron. The securing of the wires as well as the solder connection to the nodes is illustrated in Figure 74.



Figure 74: Photograph showing the solder connections between conductors and the nodes of the wagon during the wagon measurements.

The wheels and couplers are significantly large in volume. Thus the heat provided by the soldering iron was quickly dissipated in the steel. This at times resulted in an insufficient electrical connection. To ensure electrical conductivity between the nodes and the wires used for measurements, “Electric Paint” was used as an alternative current path between

the wires and the exposed steel of the nodes. The “Electric Paint” was commercially purchased for this purpose and once dry offers an electrically conductive path.

Before testing commenced, each electrical connection to the nodes was tested using the continuity functionality of the multi-meter. This ensured that there was electrical connection between the measurement wires and the exposed steel of the nodes to avoid inaccurate readings.

C.7 Self-Inductance Introduced by Test Apparatus

Inductance is caused by AC current in a conductive loop as described in CHAPTER 3 of the research dissertation. Thus in order to avoid introducing inductance from the test equipment, the current return wire, and all wires used in the measurements were kept as close to the wagon body as possible. This minimized any loop areas in the circuit and hence inductance due to measurement equipment. This is visually illustrated in Figure 75 where it can be seen that the measurement wire (in this case the current return) was secured to the wagon body through the use of duct tape. This allowed the current in the wagon to flow in very close proximity to the return current.



Figure 75: Photograph showing the return conductive wire in close proximity to the wagon body to avoid creating loop areas and inductances during the wagon measurements.

APPENDIX D

WAGON MODEL VERIFICATION: EXPERIMENTAL RESULTS ANALYSIS

Section 4.3 of the dissertation describes the development of the wagon model through theoretical basis. For ease of reference the wagon model proposed can be seen in Figure 76.

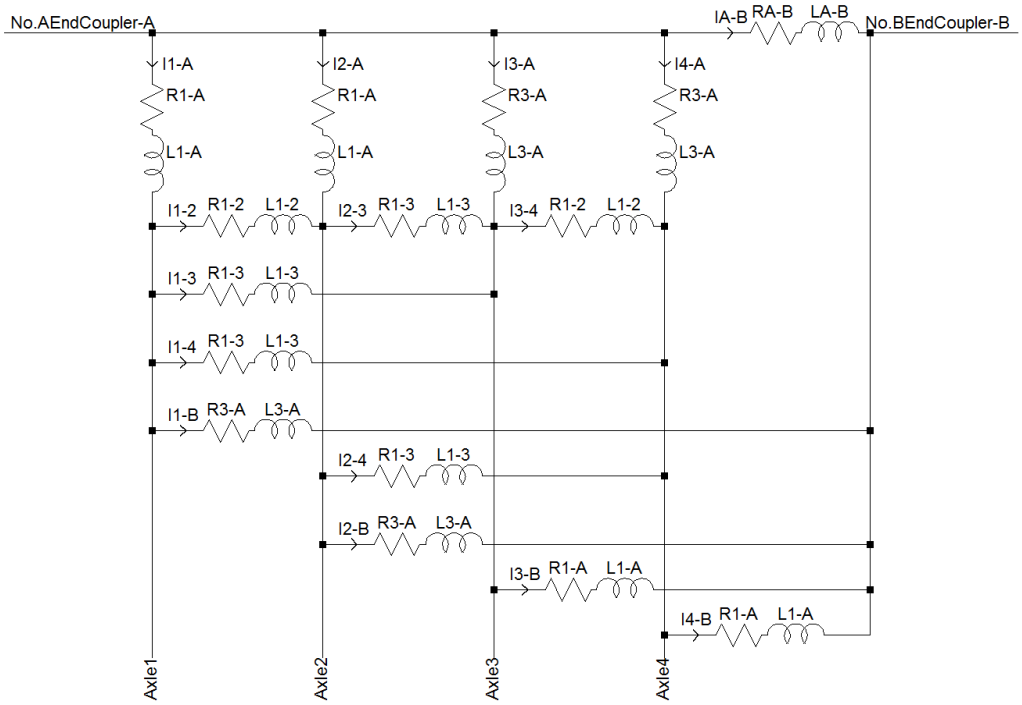


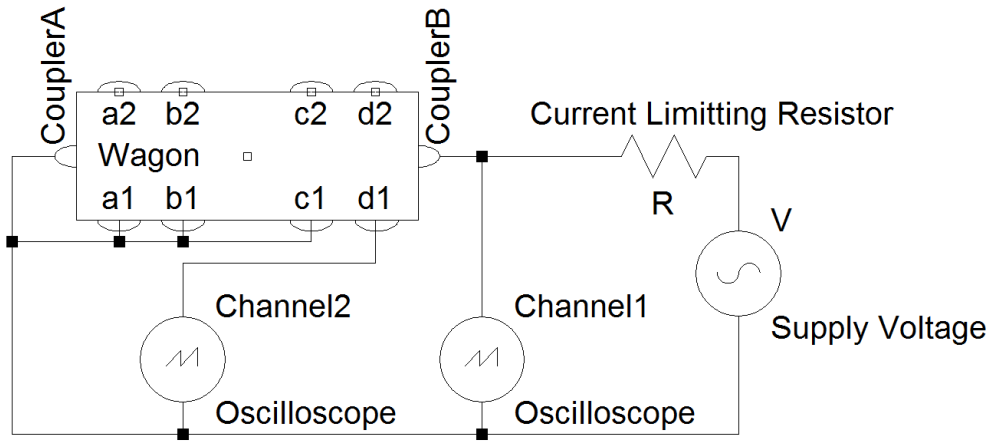
Figure 76: Diagram to show the reduced complex wagon model.

D.1 Setup of Simultaneous Equations from Wagon Measurements

In order to experimentally determine the size of components, some nodes were shorted together in order to modify the circuit topology and reduce the number of effective components. This method makes determining the sizes of parameters substantially simpler. For the each "new" circuit, appropriate circuit analysis techniques are performed and the determination of parameter sizes shown. This methodology is described in APPENDIX C.

D.1.1 Measurements on Axle D1

In order to perform measurements on axle D1, the circuit was setup as described in Figure 77. Further details of the setup and experimental methodology can be found in APPENDIX C.



where: V is a frequency generator (variable frequency) or DC supply.
R is a current limiting resistor.
$CouplerA$ is the No.1 end coupler.
$a1, a2, b1, b2, c1, c2, d1, d2$ are wheel terminals.
$CouplerB$ is the No.2 end coupler.

Figure 77: Diagram showing electrical connections to the wagon nodes to take measurements on the wheel $D1$ during wagon measurements.

Using this circuit, the wagon model can temporarily be modified to take into account for the elements shorted together. This revised model is only applicable to the measurements on wheel $D1$. The revised circuit diagram can be seen in Figure 78.

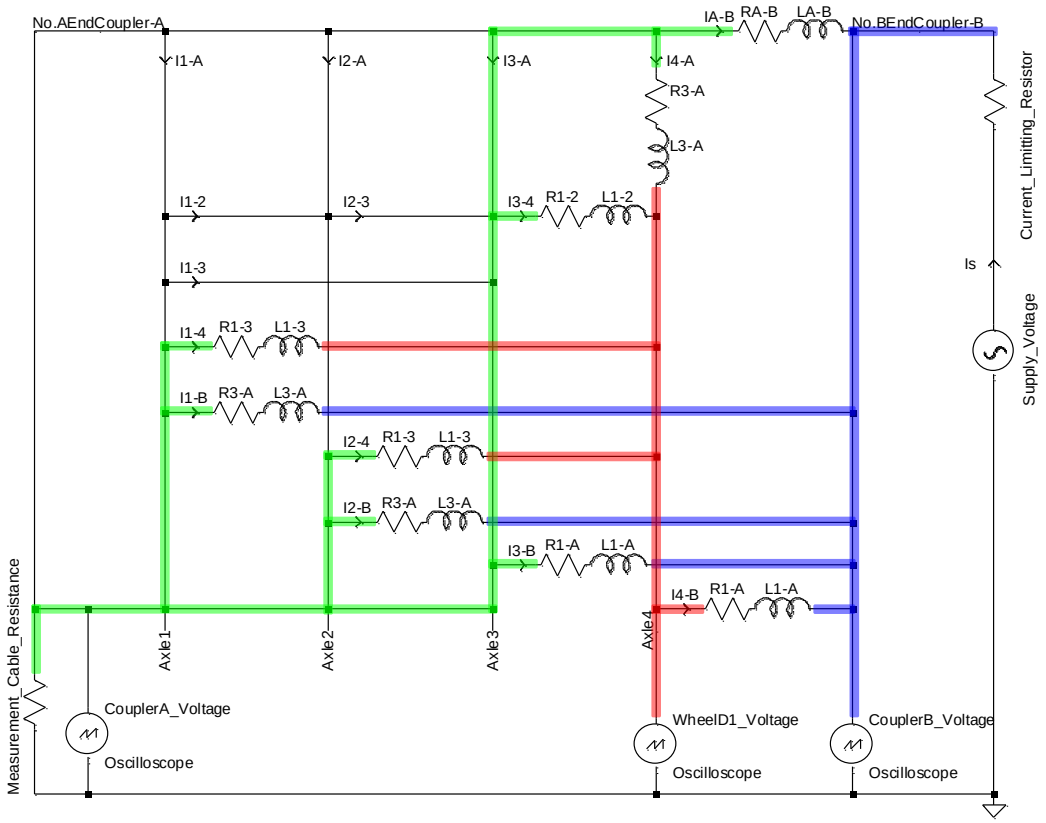


Figure 78: Circuit diagram of wagon model whilst under measurements on the wheel $D1$.

The measured values were as follows:

- Coupler B Voltage: 0.80 V_p
- Coupler A Voltage: 0.69 V_p
- Wheel D1 Voltage: 0.79 V_p
- Supply Current: 0.156 A_p

The measured voltage waveforms of Coupler B, Coupler A, Wheel D1 and the supply current waveform are shown in Figure 79. The waveforms are in phase with one another indicating that the elements of the circuit in Figure 78 do not contain imaginary components or the magnitude of the inductive and capacitive effects of the elements are negligible. Therefore the measured values are reflected as real values without imaginary components.

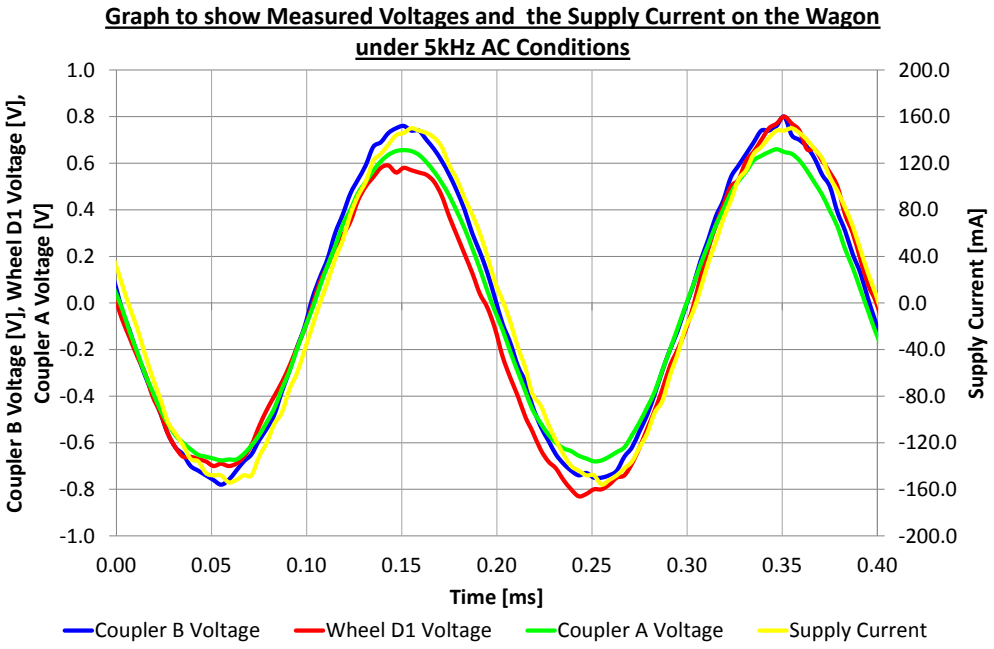


Figure 79: Graph showing wagon node voltages and supply current during measurements on the wheel $D1$.

Using the measured values, nodal analysis of the circuit is performed as follows:

Coupler B:

$$0 = i_S + i_{A-B} + i_{1-B} + i_{2-B} + i_{3-B} + i_{4-B}$$

$$0 = i_S + \frac{V(CouplerA) - V(CouplerB)}{R_{A-B}} + \frac{V(CouplerA) - V(CouplerB)}{R_{3-A}} \ldots + \frac{V(CouplerA) - V(CouplerB)}{R_{3-A}} + \frac{V(CouplerA) - V(CouplerB)}{R_{1-A}} \ldots + \frac{V(WheelD1) - V(CouplerB)}{R_{1-A}}$$

$$0 = 0.156 + \frac{0.69 - 0.80}{R_{A-B}} + \frac{0.69 - 0.80}{R_{3-A}} + \frac{0.69 - 0.80}{R_{3-A}} + \frac{0.69 - 0.80}{R_{1-A}} + \frac{0.79 - 0.80}{R_{1-A}}$$

$$0 = 0.156 + \frac{-0.11}{R_{A-B}} + \frac{-0.11}{R_{3-A}} + \frac{-0.11}{R_{3-A}} + \frac{-0.11}{R_{1-A}} + \frac{-0.01}{R_{1-A}}$$

$$0.156 = (0.11)\left(\frac{1}{R_{A-B}}\right) + (0.12)\left(\frac{1}{R_{1-A}}\right) + (0)\left(\frac{1}{R_{1-2}}\right) + (0)\left(\frac{1}{R_{1-3}}\right) + (0.22)\left(\frac{1}{R_{3-A}}\right) \quad ①$$

Wheel D1:

$$i_{4-B} = i_{4-A} + i_{3-4} + i_{1-4} + i_{2-4}$$

$$\frac{V(WheelD1)-V(CouplerB)}{R_{1-A}} = \frac{\frac{V(CouplerA)-V(CouplerB)}{R_{3-A}}+\frac{V(CouplerA)-V(CouplerB)}{R_{1-2}}\ldots}{+\frac{V(CouplerA)-V(WheelD1)}{R_{1-3}}+\frac{V(CouplerA)-V(WheelD1)}{R_{1-3}}}$$

$$\frac{0.79-0.80}{R_{1-A}} = \frac{0.69-0.80}{R_{3-A}}+\frac{0.69-0.80}{R_{1-2}}+\frac{0.69-0.79}{R_{1-3}}+\frac{0.69-0.79}{R_{1-3}}$$

$$\frac{-0.01}{R_{1-A}} = \frac{-0.11}{R_{3-A}}+\frac{-0.11}{R_{1-2}}+\frac{-0.1}{R_{1-3}}+\frac{-0.1}{R_{1-3}}$$

$$0 = (0)\left(\frac{1}{R_{A-B}}\right)+(0.01)\left(\frac{1}{R_{1-A}}\right)+(-0.21)\left(\frac{1}{R_{1-2}}\right)+(-0.2)\left(\frac{1}{R_{1-3}}\right)+(-0.11)\left(\frac{1}{R_{3-A}}\right) \quad ②$$

CouplerA:

$$0 = i_S + i_{A-B} + i_{4-A} + i_{3-4} + i_{1-4} + i_{1-B} + i_{2-4} + i_{2-B} + i_{3-B}$$

$$0 = \frac{i_S+\frac{V(CouplerA)-V(CouplerB)}{R_{A-B}}+\frac{V(CouplerA)-V(WheelD1)}{R_{3-A}}\ldots}{+\frac{V(CouplerA)-V(WheelD1)}{R_{1-2}}+\frac{V(CouplerA)-V(WheelD1)}{R_{1-3}}\ldots}$$
$$+\frac{V(CouplerA)-V(CouplerB)}{R_{3-A}}+\frac{V(CouplerA)-V(WheelD1)}{R_{1-3}}\ldots$$
$$+\frac{V(CouplerA)-V(CouplerB)}{R_{3-A}}+\frac{V(CouplerA)-V(CouplerB)}{R_{1-A}}$$

$$0 = \frac{0.156+\frac{0.69-0.80}{R_{A-B}}+\frac{0.69-0.79}{R_{3-A}}+\frac{0.69-0.79}{R_{1-2}}+\frac{0.69-0.79}{R_{1-3}}+\frac{0.69-0.80}{R_{3-A}}\ldots}{+\frac{0.69-0.79}{R_{1-3}}+\frac{0.69-0.80}{R_{3-A}}+\frac{0.69-0.80}{R_{1-A}}}$$

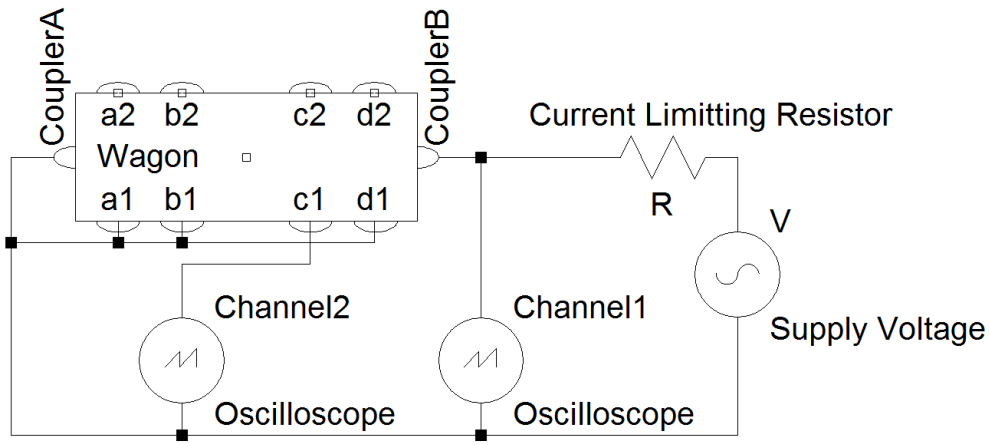
$$0 = 0.156+\frac{-0.11}{R_{A-B}}+\frac{-0.1}{R_{3-A}}+\frac{-0.1}{R_{1-2}}+\frac{-0.1}{R_{1-3}}+\frac{-0.11}{R_{3-A}}+\frac{-0.1}{R_{1-3}}+\frac{-0.11}{R_{3-A}}+\frac{-0.11}{R_{1-A}}$$

$$0.156 = (0.11)\left(\frac{1}{R_{A-B}}\right)+(0.11)\left(\frac{1}{R_{1-A}}\right)+(0.1)\left(\frac{1}{R_{1-2}}\right)+(0.2)\left(\frac{1}{R_{1-3}}\right)+(0.32)\left(\frac{1}{R_{3-A}}\right) \quad ③$$

These measurements result in simultaneous equation ①, ② and ③.

D.1.2 Measurements on Axle C1

In order to perform measurements on axle C1, the circuit was setup as described in Figure 80. Further details of the setup and experimental methodology can be found in APPENDIX C.



where: V is a frequency generator (variable frequency) or DC supply.

R is a current limiting resistor.

$CouplerA$ is the No.1 end coupler.

$a1, a2, b1, b2, c1, c2, d1, d2$ are wheel terminals.

$CouplerB$ is the No.2 end coupler.

Figure 80: Diagram showing electrical connections to the wagon nodes to take measurements on the wheel $C1$ during wagon measurements.

Using this circuit, the wagon model can temporarily be modified to take into account for the elements shorted together. This revised model is only applicable to the measurements on wheel $C1$. The revised circuit diagram can be seen in Figure 81.

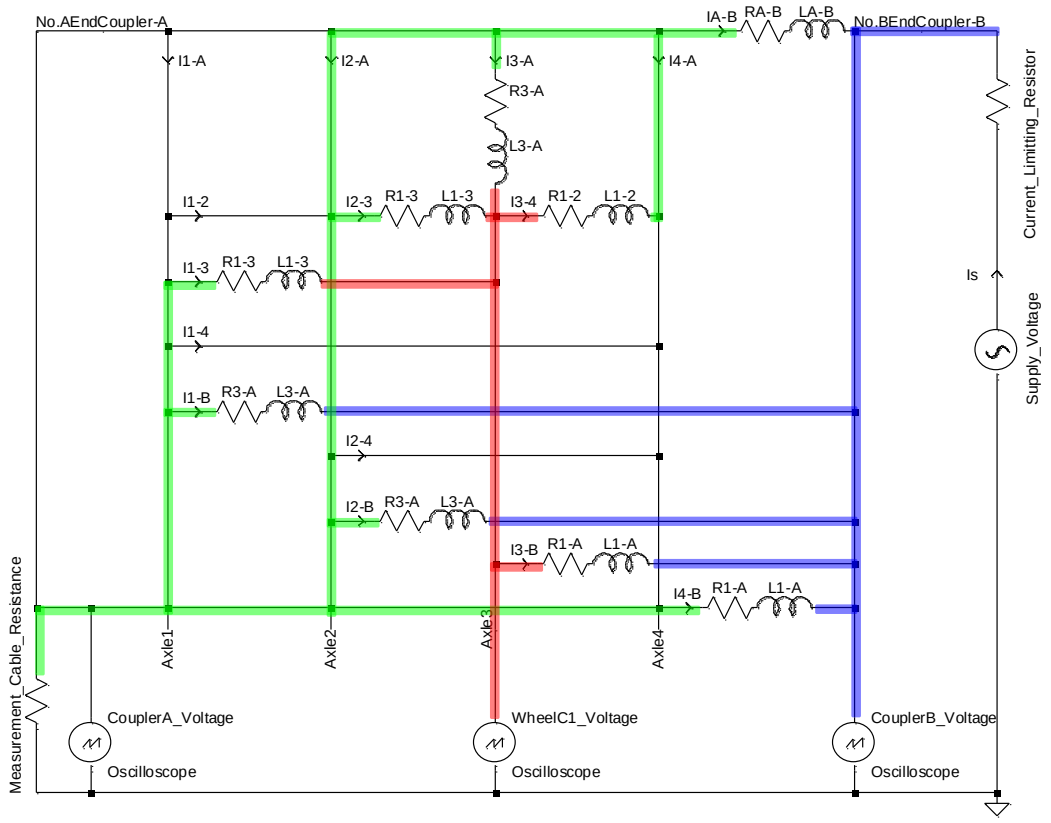


Figure 81: Circuit diagram of wagon model whilst under measurements on the wheel $C1$.

The measured values were as follows:

- Coupler B Voltage: 0.76 V_p
- Coupler A Voltage: 0.68 V_p
- Wheel C1 Voltage: 0.70 V_p
- Supply Current: 0.155 A_p

The measured voltage waveforms of Coupler B, Coupler A, Wheel C1 and the supply current waveform are shown in Figure 82. The waveforms are in phase with one another indicating that the elements of the circuit in Figure 81 do not contain imaginary components or the magnitude of the inductive and capacitive effects of the elements are negligible. Therefore the measured values are reflected as real values without imaginary components.

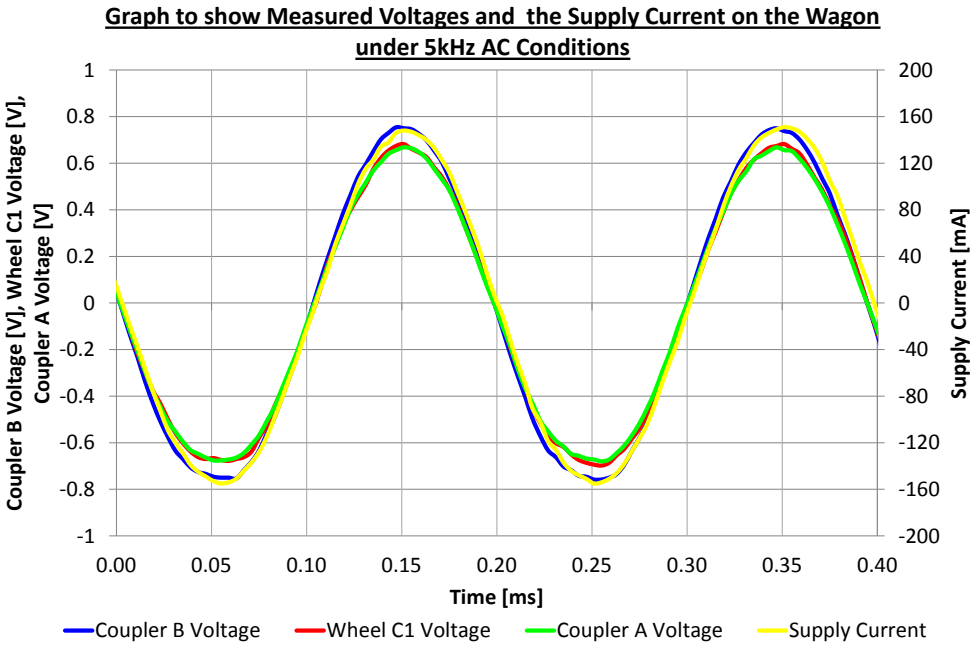


Figure 82: Graph showing wagon node voltages and supply current during measurements on the wheel $C1$.

Coupler B:

$$0 = i_S + i_{A-B} + i_{1-B} + i_{2-B} + i_{3-B} + i_{4-B}$$

$$0 = i_S + \frac{V(CouplerA) - V(CouplerB)}{R_{A-B}} + \frac{V(CouplerA) - V(CouplerB)}{R_{3-A}} \ldots + \frac{V(CouplerA) - V(CouplerB)}{R_{3-A}} + \frac{V(WheelC1) - V(CouplerB)}{R_{1-A}} \ldots + \frac{V(CouplerA) - V(CouplerB)}{R_{1-A}}$$

$$0 = 0.155 + \frac{0.68-0.76}{R_{A-B}} + \frac{0.68-0.76}{R_{3-A}} + \frac{0.68-0.76}{R_{3-A}} + \frac{0.70-0.76}{R_{1-A}} + \frac{0.68-0.76}{R_{1-A}}$$

$$0 = 0.155 + \frac{-0.08}{R_{A-B}} + \frac{-0.08}{R_{3-A}} + \frac{-0.08}{R_{3-A}} + \frac{-0.06}{R_{1-A}} + \frac{-0.08}{R_{1-A}}$$

$$0.155 = (0.08)\left(\frac{1}{R_{A-B}}\right) + (0.14)\left(\frac{1}{R_{1-A}}\right) + (0)\left(\frac{1}{R_{1-2}}\right) + (0)\left(\frac{1}{R_{1-3}}\right) + (0.16)\left(\frac{1}{R_{3-A}}\right) \quad ④$$

Wheel C1:

$$0 = i_{3-4} + i_{3-B} - i_{3-A} - i_{2-3} - i_{1-3}$$

$$0 = \frac{V(WheelC1)-V(CouplerA)}{R_{1-2}} + \frac{V(WheelC1)-V(CouplerB)}{R_{1-A}} \ldots - \frac{V(CouplerA)-V(WheelC1)}{R_{3-A}} - \frac{V(CouplerA)-V(WheelC1)}{R_{1-3}} \ldots - \frac{V(CouplerA)-V(WheelC1)}{R_{1-3}}$$

$$0 = \frac{0.70-0.68}{R_{1-2}} + \frac{0.70-0.76}{R_{1-A}} - \frac{0.68-0.70}{R_{3-A}} - \frac{0.68-0.70}{R_{1-3}} - \frac{0.68-0.70}{R_{1-3}}$$

$$0 = \frac{-0.02}{R_{1-2}} + \frac{-0.06}{R_{1-A}} - \frac{-0.02}{R_{3-A}} - \frac{-0.02}{R_{1-3}} - \frac{-0.02}{R_{1-3}}$$

$$0 = (0)\left(\frac{1}{R_{A-B}}\right) + (-0.06)\left(\frac{1}{R_{1-A}}\right) + (-0.02)\left(\frac{1}{R_{1-2}}\right) + (0.04)\left(\frac{1}{R_{1-3}}\right) + (0.02)\left(\frac{1}{R_{3-A}}\right) \quad ⑤$$

Coupler A:

$$0 = i_S + i_{A-B} + i_{3-A} + i_{2-3} + i_{1-3} + i_{1-B} + i_{2-B} + i_{4-B} - i_{3-4}$$

$$i_S + \frac{V(CouplerA)-V(CouplerB)}{R_{A-B}} + \frac{V(CouplerA)-V(WheelC1)}{R_{3-A}} \ldots$$

$$0 = + \frac{V(CouplerA)-V(WheelC1)}{R_{1-3}} + \frac{V(CouplerA)-V(WheelC1)}{R_{1-3}} \ldots$$

$$+ \frac{V(CouplerA)-V(CouplerB)}{R_{3-A}} + \frac{V(CouplerA)-V(CouplerB)}{R_{3-A}} \ldots$$

$$+ \frac{V(CouplerA)-V(CouplerB)}{R_{1-A}} - \frac{V(WheelC1)-V(CouplerA)}{R_{1-2}}$$

$$0 = 0.155 + \frac{0.68-0.76}{R_{A-B}} + \frac{0.68-0.70}{R_{3-A}} + \frac{0.68-0.70}{R_{1-3}} + \frac{0.68-0.70}{R_{1-3}} + \frac{0.68-0.76}{R_{3-A}} \ldots$$

$$+ \frac{0.68-0.76}{R_{3-A}} + \frac{0.68-0.76}{R_{1-A}} - \frac{0.70-0.68}{R_{1-2}}$$

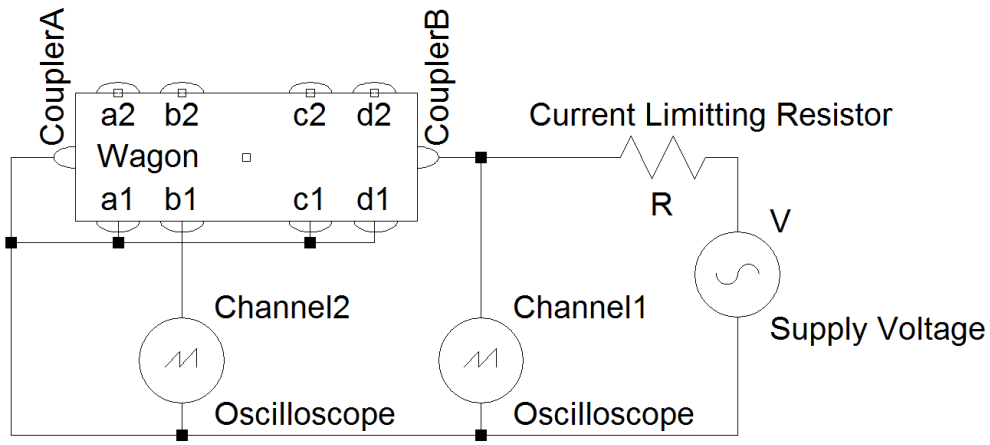
$$0 = 0.155 + \frac{-0.08}{R_{A-B}} + \frac{-0.02}{R_{3-A}} + \frac{-0.02}{R_{1-3}} + \frac{-0.02}{R_{1-3}} + \frac{-0.08}{R_{3-A}} + \frac{-0.08}{R_{3-A}} + \frac{-0.08}{R_{1-A}} - \frac{0.02}{R_{1-2}}$$

$$0.155 = (0.08)\left(\frac{1}{R_{A-B}}\right) + (0.08)\left(\frac{1}{R_{1-A}}\right) + (0.02)\left(\frac{1}{R_{1-2}}\right) + (0.04)\left(\frac{1}{R_{1-3}}\right) + (0.18)\left(\frac{1}{R_{3-A}}\right) \quad ⑥$$

These measurements result in simultaneous equation ④, ⑤ and ⑥.

D.1.3 Measurements on Axle B1

In order to perform measurements on axle B1, the circuit was setup as described in Figure 83. Further details of the setup and experimental methodology can be found in APPENDIX C.



where: V is a frequency generator (variable frequency) or DC supply.

R is a current limiting resistor.

$CouplerA$ is the No.1 end coupler.

$a1, a2, b1, b2, c1, c2, d1, d2$ are wheel terminals.

$CouplerB$ is the No.2 end coupler.

Figure 83: Diagram showing electrical connections to the wagon nodes to take measurements on the wheel $B1$ during wagon measurements.

Using this circuit, the wagon model can temporarily be modified to take into account for the elements shorted together. This revised model is only applicable to the measurements on wheel $B1$. The revised circuit diagram can be seen in Figure 84.

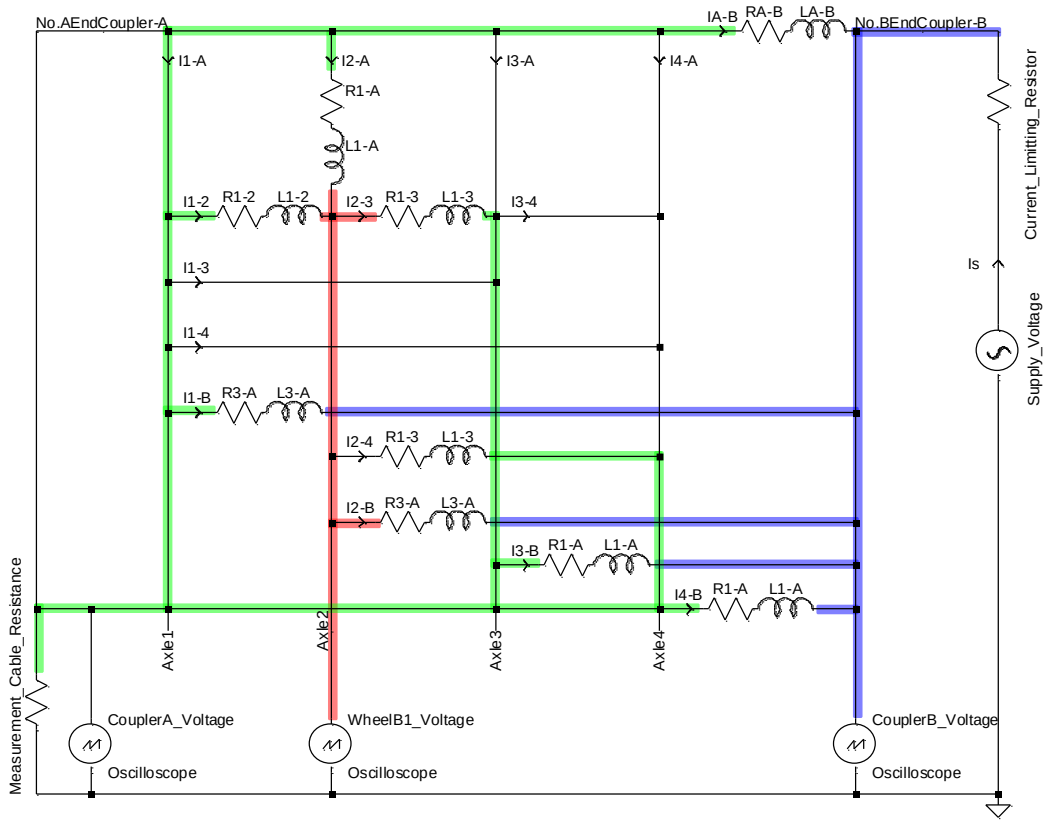


Figure 84: Circuit diagram of wagon model whilst under measurements on the wheel $B1$.

The measured values were as follows:

- Coupler B Voltage: 0.80 V_p
- Coupler A Voltage: 0.68 V_p
- Wheel B1 Voltage: 0.75 V_p
- Supply Current: 0.154 A_p

The measured voltage waveforms of Coupler B, Coupler A, Wheel B1 and the supply current waveform are shown in Figure 85. The waveforms are in phase with one another indicating that the elements of the circuit in Figure 84 do not contain imaginary components or the magnitude of the inductive and capacitive effects of the elements are negligible. Therefore the measured values are reflected as real values without imaginary components.

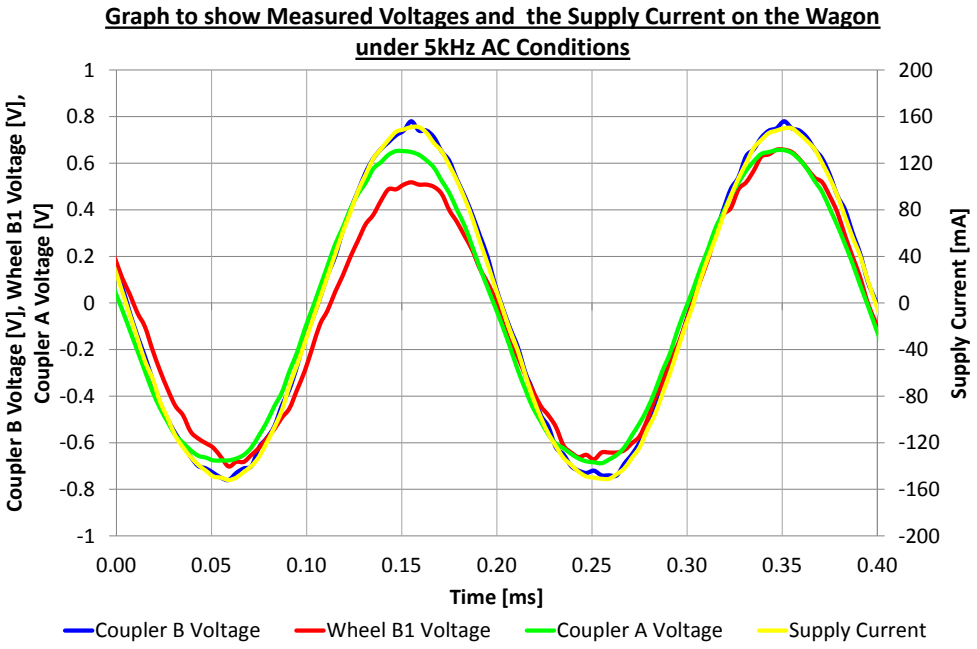


Figure 85: Graph showing wagon node voltages and supply current during measurements on the wheel *B*1.

Coupler B:

$$0 = i_S + i_{A-B} + i_{1-B} + i_{2-B} + i_{3-B} + i_{4-B}$$

$$0 \quad i_S + \frac{V(CouplerA) - V(CouplerB)}{R_{A-B}} + \frac{V(CouplerA) - V(CouplerB)}{R_{3-A}} \ldots$$
$$= + \frac{V(WheelB1) - V(CouplerB)}{R_{3-A}} + \frac{V(CouplerA) - V(CouplerB)}{R_{1-A}} \ldots$$
$$+ \frac{V(CouplerA) - V(CouplerB)}{R_{1-A}}$$

$$0 = 0.154 + \frac{0.68-0.80}{R_{A-B}} + \frac{0.68-0.80}{R_{3-A}} + \frac{0.75-0.80}{R_{3-A}} + \frac{0.68-0.80}{R_{1-A}} + \frac{0.68-0.80}{R_{1-A}}$$

$$0.154 = \frac{0.12}{R_{A-B}} + \frac{0.12}{R_{3-A}} + \frac{0.05}{R_{3-A}} + \frac{0.12}{R_{1-A}} + \frac{0.12}{R_{1-A}}$$

$$0.154 = (0.12)\left(\frac{1}{R_{A-B}}\right) + (0.24)\left(\frac{1}{R_{1-A}}\right) + (0)\left(\frac{1}{R_{1-2}}\right) + (0)\left(\frac{1}{R_{1-3}}\right) + (0.17)\left(\frac{1}{R_{3-A}}\right) \quad ⑦$$

Wheel B1:

$$0 = i_{2-3} + i_{2-4} + i_{2-B} - i_{2-A} - i_{1-2}$$

$$0 = \frac{V(WheelB1)-V(CouplerA)}{R_{1-3}} + \frac{V(WheelB1)-V(CouplerA)}{R_{1-3}} \ldots + \frac{V(WheelB1)-V(CouplerB)}{R_{3-A}} - \frac{V(CouplerA)-V(WheelB1)}{R_{1-A}} \ldots - \frac{V(CouplerA)-V(WheelB1)}{R_{1-2}}$$

$$0 = \frac{0.75-0.68}{R_{1-3}} + \frac{0.75-0.68}{R_{1-3}} + \frac{0.75-0.80}{R_{3-A}} - \frac{0.68-0.75}{R_{1-A}} - \frac{0.68-0.75}{R_{1-2}}$$

$$0 = \frac{0.07}{R_{1-3}} + \frac{0.07}{R_{1-3}} + \frac{-0.05}{R_{3-A}} - \frac{-0.07}{R_{1-A}} - \frac{-0.07}{R_{1-2}}$$

$$0 = (0)\left(\frac{1}{R_{A-B}}\right) + (0.07)\left(\frac{1}{R_{1-A}}\right) + (0.07)\left(\frac{1}{R_{1-2}}\right) + (0.14)\left(\frac{1}{R_{1-3}}\right) + (-0.05)\left(\frac{1}{R_{3-A}}\right) \quad ⑧$$

Coupler A:

$$0 = i_S + i_{1-2} + i_{1-B} + i_{2-A} + i_{3-B} + i_{4-B} + i_{A-B} - i_{2-3} - i_{2-4}$$

$$0 = i_S + \frac{V(CouplerA)-V(WheelB1)}{R_{1-2}} + \frac{V(CouplerA)-V(CouplerB)}{R_{3-A}} \ldots + \frac{V(CouplerA)-V(WheelB1)}{R_{1-A}} + \frac{V(CouplerA)-V(CouplerB)}{R_{1-A}} \ldots + \frac{V(CouplerA)-V(CouplerB)}{R_{1-A}} + \frac{V(CouplerA)-V(CouplerB)}{R_{A-B}} \ldots - \frac{V(WheelB1)-V(CouplerA)}{R_{1-3}} - \frac{V(WheelB1)-V(CouplerA)}{R_{1-3}}$$

$$0 = 0.154 + \frac{0.68-0.75}{R_{1-2}} + \frac{0.68-0.80}{R_{3-A}} + \frac{0.68-0.75}{R_{1-A}} + \frac{0.68-0.80}{R_{1-A}} + \frac{0.68-0.80}{R_{1-A}} \ldots + \frac{0.68-0.80}{R_{A-B}} - \frac{0.75-0.68}{R_{1-3}} - \frac{0.75-0.68}{R_{1-3}}$$

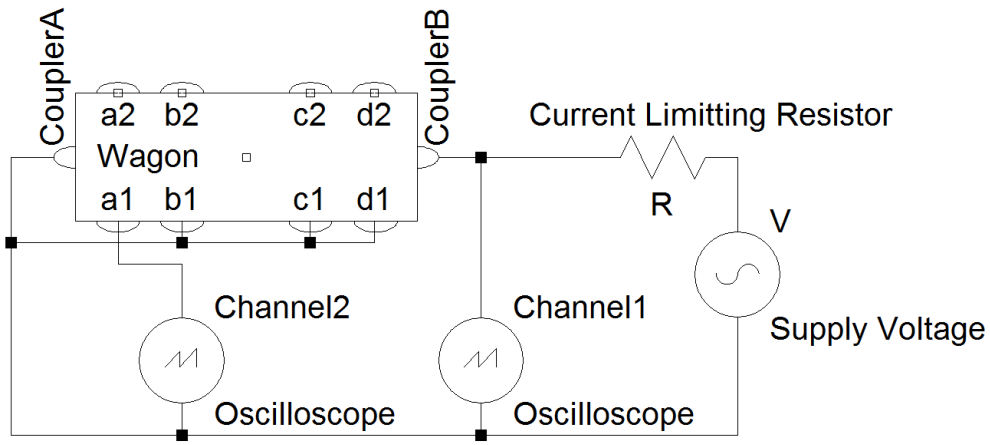
$$0 = 0.154 + \frac{-0.07}{R_{1-2}} + \frac{-0.12}{R_{3-A}} + \frac{-0.07}{R_{1-A}} + \frac{-0.12}{R_{1-A}} + \frac{-0.12}{R_{1-A}} + \frac{-0.12}{R_{A-B}} - \frac{0.07}{R_{1-3}} - \frac{0.07}{R_{1-3}}$$

$$0.154 = (0.12)\left(\frac{1}{R_{A-B}}\right) + (0.31)\left(\frac{1}{R_{1-A}}\right) + (0.07)\left(\frac{1}{R_{1-2}}\right) + (0.14)\left(\frac{1}{R_{1-3}}\right) + (0.12)\left(\frac{1}{R_{3-A}}\right) \quad ⑨$$

These measurements result in simultaneous equation ⑦, ⑧ and ⑨.

D.1.4 Measurements on Axle A1

In order to perform measurements on axle A1, the circuit was setup as described in Figure 86. Further details of the setup and experimental methodology can be found in APPENDIX C.



where: V is a frequency generator (variable frequency) or DC supply.

R is a current limiting resistor.

$CouplerA$ is the No.1 end coupler.

$a1, a2, b1, b2, c1, c2, d1, d2$ are wheel terminals.

$CouplerB$ is the No.2 end coupler.

Figure 86: Diagram showing electrical connections to the wagon nodes to take measurements on the wheel $A1$ during wagon measurements.

Using this circuit, the wagon model can temporarily be modified to take into account for the elements shorted together. This revised model is only applicable to the measurements on wheel $A1$. The revised circuit diagram can be seen in Figure 87.

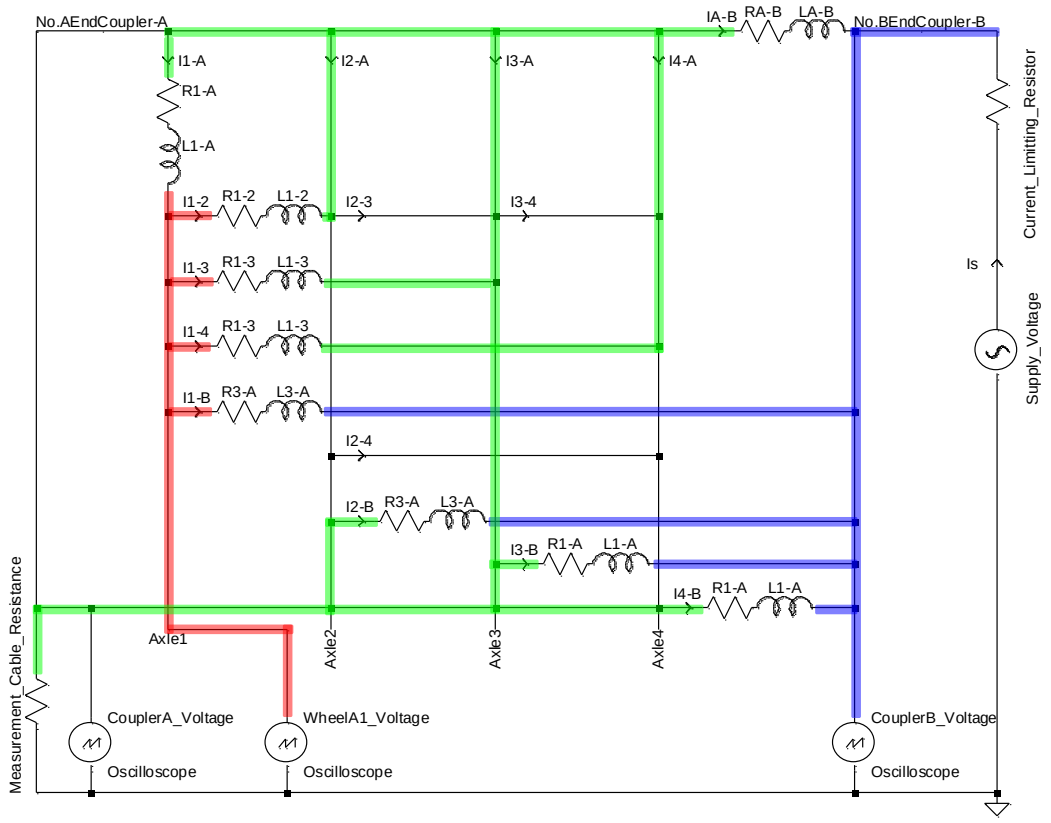


Figure 87: Circuit diagram of wagon model whilst under measurements on the wheel $A1$.

The measured values were as follows:

- Coupler B Voltage: 0.75 V_p
- Coupler A Voltage: 0.65 V_p
- Wheel A1 Voltage: 0.70 V_p
- Supply Current: 0.152 A_p

The measured voltage waveforms of Coupler B, Coupler A, Wheel A1 and the supply current waveform are shown in Figure 88. The waveforms are in phase with one another indicating that the elements of the circuit in Figure 87 do not contain imaginary components or the magnitude of the inductive and capacitive effects of the elements are negligible. Therefore the measured values are reflected as real values without imaginary components.

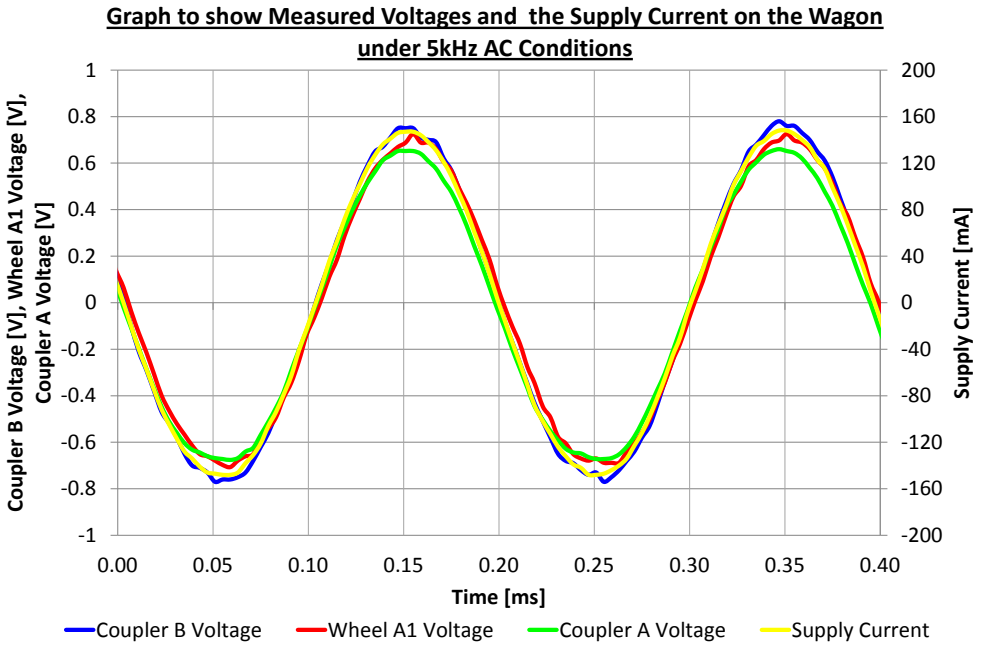


Figure 88: Graph showing wagon node voltages and supply current during measurements on the wheel $A1$.

Coupler B:

$$0 = i_S + i_{A-B} + i_{1-B} + i_{2-B} + i_{3-B} + i_{4-B}$$

$$0 \quad i_S + \frac{V(CouplerA) - V(CouplerB)}{R_{A-B}} + \frac{V(WheelA1) - V(CouplerB)}{R_{3-A}} \ldots$$
$$= + \frac{V(CouplerA) - V(CouplerB)}{R_{3-A}} + \frac{V(CouplerA) - V(CouplerB)}{R_{1-A}} \ldots$$
$$+ \frac{V(CouplerA) - V(CouplerB)}{R_{1-A}}$$

$$0 = 0.152 + \frac{0.65 - 0.75}{R_{A-B}} + \frac{0.70 - 0.75}{R_{3-A}} + \frac{0.65 - 0.75}{R_{3-A}} + \frac{0.65 - 0.75}{R_{1-A}} + \frac{0.65 - 0.75}{R_{1-A}}$$

$$0 = 0.152 + \frac{-0.10}{R_{A-B}} + \frac{-0.05}{R_{3-A}} + \frac{-0.10}{R_{3-A}} + \frac{-0.10}{R_{1-A}} + \frac{-0.10}{R_{1-A}}$$

$$0.152 = (0.10)\left(\frac{1}{R_{A-B}}\right) + (0.20)\left(\frac{1}{R_{1-A}}\right) + (0)\left(\frac{1}{R_{1-2}}\right) + (0)\left(\frac{1}{R_{1-3}}\right) + (0.15)\left(\frac{1}{R_{3-A}}\right) \quad ⑩$$

Wheel A1:

$$i_{1-A} = i_{1-2} + i_{1-3} + i_{1-4} + i_{1-B}$$

$$\frac{V(CouplerA)-V(WheelA1)}{R_{1-A}} = \frac{V(WheelA1)-V(CouplerA)}{R_{1-2}}+\frac{V(WheelA1)-V(CouplerA)}{R_{1-3}}\ldots$$
$$+\frac{V(WheelA1)-V(CouplerA)}{R_{1-3}}+\frac{V(CouplerA)-V(CouplerB)}{R_{3-A}}$$

$$\frac{0.65-0.70}{R_{1-A}} = \frac{0.70-0.65}{R_{1-2}}+\frac{0.70-0.65}{R_{1-3}}+\frac{0.70-0.65}{R_{1-3}}+\frac{0.65-0.75}{R_{3-A}}$$

$$\frac{-0.05}{R_{1-A}} = \frac{0.05}{R_{1-2}}+\frac{0.05}{R_{1-3}}+\frac{0.05}{R_{1-3}}+\frac{-0.10}{R_{3-A}}$$

$$0 = (0)\left(\frac{1}{R_{A-B}}\right)+(0.05)\left(\frac{1}{R_{1-A}}\right)+(0.05)\left(\frac{1}{R_{1-2}}\right)+(0.10)\left(\frac{1}{R_{1-3}}\right)+(-0.10)\left(\frac{1}{R_{3-A}}\right) \quad ⑪$$

Coupler A:

$$0 = i_S + i_{1-A} + i_{2-B} + i_{3-B} + i_{4-B} + i_{A-B} - i_{1-2} - i_{1-3} - i_{1-4}$$

$$0 \quad i_S+\frac{V(CouplerA)-V(WheelA1)}{R_{1-A}}+\frac{V(CouplerA)-V(CouplerB)}{R_{3-A}}\ldots$$
$$= +\frac{V(CouplerA)-V(CouplerB)}{R_{1-A}}+\frac{V(CouplerA)-V(CouplerB)}{R_{1-A}}\ldots$$
$$+\frac{V(CouplerA)-V(CouplerB)}{R_{A-B}}-\frac{V(WheelA1)-V(CouplerA)}{R_{1-2}}\ldots$$
$$-\frac{V(WheelA1)-V(CouplerA)}{R_{1-3}}-\frac{V(WheelA1)-V(CouplerA)}{R_{1-3}}$$

$$0 = 0.152+\frac{0.65-0.70}{R_{1-A}}+\frac{0.65-0.75}{R_{3-A}}+\frac{0.65-0.75}{R_{1-A}}+\frac{0.65-0.75}{R_{1-A}}+\frac{0.65-0.75}{R_{A-B}}\ldots$$
$$-\frac{0.70-0.65}{R_{1-2}}-\frac{0.70-0.65}{R_{1-3}}-\frac{0.70-0.65}{R_{1-3}}$$

$$0 = 0.152+\frac{-0.05}{R_{1-A}}+\frac{-0.10}{R_{3-A}}+\frac{-0.10}{R_{1-A}}+\frac{-0.10}{R_{1-A}}+\frac{-0.10}{R_{A-B}}-\frac{0.05}{R_{1-2}}-\frac{0.05}{R_{1-3}}-\frac{0.05}{R_{1-3}}$$

$$0.152 = (0.10)\left(\frac{1}{R_{A-B}}\right)+(0.25)\left(\frac{1}{R_{1-A}}\right)+(0.05)\left(\frac{1}{R_{1-2}}\right)+(0.10)\left(\frac{1}{R_{1-3}}\right)+(0.10)\left(\frac{1}{R_{3-A}}\right) \quad ⑫$$

These measurements result in simultaneous equation ⑩, ⑪ and ⑫.

D.2 Solving Simultaneous equations

Due to the simplification of the wagon model discussed in CHAPTER 4, section 4.3 of the research dissertation, there are only 5 unknown variables in the wagon model, however 12 simultaneous equations have been derived. The additional simultaneous equations were derived for completeness, however are not required to determine the wagon model. Thus equations ①, ②, ③, ⑥ and ⑨ are used in the wagon parameter determination.

Equations ①, ②, ③, ⑥ and ⑨ can now be represented in matrix format such that:

$$\boldsymbol{Zv = k}$$

Where $\boldsymbol{A}$ is a square matric of size 5, $\boldsymbol{v}$ is a unknown vector and $\boldsymbol{k}$ is the system constant vector.

$$\begin{bmatrix} z_{1-1} & \cdots & z_{1-5} \\ \vdots & \ddots & \vdots \\ z_{5-1} & \cdots & z_{5-5} \end{bmatrix} \begin{bmatrix} v_1 \\ \vdots \\ v_5 \end{bmatrix} = \begin{bmatrix} k_1 \\ \vdots \\ k_5 \end{bmatrix}$$

The solution to the system is found by calculating the inverse matrix of $\boldsymbol{Z}, \boldsymbol{Z^{-1}}$ such that $\boldsymbol{v}$ can be solved for.

$$\boldsymbol{Z^{-1}Zv = Z^{-1}k}$$
$$\boldsymbol{v = Z^{-1}k}$$

Thus simultaneous equations ①, ②, ③, ⑥ and ⑨ are represented in matrix format as:

$$\boldsymbol{Av_1 = k_1}$$

$$\begin{bmatrix} 0.11 & 0.12 & 0 & 0 & 0.22 \\ 0 & 0.01 & -0.21 & -0.20 & -0.11 \\ 0.11 & 0.11 & 0.1 & 0.2 & 0.32 \\ 0.08 & 0.08 & 0.02 & 0.04 & 0.18 \\ 0.12 & 0.31 & 0.07 & 0.14 & 0.12 \end{bmatrix} \begin{bmatrix} \left(\frac{1}{R_{A-B}}\right) \\ \left(\frac{1}{R_{1-A}}\right) \\ \left(\frac{1}{R_{1-2}}\right) \\ \left(\frac{1}{R_{1-3}}\right) \\ \left(\frac{1}{R_{3-A}}\right) \end{bmatrix} = \begin{bmatrix} 0.156 \\ 0 \\ 0.156 \\ 0.155 \\ 0.154 \end{bmatrix}$$

In ideal conditions, the mathematical matrix calculations would be able to determine the wagon parameter, however, due to unavoidable measurement inaccuracies this matrix manipulation becomes unfeasible. This is because the mathematical matrix calculations are exact and do not allow for any inaccuracies. As a result, solving this matrix would result in physically unfeasible (very large and small) parameter values.

In order to determine the wagon parameters, considering the inaccuracies in measurement data, and a mathematic software tool, such as MatLab, Octave or similar (for this research, GNU Octave version 3.8.2 was used), can be used to iterate through a series of values and store the error between the calculated result, and the measured result. The simulation results can then be sorted and the solution with the smallest error used as the wagon parameters. The simulation code for this section of the research can be seen in APPENDIX G, G.1.

Following the iterative simulation, the values for the wagon parameters with the lowest average error of 7.65 % are obtained as follows:

- $R_{A-B} = 0.72\ \Omega$
- $R_{1-A} = 200\ \Omega$

- $R_{1-2} = 1500\,\Omega$
- $R_{1-3} = 1500\,\Omega$
- $R_{3-A} = 120\,\Omega$

The reason that these parameters are round numbers is due to the iteration increments of the parameters. The increments were rational and hence the parameters have an accuracy which is limited by the boundaries of the iterative process. With and average error of only 7.65 %, the parameters were deemed acceptable and further iterative processes around the initial parameters using smaller increments was not necessary.

Using the these parameters, equations ①, ②, ③, ⑥ and ⑨ can be redefined using the newly obtained wagon parameters, which results in equations ⑬, ⑭, ⑮, ⑯ and ⑰ respectively as shown below:

$$0.1552111111 = (0.11)\left(\frac{1}{R_{A-B}}\right)+(0.12)\left(\frac{1}{R_{1-A}}\right)+(0)\left(\frac{1}{R_{1-2}}\right)+(0)\left(\frac{1}{R_{1-3}}\right)+(0.22)\left(\frac{1}{R_{3-A}}\right) \quad ⑬$$

$$-0.00114 = (0)\left(\frac{1}{R_{A-B}}\right)+(0.01)\left(\frac{1}{R_{1-A}}\right)+(-0.21)\left(\frac{1}{R_{1-2}}\right)+(-0.2)\left(\frac{1}{R_{1-3}}\right)+(-0.11)\left(\frac{1}{R_{3-A}}\right) \quad ⑭$$

$$0.1561944444 = (0.11)\left(\frac{1}{R_{A-B}}\right)+(0.11)\left(\frac{1}{R_{1-A}}\right)+(0.1)\left(\frac{1}{R_{1-2}}\right)+(0.2)\left(\frac{1}{R_{1-3}}\right)+(0.32)\left(\frac{1}{R_{3-A}}\right) \quad ⑮$$

$$0.1130511111 = (0.08)\left(\frac{1}{R_{A-B}}\right)+(0.08)\left(\frac{1}{R_{1-A}}\right)+(0.02)\left(\frac{1}{R_{1-2}}\right)+(0.04)\left(\frac{1}{R_{1-3}}\right)+(0.18)\left(\frac{1}{R_{3-A}}\right) \quad ⑯$$

$$0.1693566667 = (0.12)\left(\frac{1}{R_{A-B}}\right)+(0.31)\left(\frac{1}{R_{1-A}}\right)+(0.07)\left(\frac{1}{R_{1-2}}\right)+(0.14)\left(\frac{1}{R_{1-3}}\right)+(0.12)\left(\frac{1}{R_{3-A}}\right) \quad ⑰$$

Thus simultaneous equations ⑬, ⑭, ⑮, ⑯ and ⑰ are represented in matrix format as:

$$\boldsymbol{A v_1 = k_2}$$

$$\begin{bmatrix} 0.11 & 0.12 & 0 & 0 & 0.22 \\ 0 & 0.01 & -0.21 & -0.20 & -0.11 \\ 0.11 & 0.11 & 0.1 & 0.2 & 0.32 \\ 0.08 & 0.08 & 0.02 & 0.04 & 0.18 \\ 0.12 & 0.31 & 0.07 & 0.14 & 0.12 \end{bmatrix} \begin{bmatrix} \left(\frac{1}{R_{A-B}}\right) \\ \left(\frac{1}{R_{1-A}}\right) \\ \left(\frac{1}{R_{1-2}}\right) \\ \left(\frac{1}{R_{1-3}}\right) \\ \left(\frac{1}{R_{3-A}}\right) \end{bmatrix} = \begin{bmatrix} 0.1552111111 \\ -0.00114 \\ 0.1561944444 \\ 0.1130511111 \\ 0.1693566667 \end{bmatrix}$$

Setting up a new Octave simulation, to solve the matrix calculations, the parameter values can be confirmed using matrix algebra. The Octave simulation code for the matrix

calculations can be seen in APPENDIX G, G.2, and the results presented in the following paragraphs.

The inverse of a square matrix can only be determined if its determinant is non-zero. The determinant of the $\boldsymbol{A}$ matrix is found through the simulation:

$$\begin{aligned} x &= det(\boldsymbol{A}) \\ &= -2.4244 \times 10^{-6} \end{aligned}$$

Thus the inverse of matrix $\boldsymbol{A}$ can be found and multiplied by the matrix $\boldsymbol{k_2}$:

$$\boldsymbol{v_1} = \boldsymbol{A^{-1}k_2}$$

$$= \begin{bmatrix} 1.3889 \\ 5 \times 10^{-3} \\ 6.667 \times 10^{-4} \\ 6.667 \times 10^{-4} \\ 8.3333 \times 10^{-3} \end{bmatrix}$$

To determine the parameters of the wagon, each element of the matrix v_1 needs to be inverted. This results in the confirmation of the wagon parameters from static wagon measurements to be:

- $R_{A-B} = 0.72\ \Omega$
- $R_{1-A} = 200\ \Omega$
- $R_{1-2} = 1500\ \Omega$
- $R_{1-3} = 1500\ \Omega$
- $R_{3-A} = 120\ \Omega$

The parameter determination, based on the minimum error, was performed through the iterative simulation against measured data. The matrix calculations provided above verify the mathematic calculations in the iterative simulation were indeed correct, but it does not further verify the parameters determined by minimum error iteration are correct.

These parameters are configured into the system model for simulation and tuned or adjusted against measured coupler current data. The comparison between the wagon model parameter values determined in this section against those used in the system model simulation is discussed in CHAPTER 7, section 7.2.

APPENDIX E

TRANSNET FREIGHT RAIL COAL LINE MEASUREMENTS: EXPERIMENTAL METHODOLOGY

As part of the research, verification of the system model against current Transnet Freight Rail measurements is necessary. Measurements were performed on in-service revenue earning trains.

The following section of the Appendices describes the experimental setup and methodology in measuring the wagon currents on Transnet Freight Rail's Coal Line.

E.1 Experiment Location

The South African Coal Line or Coal Link is a Transnet Freight Rail operated corridor between the Coal mine fields north of Ermelo and the Richards Bay Coal Terminal (RBCT). The measurements were performed on revenue earning trains on this corridor.

North of Ermelo, where the coal is collected from various coal mining clients, is DC infrastructure. As discussed the main document, DC infrastructure falls outside the scope of this research and hence no measurements north of Ermelo were taken.

When collecting coal from the mines, trains are compiled of 4 locomotives and 100 trailing wagons. Once the coal has been collected from the mines, these trains return to the Ermelo depot where the locomotive and wagons are split. In the Ermelo depot, trains for departure to Richards Bay Coal Terminal are assembled. These trains are built with 6 locomotives in the front of the train and 200 trailing locomotives.

The infrastructure between Ermelo and Richards Bay Coal Terminal is 25kV AC at 50 Hz. Thus coal line measurements were obtained whilst the trains operated from Ermelo depot to Richards Bay Coal Terminal whilst loaded with coal as well as from Richards Bay Coal Terminal to Ermelo depot with empty wagons.

E.2 Experiment Apparatus

Transnet Freight Rail is a significantly large company with the need for continuous technological advancement, new assets testing and fault investigation. As a result, Transnet Freight Rail operates a department named Technology Management. This department owns testing equipment and specialized staff for such activities.

During the measurements performed on the Coal line, these resources were utilized. Namely, the use of Test Coaches which are passenger coaches converted into the mobile laboratories equipped with a large amount of testing instruments.

These test coaches are equipped with onboard computers which are designed to record a number of sensor signals continuously. Both digital and analog signals can be simultaneously viewed or monitored and recorded for later analysis. The display system of the Transnet Freight Rail Data Acquisition System can be seen in Figure 89. This shows the graphical representation of sensor data in real-time.

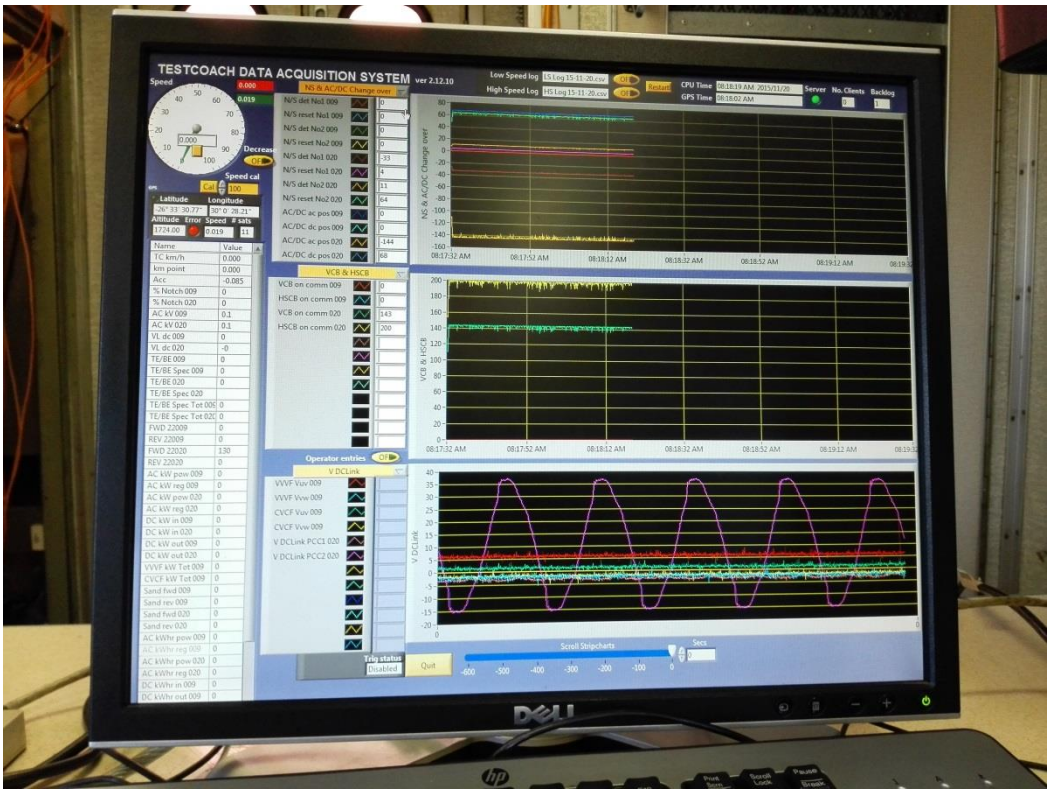


Figure 89: Photograph showing the Transnet Freight Rail data acquisition system on one of their test coaches.

Signals are provided to the computer through a patch panel. The patch panel receives a scaled voltage signal representative of the sensor signal. This is then converted to a digital representation of the signal and transmitted to the computer or recorder. In essence, the patch panel acts as an analog to digital converter. Figure 90 shows the front of the patch panel with various signals being input to the panel through the use of banana clips. Figure 91 shows the back of the patch panel with data busses from the panel to the Data Acquisition System main computer shown in Figure 89.

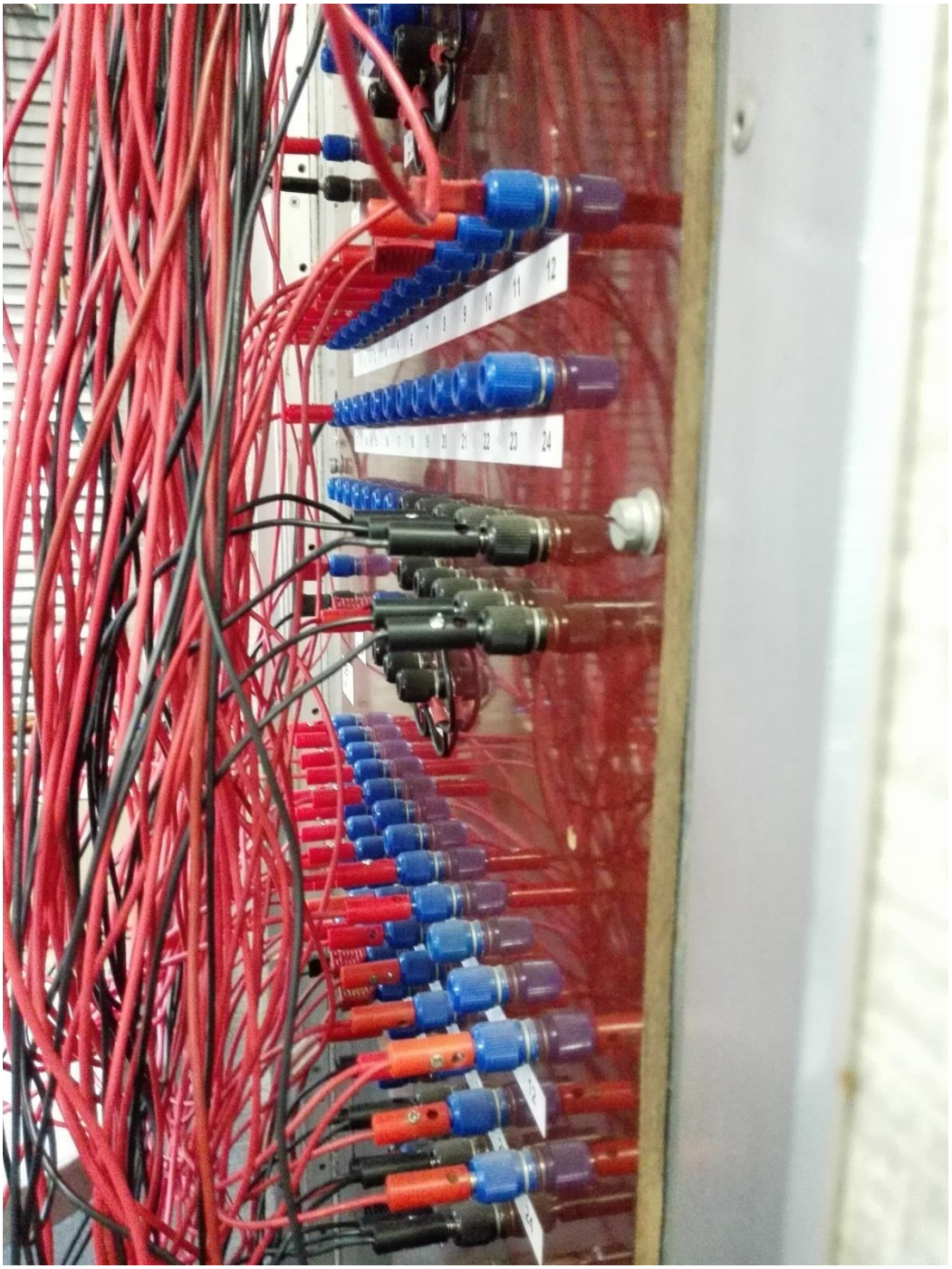


Figure 90: Photograph showing the front of the Transnet Freight Rail patch panel on one of their test coaches.

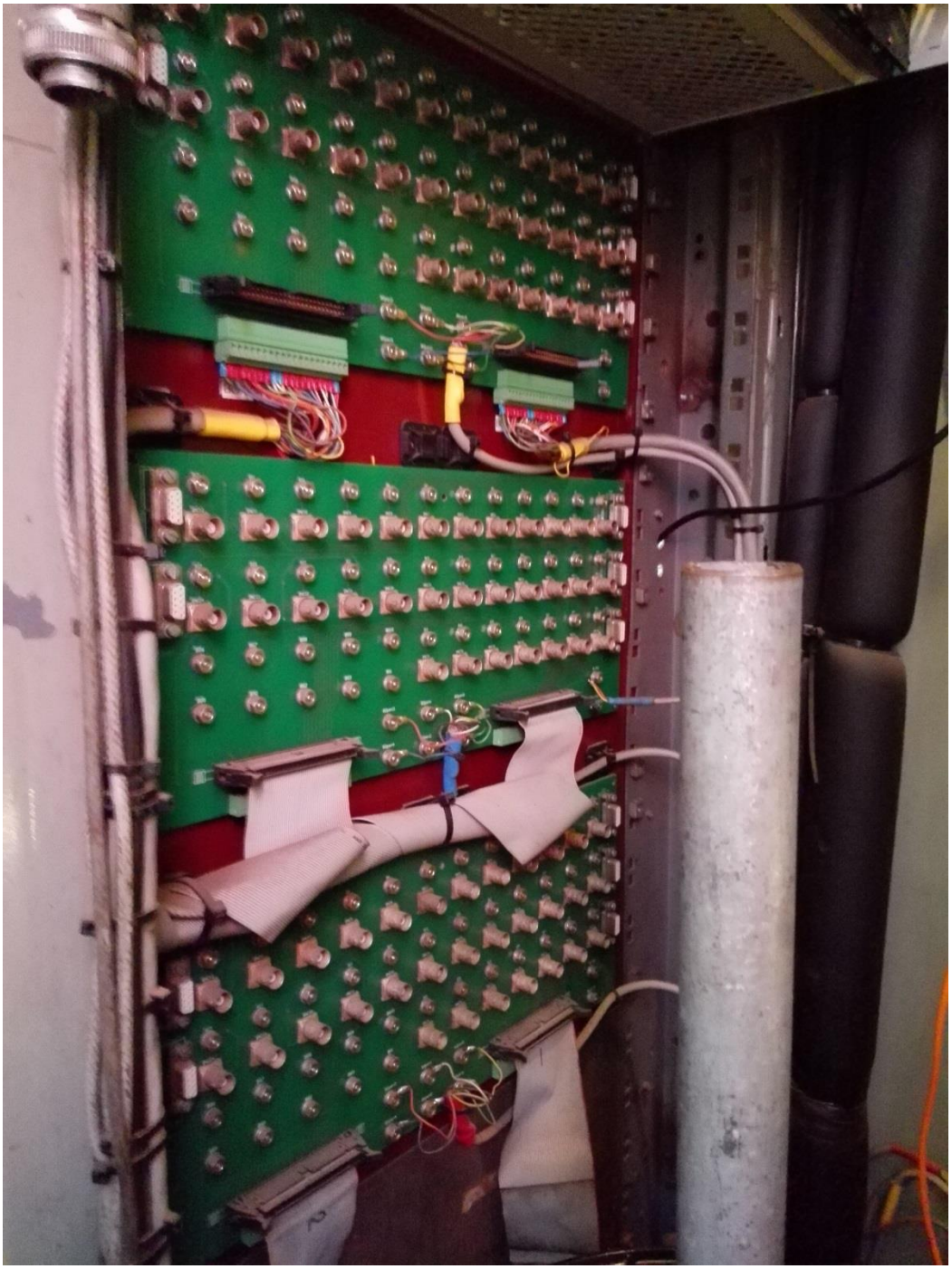


Figure 91: Photograph showing the back of the Transnet Freight Rail patch panel on one of their test coaches.

The patch panel receives signals from fiber optic receivers. These receivers are accompanied by fiber optic transmitters which are setup at the location of the transducer. Optical signals are relayed between the transmitter and receiver in order to communicate the status of transducers.

This is a measurement technique employed in most Transnet Freight Rail testing. There are numerous reasons for this; however a few will be mentioned:

1. Complete electrical isolation of testing staff and recorders from transducers, this is particularly important when working with high voltage measurements or in a high voltage environment.
2. High speed transmission of data.
3. Low attenuation of signals, thus transducers can be located at significant distances from the test coach.

The fiber optic receivers convert optic signals, received from the transmitters, to voltage signals. The front of the fiber optic receivers can be seen in Figure 92 which illustrates the voltage outputs from the optic receivers. These voltage signals are then provided to the patch panel as seen in Figure 90 and Figure 93.

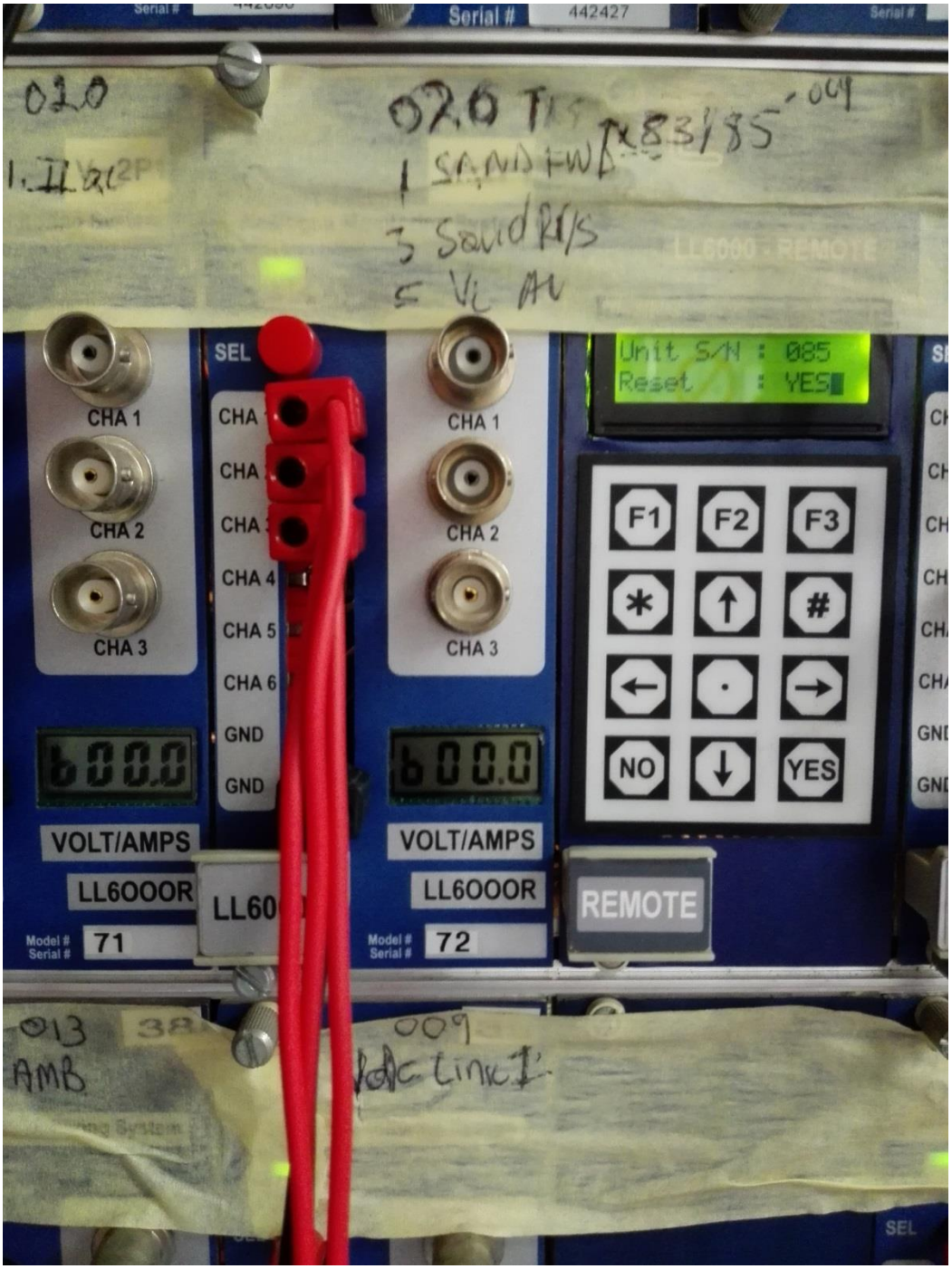


Figure 92: Photograph showing the front of the Transnet Freight Rail fiber optic receivers on one of their test coaches.

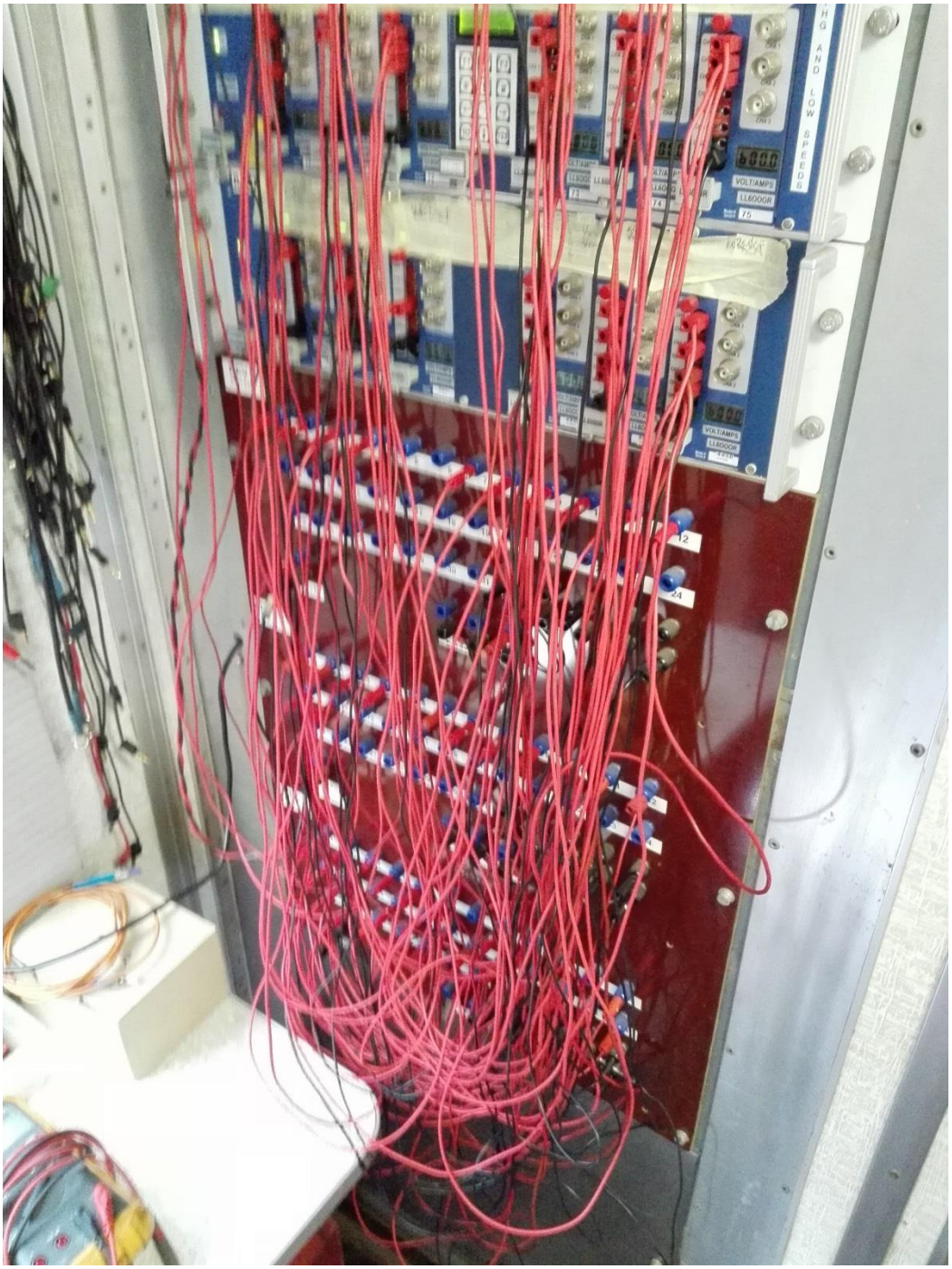


Figure 93: Photograph showing the connection from the optic receivers to the patch panel on one of Transnet Freight Rail's test coaches.

The input to the optic receivers is an optic cable from the transmitter. These optic cables enter the test coach after being routed from the transducers, as can be seen in Figure 94 and are connected to the back of the receivers as seen in Figure 95.



Figure 94: Photograph showing the fiber optic cables entering one of the Transnet Freight Rail test coaches.

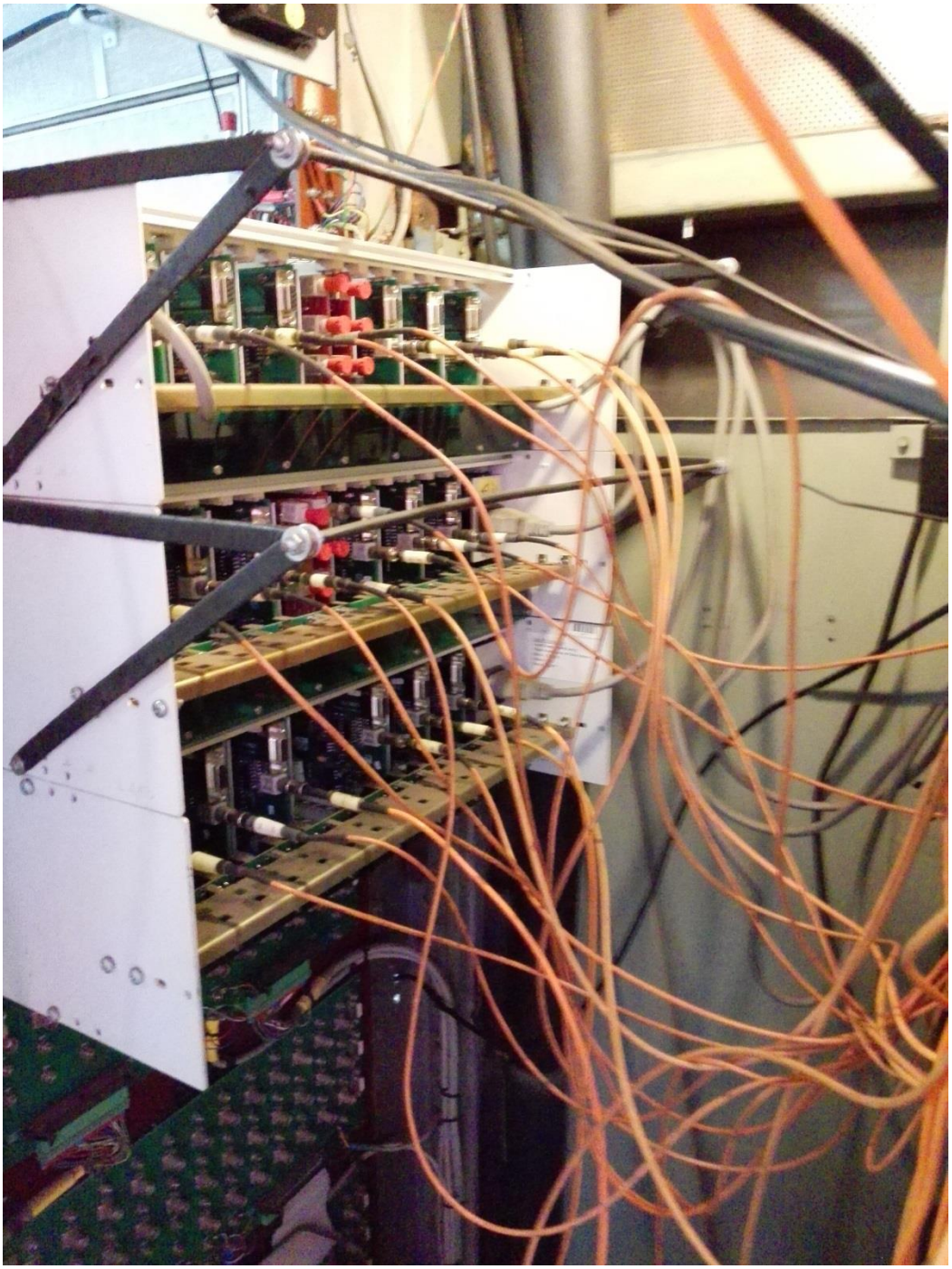


Figure 95: Photograph showing the connection of the optic cables to the receivers on one of Transnet Freight Rail's test coaches.

The fibre optic cables are routed from the location of the transducer. The fibre optic cable is then connected to the output of the optic transmitter. The front of the optic transmitted can be seen in Figure 96.



Figure 96: Photograph showing the front of the fibre optic transmitter on one of Transnet Freight Rail's test coaches.

Figure 97 provides an illustration of the overview of the equipment internal to one of Transnet Freight Rail's test coaches.



Figure 97: Photograph showing an overview of equipment found on one of Transnet Freight Rail's test coaches.

The transducer/s are connected to the optic transmitter input. In terms of measuring wagon currents, the transducer used to measure the current through couplers was a flexible current clamp. For reference purposes, the model number is GMC-I Prosys ACP 3000. The current clamp was placed around draw bar of the wagon. This is illustrated in Figure 98.



Figure 98: Photograph showing placement of the current clamp around the draw bar of one Transnet Freight Rail's coal wagon sets.

The output from the current clamp was then connected to the input of the fibre optic transmitter as seen in Figure 99. The signal was then routed to the test coach through fibre optic cables for monitoring and recording.



Figure 99: Photograph showing placement of the connection from the current clamp to the optic transmitter on one Transnet Freight Rail's coal wagon sets.

In the case of remote measurements at large distances from the test coach such as at the middle or end of the train, remote loggers were deployed. Figure 100 show the remote logger.

These remote loggers are battery operated and record the RMS value of the signal at a predefined sampling rate. For the purposes of this research, the sampling rate was set to 1 second.

The remote loggers and current clamps are installed at the remote measurement positions in the train, recording was started and then the equipment was protected from the weather. The recordings from remote loggers thus needed to be synchronized with the data from the test coach. Figure 101 shows the remote logger and current clamp setup at the remote location on the train.



Figure 100: Photograph showing the remote logger used to measure wagon currents at significant distance from the Transnet Freight Rail test coach.

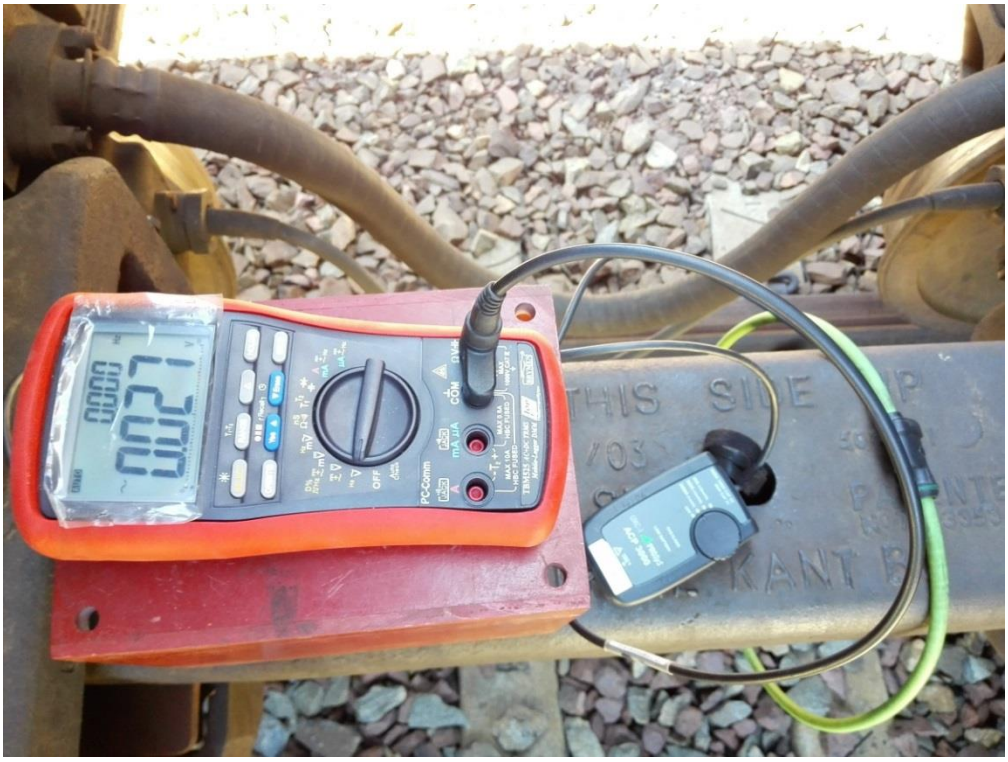


Figure 101: Photograph showing the remote logger and current clamp used to measure wagon currents at significant distance from the Transnet Freight Rail test coach.

E.3 Experimental Method

In order to minimize effect of normal revenue earning service, the wagon current measurements were conducted on in-service trains. Transducers, optic transmitters, fiber optic cables, optic receivers, patch panel and data acquisition system was thus setup in advance of train's scheduled departure.

The signals monitored during the wagon current measurements can be seen in Table 18. However, not all signals were necessarily used in the data analysis.

Table 18: Table showing signals recorded whilst performing in-service wagon coupler current measurements.

Signal Description	Signal Unit	Sampling Rate
Time	hh:mm:ss	1 second
GPS Latitude	Degrees, minutes, seconds	1 second
GPS Longitude	Degrees, minutes, seconds	1 second
GPS Altitude	meters	1 second
Speed	km/h	1 second
Notch	percentage	1 second
Line Current	RMS Amps	1 second
Line Voltage	RMS Volts	1 second
1st Wagon drawbar current	RMS Amps	1 second

APPENDIX F

LTSPICE NETLISTS

F.1 Main Simulation Circuit Netlist (LTSpice Generated)

```
* D:\Users\0001117\Documents\Transnet\Masters\LTSPICE\Supply Model\Ekman
Simulation\Figure8        Simulation Final 16.03.16D01.asc
R_FeederA N001 N002 {R_FeederA}
L_FeederA N003 N002 {L_FeederA}
R_CatenaryA N001 N007 {R_CatenaryA}
L_CatenaryA N008 N007 {L_CatenaryA}
R_ContactA N001 N015 {R_ContactA}
L_ContactA N016 N015 {L_ContactA}
R_LeftRailA 0 N053 {R_LeftRailA}
L_LeftRailA N039 N053 {L_LeftRailA}
R_RightRailA 0 N058 {R_RightRailA}
L_RightRailA N045 N058 {L_RightRailA}
R_ReturnA 0 N060 {R_ReturnA}
V§Supply_A N001 0 SINE(0 {SupplyVoltage} {fundamentalFreq} 0 0 0 200)
R_FeederB N006 N005 {R_FeederB}
L_FeederB N005 N004 {L_FeederB}
R_CatenaryB N006 N014 {R_CatenaryB}
L_CatenaryB N014 N004 {L_CatenaryB}
R_ContactB N006 N022 {R_ContactB}
L_ContactB N022 N004 {L_ContactB}
R_LeftRailB N057 N056 {R_LeftRailB}
L_LeftRailB N056 N055 {L_LeftRailB}
R_RightRailB N057 N059 {R_LeftRailB}
L_RightRailB N059 N055 {L_RightRailB}
R_ReturnB N057 N074 {R_ReturnB}
V§Supply_B N006 N057 SINE(0 {SupplyVoltage} {fundamentalFreq} 0 0 0 200)
I1 N004 N052 SINE(0 {PrimaryCurrent} {fundamentalFreq})
I2 N004 N052 SINE(0 0.105 '2*{fundamentalFreq}')
I3 N004 N052 SINE(0 0.007 '3*{fundamentalFreq}')
I4 N004 N052 SINE(0 0.015 '4*{fundamentalFreq}')
I5 N004 N052 SINE(0 0.0015 '5*{fundamentalFreq}')
I6 N004 N052 SINE(0 0.006 '6*{fundamentalFreq}')
I7 N004 N052 SINE(0 0.0009 '7*{fundamentalFreq}')
I8 N004 N052 SINE(0 0.004 '8*{fundamentalFreq}')
I9 N004 N052 SINE(0 0.0007 '9*{fundamentalFreq}')
I10 N004 N052 SINE(0 0.002 '10*{fundamentalFreq}')
R_Termination N033 N039 1T
XU9 N017 N023 N028 N034 N040 N046 N051 N018 N024 N029 N035 N041 N047 N010 SingleHighWagon
XU10 N003 N008 N016 N033 N039 N045 N009 N017 N023 N028 N034 N040 N046 N051 SingleHighWagon
R2M1 N055 N073 {R2M1}
R2M2 N082 N090 {R2M2}
R2M3 N081 N089 {R2M3}
R2M4 N080 N088 {R2M4}
R2M5 N079 N087 {R2M5}
R2M6 N013 N044 {R2M6}
R2M7 N012 N043 {R2M7}
R2M8 N011 N042 {R2M8}
R2M9 N010 N041 {R2M9}
XU1 N064 N068 N072 N078 N082 N086 N090 N004 N004 N004 N054 N055 N055 N073 7HighWagon
XU2 N063 N067 N071 N077 N081 N085 N089 N064 N068 N072 N078 N082 N086 N090 7HighWagon
XU3 N062 N066 N070 N076 N080 N084 N088 N063 N067 N071 N077 N081 N085 N089 7HighWagon
XU4 N061 N065 N069 N075 N079 N083 N087 N062 N066 N070 N076 N080 N084 N088 7HighWagon
XU5 N021 N027 N032 N038 N044 N050 N013 N061 N065 N069 N075 N079 N083 N087 7HighWagon
XU6 N020 N026 N031 N037 N043 N049 N012 N021 N027 N032 N038 N044 N050 N013 7HighWagon
XU7 N019 N025 N030 N036 N042 N048 N011 N020 N026 N031 N037 N043 N049 N012 7HighWagon
XU8 N018 N024 N029 N035 N041 N047 N010 N019 N025 N030 N036 N042 N048 N011 7HighWagon
L_ReturnA N009 N060 {L_ReturnA}
L_ReturnB N074 N073 {L_ReturnB}
R2M10 N009 N039 {R2M10}
R1 N052 N054 0.0002
R2 N052 N055 0.00365
.tran 0 0.1 0.04 0.1
.param L_FeederA='(({d}-{TrainLength})*({L_Feeder_pm}))'
.param L_CatenaryA='(({d}-{TrainLength})*({L_Catenary_pm}))'
.param L_ContactA='(({d}-{TrainLength})*({L_Contact_pm}))'
.param L_LeftRailA='(({d}-{TrainLength})*({L_LeftRail_pm}))'
.param L_RightRailA='(({d}-{TrainLength})*({L_RightRail_pm}))'
.param R_FeederA='(({d}-{TrainLength})*(2.316E-04))'
.param R_CatenaryA='(({d}-{TrainLength})*(3.230E-04))'
```

```
.param R_ContactA='(({d}-{TrainLength}))*(2.186E-04))'
.param R_LeftRailA='(({d}-{TrainLength}))*(4.000E-05))'
.param R_RightRailA='(({d}-{TrainLength}))*(4.000E-05))'
.param R_ReturnA='(({d}-{TrainLength}))*(2.316E-04))'
.param L_FeederB='((15000-{d}))*({L_Feeder_pm}))'
.param L_CatenaryB='((15000-{d}))*({L_Catenary_pm}))'
.param L_ContactB='((15000-{d}))*({L_Contact_pm}))'
.param L_LeftRailB='((15000-{d}))*({L_LeftRail_pm}))'
.param L_RightRailB='((15000-{d}))*({L_RightRail_pm}))'
.param R_FeederB='((15000-{d}))*(2.316E-04))'
.param R_CatenaryB='((15000-{d}))*(3.230E-04))'
.param R_ContactB='((15000-{d}))*(2.186E-04))'
.param R_LeftRailB='((15000-{d}))*(4.000E-05))'
.param R_RightRailB='((15000-{d}))*(4.000E-05))'
.param R_ReturnB='((15000-{d}))*(2.316E-04))'
.param R2M1='{limit(R_R2M_DownLim, R_R2M_UpLim,
R_R2M_pm*((71/2)*sin((d)/(5*71)+1)+15.42)))}'
.param R2M2='{limit(R_R2M_DownLim, R_R2M_UpLim, R_R2M_pm*((71/2)*sin((d-
        (1*68.18))/(5*71)+1)+15.42)))}'
.param R2M3='{limit(R_R2M_DownLim, R_R2M_UpLim, R_R2M_pm*((71/2)*sin((d-
        (2*68.18))/(5*71)+1)+15.42)))}'
.param R2M4='{limit(R_R2M_DownLim, R_R2M_UpLim, R_R2M_pm*((71/2)*sin((d-
        (3*68.18))/(5*71)+1)+15.42)))}'
.param R2M5='{limit(R_R2M_DownLim, R_R2M_UpLim, R_R2M_pm*((71/2)*sin((d-
        (4*68.18))/(5*71)+1)+15.42)))}'
.param R2M6='{limit(R_R2M_DownLim, R_R2M_UpLim, R_R2M_pm*((71/2)*sin((d-
        (5*68.18))/(5*71)+1)+15.42)))}'
.param R2M7='{limit(R_R2M_DownLim, R_R2M_UpLim, R_R2M_pm*((71/2)*sin((d-
        (6*68.18))/(5*71)+1)+15.42)))}'
.param R2M8='{limit(R_R2M_DownLim, R_R2M_UpLim, R_R2M_pm*((71/2)*sin((d-
        (7*68.18))/(5*71)+1)+15.42)))}'
.param R2M9='{limit(R_R2M_DownLim, R_R2M_UpLim, R_R2M_pm*((71/2)*sin((d-
        (8*68.18))/(5*71)+1)+15.42)))}'
.param R2M10='{limit(R_R2M_DownLim, R_R2M_UpLim, R_R2M_pm*((71/2)*sin((d-
        (9*68.18))/(5*71)+1)+15.42)))}'
.param R2M11='{limit(R_R2M_DownLim, R_R2M_UpLim, R_R2M_pm*((71/2)*sin((d-
        (10*68.18))/(5*71)+1)+15.42)))}'
.param R2M12='{limit(R_R2M_DownLim, R_R2M_UpLim, R_R2M_pm*((71/2)*sin((d-
        (11*68.18))/(5*71)+1)+15.42)))}'
.param R2M13='{limit(R_R2M_DownLim, R_R2M_UpLim, R_R2M_pm*((71/2)*sin((d-
        (12*68.18))/(5*71)+1)+15.42)))}'
.param R2M14='{limit(R_R2M_DownLim, R_R2M_UpLim, R_R2M_pm*((71/2)*sin((d-
        (13*68.18))/(5*71)+1)+15.42)))}'
.step param d list 1005, 1014, 1045, 1094, 1143, 1192, 1241, 1290, 1339, 1388, 1437, 1473,
        1491, 1500, 1526, 1575, 1624, 1674, 1723, 1772, 1808, 1821, 1829, 1838, 1847,
1856,   1865, 1874, 1899, 1950, 1999, 2034, 2046, 2051, 2056, 2058, 2063, 2068, 2072,
2078,   2083, 2088, 2092, 2101, 2112, 2143, 2164, 2173, 2182, 2191, 2204, 2235, 2284,
2333,   2382, 2431, 2461, 2467, 2476, 2485, 2493, 2510, 2532, 2574, 2623, 2672
.param PrimaryCurrent table(d, 1005, 131, 1014, 92, 1045, 64, 1094, 61, 1143, 63, 1192,
69,     1241, 69, 1290, 69, 1339, 78, 1388, 110, 1437, 115, 1473, 126, 1491, 157, 1500,
191,    1526, 228, 1575, 231, 1624, 231, 1674, 230, 1723, 231, 1772, 231, 1808, 254,
1821,   291, 1829, 330, 1838, 365, 1847, 401, 1856, 443, 1865, 477, 1874, 512, 1899, 559,
        1950, 565, 1999, 567, 2034, 558, 2046, 512, 2051, 468, 2056, 425, 2058, 391,
2063,   357, 2068, 315, 2072, 274, 2078, 229, 2083, 191, 2088, 159, 2092, 133, 2101, 99,
        2112, 67, 2143, 45, 2164, 82, 2173, 119, 2182, 161, 2191, 194, 2204, 228, 2235,
254,    2284, 258, 2333, 252, 2382, 252, 2431, 250, 2461, 222, 2467, 198, 2476, 168,
2485,   132, 2493, 98, 2510, 62, 2532, 48, 2574, 89, 2623, 90, 2672, 90)
.param TrainLength='481'
.param fundamentalFreq='16.7'
.param SupplyVoltage='16000'

;Simulation & Save Options
.options plotwinsize=0 numdgt=15
.save I(I1) I(u1:u1:Coupler_Current) I(u3:u6:Coupler_Current) I(u10:Coupler_Current)

;RMS Calculations
.meas PrimaryCurrentRMS RMS I(I1)
.meas 1stCouplerCurrentRMS RMS I(u1:u1:Coupler_Current)
.meas 20thCouplerCurrentRMS RMS I(u3:u6:Coupler_Current)
.meas 51stCouplerCurrentRMS RMS I(u10:Coupler_Current)
.param R_Feeder_pm='2.316E-04'
.param R_Catenary_pm='3.230E-04'
.param R_Contact_pm='2.186E-04'
.param R_LeftRail_pm='4.00E-05'
.param R_RightRail_pm='4.00E-05'
.param R_Return_pm='2.32E-04'

.param L_Feeder_pm='2.827E-06'
.param L_Catenary_pm='2.813E-06'
.param L_Contact_pm='2.679E-06'
.param L_LeftRail_pm='1.345E-06'
.param L_RightRail_pm='1.345E-06'
```

```
.param L_Return_pm='2.819E-06'
.param L_ReturnA='(({d}-{TrainLength})*({L_Return_pm}))'
.param L_ReturnB='((15000-{d})*({L_Return_pm}))'
K1001 L_FeederA L_CatenaryA {K_Feeder_Catenary}
K1002 L_FeederA L_ContactA {K_Feeder_Contact}
K1004 L_FeederA L_LeftRailA {K_Feeder_LeftRail}
K1005 L_FeederA L_RightRailA {K_Feeder_RightRail}
K1006 L_CatenaryA L_ContactA {K_Catenary_Contact}
K1008 L_CatenaryA L_LeftRailA {K_Catenary_LeftRail}
K1009 L_CatenaryA L_RightRailA {K_Catenary_RightRail}
K1011 L_ContactA L_LeftRailA {K_Contact_LeftRail}
K1012 L_ContactA L_RightRailA {K_Contact_RightRail}
K1015 L_LeftRailA L_RightRailA {K_LeftRail_RightRail}
K1016 L_FeederA L_ReturnA {K_Feeder_Return}
K1017 L_CatenaryA L_ReturnA {K_Catenary_Return}
K1018 L_ContactA L_ReturnA {K_Contact_Return}
K1020 L_LeftRailA L_ReturnA {K_LeftRail_Return}
K1021 L_RightRailA L_ReturnA {K_RightRail_Return}
K2001 L_FeederB L_CatenaryB {K_Feeder_Catenary}
K2002 L_FeederB L_ContactB {K_Feeder_Contact}
K2004 L_FeederB L_LeftRailB {K_Feeder_LeftRail}
K2005 L_FeederB L_RightRailB {K_Feeder_RightRail}
K2006 L_CatenaryB L_ContactB {K_Catenary_Contact}
K2008 L_CatenaryB L_LeftRailB {K_Catenary_LeftRail}
K2009 L_CatenaryB L_RightRailB {K_Catenary_RightRail}
K2011 L_ContactB L_LeftRailB {K_Contact_LeftRail}
K2012 L_ContactB L_RightRailB {K_Contact_RightRail}
K2015 L_LeftRailB L_RightRailB {K_LeftRail_RightRail}
K2016 L_FeederB L_ReturnB {K_Feeder_Return}
K2017 L_CatenaryB L_ReturnB {K_Catenary_Return}
K2018 L_ContactB L_ReturnB {K_Contact_Return}
K2020 L_LeftRailB L_ReturnB {K_LeftRail_Return}
K2021 L_RightRailB L_ReturnB {K_RightRail_Return}
.param R2M15='{limit(R_R2M_DownLim, R_R2M_UpLim, R_R2M_pm*((71/2)*sin((d-
        (14*68.18))/(5*71)+1)+15.42)))}'
.param R2M16='{limit(R_R2M_DownLim, R_R2M_UpLim, R_R2M_pm*((71/2)*sin((d-
        (15*68.18))/(5*71)+1)+15.42)))}'
.param R2M17='{limit(R_R2M_DownLim, R_R2M_UpLim, R_R2M_pm*((71/2)*sin((d-
        (16*68.18))/(5*71)+1)+15.42)))}'
.param R2M18='{limit(R_R2M_DownLim, R_R2M_UpLim, R_R2M_pm*((71/2)*sin((d-
        (17*68.18))/(5*71)+1)+15.42)))}'
.param R2M19='{limit(R_R2M_DownLim, R_R2M_UpLim, R_R2M_pm*((71/2)*sin((d-
        (18*68.18))/(5*71)+1)+15.42)))}'
.param R2M20='{limit(R_R2M_DownLim, R_R2M_UpLim, R_R2M_pm*((71/2)*sin((d-
        (19*68.18))/(5*71)+1)+15.42)))}'
.param R2M21='{limit(R_R2M_DownLim, R_R2M_UpLim, R_R2M_pm*((71/2)*sin((d-
        (20*68.18))/(5*71)+1)+15.42)))}'
.param R2M22='{limit(R_R2M_DownLim, R_R2M_UpLim, R_R2M_pm*((71/2)*sin((d-
        (21*68.18))/(5*71)+1)+15.42)))}'
.param R2M23='{limit(R_R2M_DownLim, R_R2M_UpLim, R_R2M_pm*((71/2)*sin((d-
        (22*68.18))/(5*71)+1)+15.42)))}'
.param R2M24='{limit(R_R2M_DownLim, R_R2M_UpLim, R_R2M_pm*((71/2)*sin((d-
        (23*68.18))/(5*71)+1)+15.42)))}'
.param R2M25='{limit(R_R2M_DownLim, R_R2M_UpLim, R_R2M_pm*((71/2)*sin((d-
        (24*68.18))/(5*71)+1)+15.42)))}'
.param R2M26='{limit(R_R2M_DownLim, R_R2M_UpLim, R_R2M_pm*((71/2)*sin((d-
        (25*68.18))/(5*71)+1)+15.42)))}'
.param R2M27='{limit(R_R2M_DownLim, R_R2M_UpLim, R_R2M_pm*((71/2)*sin((d-
        (26*68.18))/(5*71)+1)+15.42)))}'
.param R2M28='{limit(R_R2M_DownLim, R_R2M_UpLim, R_R2M_pm*((71/2)*sin((d-
        (27*68.18))/(5*71)+1)+15.42)))}'
.param K_Feeder_Catenary='5.329E-01'
.param K_Feeder_Contact='5.245E-01'
.param K_Feeder_LeftRail='4.489E-01'
.param K_Feeder_RightRail='4.423E-01'
.param K_Feeder_Return='5.476E-01'
.param K_Catenary_Contact='6.032E-01'
.param K_Catenary_LeftRail='4.465E-01'
.param K_Catenary_RightRail='4.465E-01'
.param K_Catenary_Return='5.985E-01'
.param K_Contact_LeftRail='4.573E-01'
.param K_Contact_RightRail='4.573E-01'
.param K_Contact_Return='7.525E-01'
.param K_LeftRail_RightRail='5.431E-01'
.param K_LeftRail_Return='4.462E-01'
.param K_RightRail_Return='4.462E-01'
* Simulation Settings and Configuration
* Feed_A
* Wagons
* Locomotive Consist
* Feed_B
.param R_R2M_pm='0.2'
```

```
.param R_R2M_UpLim='1000'
.param R_R2M_DownLim='0.000004'
.lib D:\Users\0001117\Documents\Transnet\Masters\LTSPICE\Supply Model\Ekman Simulation\7
HighWagon 15.12.29 D01.sub
.lib D:\Users\0001117\Documents\Transnet\Masters\LTSPICE\Supply Model\Ekman
Simulation\SingleHighWagon 15.12.29.sub
.backanno
.end
```

F.2 Wagon Set Sub-Circuit Netlist (LTSpice Generated)

```
* D:\Users\0001117\Documents\Transnet\Masters\LTSPICE\Supply Model\Ekman Simulation\7
        HighWagon 16.01.19 D01.asc
XU1 N024 N027 N030 N033 N036 N039 N042 FeederFront_Port CatenaryFront_Port
ContactFront_Port         WagonFront_Port LeftRailFront_Port RightRailFront_Port
ReturnFront_Port SingleHighWagon
XU2 N023 N026 N029 N032 N035 N038 N041 N024 N027 N030 N033 N036 N039 N042 SingleHighWagon
XU3 N022 N025 N028 N031 N034 N037 N040 N023 N026 N029 N032 N035 N038 N041 SingleHighWagon
XU4 N003 N006 N009 N012 N015 N018 N021 N022 N025 N028 N031 N034 N037 N040 SingleHighWagon
XU5 N002 N005 N008 N011 N014 N017 N020 N003 N006 N009 N012 N015 N018 N021 SingleHighWagon
XU6 N001 N004 N007 N010 N013 N016 N019 N002 N005 N008 N011 N014 N017 N020 SingleHighWagon
XU7 FeederBack_Port CatenaryBack_Port ContactBack_Port WagonBack_Port LeftRailBack_Port
        RightRailBack_Port ReturnBack_Port N001 N004 N007 N010 N013 N016 N019
        SingleHighWagon
.lib D:\Users\0001117\Documents\Transnet\Masters\LTSPICE\Supply Model\Ekman
        Simulation\SingleHighWagon 15.12.29.sub
.backanno
.end
```

F.3 Individual Wagon Sub-Sub-Circuit Netlist (LTSpice Generated)

```
* D:\Users\0001117\Documents\Transnet\Masters\LTSPICE\Supply Model\TFR
        Simulation\SingleWagon3095High160222D02.asc
R_Feeder_5 N008 N009 {R_Feeder_5}
L_Feeder_5 FeederFront_Port N009 {L_Feeder_5}
R_Catenary_5 N017 N018 {R_Catenary_5}
L_Catenary_5 CatenaryFront_Port N018 {L_Catenary_5}
R_Contact_5 N026 N027 {R_Contact_5}
L_Contact_5 ContactFront_Port N027 {L_Contact_5}
R_LeftRail_5 N045 N046 {R_LeftRail_5}
L_LeftRail_5 LeftRailFront_Port N046 {L_LeftRail_5}
R_RightRail_5 N054 N055 {R_RightRail_5}
L_RightRail_5 RightRailFront_Port N055 {L_RightRail_5}
L_ab_5 N037 N036 {L_ab_5}
R1a WagonBack_Port Axle1 {R1a}
R3a WagonBack_Port Axle3 {R3a}
R4a WagonBack_Port Axle4 {R3a}
R2a WagonBack_Port Axle2 {R1a}
R12 Axle1 Axle2 {R12}
R23 Axle2 Axle3 {R13}
R34 Axle3 Axle4 {R12}
R13 Axle1 Axle3 {R13}
R14 Axle1 Axle4 {R13}
R1b Axle1 N037 {R3a}
R24 Axle2 Axle4 {R13}
R2b Axle2 N037 {R3a}
R3b Axle3 N037 {R1a}
R4b Axle4 N037 {R1a}
R_ab_5 N035 N036 {R_ab_5}
R_Feeder_4 N006 N007 {R_Feeder_4}
L_Feeder_4 N008 N007 {L_Feeder_4}
R_Catenary_4 N015 N016 {R_Catenary_4}
L_Catenary_4 N017 N016 {L_Catenary_4}
R_Contact_4 N024 N025 {R_Contact_4}
L_Contact_4 N026 N025 {L_Contact_4}
R_LeftRail_4 N043 N044 {R_LeftRail_4}
L_LeftRail_4 N045 N044 {L_LeftRail_4}
R_RightRail_4 N052 N053 {R_RightRail_4}
L_RightRail_4 N054 N053 {L_RightRail_4}
L_ab_4 N035 N034 {L_ab_4}
```

```
R_ab_4 N033 N034 {R_ab_4}
R_Feeder_3 N004 N005 {R_Feeder_3}
L_Feeder_3 N006 N005 {L_Feeder_3}
R_Catenary_3 N013 N014 {R_Catenary_3}
L_Catenary_3 N015 N014 {L_Catenary_3}
R_Contact_3 N022 N023 {R_Contact_3}
L_Contact_3 N024 N023 {L_Contact_3}
R_LeftRail_3 N041 N042 {R_LeftRail_3}
L_LeftRail_3 N043 N042 {L_LeftRail_3}
R_RightRail_3 N050 N051 {R_RightRail_3}
L_RightRail_3 N052 N051 {L_RightRail_3}
L_ab_3 N033 N032 {L_ab_3}
R_ab_3 N031 N032 {R_ab_3}
R_Feeder_2 N002 N003 {R_Feeder_2}
L_Feeder_2 N004 N003 {L_Feeder_2}
R_Catenary_2 N011 N012 {R_Catenary_2}
L_Catenary_2 N013 N012 {L_Catenary_2}
R_Contact_2 N020 N021 {R_Contact_2}
L_Contact_2 N022 N021 {L_Contact_2}
R_LeftRail_2 N039 N040 {R_LeftRail_2}
L_LeftRail_2 N041 N040 {L_LeftRail_2}
R_RightRail_2 N048 N049 {R_RightRail_2}
L_RightRail_2 N050 N049 {L_RightRail_2}
L_ab_2 N031 N030 {L_ab_2}
R_ab_2 N029 N030 {R_ab_2}
R_Feeder_1 FeederBack_Port N001 {R_Feeder_1}
L_Feeder_1 N002 N001 {L_Feeder_1}
R_Catenary_1 CatenaryBack_Port N010 {R_Catenary_1}
L_Catenary_1 N011 N010 {L_Catenary_1}
R_Contact_1 ContactBack_Port N019 {R_Contact_1}
L_Contact_1 N020 N019 {L_Contact_1}
R_LeftRail_1 LeftRailBack_Port N038 {R_LeftRail_1}
L_LeftRail_1 N039 N038 {L_LeftRail_1}
R_RightRail_1 RightRailBack_Port N047 {R_RightRail_1}
L_RightRail_1 N048 N047 {L_RightRail_1}
R_ab_1 N028 N029 {R_ab_1}
R_Axle1L N039 Axle1 1E-03
L_ab_1 N028 WagonBack_Port {L_ab_1}
R_Return_1 ReturnBack_Port N056 {R_Return_1}
L_Return_1 N057 N056 {L_Return_1}
R_Return_2 N057 N058 {R_Return_2}
L_Return_2 N059 N058 {L_Return_2}
R_Return_3 N059 N060 {R_Return_3}
L_Return_3 N061 N060 {L_Return_3}
R_Return_4 N061 N062 {R_Return_4}
L_Return_4 N063 N062 {L_Return_4}
R_Return_5 N063 N064 {R_Return_5}
L_Return_5 ReturnFront_Port N064 {L_Return_5}
R§Coupler_Current WagonFront_Port N037 1E-9
R_Axle1R N048 Axle1 1E-03
R_Axle2L N041 Axle2 1E-03
R_Axle2R N050 Axle2 1E-03
R_Axle3L N043 Axle3 1E-03
R_Axle3R N052 Axle3 1E-03
R_Axle4L N045 Axle4 1E-03
R_Axle4R N054 Axle4 1E-03
* 0.805 meters
* 2.133 meters
* 3.963 meters
* 2.133 meters
* 0.805 meters
.param Rab='0.003'
.param R1a='125'
.param R12='1200'
.param R13='1200'
.param R3a='125'
.param R_Feeder_pm='2.316E-04'
.param R_Catenary_pm='3.230E-04'
.param R_Contact_pm='2.186E-04'
.param R_ab_pm='{Rab}/9.034'
.param R_LeftRail_pm='4.00E-05'
.param R_RightRail_pm='4.00E-05'
.param R_Return_pm='2.32E-04'

.param L_Feeder_pm='2.827E-06'
.param L_Catenary_pm='2.813E-06'
.param L_Contact_pm='2.679E-06'
.param L_ab_pm='1.996E-06'
.param L_LeftRail_pm='1.345E-06'
.param L_RightRail_pm='1.345E-06'
.param L_Return_pm='2.819E-06'
```

```
.param K_Feeder_Catenary='5.329E-01'
.param K_Feeder_Contact='5.245E-01'
.param K_Feeder_ab='5.447E-01'
.param K_Feeder_LeftRail='4.489E-01'
.param K_Feeder_RightRail='4.423E-01'
.param K_Feeder_Return='5.476E-01'
.param K_Catenary_Contact='6.032E-01'
.param K_Catenary_ab='5.716E-01'
.param K_Catenary_LeftRail='4.465E-01'
.param K_Catenary_RightRail='4.465E-01'
.param K_Catenary_Return='5.985E-01'
.param K_Contact_ab='6.074E-01'
.param K_Contact_LeftRail='4.573E-01'
.param K_Contact_RightRail='4.573E-01'
.param K_Contact_Return='7.525E-01'
.param K_ab_LeftRail='5.287E-01'
.param K_ab_RightRail='5.287E-01'
.param K_ab_Return='3.621E-01'
.param K_LeftRail_RightRail='5.431E-01'
.param K_LeftRail_Return='4.462E-01'
.param K_RightRail_Return='4.462E-01'
.param Dist_1='0.805'

.param L_Feeder_1='({Dist_1}*{L_Feeder_pm})'
.param L_Catenary_1='({Dist_1}*{L_Catenary_pm})'
.param L_Contact_1='({Dist_1}*{L_Contact_pm})'
.param L_ab_1='({Dist_1}*{L_ab_pm})'
.param L_LeftRail_1='({Dist_1}*{L_LeftRail_pm})'
.param L_RightRail_1='({Dist_1}*{L_RightRail_pm})'
.param L_Return_1='({Dist_1}*{L_Return_pm})'

.param R_Feeder_1='{Dist_1}*{R_Feeder_pm}'
.param R_Catenary_1='{Dist_1}*{R_Catenary_pm}'
.param R_Contact_1='{Dist_1}*{R_Contact_pm}'
.param R_ab_1='{Dist_1}*{R_ab_pm}'
.param R_LeftRail_1='{Dist_1}*{R_LeftRail_pm}'
.param R_RightRail_1='{Dist_1}*{R_RightRail_pm}'
.param R_Return_1='({Dist_1}*{R_Return_pm})'

K1001 L_Feeder_1 L_Catenary_1 {K_Feeder_Catenary}
K1002 L_Feeder_1 L_Contact_1 {K_Feeder_Contact}
K1003 L_Feeder_1 L_ab_1 {K_Feeder_ab}
K1004 L_Feeder_1 L_LeftRail_1 {K_Feeder_LeftRail}
K1005 L_Feeder_1 L_RightRail_1 {K_Feeder_RightRail}
K1006 L_Feeder_1 L_Return_1 {K_Feeder_Return}
K1007 L_Catenary_1 L_Contact_1 {K_Catenary_Contact}
K1008 L_Catenary_1 L_ab_1 {K_Catenary_ab}
K1009 L_Catenary_1 L_LeftRail_1 {K_Catenary_LeftRail}
K1010 L_Catenary_1 L_RightRail_1 {K_Catenary_RightRail}
K1011 L_Catenary_1 L_Return_1 {K_Catenary_Return}
K1012 L_Contact_1 L_ab_1 {K_Contact_ab}
K1013 L_Contact_1 L_LeftRail_1 {K_Contact_LeftRail}
K1014 L_Contact_1 L_RightRail_1 {K_Contact_RightRail}
K1015 L_Contact_1 L_Return_1 {K_Contact_Return}
K1016 L_ab_1 L_LeftRail_1 {K_ab_LeftRail}
K1017 L_ab_1 L_RightRail_1 {K_ab_RightRail}
K1018 L_ab_1 L_Return_1 {K_ab_Return}
K1019 L_LeftRail_1 L_RightRail_1 {K_LeftRail_RightRail}
K1020 L_LeftRail_1 L_Return_1 {K_LeftRail_Return}
K1021 L_RightRail_1 L_Return_1 {K_RightRail_Return}
.param Dist_2='2.133'

.param L_Feeder_2='({Dist_2}*{L_Feeder_pm})'
.param L_Catenary_2='({Dist_2}*{L_Catenary_pm})'
.param L_Contact_2='({Dist_2}*{L_Contact_pm})'
.param L_ab_2='({Dist_2}*{L_ab_pm})'
.param L_LeftRail_2='({Dist_2}*{L_LeftRail_pm})'
.param L_RightRail_2='({Dist_2}*{L_RightRail_pm})'
.param L_Return_2='({Dist_2}*{L_Return_pm})'

.param R_Feeder_2='{Dist_2}*{R_Feeder_pm}'
.param R_Catenary_2='{Dist_2}*{R_Catenary_pm}'
.param R_Contact_2='{Dist_2}*{R_Contact_pm}'
.param R_ab_2='{Dist_2}*{R_ab_pm}'
.param R_LeftRail_2='{Dist_2}*{R_LeftRail_pm}'
.param R_RightRail_2='{Dist_2}*{R_RightRail_pm}'
.param R_Return_2='({Dist_2}*{R_Return_pm})'

K2001 L_Feeder_2 L_Catenary_2 {K_Feeder_Catenary}
K2002 L_Feeder_2 L_Contact_2 {K_Feeder_Contact}
K2003 L_Feeder_2 L_ab_2 {K_Feeder_ab}
K2004 L_Feeder_2 L_LeftRail_2 {K_Feeder_LeftRail}
```

```
K2005 L_Feeder_2 L_RightRail_2 {K_Feeder_RightRail}
K2006 L_Feeder_2 L_Return_2 {K_Feeder_Return}
K2007 L_Catenary_2 L_Contact_2 {K_Catenary_Contact}
K2008 L_Catenary_2 L_ab_2 {K_Catenary_ab}
K2009 L_Catenary_2 L_LeftRail_2 {K_Catenary_LeftRail}
K2010 L_Catenary_2 L_RightRail_2 {K_Catenary_RightRail}
K2011 L_Catenary_2 L_Return_2 {K_Catenary_Return}
K2012 L_Contact_2 L_ab_2 {K_Contact_ab}
K2013 L_Contact_2 L_LeftRail_2 {K_Contact_LeftRail}
K2014 L_Contact_2 L_RightRail_2 {K_Contact_RightRail}
K2015 L_Contact_2 L_Return_2 {K_Contact_Return}
K2016 L_ab_2 L_LeftRail_2 {K_ab_LeftRail}
K2017 L_ab_2 L_RightRail_2 {K_ab_RightRail}
K2018 L_ab_2 L_Return_2 {K_ab_Return}
K2019 L_LeftRail_2 L_RightRail_2 {K_LeftRail_RightRail}
K2020 L_LeftRail_2 L_Return_2 {K_LeftRail_Return}
K2021 L_RightRail_2 L_Return_2 {K_RightRail_Return}
.param Dist_3='3.963'

.param L_Feeder_3='({Dist_3}*{L_Feeder_pm})'
.param L_Catenary_3='({Dist_3}*{L_Catenary_pm})'
.param L_Contact_3='({Dist_3}*{L_Contact_pm})'
.param L_ab_3='({Dist_3}*{L_ab_pm})'
.param L_LeftRail_3='({Dist_3}*{L_LeftRail_pm})'
.param L_RightRail_3='({Dist_3}*{L_RightRail_pm})'
.param L_Return_3='({Dist_3}*{L_Return_pm})'

.param R_Feeder_3='{Dist_3}*{R_Feeder_pm}'
.param R_Catenary_3='{Dist_3}*{R_Catenary_pm}'
.param R_Contact_3='{Dist_3}*{R_Contact_pm}'
.param R_ab_3='{Dist_3}*{R_ab_pm}'
.param R_LeftRail_3='{Dist_3}*{R_LeftRail_pm}'
.param R_RightRail_3='{Dist_3}*{R_RightRail_pm}'
.param R_Return_3='({Dist_3}*{R_Return_pm})'

K3001 L_Feeder_3 L_Catenary_3 {K_Feeder_Catenary}
K3002 L_Feeder_3 L_Contact_3 {K_Feeder_Contact}
K3003 L_Feeder_3 L_ab_3 {K_Feeder_ab}
K3004 L_Feeder_3 L_LeftRail_3 {K_Feeder_LeftRail}
K3005 L_Feeder_3 L_RightRail_3 {K_Feeder_RightRail}
K3006 L_Feeder_3 L_Return_3 {K_Feeder_Return}
K3007 L_Catenary_3 L_Contact_3 {K_Catenary_Contact}
K3008 L_Catenary_3 L_ab_3 {K_Catenary_ab}
K3009 L_Catenary_3 L_LeftRail_3 {K_Catenary_LeftRail}
K3010 L_Catenary_3 L_RightRail_3 {K_Catenary_RightRail}
K3011 L_Catenary_3 L_Return_3 {K_Catenary_Return}
K3012 L_Contact_3 L_ab_3 {K_Contact_ab}
K3013 L_Contact_3 L_LeftRail_3 {K_Contact_LeftRail}
K3014 L_Contact_3 L_RightRail_3 {K_Contact_RightRail}
K3015 L_Contact_3 L_Return_3 {K_Contact_Return}
K3016 L_ab_3 L_LeftRail_3 {K_ab_LeftRail}
K3017 L_ab_3 L_RightRail_3 {K_ab_RightRail}
K3018 L_ab_3 L_Return_3 {K_ab_Return}
K3019 L_LeftRail_3 L_RightRail_3 {K_LeftRail_RightRail}
K3020 L_LeftRail_3 L_Return_3 {K_LeftRail_Return}
K3021 L_RightRail_3 L_Return_3 {K_RightRail_Return}
.param Dist_4='2.133'

.param L_Feeder_4='({Dist_4}*{L_Feeder_pm})'
.param L_Catenary_4='({Dist_4}*{L_Catenary_pm})'
.param L_Contact_4='({Dist_4}*{L_Contact_pm})'
.param L_ab_4='({Dist_4}*{L_ab_pm})'
.param L_LeftRail_4='({Dist_4}*{L_LeftRail_pm})'
.param L_RightRail_4='({Dist_4}*{L_RightRail_pm})'
.param L_Return_4='({Dist_4}*{L_Return_pm})'

.param R_Feeder_4='{Dist_4}*{R_Feeder_pm}'
.param R_Catenary_4='{Dist_4}*{R_Catenary_pm}'
.param R_Contact_4='{Dist_4}*{R_Contact_pm}'
.param R_ab_4='{Dist_4}*{R_ab_pm}'
.param R_LeftRail_4='{Dist_4}*{R_LeftRail_pm}'
.param R_RightRail_4='{Dist_4}*{R_RightRail_pm}'
.param R_Return_4='({Dist_4}*{R_Return_pm})'

K4001 L_Feeder_4 L_Catenary_4 {K_Feeder_Catenary}
K4002 L_Feeder_4 L_Contact_4 {K_Feeder_Contact}
K4003 L_Feeder_4 L_ab_4 {K_Feeder_ab}
K4004 L_Feeder_4 L_LeftRail_4 {K_Feeder_LeftRail}
K4005 L_Feeder_4 L_RightRail_4 {K_Feeder_RightRail}
K4006 L_Feeder_4 L_Return_4 {K_Feeder_Return}
K4007 L_Catenary_4 L_Contact_4 {K_Catenary_Contact}
K4008 L_Catenary_4 L_ab_4 {K_Catenary_ab}
```

```
K4009 L_Catenary_4 L_LeftRail_4 {K_Catenary_LeftRail}
K4010 L_Catenary_4 L_RightRail_4 {K_Catenary_RightRail}
K4011 L_Catenary_4 L_Return_4 {K_Catenary_Return}
K4012 L_Contact_4 L_ab_4 {K_Contact_ab}
K4013 L_Contact_4 L_LeftRail_4 {K_Contact_LeftRail}
K4014 L_Contact_4 L_RightRail_4 {K_Contact_RightRail}
K4015 L_Contact_4 L_Return_4 {K_Contact_Return}
K4016 L_ab_4 L_LeftRail_4 {K_ab_LeftRail}
K4017 L_ab_4 L_RightRail_4 {K_ab_RightRail}
K4018 L_ab_4 L_Return_4 {K_ab_Return}
K4019 L_LeftRail_4 L_RightRail_4 {K_LeftRail_RightRail}
K4020 L_LeftRail_4 L_Return_4 {K_LeftRail_Return}
K4021 L_RightRail_4 L_Return_4 {K_RightRail_Return}
.param Dist_5='2.133'

.param L_Feeder_5='({Dist_5}*{L_Feeder_pm})'
.param L_Catenary_5='({Dist_5}*{L_Catenary_pm})'
.param L_Contact_5='({Dist_5}*{L_Contact_pm})'
.param L_ab_5='({Dist_5}*{L_ab_pm})'
.param L_LeftRail_5='({Dist_5}*{L_LeftRail_pm})'
.param L_RightRail_5='({Dist_5}*{L_RightRail_pm})'
.param L_Return_5='({Dist_5}*{L_Return_pm})'

.param R_Feeder_5='{Dist_5}*{R_Feeder_pm}'
.param R_Catenary_5='{Dist_5}*{R_Catenary_pm}'
.param R_Contact_5='{Dist_5}*{R_Contact_pm}'
.param R_ab_5='{Dist_5}*{R_ab_pm}'
.param R_LeftRail_5='{Dist_5}*{R_LeftRail_pm}'
.param R_RightRail_5='{Dist_5}*{R_RightRail_pm}'
.param R_Return_5='({Dist_5}*{R_Return_pm})'

K5001 L_Feeder_5 L_Catenary_5 {K_Feeder_Catenary}
K5002 L_Feeder_5 L_Contact_5 {K_Feeder_Contact}
K5003 L_Feeder_5 L_ab_5 {K_Feeder_ab}
K5004 L_Feeder_5 L_LeftRail_5 {K_Feeder_LeftRail}
K5005 L_Feeder_5 L_RightRail_5 {K_Feeder_RightRail}
K5006 L_Feeder_5 L_Return_5 {K_Feeder_Return}
K5007 L_Catenary_5 L_Contact_5 {K_Catenary_Contact}
K5008 L_Catenary_5 L_ab_5 {K_Catenary_ab}
K5009 L_Catenary_5 L_LeftRail_5 {K_Catenary_LeftRail}
K5010 L_Catenary_5 L_RightRail_5 {K_Catenary_RightRail}
K5011 L_Catenary_5 L_Return_5 {K_Catenary_Return}
K5012 L_Contact_5 L_ab_5 {K_Contact_ab}
K5013 L_Contact_5 L_LeftRail_5 {K_Contact_LeftRail}
K5014 L_Contact_5 L_RightRail_5 {K_Contact_RightRail}
K5015 L_Contact_5 L_Return_5 {K_Contact_Return}
K5016 L_ab_5 L_LeftRail_5 {K_ab_LeftRail}
K5017 L_ab_5 L_RightRail_5 {K_ab_RightRail}
K5018 L_ab_5 L_Return_5 {K_ab_Return}
K5019 L_LeftRail_5 L_RightRail_5 {K_LeftRail_RightRail}
K5020 L_LeftRail_5 L_Return_5 {K_LeftRail_Return}
K5021 L_RightRail_5 L_Return_5 {K_RightRail_Return}
* Parameter Configuration
.backanno
.end
```

APPENDIX G

OCTAVE SIMULATION SOURCE CODE

G.1 Wagon Parameter Iterative Determination Simulation Code

```
################################################################################
##
#
#
#    Octave V3.8.2 Simulation
#
#    Title: Wagon Parameter Iterative
#
#               Determination
#
#    Author: James Clay
#
#    Student Number: 325609
#
#
#
################################################################################
##

itr = 0;                                    # Iteration Count Variable

filename = "PossibleSolutionsAC_D01.csv";   # Store Filename as a Variable
fid = fopen (filename, "w");                # Open/Create file

line = "Iteration, Rab, R1a, R12, R13, ...
          R3a, SupplyCurrent1Error, ...
          SupplyCurrent1aError, ...
          SupplyCurrent1bError, ...
          SupplyCurrent2Error, ...
          SupplyCurrent3Error, AvgError\n"; # Store Column headers as a Variable

fputs (fid, line);                          # Write the Column headers to the file

CouplerB1Voltage = 0.8;                     # Initialization of Measurement to Variable
CouplerA1Voltage = 0.69;                    # Initialization of Measurement to Variable
WheelD1Voltage = 0.79;                      # Initialization of Measurement to Variable
SupplyCurrent1 = 0.156;                     # Initialization of Measurement to Variable

CouplerB2Voltage = 0.76;                    # Initialization of Measurement to Variable
CouplerA2Voltage = 0.68;                    # Initialization of Measurement to Variable
WheelD2Voltage = 0.7;                       # Initialization of Measurement to Variable
SupplyCurrent2 = 0.155;                     # Initialization of Measurement to Variable

CouplerB3Voltage = 0.8;                     # Initialization of Measurement to Variable
CouplerA3Voltage = 0.68;                    # Initialization of Measurement to Variable
WheelD3Voltage = 0.75;                      # Initialization of Measurement to Variable
SupplyCurrent3 = 0.154;                     # Initialization of Measurement to Variable

Rab = 0;                                    # Initialization of Iteration Limit for Rab
RabStep = 0.0001;                           # Initialization of Iteration increment for
Rab
RabEnd = 0.005;                             # Initialization of Iteration Limit for Rab

progress = 0;                               # Initialization of progress Variable



do                                          # Begin iterative loop
  Rab = Rab+RabStep;                        # Increment Rab

  R1a = 5;                                  # Set Iteration Limit for R1a
  do
    R1a = R1a+5;                            # Increment R1a
    R12 = 50;                               # Set Iteration Limit for R12
    do
      R12 = R12+50;                         # Increment R12
```

```
R13 = 50;                               # Set Iteration Limit for R13
do
  R13 = R13+50;                         # Increment R13
  R3a = 5;                              # Set Iteration Limit for R3a
  do
    R3a = R3a+5;                        # Increment R3a

    itr++;                              # Increment Iteration Count Variable

    SupplyCurrent1Temp = ...
      -1*((CouplerA1Voltage...
      -CouplerB1Voltage)/Rab)...
      -1*((CouplerA1Voltage...
      +WheelD1Voltage...
      -(2*CouplerB1Voltage))/R1a)...
      -2*((CouplerA1Voltage...
      -CouplerB1Voltage)/R3a);          # Calculation of Simultaneous Equation 1

    SupplyCurrent1Error = ...
      1-(SupplyCurrent1Temp...
      /SupplyCurrent1);                 # Calculation of Error for Equation 1

    SupplyCurrent1aTemp = ...
      -1*((WheelD1Voltage...
      -CouplerB1Voltage)/R1a)...
      +((CouplerA1Voltage...
      -CouplerB1Voltage)/R12)...
      +2*((CouplerA1Voltage...
      -WheelD1Voltage)/R13)...
      +((CouplerA1Voltage...
      -CouplerB1Voltage)/R3a);          # Calculation of Simultaneous Equation 2

    SupplyCurrent1aError = ...
      1-((SupplyCurrent1...
      -SupplyCurrent1aTemp)...
      /SupplyCurrent1);                 # Calculation of Error for Equation 2

    SupplyCurrent1bTemp = ...
      -1*((CouplerA1Voltage...
      -CouplerB1Voltage)/Rab)...
      -1*((CouplerA1Voltage...
      -CouplerB1Voltage)/R1a)...
      -((CouplerA1Voltage...
      -WheelD1Voltage)/R12)...
      -((2*(CouplerA1Voltage...
      -CouplerB1Voltage)...
      +(CouplerA1Voltage...
      -WheelD1Voltage))/R3a);           # Calculation of Simultaneous Equation 3

    SupplyCurrent1bError = ...
      1-(SupplyCurrent1bTemp...
      /SupplyCurrent1);                 # Calculation of Error for Equation 3

    SupplyCurrent2Temp = ...
      -((CouplerA2Voltage...
      -CouplerB2Voltage)/Rab)...
      -((CouplerA2Voltage...
      -CouplerB2Voltage)/R1a)...
      +((WheelD2Voltage...
      -CouplerA2Voltage)/R12)...
      -2*((CouplerA2Voltage...
      -WheelD2Voltage)/R13)...
      -1*((3*CouplerA2Voltage...
      -WheelD2Voltage...
      -2*CouplerB2Voltage)/R3a);        # Calculation of Simultaneous Equation 6

    SupplyCurrent2Error = ...
      1-(SupplyCurrent2Temp...
      /SupplyCurrent2);                 # Calculation of Error for Equation 6

    SupplyCurrent3Temp = ...
      -((CouplerA3Voltage...
      -CouplerB3Voltage)/Rab)...
      -(((CouplerA3Voltage...
      -WheelD3Voltage)...
      +2*(CouplerA3Voltage...
      -CouplerB3Voltage))/R1a)...
      -((CouplerA3Voltage...
      -WheelD3Voltage)/R12)...
      +2*((WheelD3Voltage...
```

```
          -CouplerA3Voltage)/R13)...
          -((CouplerA3Voltage...
          -CouplerB3Voltage)/R3a);        # Calculation of Simultaneous Equation 9

        SupplyCurrent3Error = ...
          1-(SupplyCurrent3Temp...
          /SupplyCurrent3);               # Calculation of Error for Equation 9

        AvgCurrError = ...
          ((abs(SupplyCurrent1Error)...
          +abs(SupplyCurrent2Error)...
          +abs(SupplyCurrent3Error)...
          +abs(SupplyCurrent1aError)...
          +abs(SupplyCurrent1bError))/5); # Calculation of Average Error

        if(AvgCurrError<=0.3)             # If the Average Error is less than 30%
          line = [mat2str(itr) ", " ...
            mat2str(Rab) ", " ...
            mat2str(R1a) ", " ...
            mat2str(R12) ", " ...
            mat2str(R13) ", " ...
            mat2str(R3a) ", " ...
            mat2str(SupplyCurrent1Error)...
            ", " ...
            mat2str(SupplyCurrent1aError)...
            ", " ...
            mat2str(SupplyCurrent1bError)...
            ", " ...
            mat2str(SupplyCurrent2Err)...
            ", Error" ...
            mat2str(SupplyCurrent3Error)...
            ", " mat2str(AvgCurrError)...
            "\n"];                        # Store the Supply Currents and Errors
          fputs (fid, line);              # Write this iteration to file
        endif

        clc;                              # Clear the display
        disp ("Progress Summary")
        disp ("The value of Rab is:"),
          disp (Rab)
        disp ("The value of R1a is:"),
          disp (R1a)
        disp ("The value of R12 is:"),
          disp (R12)
        disp ("The value of R13 is:"),
          disp (R13)
        disp ("The value of R3a is:"),
          disp (R3a);                     # Display parameters
        progress = (Rab/RabEnd)*100;      # Calculate the and progress of simulation
        disp ("Progress (%):"),
          disp (progress);                # Display the progress


      until(R3a>=200)                     # Iteration Limit for R3a
    until(R13>=1500)                      # Iteration Limit for R13
  until(R12>=1500)                        # Iteration Limit for R12
until(R1a>=200)                           # Iteration Limit for R1a
until(Rab>=RabEnd)                        # End Iterations

fclose (fid);                             # Close the results file

##############################################################################################
##
#
#
#                                        END
#
#
#
##############################################################################################
##
```

G.2 Wagon Parameter Matrix Calculation Verification Simulation Code

```
################################################################################################
##
#
#
#    Octave V3.8.2 Simulation
#
#    Title: Wagon Parameter Matrix Calculations
#
#
#
#    Author: James Clay
#
#    Student Number: 325609
#
#
#
################################################################################################
##

MatrixA=[0.11, 0.12, 0, 0, 0.22;...
         0, 0.01, -0.21, -0.2, -0.11;...
         0.11, 0.11, 0.1, 0.2, 0.32;...
         0.08, 0.08, 0.02, 0.04, 0.18;...
         0.12, 0.31, 0.07, 0.14, 0.12]       # Declaration of MatrixA

Constantk2 = [0.1552111111;...
              -0.00114;...
              0.1561944444;...
              0.1130511111;...
              0.1693566667]                  # Declaration of Matrixk2

detA = det(MatrixA)                          # Calculate the determinant of MatrixA
invA = inv(MatrixA)                          # Calculate the inverse of MatrixA

solA = invA*Constantk2                       # Multiply the inverse of MatrixA by
Matrixk2

invSolA = solA.^-1                           # Find the inverse of the elements of solA
save MatrixCalculations_D01.txt...
       MatrixA Constantk2 detA...
       invA solA invSolA                     # Write the results to a text file

################################################################################################
##
#
#
#                                          END
#
#
#
################################################################################################
##
```